NCAR-TN/IA-99
NCAR TECHNICAL NOTE

May 1975

Scientific Ballooning Handbook

Alvin L. Morris, Editor

ATMOSPHERIC TECHNOLOGY DIVISION

NATIONAL CENTER FOR ATMOSPHERIC RESEARCH
BOULDER, COLORADO

PREFACE

The scientific foundations for ascent by balloon were established as early as Archimedes; a practical application of his principles, however, was to await another twenty centuries. From the moment the Montgolfier brothers succeeded in flying balloons that could carry useful loads, scientists were eager to use them. Today, employing technological developments in materials, communications, and electronics, and taking advantage of new information about the circulation of the atmosphere, man has made balloon systems servants of science which can be used virtually anywhere on earth. He is even contemplating their use on other planets.

The current revolution in scientific ballooning has resulted in a technology that is, in its own right, important to many groups; unfortunately the literature of that technology is not readily available. Much of it was classified when written and received extremely limited distribution. In particular, reports of the excellent work done at the

University of Minnesota, although now declassified, are not generally accessible. Other important work has been published in scientific or trade journals that are not identified with ballooning.

It was my purpose when I undertook the preparation of this handbook to summarize the current technology of ballooning as completely as possible. I have been fortunate in obtaining contributions from experts in most of the technological areas I consider important. When no one could be found to contribute a section dealing with an important area, other contributors were asked to include in their sections pertinent material from the missing area. The most notable omission is a section on materials. Therefore, more information on materials is included in several other sections than the authors of those sections might otherwise have chosen to include.

Each contribution was reviewed by at least one person other than the author in an effort to minimize errors and avoid major omissions. The final content of each section was determined by the author, however.

To limit the size of the book, I have included only those techno-

logical areas which I feel are rather directly associated with scientific ballooning and about which information is not readily available. Thus, there are no general mathematical tables. Given the abundance of handbooks available in most technical libraries and the nearly universal use of high speed computers by technologists, this elimination seems justifiable.

Material for this handbook was selected and organized with several groups of people in mind. The scientist whose experiment will be flown on a balloon, the engineer who designs the balloon or the equipment to be flown, and flight operations engineers and technicians will all find useful information in it.

Principles have been emphasized, but "cookbook" procedures are also given for a few facets of balloon operations, e.g., selecting a parachute. Tables have been made short, but linear interpolation is acceptable in nearly all of them. Equations from which more complete data may be generated are usually included for the convenience of anyone using a computer.

The help of experts from many fields was essential in the compilation of this book, and I am grateful to each author for his contribution. Many others also contributed and while I cannot list all of their names, I would like to thank the following people for their special efforts: Justin Smalley, John Sparkman, and Karl Stefan for their critical review of the sections I wrote; Jay Chalmers and Matthew Reynolds for extensive computer programming aid; and Carolyn Morris for typing the manuscript, helping with the editing, and providing constant encouragement.

Alvin L. Morris

October 1972

CONTENTS

SECTION I

EVOLUTION OF BALLOONING

by

Ralph H. Upson

LIST OF SYMBOLS

Symbol	Description	Dimensions
b	specific lift of gas	$ML^{-2}T^{-2}$
G	total weight carried at attachment point of balloon	MLT^{-2}
K	a shape constant [defined by Eq. (1)] which is determined by the design and operational conditions of a balloon	L^{-3}
m	subscript identifying its symbol with the equator of a balloon	
n	subscript identifying its symbol with the natural shape	
o	subscript identifying its symbol with a reference level far below a balloon's ceiling	
p	pressure	$ML^{-1}T^{-2}$
R_m	radius of curvature of a meridional section of a balloon	L
R_s	radius of a spherical balloon	L
s	gore length measured downward from the top of a balloon	L
s	subscript identifying its symbol with a sphere	
t_c	circumferential (horizontal) tension per unit of material width	MT^{-2}
t_m	meridional tension per unit of material width	MT^{-2}

t_s	meridional tension per unit of material width in a spherical balloon	MT^{-2}
V	volume (of gas or balloon)	L^3
V_o	volume of a balloon at a reference level far below the balloon's ceiling	L^3
V_s	volume of a spherical balloon	L^3
x	distance measured radially outward from the vertical axis of a balloon	L
x_o	radial distance from axis to balloon skin at level of zero differential pressure	L
x_1	radial distance from axis to edge of taut cap	L
y	distance measured upward	L
y_n	vertical distance measured from the top of a natural shape balloon to a point on the balloon skin. This distance may be given approximately by a cubic equation	L
y_o	vertical distance measured from the level of zero differential pressure to the top of a balloon	L
y_s	vertical distance measured from the top of a spherical balloon to a point on the balloon skin. This distance may be given approximately by a quadratic equation	L

Greek letters

ρ	air density	ML^{-3}

π	3.14159	
θ	angle balloon skin makes with the vertical	

List of Figures

EVOLUTION OF BALLOONING

A. HISTORICAL INTRODUCTION

Balloons, like all floating bodies, demonstrate the principle of Archimedes (see Chronology). He not only proved the principle experimentally but showed by sound reasoning that a statically floating body must displace its own weight of the fluid in which it floats. This principle in its original form is as valid in air as in water, yet for 2000 years thereafter, men watch smoke rising through the air without thinking how it could be put to practical use. This long period was broken by two flashes of inspiration--Roger Bacon's proposal in the middle of the 13th century of a (then hypothetical) lighter-than-air filling, and Father Lana's proposal in 1670 of a vacuum balloon. The latter device, which is theoretically sound, is still frequently reinvented by people unfamiliar with shell structures, available materials, and the realities of atmospheric pressure. Here, as usual, faith in an idea can be effective only when combined with knowledge of the difficulties to be faced and with realizable means of meeting them.

The practical breakthrough--the French Montgolfier brothers' hot-air balloon--was a tribute to the intelligent artisans' powers of observation and flair for feasible construction. Still, it was the noted scientist Charles, in collaboration with two artisans, the Robert brothers, who shortly afterward introduced the hydrogen-filled balloon, with features of construction that remained standard for over 150 years. Even the basic instruments have been retained for nearly as long as the general features developed in the early days.

The technological developments most effective in dictating modern balloon design and use are probably improved plastics, helium gas, and for sport use, a reversion to hot air. These developments are still far from complete. In general, however, flexible, high-strength film permits making the balloon a self-contained unit with no net to carry the load and with a weight saving that greatly extends the altitude capability. Gas-tight, high-strength material also makes feasible for the first time altitude stabilization by superpressure. Helium not only disposes of the fire risk but also significantly stabilizes the balloon with respect to altitude changes.

For special purposes older methods are still useful. The self-adjusting, load-carrying net might well be reconsidered for conditions varying from partial inflation to superpressure, and hydrogen is relatively inexpensive, readily available, and well suited to any demand for a fast-rising balloon or for one designed to float in a strongly stable layer of the atmosphere (1). The long and successful record in the use of flammable gas for free balloons seems to justify a re-evaluation of hydrogen for the more demanding of these conditions, with due consideration of the skin material's electrostatic properties, avoidance of flame in operation, and suitable precautions generally. Experience shows Mylar to be much more prone to static sparks than polyethylene.

A modern plastic balloon is essentially a shell structure of material incapable of carrying compression and having a small but appreciable weight. Each element of skin is in static balance from its own tangential tension and the normal pressure difference between inside and outside. This pressure difference, usually positive, can also be negative in gas below the level of zero-pressure difference.

A balloon's profile or axial section was formerly quite arbitrarily assumed, and common designed to be a circle. In fact, a free balloon was referred to as a spherical balloon to distinguish it from the elongated kite balloon or dirigible balloon (airship). Even the early netless balloons were close to spherical, with long footropes attached to loading points near the equator (1). The spherical concept had a further lingering death in the cone-on-sphere shape of the early plastic designs, but its structural limitations for high altitude use had already be recognized.

B. OPERATING CONDITIONS

We must here recall the status of balloon theory 40 years ago. In 1898 the term "scientific ballooning" was applied to physical and atmospheric research and was later applied to the use of scientific principles in balloon operation to replace the largely rule-of-thumb techniques in almost exclusive use up to 1913. These principles were at first applied mainly to the winning of balloon races with the objective of spanning the greatest distance from the starting point. As outlined in reference (1), the operational improvements introduced after 1913 included better instruments, precise navigation, a means of sounding for air currents, establish-

ment of quantitative balloon response to measured discharge of gas and ballast through the use of a stop watch with a calibrated gas valve; all of these were coupled with the best possible appraisal of the general weather conditions.

As shown by Fig. 1, two operational conditions of the balloon had long been recognized: full and partially full (slack or flabby). A rising, full balloon would discharge gas by automatic spillage; a slack balloon would not. Except for the final landing approach, this means of gas control remained the only one in practical use until the advent of the calibrated valve. Here it should be noted that vertical control was especially critical in the usual daytime unstable conditions dictated by the use of moist gas having two or more atoms per molecule. Such gas responded to altitude change with a temperature change numerically less than the average or standard lapse rate (negative gradient) in the troposphere.

It seemed to be tacitly assumed that the partially-filled balloon would necessarily be in a less critical condition structurally than a full one. The error in this assumption was not serious as long as operation was

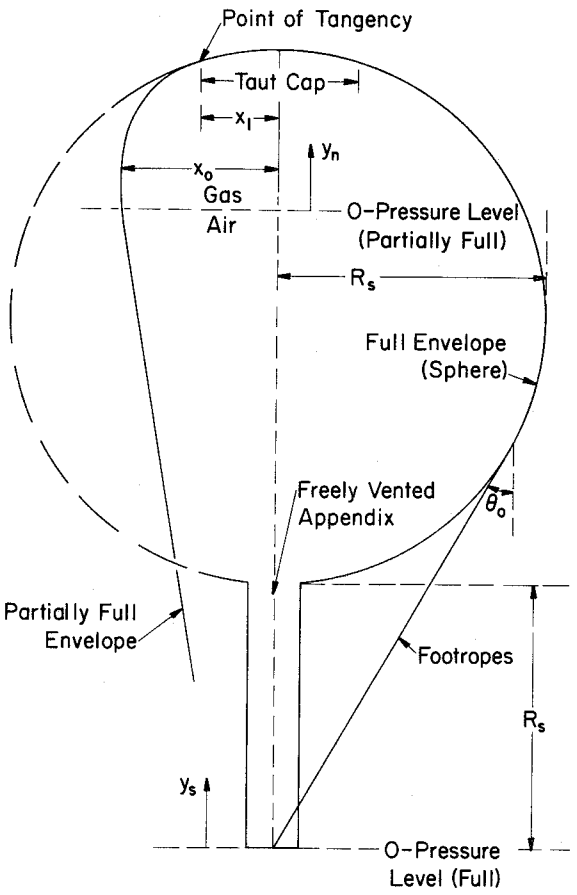

Fig. 1. Spherical balloon shapes under full and partially full (slack) conditions. Note that the balloon is vented at the bottom so that air fills the slack balloon below the zero-pressure level.

confined to the lower troposphere, but with stratosphere expeditions using netless balloons it was a different story (2).

An important property of the traditional balloon net is its distribution of load in two dimensions over a substantial range of shape and pressure variation, especially if similarly shaped meshes are retained toward the top. A similar property can theoretically be had by a suitable arrangements of threads and panels of woven fabric, but this property is practically destroyed in conventional two-ply rubberized fabric in which only one ply is laid on the bias. The same applies to any flexible but essentially inextensible membrane, for reasons that will now be apparent.

In a balloon carrying the usually concentrated payload, this gravity load must, of course, reappear in the axial component of circumferentially integrated (total) meridional tension adjacent to the load attachment level, where such stress must also be in normal balance with the local gas pressure. Since there must always be stress in the meridional direction, it is clear that any slack to accommodate a less-than-full condition must be in the circumferential direction. It is also clear that with gas pressure normal to the surface, only the skin weight, or other applied load, can

change the total tension within a slack portion of the balloon at a given altitude. Thus, in such a portion of the balloon, aside from skin weight, the stress or tension, t_m, per unit of horizontal circumference varies inversely as the circumference $t_m = G/(2\pi \times \cos \Theta_o) = bV/(2\pi \times \cos \Theta_o) = pR_m$, where G is the total weight carried at the concentration point. Also, the same stress is all that carries the pressure, which in this simplified case varies as the gas head measured from the level of zero gage pressure, or $p = by$. Then $t_m \propto 1/x$ and $p \propto y$, or

$$p/t_m = 1/R_m = Kxy = \frac{2\pi xy}{V} \cos \Theta_o \qquad (1)$$

where x and y are the coordinates of the profile curve, $1/R_m$ is the meridional curvature at the same point, and K is a constant applying to a particular slack portion of a balloon, which is quantitatively determined by the design and operational conditions. For finite skin weight the effective pressure p must include the normal weight component of unit skin weight and the integrated meridional component of skin weight t_m.

This is the basic equation of what has come to be known as the natural shape. Even in its elementary form for weightless skin carrying zero circumferential stress, the integrated curve of the profile can take an infinite

variety of shapes depending on the starting coordinates and slope and on the value of K. Several examples are qualitatively shown in Fig. 2. A particular shape studied in reference (2) was approximately the profile of a gas bubble in a partially-filled balloon designed as a sphere, as shown in Fig. 1. Here at the left the circumferential elements of the skin are slack below a certain critical level where the designed circle and the natural shape come tangent to each other. Above this level the envelope is free to fill out to its full designed shape in what has been called the taut cap, and the maximum stress is determined by the meridional stress at its edge.

The next step in design development came with the thought that the natural shape, prevailing over most of the surface during most of an ascent to high altitude, might logically be made the designed shape of the full balloon. In other words, for a balloon vented to the atmosphere the circumferential stress is of so little use that it may as well be assumed of no use and the balloon designed accordingly. This assumption also fitted well the commonly prevailing condition of meridional gores joined by relatively low-strength, unreliable seams carrying meridional reinforcing tapes.

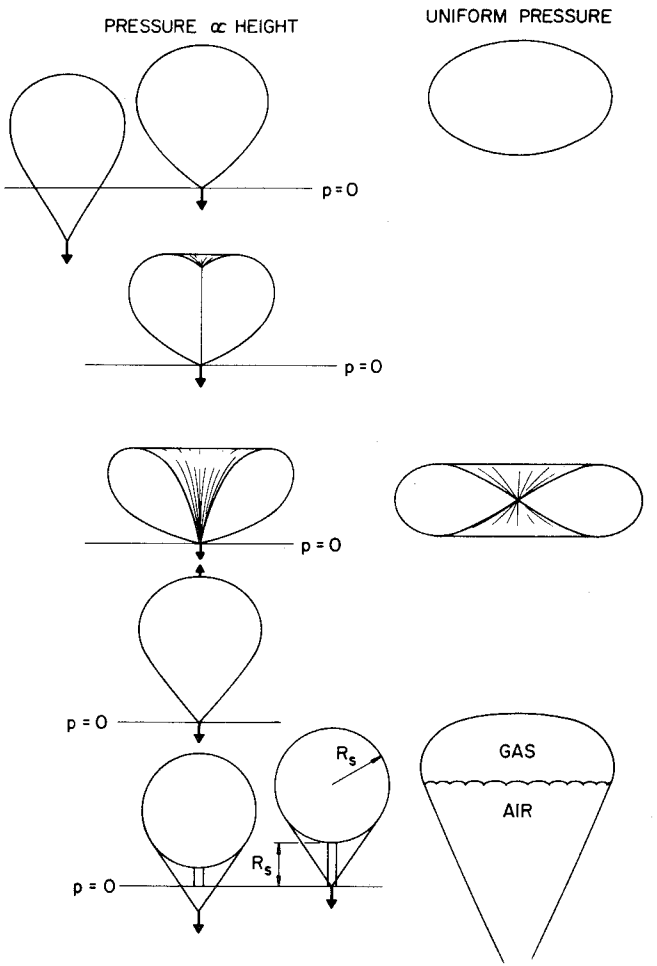

Fig. 2. Some forms which a natural shape balloon may take.

An idealized complete profile from the same equation is shown by the outer curve on the right in Fig. 3. It is based on the assumption that at the bottom x = y = 0 where θ_o is 50.15°; K = 8.53 throughout for balloon height = 1, reference (3). For comparison, the inner curve (right) in the same figure shows a full balloon with an appendix vent of length a = 0.03 (K = 8.80) on the same scale of y_{max} = 1. Subsequent developments to date have been mainly refinements in balloons of this general shape, which, however, still present some problems of a rather basic nature.

C. ENVELOPE CONSTRUCTION

Beginning in 1910, the aspect of the aeronautical awakening of most interest to the management of the Goodyear Company was finding a new outlet for rubber products. After a brief and unsuccessful trial of rubberized fabric for wing covering, it was decided that a much better market for such fabric was balloons and airships. Also, since there was no fully established manufacturer of lighter-than-air (LTA) aircraft in this country, there appeared no alternative to the development of their own complete product in this field. As applied to free balloons, components of

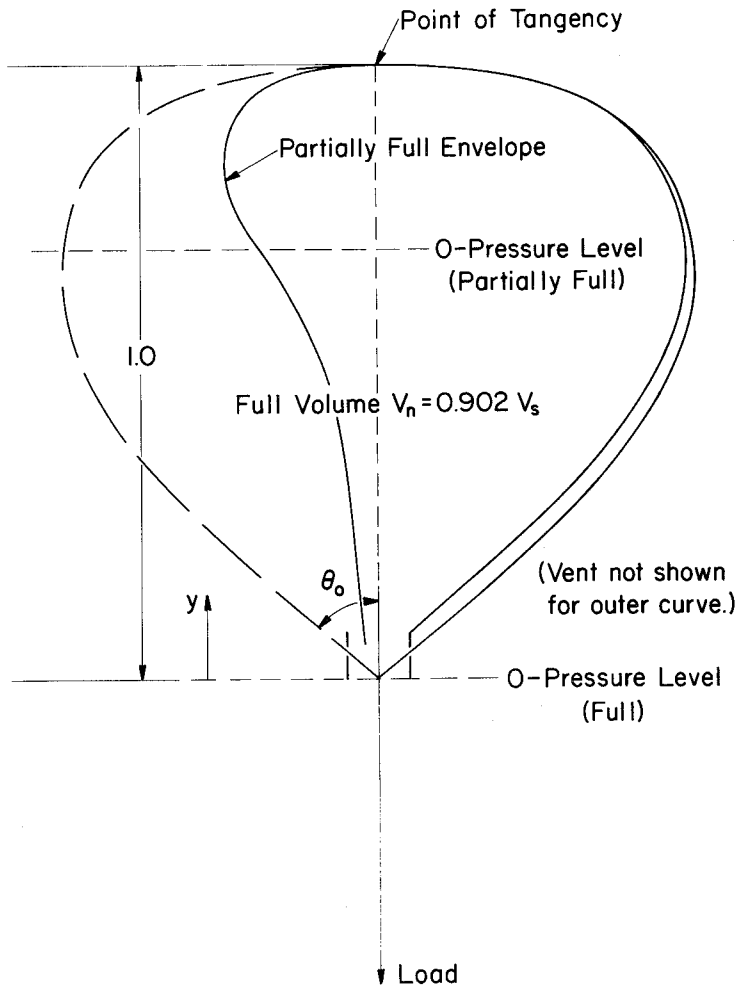

Fig. 3. Natural shape balloon fully inflated right and partially inflated left. There is no air inside the balloon.

the overall problem seemed to be as follows: material, general configuration, size and panel geometry, assembly, flight testing and operation.

Work proceeded at first with a relatively conventional shape and arrangement. With the type of fabric selected, it was obvious that its strength was not a critical factor, especially with a net to take the greater part of the load. Hence, the spherical shape was retained as having the maximum volume/weight ratio. This did not take into account at the time, however, the actual deformation of the shape in free flight with an open appendix of usual length and with a net proportioned to make its circumferential stress one-quarter of its meridional stress (width of each diamond mesh one-half of its height).

In approximating a sphere from initially flat panels, two arrangements were considered: 1) the commonly used meridional-gore system, and 2) conical rings. The latter was chosen for the first balloon, mainly for appearance and to facilitate arranging the panels brick fashion, thus avoiding four thicknesses of material at the corners. Each circumferential ring had the same number of identical panels except near the extreme top and bottom and allowed for seam overlap. The number of panels per circumference was

dictated by the need to economize labor and at the same time avoid excessive trim waste. Each pattern had typical dimensions tabulated as follows: chord length and off-set for convex side, same for concave side, width (end dimension). The chord length and off-set, setting up the required arc length and radius, were laid off by direct measurement on a simple double-bow device shaped to closely approximate a circular arc of any desired long radius, as determined by the setting of a central screw. The bias ply was run in the same helical direction (not herringbone) around the balloon, since the resultant slight twist about the center axis would be of no conceivable harm in a free balloon.

Seams were at first cemented, then sewed, and then taped, a procedure inherited from construction of the Vaniman airship envelope. The sewing was always a major headache, however, as the cement kept fouling the machines. Later, a properly made and aged seam was found to be adequate without the sewing. Some experimenting was done with small varnished balloons; one, built for an advertising contract, had an internal electric light. It was generally unsuccessful, however, because of the difficulty of tethering an

essentially spherical balloon. Sticking, cracking, and spontaneous combustion were other difficulties.

D. INSTRUMENTATION

Starting in 1910 there were several years of experiment and development for improving the sensitivity and utility of vertical-motion detectors. The European stratoscope, with a mechanical pointer, and the American Custer, a liquid type, were both good but lacked full quantitative significance. Tossing out a handful of fragmented tissue paper was about as informative. A more quantitative vertical airspeed meter consisted of a light counter-balanced vane, pivoted slightly above the center of gravity and free to swing over a calibrated scale. The utility of any aerodynamic indicator, however, depended largely on how closely a movement through the air correlated with a change in pressure altitude. This correlation was not always perfect and tended to break down completely with the much later introduction of dry helium.

A hypersensitive accelerometer was developed with the help of the Pioneer Instrument Company. It had a scale readable to 0.0001 of g, corresponding to less than 1.0 lb or 1/30 of a sandbag on an 80,000 ft^3 balloon,

just the kind of accuracy wanted. It proved to be useless, however, because random creep, presumably due to elastic hysteresis, temperature change, and the passage of time, effectively destroyed any knowledge of the zero position. Present know-how would probably permit a satisfactory solution to this problem.

At the time the best solution was a sensitive change-of-altitude meter. This instrument was a long U tube containing two non-miscible liquids of slightly differing densities, one red, the other colorless. The line of separation was observed in a long glass tube of contracted section. One arm of the U vented directly to the atmosphere, the other through a chamber of finite volume whose atmospheric outlet could be closed off. The scale was calibrated so that when this outlet was closed, it read change of altitude. Watching and timing the change gave a fair idea of acceleration and vertical unbalance. The leak-type climb meter, subsequently developed for airplanes, was not too good because of its considerable lag and inadequate sensitivity.

E. FABRIC TESTING

A fabric testing program at Goodyear which was essential to the largely

parallel airship development gave results also of interest in ballooning. The mere handling of woven fabric shows the great difference in yield between the warp and web directions and the indefinitely large local yield in the diagonal direction of a single ply. Early tests showed that the strength of a sample tested rapidly in a standard tensile machine was deceptively large compared to strength of a sample under long-continued loading. The reduction of strength, although presumably asymptotic, seemed substantially complete after one or two days. With allowance for random variations, it was established that none of the fabrics tested could be expected to hold, for an indefinite time, more than about half of the machine-tested strength.

Another important material test was resistance to exposure. In this program, hundreds of samples were labeled, dated, and exposed to the elements on the roof and then strength-tested at specified intervals. In general, the rubberized fabrics were much more affected by sunlight than by any other agency. Almost all samples proved capable of going through a winter of cold, wet, ice, and snow, but many were almost ready to fall apart after a month of hot summer sun. Samples kept in the shade were much better

off. A fabric found most resistant to such deterioration was one heavily compounded with carbon black and externally aluminized. In 1919, this fabric was used in the construction of a racing balloon, Goodyear II, winner of the national race that year (Upson and Van Orman).

A series of tests on internal heating from radiation was also carried out. For this purpose, closed fabric envelopes containing thermometers were exposed to identical conditions of sun. From appearancce the aluminized fabric already mentioned seemed a likely candidate for minimum heating but, to save time, was not actually tested prior to construction of the balloon. Its performance in flight was, in this respect, somewhat disappointing, and a subsequent comparative test showed it to heat more than the yellow fabric used in Goodyear I, possibly because of the carbon black under the thin aluminum surface since similar fabric without the aluminum heated most of all. A chalky white surface was the best, although not much better than yellow. No transparent material was tested since none then appeared suitable for balloon use. Considerable study was devoted to the relative importance of various fabric improvements (4).

F. INTERMEDIATE DEVELOPMENTS

In 1923 a balloon, designed by Upson but made by Goodyear, was tested with complete success. This balloon (1) is interesting as a transition between early and modern designs. It had a single thickness of white rubberized woven fabric laid herringbone fashion as in the old Upson parachute patent, and strengthened with meridional load-carrying tapes. These tapes were carried into a heavily reinforced conical cap at the top. The bias-laid fabric was self-adjusting to the effects of varying volumes and pressures. Rain was perfectly shed by the conical top, off-set valve, and an equatorial rim--the latter serving also to dampen the vertical motion, a feature not recommended for use with helium, however. The single, precise valve served all gas discharge purposes except quick deflation, for which a conventional rip panel was provided.

The following year (1924) the use of white, single-ply fabric was continued by W. T. Van Orman in Goodyear III with an envelope weighing 315 lbs as compared with 720 lbs for Goodyear II of the same size. In this and subsequent balloons up to Goodyear X in 1933, Van Orman set a phenomenal record by winning five national and three international distance races, three

times beating Belgium's Demuyter. A similar single-ply fabric was used in the record altitude Explorer II of Stevens and Anderson in 1935. Other improvements by Van Orman were the use of radio compass and celestial navigation, both later adopted by air transport and navigators.

Structural and aerodynamic experience with kite balloons and airships, particularly the metal-clad ZMC-2 (5), resulted in indirect benefits to all balloon development. Progress in airplanes and seemingly unrelated fields contributed its share. In the meantime, rubber and neoprene balloons had been improved to an extent permitting instrumented flights to altitudes previously unreached by the more conventional, vented type. However, the usual bursting of the balloon at ceiling was an effective bar to prolonged flight. The time seemed ripe for new ideas.

Development of the modern plastic balloon started with a series of cellophane balloon flights by Jean Piccard with T. H. Johnson and John D. Ackerman, mainly at the University of Minnesota in 1936 (6). These flights were unmanned and were controlled by an automatic ballast dispenser based on aerodynamic vertical motion, like the vertical airspeed meter previously mentioned. These balloons and the succeeding ones of polyethylene built by

the General Mills Company had a rough approach to a natural shape approximated by a cone-on-sphere (6).

Studies at the University of Minnesota by Ney, Winckler, and others resulted in particularly valuable advances in launching techniques and in increased knowledge of the flight thermodynamics of helium-filled balloons.

Reference has already been made to the still impractical idea of a vacuum balloon, but the same type of equation, with modern materials, has definitely feasible application to superpressure balloons. A generally sound example of such application is in the mathematics of Zahm (7), which shows the relationship of stress and elastic yield required to maintain altitude in event of leakage. As may be noted in the Chronology, the superpressure idea was also proposed by Vaniman in 1912. The first structure capable of acting in this manner, however, was the metalclad ZMC-2 launched in 1929. Tested strength of the metal and seams, confirmed by water-model tests, showed that the hull could carry an ample reserve of pressure for altitude stabilization, although this was not a feature important in airship operation under power.

G. INTRODUCTION OF THE NATURAL SHAPE

The so-called natural shape of the freely vented balloon dates back to 1934 when the failure of the first Explorer balloon was the stimulus for a shape-and-stress analysis of a partially-inflated balloon in Upson's lecture to a lighter-than-air class at the University of Michigan. These lecture notes reappeared in an IAS paper published in 1939 (2). As a result of several studies for General Mills (3), a mathematically derived curve was applied to the designed profile of the entire balloon. In the meantime, Arnstein and Swan at Goodyear had simulated a form of the same curve by a system of weights and pulleys acting on a chain (8). Further development of this type of profile resulted in its becoming practically standard for vented plastic balloons. It is perhaps unfortunate that the natural shape has come to be so closely associated with the one general form typified by Fig. 3, with only minor variations in the design geometry due to skin weight, vent location, and load attachment. Experience continues to remind us that it is not the full balloon, envisioned by the design geometry, which usually poses the most critical problem. The really critical condition in any high-altitude operation almost invariably occurs as it did with the old Explorer,

when the balloon is inflated to a small fraction of the design volume. Under these conditions any netless balloon of the type here considered takes a natural shape over a substantial portion of its surface, but this is a natural shape only in the mathematical sense, as defined by Eq. (1). It has little apparent resemblance to the full profile of Fig. 3 and is highly variable as changes of altitude change the volume ratio.

To summarize the physical conditions to which Eq. (1) applies: it is any portion of a pressure-and-load-balanced curve of polar symmetry, generated by weightless, flexible skin carrying zero circumferential stress with linear variation of pressure. In a preliminary analysis of this kind, simplifying assumptions serve the same purpose as those appropriate to slender struts, Newtonian orbits, and other inherently complicated concepts of science and engineering.

It is instructive now to compare the spherical design of Fig. 1 with the special form of the natural shape typified in Fig. 3. In the latter case, the partially inflated condition is shown with the gas filling below the same zero-pressure level. Broadly speaking, in each case for any less-than-full condition, the skin is circumferentially slack at all points up

to where the natural profile of the less-than-full shape comes tangent to the full designed shape. The most meaningful difference between the two cases is that for the spherical design the point of tangency rises gradually as the gas volume decreases, whereas for the natural-shape design the entire profile is circumferentially slack for anything less than full volume. Quantitative consideration of this difference in behavior should do much in answering the question as to whether a real improvement in design has been made, and if so, what potential it may hold for further improvement.

As shown in Fig. 1, the full spherical form is attained with an appendix venting one radius length below the balloon, on the assumption of 30^{o} footropes and material of negligible weight. The same condition can, of course, be had by throttling the usually shorter appendix to a slight super pressure, a condition assumed equivalent to that at the pressure ceiling. For any predetermined shape, the meridional stresses are simply determined by a balance of forces on either the top or bottom portion of the balloon, cut on a horizontal plane at a given level.

If the design radius of the spherical balloon is R_s and the unit lift b_s, the maximum stress in the full balloon is found to be

$t_s = 1.5\ b_s R_s^2$ force per unit of circumferential length. (2)

This value of the merional stress occurs at the top and also just above the suspension band. A balance of force on an increment of skin area normal to the surface makes the circumferential stress of equal magnitude at the top but zero just above the suspension band. The general distribution of stress is shown in Fig. 4.

The above stresses are for the full volume $V_s = (4/3)\pi R_s^3$. When filled to a small fraction of this design volume, far below pressure ceiling, where the unit lift is b_o and the volume V_o, the distorted profile approximates the form shown by the innermost curve, top left, in Fig. 4. Trial integration of this curve shows the volume to be approximately $V_o = 0.77\ \pi\ y_o^3$ with $K = 2.60/y_o^3$ in Eq. (1).

Inspection of Eq. (1) shows that the natural curve approaches a cubic parabola at the top (3), whereas the spherical profile there approaches an ordinary parabola. These curves are shown in Fig. 4. By equating their slopes at x_1, where $x_1 \ll R_s$ and $y \approx y_o$, we get immediately $R_s = 2\ R_m$. In other words, where the slack portion of the balloon merges into the taut

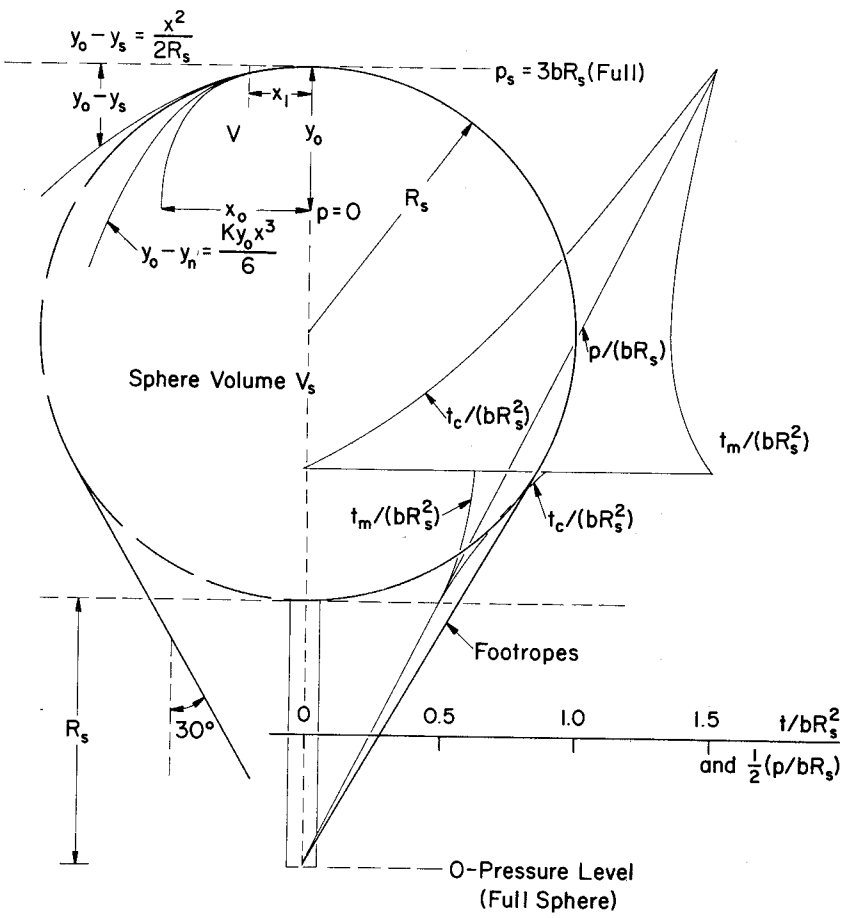

Fig. 4. Distribution of stress on a spherical balloon and comparison of the spherical and natural shapes.

portion, the meridional radius suddenly doubles. Just above this point, the normal force balance on an incremental area of fabric requires the meridional stress to remain unchanged, but now with a circumferential stress of equal magnitude, a condition which then prevails throughout the entire taut cap (if small).

Use of the above principles permits a simple comparison of stress between the full balloon and the same balloon with a small fraction of full inflation, but for constant gross lift and weightless fabric. As already noted, the maximum stress in the full spherical balloon is

$$t_s = 1.5bR_s^2 = 0.577bV_s^{2/3}$$

where b is the unit lift at ceiling. For partial inflation, at low altitude, where the unit lift is b_o, the maximum stress at the edge of the taut cap of radius x_1 is given by

$$t_m = b_o V_o / (2\pi x_1)$$

where

$$V_o/\pi = 0.77y_o^3$$

also

$$x_1/R_s = 0.77\ (y_o/R_s)^2 = 1.11\ (V_o/V_s)^{2/3}$$

and

$$y_o/R_s = 1.20\ (V_o/V_s)^{1/3}$$

The volume $V_s = (4/3)\pi R_s^3$ for the full sphere, $V_o = 0.77\pi y_o^3 = \pi R_s x_1 y_o$ for variable inflation to a small fraction of V_s. Furthermore, $b/b_o = V_o/V_s$ for expansion of the same mass of gas. Use of the above relationships now gives the stress ratio at partial inflation relative to full inflation as

$$t_m/t_s = \frac{(4/3\pi^2)^{1/3}}{2 \times 1.11 \times 0.577}\ (V_s/V_o)^{2/3} \approx 0.40\ (V_s/V_o)^{2/3} = 0.40(\rho_o/\rho)^{2/3} \qquad (3)$$

Results are plotted in Fig. 5 with the dashed curves corrected for the otherwise neglected volume difference of the spherical segment comprising the taut cap and the finite value of the meridional angle at the bottom of the gas-filled portion, as shown in Fig. 1.

It is clear from Eq. (3) that the stress tends rapidly to approach an infinite value as the design ratio V_s/V_o increases. This theoretical value would actually be approximated were it not for the elastic and plastic yield of the material. The same condition is designed into the full natural shape of Fig. 3, since here the stress is concentrated at the top--the theoretical stress center--for all volume ratios, but the meridional force is finite per

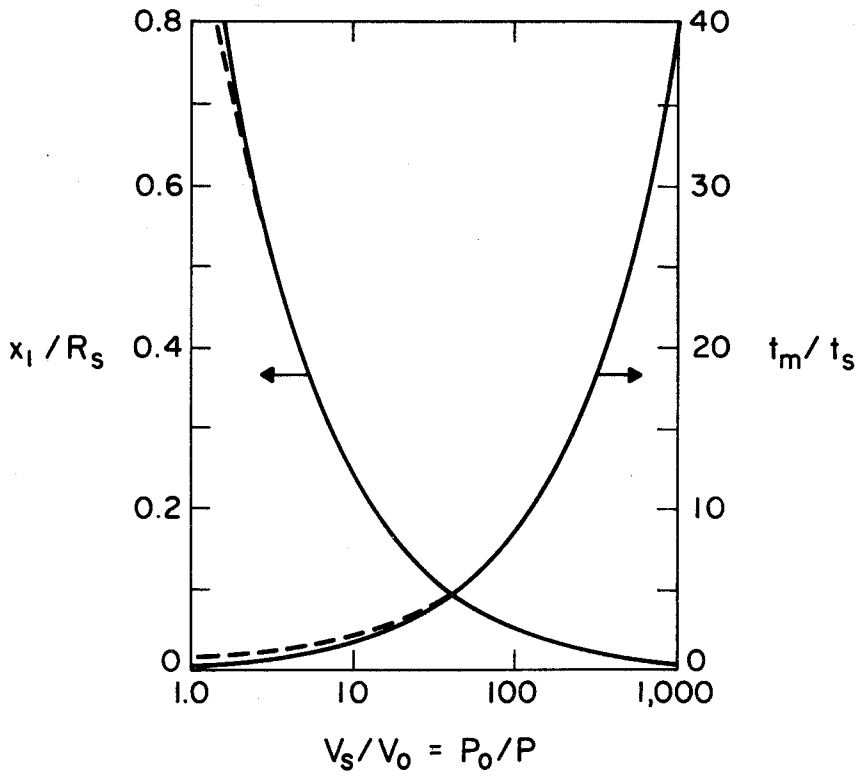

Fig. 5. Comparison of meridional stress at the edge of the taut cap in a partially inflated spherical balloon with stress in the same balloon after it is fully inflated.

meridian tape. On this basis, the load carried per tape actually increases as the volume expands, due to the increased cone angle at the bottom, but is constant along the meridian for any weightless natural shape. The area increment on which the pressure acts still varies with the circumference, making the mathematics basically the same as for any slack condition. The tape construction, however, seems no panacea for problems of the spherical shape, if any of it remains, since the stress in a small taut cap is theoretically the same in all directions, including the normally untaped circumferential direction. By the same theory, in the full natural shape we have reduced the dimensions of the taut cap to zero for all volume ratios. However, can we be sure of this actual result? A second look seems in order.

It is apparent, even from the rough sketches presented here, that practically all smooth curves become indistinguishable as we move close enough to the top. Specifically, we are interested in the difference of meridian or gore length in the taut cap between the spherical and natural shape ($s_s - s_n$), represented respectively by ordinary and cubic parabolas (3). Using the simplified integration of (9), we get for the "geometric strain" or relative difference between the two curve lengths out to a radius x

$$(s_s - s_n)/x = x^2/8R^2 \qquad (4)$$

For example, if the cap has a radius one-tenth that of the full balloon, a material strain of 1/800 will make up the difference. Practically speaking, this means that the top of any balloon with a continuous curve and an unwrinkled surface is structurally indeterminate. The same point is brought out more fully in references (3) and (10).

Alleviation of this tendency toward over-stressing near the top may be approached in one or both of two ways: 1) insuring that the stress center--where the tapes cross--remains exactly in the designed position; for example, depressing the top by an axial suspension member or extending it by the lift of a smaller balloon above; 2) reinforcement of the top surface to an extent making the circumferential strength approach that of the meridian strength.

For reasons already brought out, need for the latter provision is not appreciably discounted by use of a spherical top. Return to the spherical upper portion is not ruled out, however, to make maximum use of the designed volume in the full condition, if kept within safe stresses for all conditions.

The concept of the natural shape can be readily applied to a super pressure balloon and deserves some attention here. The theory is the same as already explained, all forces being carried by meridional elements and none circumferentially. With uniform pressure (equivalent to an infinite head of lifting gas) and negligible weight in comparison, the curve is a true elastica, which can be solved by elliptic integrals. The mechanical analogue is a straight elastic rod bent into a hoop and then compressed by two diametric forces until the curvature just disappears on opposite sides. With equatorial radius $x_m = 1$, a closely approximate algebraic equation is: $y = 0.598\sqrt{1 - (x)^{2.8}}$. The resulting surface of revolution has a half-gore length of $1.31\ x_m$, an enclosed volume of $2.75\ x_m^3$, and a meridional radius at the equator of $R_m = \frac{1}{2}\ x_m$. It is a relatively unfavorable application of the natural shape or meridian-tape construction.

For a given volume, the elastica must carry a tape stress-to-density ratio double that of the sphere's skin material to equal the same structural weight. Also, this natural shape has 15% more frontal area in vertical motion and roughly 50% more drag. This is but one example of how overall conditions affect design.

I have attempted in this section to show not only the development to date, but the great amount of work still to be done, as may be facilitated by the more detailed coverage in subsequent sections. With suitable interpretation, the principles brought out will be found applicable not only to balloons but to flexible fluid containers in general: fuel tanks, inflated satellites, decoys and targets, deceleration gear, underwater craft, air-supported roofs, pneumatic boats, airplanes, etc.

A CHRONOLOGY OF BALLOONING

c. 240 BC: Archimedes discovered the principle of flotation.

c. 1250 AD: Roger Bacon suggested that a light vessel filled with some (hypothetical) fluid lighter than air could use the same flotation principle in the atmosphere.

c. 1600: Galileo determined the approximate density of low-level air.

c. 1670: Francesco de Lana proposed a vacuum balloon to be driven by a sail--the latter, of course, a fallacy for free flight. He also confirmed the density of air and the effect of heat.

c. 1766: Henry Cavendish discovered hydrogen and showed it to be at least seven times lighter than air.

c. 1781: Tiberius Cavallo made hydrogen-filled soap bubbles that floated.

1782: Joseph and Jacques Montgolfier floated small paper balloons filled with smoke, called Montgolfier's gas.

June 4, 1783: The Montgolfiers, in a public exhibition, sent up a paper-lined linen balloon about 10 m in diameter which floated about 3 km in 10 min. Although inflated with smoke from a straw fire, heat was not yet recognized as the dominant source of reduced density.

Aug. 27, 1783: Under the auspices of the French Academy of Sciences, J. A. C. Charles sent up a hydrogen-filled balloon of rubber-coated silk, 4 m in diameter, made by the Robert brothers. It rose to about 1000 m and traveled 24 km

in 45 min. Charles's name is also well-known for his work on gas expansion by heat.

Sept. 19, 1783: A Montgolfier balloon successfully carried a sheep, a cock, and a duck about 3 km in 8 min.

Nov. 21, 1783: First manned flight: Pilatre de Rozier and the Marquis d'Arlandes flew in a Montgolfier in which the heat was replenished in flight by a straw fire. The balloon, 15 m in diameter, ascended about 100 m and traveled 8 km in 20 min, during which time the balloon caught fire but was extinguished with water carried for that purpose.

Dec. 1, 1783: J. A. C. Charles and M. N. Robert ascended from Paris to about 600 m and landed 43 km away after 2 hr in the air. Robert then alighted and Charles continued the flight briefly to 2700 m altitude as measured by a barometer. This hydrogen-filled balloon was substantially spherical and used a net, load ring, valve, open appendix, and sand ballast, all of which were later to be almost universally adopted.

1783: D. Rittenhouse and F. Hopkinson at Philadelphia experimented with a cluster of up to 47 small hydrogen-filled balloons with which James Wilcox was reportedly paid to make a flight of about 10 min, his downward control being effected by puncturing several of the balloons (the same in principle as Jean Piccard's control of a cluster a century and a half later). The evidence of Wilcox's flight seems not entirely convincing.

Jan. 19, 1784: The largest hot-air balloon on record, over 30 m diameter, made one ascent (from Lyons), terminated in 15 min by a rent in the fabric--a seeming premonition of some modern failures. Although presumably netless like other Montgolfiers, its large area with whatever volume remained, was enough to land its seven passengers with no casualties.

1784: Dr. John Jeffries, with J-P. F. Blanchard as pilot, made observations of temperature and moisture and collected samples of air at various (moderate) altitudes over England, using a hydrogen-filled balloon of the usual varnished fabric.

Jan. 7, 1785: Jeffries and Blanchard crossed the English Channel from England to France in an allegedly leaky, varnished balloon, sacrificing practically every available item of weight for ballast. Oars and a rudder proved ineffective.

June 15, 1785: de Rozier and P. A. Romain attempted a reverse Channel crossing (France to England) in a tandem balloon consisting of an upper gas balloon 11.3 m diameter and a lower hot-air or fire balloon 3 m diameter, the latter intended for vertical control instead of ballast. (They may well have surmised that Jeffries and Blanchard's difficulties had been due more to instability than to leakage, not knowing, however, that whereas air over water is likely to be unstable in winter, it is the opposite in summer.) A chance was taken on the flammability

of hydrogen in apparent confidence that its lightness would carry it up and away and that sparks could be contained. But less than a half-hour after the start, at about 1000 m, the craft was seen to burst into flame, with fatal results.

Jan. 9, 1793: Blanchard made the first free flight in America (at least in a single balloon) under full control. He continued exhibitions over Europe but died from an unrecorded illness, impoverished by political complications. His widow continued successful exhibitions.

Oct. 22, 1797: First successful parachute drop by Andre Garnerin over Paris, although Blanchard and others are credited with the original idea.

1804: The French Academy of Sciences, questioning the accuracy of previous upper-air data, commissioned physicists J. B. Biot and J. L. Gay-Lussac to make scientific observations. In flights together on Aug. 24 to 4000 m and by Gay-Lussac alone on Sept. 16 to 7000 m (hydrogen inflation) they established within this atmospheric layer substantial uniformity of gravitation, terrestial magnetism, and air composition (except moisture content).

1819: Madam Blanchard, after about 60 other flights, died in attempting a fireworks display from a gas balloon. It seems such displays were fairly common, continuing even after her death.

1821: First balloon use of coal gas by the leading British balloonist Charles Green, at the coronation of George IV. Green is credited with first use of the drag rope (then termed 'guide rope').

Nov. 7, 1836: Green, Monck Mason, R. Holland, M.P. set a distance record of 772 km from London to Weilburg, Germany, in flight of 18 hr with a balloon of about 2100 cu m.

1837: Dr. John Rae, a trader and surgeon for the Hudson's Bay Co., tried unsuccessfully to raise a balloon by sun heat alone. He attributed his failure to the weakness of sunlight in northern latitudes, but this could have been only a minor factor. The experiment has been done successfully with modern light plastic, blackened to absorb maximum heat.

July 1-2, 1859: John Wise, leading American balloonist, made the first airmail flight and, incidentally, set a new world distance record of about 1300 km from St. Louis to Henderson, N.Y. (not shown on available maps). The first flight carrying official U.S. mail started from Lafayette, Ind., July 17, 1859, descending only a short distance away. To Wise is attributed first use of the rip panel. (Although the rip panel has virtually supplanted the anchor or grapnel in modern balloon operation, accounts indicate that Wise continued to use an anchor with continuing poor results.) Wise also demonstrated the ability of a collapsed balloon to spread out enough in the top of a net

to parachute down. His monumental book, Through the Air, 1873, is a comprehensive collection of experiences, methods, and ideas from hundreds of flights.

1861-63: Tethered observation balloons used by both Union and Confederate armies. As with previous similar use in the French Revolutionary Wars, these balloons were of conventional spherical shape, prohibiting use in much wind.

Sept. 5, 1862: Under auspices of the British Association for the Advancement of Science, Henry Coxwell and James Glaisher, meteorologist, made an apparent new altitude record (without oxygen) with various physical and physiological observations. The highest altitude reading--from a non-recording barometer--claimed to be 8800 m while still rising, but this observation is questionable due to the physical condition of the men. Both became unconscious as the altitude increased. Tragedy was averted by Coxwell, who, with his hands already paralyzed, pulled the valve rope with his teeth. Consciousness was regained and readings resumed about 13 min later with barometer at 293 mm of mercury or 7300 m altitude. Of two pigeons carried, one died.

1864: A hot-air balloon of about 11,000 cu m was built and flown by E. Godard in England. It had a straw-burning stove weighing about 450 kg. Except for the county-fair type with air heated only on the ground, used for exhibition parachutes drops, the hot-air type now seemed to disappear until its modern revival.

1870-71: A total of 66 balloons, carrying 164 people and miscellaneous cargo, left Paris during its siege by the Germans in the Franco-Prussian War; for 4 months balloons provided the only contact between the city and the outside world.

April 15, 1875: First use of oxygen, and also first anoxia victims, in a flight from Paris. H. T. Sivel, Croce-Spinnelli, and G. Tissandier reached 8500 m, but only Tissandier survived. They didn't start using oxygen soon enough, not realizing the insidious approach of paralysis.

1878: Paul Bert published his classic work, La Pression Barometrique, on the physiological effects of altitude.

1885: Renard and Krebs in France made first fully successful application of power (electric motor) to an elongated balloon with a ballonet and steering organs. It was steered in a figure 8 at a speed of about 23 km/hr. (No further references to airship development will be given except as related to ballooning.)

1892: Hermite and Besancon developed instruments for unmanned high-altitude flight.

1895: Wm. Ramsay discovered helium in the atmosphere (previously observed by Janssen and Lockyer in the sun's spectrum in 1868).

1897: Andrée and crew started from Spitsbergen on a projected balloon trip to the North Pole. Bodies found at White Island in 1930.

1898: Aero Club de France founded, primarily to promote ballooning

(parent organization of F.A.I. which sponsors international contests and controls official records).

1900: Comte de la Vaux set world distance record of 1920 km.

July 31, 1901 Suring and Berson set world altitude record of 10,800 m.

1901: Assman in Germany developed rubber sounding balloons.

1903: Cady and McFarland discovered helium in natural gas.

1904: First record of modern rubberized fabric used in Europe.

1906: First contest for the Gordon-Bennett Trophy, a distance race from Paris, won by Lt. Frank P. Lahm of U.S. Santos-Dumont unsuccessful with a balloon carrying powered propellers for vertical control.

1910: Based on previous European development, Goodyear Tire and Rubber Co. started making and improving single and multi-ply rubberized fabric suitable for LTA use. Previous American balloons were exclusively of varnished single-ply fabric.

1912: Melvin Vaniman proposed wire-bound balloon to be stabilized by superpressure. Apparently while experimenting with such pressure in his airship off Atlantic City, the fabric hull burst, causing death to himself and four crew members, a disaster erroneously attributed to fire in newspaper reports.

Dec. 13-17, 1913: Duration record of 87 hr set by H. Kaulen, Germany.

Feb. 8-10, 1914: Distance record of 3053 km set by H. Berliner, Germany.

1918: By Armistice Day 147,000 cu ft of helium was ready to ship to France for inflation of observation balloons.

1920: Post-war international balloon racing resumed. E. Demuyter of Belgium winner of the Gordon-Bennett race from Birmingham, Ala.

1921: U.S. Navy C-7 non-rigid was first LTA unit to be flown with helium.

1923: Radio used for first time in free flight by balloon in American National Race (R. H. Upson and C. G. Andrus).

1924: Demuyter took permanent possession of the G-B cup for Belgium, his fourth victory and third in succession.

Nov. 4, 1927: Capt. H. C. Gray of U.S. Army Air Corps died in altitude attempt; 12,950 m attained while still conscious, but record disallowed because pilot not in control throughout. His clock stopped on ascent and oxygen apparently ran out at about 9000 m on descent. Official inquiry made particular note of unprecedentedly slow ascent and descent, but said nothing about kind of gas used. Gray definitely used hydrogen in previous altitude flights.

1926-27-28: After three successive wins, W. T. Van Orman, E. J. Hill, and W. E. Kepner took permanent possession of the second G-B Cup for the U.S.

May 27, 1931: A. Piccard and P. Kipfer used sealed, pressurized gondola for first time in setting altitude record of 15,781 m (cabin pressure equivalent to 3000 m). Max. cabin temperature 41°C with top of gondola black and bottom white.

1932: A. Piccard and M. Cosyns reached 16,200 m. An attempt to reduce inside temperature with all-white gondola, apparently was too successful--minimum temperature -18°C.

Sept. 30, 1933: Russian crew of Prokief, Birnbaum, and Gudunow reached 18,500 m altitude.

Nov. 20, 1933: U.S. Navy crew of T. Settle and C. Fordney reached 18,665 m, 183,000-cu-m spherical balloon, Piccard gondola.

Jan. 30, 1934: Fedosienko, Wasienko, and Usyskin (all of Russia) reportedly reached 22,000 m (unofficial), but gondola broke loose at about 15,000 m on descent, fatal to all.

July 28, 1934: U.S. Army Air Corps and National Geographic Society balloon Explorer of 90,000 cu m (hydrogen) burst at about 18,000 m, but crew of W. Kepner, O. Anderson, and A. Stevens parachuted safely in gondola.

1933-34-35: F. Hynck and Z. Burzynski took permanent possession of third and last G-B Cup for Poland.

Nov. 11, 1935: Explorer II, 113,000-cu-m rubberized balloon (helium) made official record of 22,066 m in collecting atmospheric, cosmic-ray, and other data (crew, Anderson and Stevens).

1936: First successful plastic balloon flights. J. F. Piccard in collaboration with T. H. Johnson and J. D. Akerman launched a series of four cellophane balloons, 65 cu m each. A summer flight traveled 990 km in 10 hr. In cold weather, however, the material proved impractical due to cracking in the folds. The aerodynamic vertical stabilizer, working well with hydrogen, would be almost worthless with helium.

1937: J. Piccard made a successful flight to 3000 m with cluster of 98 small rubber balloons; proved that motion through air tends to separate the balloons.

1943-44: Several hundred Japanese paper balloons carried bombs across the Pacific Ocean but did little damage. These balloons were spherical of about 540-cu-m volume (hydrogen); ballast release was pressure-controlled. One balloon from a total of more than 9000 reached Kingston, Ontario; perhaps as many as 900, or 10%, reached North America.

1946: Development of large polyethylene balloons undertaken by General Mills. Subsequent study of plastic balloon operation, stresses, and shape sponsored by U.S. Navy at Univ. of Minnesota.

1947: Navy Skyhook balloon carried 32-kg load to 30,500 m.

May 6-7, 1958: A. Mikesell with M. Ross, pilot, made first astronomical observations from balloon at 12,000 m.

1953-54: Successful balloon-launched rockets.

Nov. 28-29, 1959: Water vapor first observed on Venus by C. M. Moore, Ross pilot, at 25,000 m with 406-mm telescope.

1960: Balloon of 28,300 cu m launched from carrier deck.

Aug. 12, 1960: First balloon-type satellite, Echo I, 30.5 m in diameter, made by G. T. Schjeldahl, Inc., launched by NASA.

April 28, 1961: World altitude record for manned aircraft of 34,700 m set by G. Mossolov, USSR, in E-66 jet airplane; first such record made by aircraft other than a balloon.

May 4, 1961: Manned balloon altitude record set by M. D. Ross, USNR, at 34,668 m over Gulf of Mexico, 28,300-cu-m balloon made

by Winzen Research, Inc. Copilot V. A. Prather drowned in an accident after landing.

Sept. 11, 1968: Polyethylene balloon of 813,300 cu m launched at White Sands Missile Range, N.M., reached 48.5 km altitude with a scientific payload of 26.8 kg. This was the largest balloon flown to that date and set an altitude record for balloons.

A SHORT BIBLIOGRAPHY OF BALLOON HISTORY

Encyclopedia Brittanica, 1962-63 Edition, article on Ballooning by Jean and Jeannette Piccard.

Aeronautics II - Lighter-than-Air; M. J. B. Davy; Science Museum, London, Handbook of the Collections, 1934.

Through the Air; John Wise; dedicated to and with contribution by Prof. Joseph Henry, 1873.

Ballooning; G. May, London, 1885.

Navigating the Air; Aero Club of America, 1907.

Conquering the Air; Archibald Williams, 1926.

The First Century of Flight in America; Jeramia Milbank, 1943.

Files of the Wingfoot LTA Society Bulletin; Akron, Ohio.

A number of good articles in MD Medical News Magazine, April 1966.

La Pression Barometrique - Recherches de Physiologie Experimentale, (English translation by Mary and Fred Hitchcock); Paul Bert, 1878.

A Narrative of Two Aerial Voyages; John Jeffries MD, London, 1786.

Aeronautica; Monck Mason, London, 1838.

Aeronautics in the Civil War; J. D. Squires, American Historical Review, Vol. 42, 652.

The Air Arm of the Confederacy; J. K. Cornish III, Richmond Civil War Centennial Committee, Richmond, Virginia, 1963.

The Orion Book of Balloons; Charles Dollfus, (procurable from Wingfoot LTA Society).

Aircraft Year Book (yearly issue); includes various balloon events by year of occurrence.

Capt. H. C. Gray's Last Flight 1928; U.S. War Dept., Air Corps Official Report.

Ten Miles High; Alan Honour.

Exploring the Stratosphere; Gerald Heard, 1936.

Wonderful Balloon Ascents; F. Marion (Trans.), 1870.

Aeronautica Catalog of Aeronauts; Monck Mason, 1838.

Bag of Smoke; Zonzo Anderson, 1942.

A History of Aircraft; Magoun & Hodges, 1931.

Balloon & Airship Gases; Chandler, 1926 (contains good section on safety precautions against ignition).

Adventures in the Air; W. de Fonvielle (Trans.), 1877.

Aerial Navigation; C. C. Turner, 1910.

Trail Blazing in the Skies; F. Chase, 1943 (Goodyear Tire & Rubber Co.).

Ballooning; G. May, 1885.

Ballooning; Gibbs-Smith, 1948.

Scientific Ballooning; J. M. Bacon, Smithsonian Inst. Annual Report 1898 (scientific observations of atmosphere, optics, and acoustics).

Jambo; Anthony Smith, 1963 (African balloon safari).

The Flight of the Small World; Eiloart and Elstob, 1959 (attempted trans-Atlantic balloon flight).

Via Balloon Jupiter; Jerry Marlette, J. of American Aviation Historical Soc., Summer 1966. (John Wise's pioneer U.S. airmail flight)

Skyhooks; Kurt R. Stehling and William Beller, 1962.

REFERENCES

(1) Upson, R. H. and Charles deForest Chandler, 1926: Free and Captive Balloons, Ronald Press, New York.

(2) Upson, R. H., 1939: Stresses in a Partially Inflated Free Balloon. Journal of Aeronautical Sciences, Feb. 1939.

(3) Upson, R. H. and James S. Holdhusen, 1952: Balloon Shapes--or Stress Analysis and Design of Thin, Axially Symmetric Fluid Containers. General Mills Report #1143, Sept. 1952.

(4) Upson, R. H., 1915: Relative Worth of Improvements in Fabrics. Goodyear Tire & Rubber Co., NACA Report #5.

(5) Upson, R. H., 1926: Metalclad Rigid Airship Development. SEA Journal, Feb. 1926, discussion Oct. 1926. Also May 1930.

(6) Ackerman, John D. and J. Piccard, 1937: Upper Air Study by Means of Balloons, J. Aeronautical Sci., June 1937.

(7) Zahm, A. F., 1950: Some Theorems in the Mechanics of High-Speed Balloons, International Aeronautic Congress 1900. Published In Vol. I of Zahm's collected papers, University of Notre Dame Press.

(8) Arnstein, Karl, W.F.G. Swan, 1935-36: Stratosphere Series Nos. 1 & 2, Explorer I & II Balloons. National Geographic Soc. Contributed Technical Papers.

(9) Upson, R. H., 1952: Simplified Mathematical Forms for Engineering Use. Aeronautical Eng. Review, Feb. 1952.

(10) Upson, R. H., 1965: Clues to Balloon Failure. Scientific Ballooning, March 1965.

SECTION II

THEORY OF BALLOON FLIGHT

by

Alvin L. Morris

LIST OF SYMBOLS

Symbol	Description	Dimensions
a	subscript identifying its symbol with air	
A	area; subscripts may be used to make the area specific	L^2
b	angle relative wind makes with the vertical axis of a balloon	deg
b	subscript identifying its symbol with ballast	
B	buoyant force	MLT^{-2}
B	subscript identifying its symbol with the balloon	
C_B	added mass coefficient for a balloon undergoing acceleration through the air	
C_D	aerodynamic drag coefficient	
C_L	aerodynamic lift coefficient	
C_p	specific heat at constant pressure	$L^2T^{-2}\theta^{-1}$
C_v	specific heat at constant volume	$L^2T^{-2}\theta^{-1}$
$\vec{D}$	aerodynamic drag force exerted on a balloon system moving through the air	MLT^{-2}
D	subscript used to identify its symbol with aerodynamic drag	
e	subscript indicating that its symbol is an equilibrium value	
f	free lift ratio	

f'	fractional free lift	
f%	percentage free lift; $f\% = 100\ f'$	
$\vec{F}$	sum of all aerostatic and gravitational forces acting on a balloon	MLT^{-2}
g	acceleration due to gravity	LT^{-2}
g	subscript identifying its symbol with gas	
G	subscript identifying its symbol with gross mass, weight, or lift	
H	geopotential height	L
i	subscript used with V to indicate a fully inflated state	
$\vec{i}$	unit vector which is directed along the positive x coordinate	
$\vec{j}$	unit vector which is directed along the positive y coordinate	
$\vec{k}$	unit vector which is directed along the positive z coordinate (i.e., upward)	
ℓ	characteristic length used in Reynolds number	L
ℓ	subscript identifying its symbol with payload	
$\vec{L}_a$	aerodynamic lift force on a balloon	MLT^{-2}
L'	vertical temperature gradient; subscripts identify it with air or gas	θL^{-1}
m	mass; subscripts are used to make its identity specific	M
M	molecular weight; subscripts identify it with air or gas	$M(M\text{-mol})^{-1}$
o	subscript identifying its symbol with a base datum reference	

p	pressure; subscripts identify it with air or gas	$ML^{-1}T^{-2}$
r	radius	L
r	subscript indicating that its symbol is relative	
R	universal gas constant	$L^2T^{-2}\theta^{-1}$
Re	Reynolds number	
S	surface area	L^2
t	time	T
T	temperature; subscripts identify it with air or gas	θ
v	speed; subscripts are used to make it specific and used with a vector symbol, e.g., $\vec{v}$, it is velocity	LT^{-1}
v	subscript used with m to indicate virtual mass	
V	volume; subscripts identify it with air, gas, or balloon	L^3
x	distance along the x coordinate	L
y	distance along the y coordinate	L
z	height or distance along the z coordinate	L
z	subscript identifying its symbol with height z	

Greek letters

α	specific volume (V/m); subscripts identify it with air or gas	L^3M^{-1}
Θ	supertemperature	θ
μ	ratio of mass of gas in a balloon to gross mass of the balloon system	
μ	dynamic viscosity; subscripts identify it with air or gas	$ML^{-1}T^{-1}$

Π	superpressure	$ML^{-1}T^{-2}$
ρ_a	air density	ML^{-3}
σ	ratio of molecular weight of air to molecular weight of gas	
τ	ratio of absolute temperature of air to absolute temperature of gas	

List of Figures

List of Tables

THEORY OF BALLOON FLIGHT

A. ARCHIMEDES' PRINCIPLE

Archimedes' principle as usually applied to a balloon in the atmosphere states that a buoyant force equal to the difference in weight of the displaced air and the lifting gas will act on the balloon. Thus, if B is the buoyant force, m_a is the mass of displaced air, m_g is the mass of the lifting gas, and g is the acceleration of gravity, then

$$B = g(m_a - m_g) \tag{1}$$

B. DISTRIBUTION OF PRESSURE FORCES

Although Eq. (1) is general if the air displaced by the payload, etc. is negligible compared to the air displaced by the gas, it is instructive to look also at the distribution of pressure forces on a balloon surface. The hydrostatic equation may be written

$$dp = -g \rho \, dz \tag{2}$$

where p is the fluid pressure, ρ is the density of fluid, and z is the vertical height above an arbitrary datum plane.

This may be integrated for the atmosphere to yield

$$p_{a,z} = p_{a,o} - \int_{z_o}^{z} g\,\rho_a\,dz \tag{3}$$

in which $p_{a,z}$ is the air pressure at level z. A similar equation may be written for the lifting gas

$$p_{g,z} = p_{g,o} - \int_{z_o}^{z} g\,\rho_g\,dz \tag{4}$$

Then the pressure difference across the balloon film at level z is

$$(p_{a,z} - p_{g,z}) = (p_{a,o} - p_{g,o}) - \left(\int_{z_o}^{z} g\,\rho_a\,dz - \int_{z_o}^{z} g\,\rho_g\,dz\right) \tag{5}$$

In a balloon which is not fully inflated there is a level at which $p_a = p_g$; let that level be z_o. Then

$$p_{a,z} - p_{g,z} = -\left(\int_{z_o}^{z} g\,\rho_a\,dz - \int_{z_o}^{z} g\,\rho_g\,dz\right) \tag{6}$$

If ρ and g are constant with height, Eq. (6) may be solved to yield

$$p_{a,z} - p_{g,z} = -g\,(\rho_a - \rho_g)\,(z - z_o) \tag{7}$$

Thus, for a lifting fluid having a density less than that of the ambient fluid, the pressure of the lifting fluid is greater than the pressure of the ambient air above $z = z_o$ and less below $z = z_o$.

It is known that neither ρ nor g is constant with height, but the variation of g over the height of a balloon may be ignored. Also, in spite of the known variation with height of ρ in both the lifting gas and the atmosphere, Eq. (7) is usually employed in ballooning work without reservation. It is not difficult, however, to show that the error incurred by assuming ρ constant with height is not large.

The equation of state for an ideal gas is

$$\rho = \frac{pM}{RT} \tag{8}$$

where M is the molecular weight [kg (kg - mol)$^{-1}$], R is the universal gas constant [8314.32 J (^{o}K)$^{-1}$ (kg - mol)$^{-1}$], T is the temperature (^{o}K), p is the pressure [Nm^{-2}], and ρ is the density [kg m^{-3}].

The molecular weight for air at all altitudes of interest in scientific ballooning is 28.9644; the values of M for lifting gases are given in Table 1, Section IV. Both the air and common lift gases behave sufficiently like ideal gases at the temperatures and pressures encountered in ballooning that they may be treated as such. Substituting from Eq. (8) into Eq. (2) yields

$$dp = -g\,\frac{pM}{RT}\,dz \tag{9}$$

and

$$\ln p \Big]_{p_o}^{p_z} = -\frac{gM}{R} \int_{z_o}^{z} \frac{dz}{T} \tag{10}$$

Through most small vertical distances in the earth's atmosphere and probably within most balloons, the variation of temperature with height is approximately linear. If $L'_a = dT_a/dz$ and $L'_g = dT_g/dz$ are constants in the stratum $(z - z_o)$, then $T_{a,z} = T_{a,o} + L'_a (z - z_o)$ and $T_{g,z} = T_{g,o} + L'_g (z - z_o)$. Equation (10) may be written

$$\ln \frac{p_{a,z}}{p_{a,o}} = -\frac{gM_a}{RL'_a} \ln \left[\frac{T_{a,o} + L'_a (z - z_o)}{T_{a,o}} \right] \tag{11}$$

and

$$\ln \frac{p_{g,z}}{p_{g,o}} = -\frac{gM_g}{RL'_g} \ln \left[\frac{T_{g,o} + L'_g (z - z_o)}{T_{g,o}} \right] \tag{12}$$

for air and lift gas respectively. Also, since $p_{a,o} = p_{g,o} = p_o$,

$$p_{a,z} - p_{g,z} = p_o \left\{ \left[1 + \frac{L'_a (z - z_o)}{T_{a,o}} \right]^{-\frac{gM_a}{RL'_a}} - \left[1 + \frac{L'_g (z - z_o)}{T_{g,o}} \right]^{-\frac{gM_g}{RL'_g}} \right\} \tag{13}$$

Equation (13) may be compared with Eq. (7) by expanding the terms in brackets in Eq. (13) in a series, e.g., a binomial series. The first terms of the binomial series yield the expression on the right side of Eq. (7), and it can be shown that the sum of all other terms is small. A more straightforward way, however, is to compute and compare values of $(p_{a,z} - p_{g,z})$ for a given value of $(z - z_o)$ for both Eqs. (7) and (13). For this purpose, assume a very extreme case in which $(z - z_o) = 100$ m, $T_{a,o} = 250^{\circ}K$, $T_{g,o} = 270^{\circ}K$, $L'_a = -0.006\ ^{\circ}Km^{-1}$, $L'_g = +0.006^{\circ}Km^{-1}$, $M_a = 28.9644$, and $M_g = 4.0026$. Then from Eq. (7)

$$p_{a,z} - p_{g,z} = \frac{g (z - z_o)}{R} \left(\frac{M_a}{T_{a,o}} - \frac{M_g}{T_{g,o}} \right) p_o = -0.01191\ p_o$$

From Eq. (13)

$$p_{a,z} - p_{g,z} = -0.01184\ p_o$$

The difference is less than 1% of the value calculated by means of Eq. (13).

Pressure is a force per unit of area which acts on the balloon fabric in a direction normal to the plane of the fabric. The orientation of the fabric then determines the direction of pressure forces on it. Therefore, if an infinitesimal area of balloon film is represented by the vector $\vec{dA}$,

directed normal to the plane of the film from inside to outside, the pressure force on that area is $p\vec{dA}$. A closed, partially-inflated balloon takes approximately the shape of a solid of revolution about a vertical axis. Figure 1 depicts the intersection of the skin of such a balloon with a plane through its vertical axis and shows the distribution of the force vectors resulting from pressure difference across the balloon film. Note that the force vectors are directed outward above level z_o and inward below z_o. Note also that the balloon film is convex above z_o and concave at most levels below z_o. If the film were weightless, the inflection point in the film would occur at z_o, but since all balloon film has weight, the inflection point occurs somewhere below z_o.

The resultant, $\vec{B}$, of all pressure forces exerted on the balloon may be obtained by integrating $-(p_{a,z} - p_{g,z})\vec{dA}$ over the surface, S, of the balloon. Thus

$$-\iint_S (p_{a,z} - p_{g,z})\vec{dA} = \vec{B} \qquad (14)$$

If $(p_{a,z} - p_{g,z})$ is substituted from either Eq. (7) or Eq. (13) and the integration is carried out $\vec{B}$ is found to be a vector directed upward,

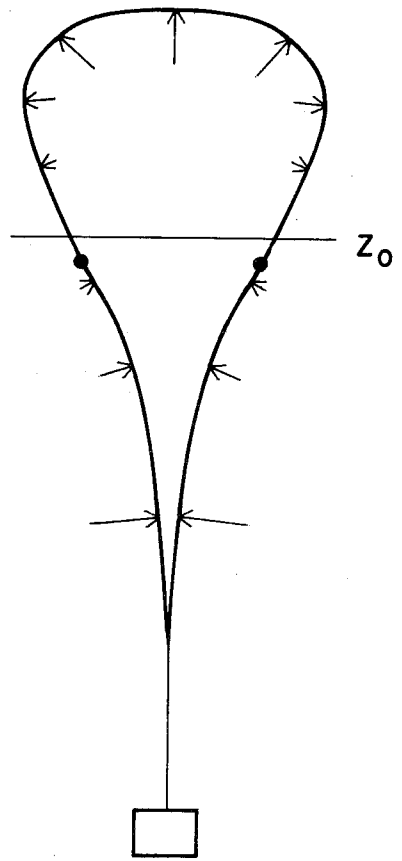

Fig. 1. Pressure force vector distribution. The inflection points are identified by the dots below the z_o line.

and its magnitude is very nearly equal to the lift B given by Eq. (1). This integration is easy to perform for some simple shapes, e.g., a cube, but Eq. (1) is much simpler and is more general.

C. COORDINATE AND UNITS SYSTEMS

The coordinate system used here is a rectangular system in which the z axis lies in the local vertical, and z increases upward. When the position of the x or y axis must be fixed relative to the earth, the orientation shown in Fig. 2 will be used. Figure 2 also shows the unit vectors $\vec{i}$, $\vec{j}$, and $\vec{k}$ at point (x,y,z) in the coordinate system.

In this coordinate system $\vec{i}x$ denotes a vector of magnitude x pointing in the $\vec{i}$ direction (i.e., east); $-\vec{i}x$ is a vector pointing west. Also the three dimensional vector, $\vec{v}_B$, which is used here to denote the velocity of the balloon system may be represented in either of the following forms:

$$\vec{v}_B = \vec{i}v_{B,x} + \vec{j}v_{B,y} + \vec{k}v_{B,z}$$

or

$$\vec{v}_B = \vec{i}\left(\frac{dx}{dt}\right)_B + \vec{j}\left(\frac{dy}{dt}\right)_B + \vec{k}\left(\frac{dz}{dt}\right)_B$$

where $v_{B,x}$, $v_{B,y}$, and $v_{B,z}$ are components of $\vec{v}_B$ along the x, y, and z axes, respectively. Likewise $(dx/dt)_B$, $(dy/dt)_B$, and $(dz/dt)_B$ are compon-

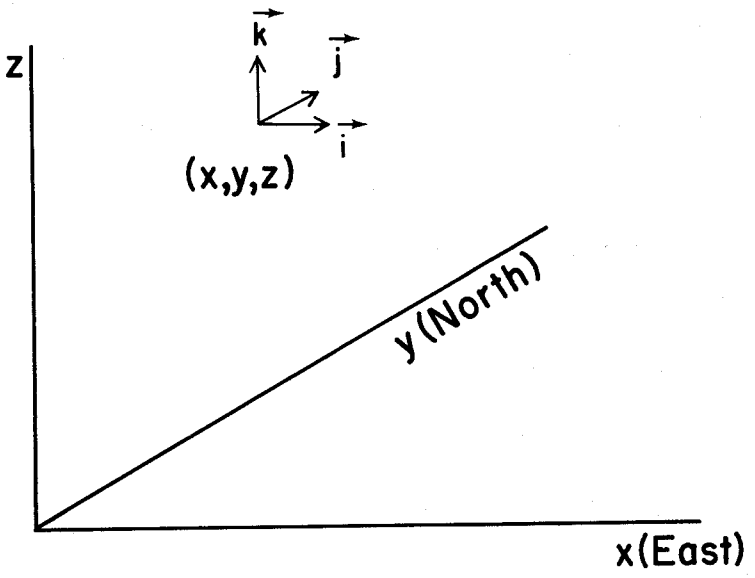

Fig. 2. Coordinate system for balloon vector analysis.

ents of $\vec{v}_B$ shown as time derivatives of distance along the three coordinate axes.

The International System of Units (SI) will be used unless otherwise stated.

D. BALLOON SYSTEM MASS

A scientific balloon system consists of the balloon, a parachute, the scientific package, a control package, and miscellaneous control devices such as valves for valving gas from the balloon and ballast for decreasing the system mass. In the treatment here we shall consider the following masses separately: m_B--the mass of the balloon, including fabric, load tapes, fittings, valves, etc.; m_ℓ--the mass of the payload, including scientific package, control package, parachute rigging, etc. but excluding ballast; m_b--the mass of the ballast; m_g--the mass of lifting gas; m_a--the mass of displaced air; and m_G--the gross mass of the system ($m_G = m_B + m_\ell + m_b$). Note that, as defined here, gross system mass does not include the mass of the lifting gas.

Figure 3 is a picture of a typical scientific balloon system on which the more significant components are marked.

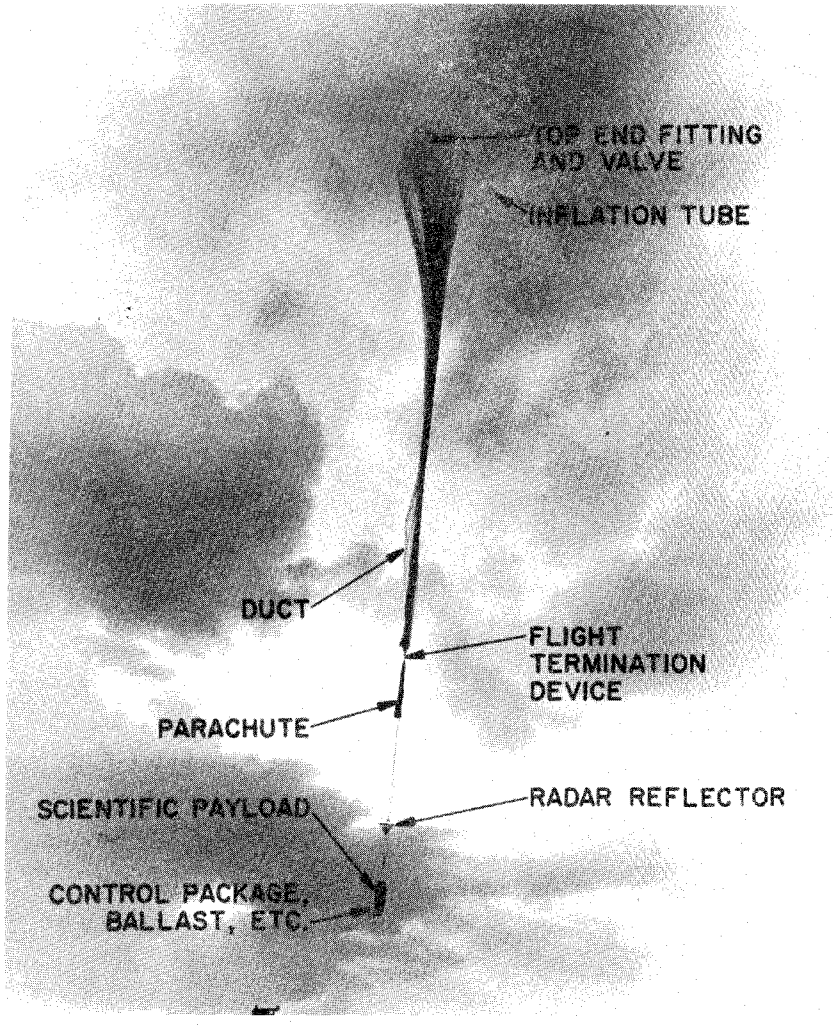

Fig. 3. Balloon system just after launch.

E. A BALLOON SYSTEM IN BUOYANT EQUILIBRIUM

A balloon system in a motionless atmosphere must displace a volume of air having a weight just equal to its own weight in order to be in buoyant equilibrium, according to Archimedes' principle. This may be written

$$g(m_G + m_g) = g(m_B + m_\ell + m_b + m_g) = gm_a \tag{15}$$

Equation (15) is identical with Eq. (1) if

$$B = g(m_B + m_\ell + m_b) = gm_G \tag{16}$$

that is, if the buoyant force is just equal to the total load to be supported. Recalling that $m_g = \rho_g V_g$ and substituting from Eq. (8) gives

$$m_g = \frac{M_g p_g V_g}{RT_g} \tag{17}$$

Also

$$m_a = \frac{M_a p_a V_a}{RT_a} \tag{18}$$

and

$$\frac{m_g}{m_a} = \frac{M_g p_g V_g T_a}{M_a p_a V_a T_g} \tag{19}$$

Substituting into Eq. (15) and rearranging gives

$$m_G + m_g \left(1 - \frac{M_a p_a V_a T_g}{M_g p_g V_g T_a}\right) = 0 \tag{20}$$

or

$$m_G + m_a \left(\frac{M_g p_g V_g T_a}{M_a p_a V_a T_g} - 1\right) = 0 \tag{21}$$

In these equations, m_g and m_a are the masses of the entire volumes of gas in the balloon and of the air displaced, respectively. Therefore, p and T as used in Eqs. (17) through (21) must be values which are representative of the entire mass. This interpretation contrasts with the interpretation of p and T used in Section II.B, where their variability within the balloon was being discussed. Nonetheless, the interpretation adopted here is not particularly restrictive, and it is consistent with the practice generally followed in ballooning.

It should be noted also that the acceleration due to gravity has been factored out of Eqs. (20) and (21) for convenience, but if the weight or lift forces are desired, the terms of Eqs. (20) and (21) must be multiplied by g. Except for the small volume of air displaced by the balloon film and the suspended load, $V_a = V_g$. Also in ballooning superpressure and supertemperature (the latter often erroneously called superheat) are frequently used. Superpressure Π is given by

$$\Pi = p_g - p_a \tag{22}$$

and supertemperature Θ by

$$\Theta = T_g - T_a \tag{23}$$

Equation (21) may now be written

$$m_G + m_a \left[\frac{(p_a + \Pi)\, T_a\, M_g}{p_a\, (T_a + \Theta)\, M_a} - 1 \right] = 0 \tag{24}$$

This is a mathematical statement of the condition for buoyant equilibrium expressed in terms of the masses involved and the measurable characteristics of the lift gas and the ambient gas. Since all masses in m_G are positive and some are not zero, the term involving m_a must be negative to satisfy the equation. This can be accomplished by a judicious selection of values of Π, Θ, and M_g/M_a. All the combinations shown in Table 1 are valid in principle. Actually only combinations 5 through 8 are attainable in a non-rigid balloon, but Π is so small in one very important class of balloons that it can be ignored, thereby simplifying many computations. Therefore, combinations 1 through 4 are useful conceptually. In ballooning, when a gas has a molecular weight less than that of air, it is said to be lighter than air. It is feasible to use a gas that is heavier than air in a balloon and

Table 1

Physical Characteristics of a Gas in a Balloon

Combination Number	Π	Θ	M_g/M_a	Comments
1	0	>0	1	Balloon filled with warmed ambient gas
2	0	0	<1	Gas lighter than ambient
3	0	>0	<1	Gas lighter and warmer than ambient
4	0	<0	<1	Gas lighter and cooler than ambient
5	>0	0	<1	Gas lighter and gas pressure greater than ambient
6	>0	>0	<1	Gas lighter and warmer and gas pressure greater than ambient
7	>0	<0	<1	Gas lighter and cooler and gas pressure greater than ambient
8	>0	>0	1	Balloon filled with warmed ambient gas under pressure greater than ambient

make it buoyant by making Θ large enough, but except to lift the gas itself there would appear to be no practical reason for doing so.

Superpressure Π cannot be negative unless the walls of the balloon are rigid enough to prevent it from collapsing. Father Francesco de Lana suggested as early as 1670 that an evacuated sphere might fly, but no one has yet developed a sufficiently strong, light material from which to make such balloons which will fly in the atmosphere. Analagous vehicles have been used in the ocean, of course. The hot-air balloonist makes use of supertemperature, and because he can change it quickly by heating the gas inside the balloon or by venting hot gas and replacing it with cooler gas, he can change the buoyant lift rapidly. Scientific ballooning usually takes advantage of the low molecular weight of helium or hydrogen to make the ratio M_g/M_a small. Other lifting gases are less satisfactory because of their higher molecular weights.

F. VIRTUAL MASS

If the numerical value of the second term of Eq. (24) is not equal to the first term, the balloon system is said to have "free lift," and the resultant force on the system in the earth's gravitational field is no longer

zero. The system will be accelerated if it is not tethered.

The mass which will be accelerated will include the gross mass of the balloon system and the mass of the lift gas, but it will also include the mass of some of the environmental fluid. This is not surprising, but the precise mass of the environmental fluid involved and the resultant acceleration are difficult to determine. It is shown in fluid dynamics, e.g., Streeter (1), that for purposes of determining the acceleration of an immersed body due to an impressed force, the acceleration of the environment may sometimes be equated with that of the immersed body if the proper environmental mass is assumed to be accelerated. The immersed body mass and the "added" environmental mass are then combined into the "virtual" mass, i.e., the total mass which is assumed to be accelerated with the immersed body. For an immersed sphere, the added mass is equal to one-half the mass of the displaced fluid. For a circular cylinder being accelerated normal to its axis, the added mass is equal to the displaced mass. There are potential difficulties such as flow separation aft of the body, or for rapid accelerations, compressibility. Although no one has determined the appropriate added mass for a nonspherical balloon system, it is common practice to assume that it is the same

as the added mass of a sphere having the same volume as the enclosed gas.

Let m_v equal the virtual mass which must be accelerated. Then, if C_B is a coefficient which when multiplied by m_a gives the added mass,

$$m_B + m_\ell + m_b + m_g + C_B m_a = m_v \tag{25}$$

From Eqs. (19), (22), and (23) and recognizing that $V_a = V_g$, m_a may be expressed in terms of m_g as follows:

$$m_a = m_g \frac{M_a p_a (T_a + \Theta)}{M_g (p_a + \Pi) T_a}$$

Then Eq. (25) may be rewritten

$$m_v = m_B + m_\ell + m_b + m_g \left(1 + C_B \frac{M_a p_a (T_a + \Theta)}{M_g (p_a + \Pi) T_a}\right) \tag{26}$$

G. FORCES ACTING ON A BALLOON IN MOTION

A rigorous analysis of all the forces to which a balloon system is subjected during inflation, launch, and flight is beyond the scope of this book; however, those of greatest importance during flight are the gravitational forces, the buoyant forces, and the aerodynamic lift and drag forces which occur only when the balloon has motion relative to the ambient air.

Buoyant or aerostatic forces were discussed in sub-Sections A, B, and E. Equation (20) which was derived for a balloon in a state of buoyant

equilibrium can be generalized to include free lift by equating the gravitational and aerostatic forces to $\vec{F}$. Thus from Eqs. (20), (22), and (23),

$$\vec{F} = -g\vec{k}\left\{m_G + m_g\left[1 - \frac{M_a p_a (T_a + \Theta)}{M_g (p_a + \Pi) T_a}\right]\right\} \tag{27}$$

The negative sign of the term on the right is necessary to preserve the convention that positive free lift is an upward force and that the weight of the system is directed downward.

The drag D exerted by a fluid upon a submersed body which is in motion through the fluid is given by

$$\vec{D} = -\tfrac{1}{2} C_D \rho_a A_D |\vec{v}_B - \vec{v}_a| (\vec{v}_B - \vec{v}_a) \tag{28}$$

where C_D is a dimensionless drag coefficient, A_D is the effective cross sectional area of the body normal to its direction of motion relative to the fluid, $\vec{v}_B$ is the velocity of the balloon, and $\vec{v}_a$ is the velocity of the fluid (the ambient air). The drag coefficient is a function of both the shape of the balloon system and the Reynolds number referred to a characteristic dimension of the system. For a spherical balloon that dimension is the diameter of the balloon; also A_D is the area of a great circle. The Reynolds number Re is given for an object in air by

$$Re = \frac{\rho_a \ell |\vec{v}_B - \vec{v}_a|}{\mu_a} \qquad (29)$$

where ℓ is the characteristic dimension and μ_a is the dynamic viscosity of the air.

For a sphere the variation of C_D with Re is not great for $Re > 5 \times 10^5$, and for most scientific balloon systems having measurable motion relative to the atmosphere, the Reynolds number exceeds 5×10^5. It is pertinent to note, however, that for lower Reynolds numbers, the variation of C_D with Re cannot be ignored. Hoerner (2) shows graphically that for Reynolds numbers between 10^4 and 4×10^5, C_D is nearly constant for a sphere and has a value of approximately 0.47. A sharp transition from laminar to turbulent flow occurs between $Re = 4 \times 10^5$ and $Re = 5 \times 10^5$, and at $Re \geq 5 \times 10^5$, C_D has a value of approximately 0.1. In a general way the drag coefficient of a natural shape balloon (see Section V) varies with Re in much the same way as a sphere at $Re \geq 4 \times 10^5$, Sherburne (3). It is sensitive to the shape, however, as shown by Fig. 4 from Peters, et al. (4). This figure was plotted from wind tunnel data obtained with a wooden, natural shape model. Tilting it to change the angle of attack changed the shape exposed to the air stream. The tests were run at $Re = 10^6$.

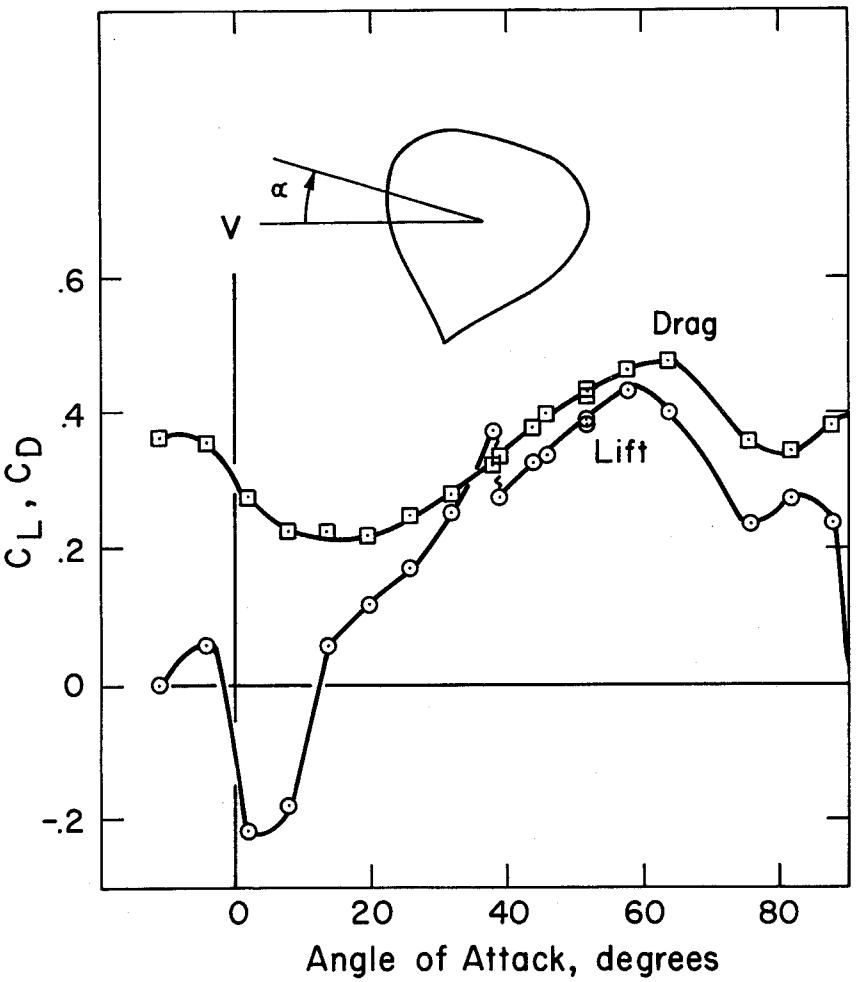

Fig. 4. Drag and lift coefficients for a modified natural shape balloon as a function of angle of attack. From Peters, et al. (4).

At best, estimates of C_D for a large balloon in flight will be coarse. The following equations may be used to make such estimates:

$$\left.\begin{aligned} C_D &= 0.47 + \frac{24}{Re + 0.01} && \text{for } Re \leq 4.5 \times 10^5 \\ C_D &= 0.3 && \text{for } Re > 4.5 \times 10^5 \end{aligned}\right\} \tag{30}$$

The equations do not take into account change of shape, and they imply that the transition from laminar to turbulent flow is discontinuous at Re = 4.5×10^5.

The lift on a tethered balloon, $\vec{L}_a$, due to horizontal motion of the atmosphere is

$$\vec{L}_a = \tfrac{1}{2}\vec{k}\, C_L\, \rho_a\, A_L\, |\vec{v}_B - \vec{v}_a|^2 \tag{31}$$

where C_L is a dimensionless lift coefficient and A_L is the effective cross sectional area of the balloon normal to the direction of lift. The lift coefficient is even more sensitive to the shape of the balloon than C_D, and it may be greater than, equal to, or less than zero. The lift $\vec{L}_a$ is usually small but it may be significant for a tethered balloon in a strong wind or for a partially inflated balloon in a stratum of the atmosphere in which the vertical wind shear is great.

The effect of the surface of the earth near a tethered balloon may also be important to the aerodynamic behavior of the balloon. It will be if it contributes to turbulence on a scale near or larger than the dimensions of the balloon. No attempt is made to account for the influence of the earth's surface here.

H. EQUATIONS OF MOTION

An equation of motion for the balloon system with free lift, embedded in a moving atmosphere, may now be written. It is

$$\vec{F} + \vec{D} + \vec{L}_a = m_v \frac{d\vec{v}_B}{dt} \tag{32}$$

or from Eqs. (26), (27), (28), and (31),

$$-\vec{k}g\left\{m_G + m_g\left[1 - \frac{M_a p_a (T_a + \Theta)}{M_g (p_a + \Pi) T_a}\right]\right\} - \tfrac{1}{2}\rho_a\left\{C_D A_D\, |\vec{v}_B - \vec{v}_a|\,(\vec{v}_B - \vec{v}_a)\right.$$
$$\left. -\vec{k}\, C_L A_L\, |\vec{v}_B - \vec{v}_a|^2\right\} = \left\{m_G + m_g\left[1 + C_B \frac{M_a p_a (T_a + \Theta)}{M_g (p_a + \Pi) T_a}\right]\right\}\frac{d\vec{v}_B}{dt} \tag{33}$$

Equation (33) is a fairly general equation of motion which makes use of the concepts of superpressure and supertemperature in the classical manner. Because Θ, T_a, C_D, C_L, Π, p_a, A_D, and A_L are all functions of position and time, Eq. (33) cannot be readily solved. It can be solved numeri-

cally and such a solution is discussed in Section III. Some knowledge of the behavior of a balloon in flight can be gained by a qualitative evaluation of Eq. (33) however; furthermore, such an evaluation helps one to understand a numerical solution.

It is convenient to classify scientific balloons into three primary categories before undertaking further discussion of balloon motion. These are 1) zero-pressure and 2) superpressure, both made of inextensible material, and 3) extensible balloons. All three have a fully inflated volume, V_i. For the zero-pressure balloon this is the volume at which the balloon is completely inflated and the lifting gas starts to escape from the vent or duct which is open to the atmosphere at the balloon base.

The expression "zero-pressure" derives from the fact that the pressure difference between the atmosphere and the lift gas is essentially zero at some level in the gas throughout flight. The so-called zero-pressure level is high on the balloon, but is near the apparent bottom of the bubble of gas, when the balloon is only slightly inflated, i.e., when $V_g \ll V_i$. It moves down the balloon away from the top as the gas expands and reaches the base just as $V_g = V_i$. If the gas continues to expand and is vented to

the atmosphere, a slight superpressure must develop in the balloon to expel the gas. In fact, too small a vent could result in sufficient superpressure in a rising balloon to cause the balloon to burst.

A superpressure balloon is a sealed balloon which is designed to contain the lifting gas at pressures greater than that of the ambient atmosphere. Ideally, when fully inflated, it becomes a fixed volume containing a fixed mass of gas. Thus, when an ascending superpressure balloon becomes fully inflated, it will continue to rise until it reaches a level at which the volume of displaced air has a weight equal to that of the balloon system, including any suspended mass. It will then float at that atmospheric density level. The superpressure balloon is such an important balloon vehicle that Section VIII is devoted to it. Below the level at which $V_g = V_i$, a superpressure balloon is no different from a zero-pressure balloon except that it is likely to be made of different material; thus it may react differently to its radiation environment.

Extensible balloons are usually made of natural or synthetic rubber. These balloons are frequently, but not always, inflated sufficiently to subject the entire volume of lift gas to a slight superpressure, even at launch.

As the balloon ascends and the lift gas expands, the forces due to the differential pressure across the film just equal the elastic restoring forces of the film. Expansion continues until the film stretches to its limit and the balloon bursts. For present purposes, the fully inflated volume is the volume at which burst occurs.

The hot-air balloon is a special type of inextensible zero-pressure balloon. Its volume is kept essentially constant, and it is vented at the base so that $\Pi = 0$ there. Lift is achieved by making $\Theta > 0$. The hot-air balloon is discussed more completely in Section IX.

Since most balloons are essentially zero-pressure balloons until they become fully inflated, it is often assumed that Π is negligible. Equation (33) can then be rewritten as follows:

$$-\vec{k}g\left[m_G + m_G\left(1 - \frac{M_a}{M_g}\right)\right] + \vec{k}gm_g\frac{M_a}{M_g}\frac{\Theta}{T_a} - \tfrac{1}{2}\rho_a\left\{C_D A_D\left|\vec{v}_B - \vec{v}_a\right|(\vec{v}_B - \vec{v}_a)\right.$$
$$\left. -\vec{k}C_L A_L\left|\vec{v}_B - \vec{v}_a\right|^2\right\} = \left\{m_G + m_g\left[1 + C_B\frac{M_a(T_a + \Theta)}{M_g T_a}\right]\right\}\frac{d}{dt}\left[\vec{i}\left(\frac{dx}{dt}\right)_B + \vec{j}\left(\frac{dy}{dt}\right)_B + \vec{k}\left(\frac{dz}{dt}\right)_B\right] \tag{34}$$

The term $-\vec{k}g\left[m_G + m_g\left(1 - \frac{M_a}{M_g}\right)\right]$ alone is often called the free lift term. It is the true free lift only if $\Pi = \Theta = 0$; therefore, it is called

nominal free lift in this section. It is customary in scientific ballooning to inflate a balloon with a sufficient mass m_g of gas having a molecular weight M_g to get the desired nominal free lift. Since the molecular weight of air does not change significantly with altitude below 70 km (230,000 ft), the nominal free lift is invariant with altitude up to the altitude at which $V_g = V_i$ unless gas is lost or the mass of the system is changed. During ascent the gas in the balloon expands. When $V_g > V_i$, gas is vented to the atmosphere, thereby decreasing m_g and reducing the nominal free lift. In zero-pressure ballooning the nominal free lift is measured in terms of a percentage fraction f% of gross system weight. Thus

$$-g\left[m_G + m_g\left(1 - \frac{M_a}{M_g}\right)\right] = \frac{f\%}{100}gm_G \tag{35}$$

The mass of the lifting gas is then

$$m_g = \frac{m_G(1 + f')}{\left(\frac{M_a}{M_g} - 1\right)} \tag{36}$$

where $f' = f\%/100$. The symbol f% is called the percentage free lift. The symbol f' is used here to designate the fractional free lift; it should be

carefully differentiated from the free lift ratio f used in superpressure ballooning practice. (See Section VIII.)

The term $\vec{k}gm_g M_a\Theta/M_g T_a$ in Eq. (34) is the thermal lift term to hot-air balloonists; it is most frequently known as the thermodynamic drag term to those who use helium to produce lift. If $\Theta > 0$, the term produces a force directed upward. If $\Theta < 0$, it produces a force directed downward. If a balloon is ascending and $\Theta < 0$, or if it is descending and $\Theta > 0$, the force opposes the motion.

A balloon system prior to launch is tethered to the earth so that its velocity is zero. The velocity of the atmosphere is essentially two dimensional, the vertical velocity being near zero. Therefore, $(\vec{v}_B - \vec{v}_a)$ in Eq. (34) is a horizontal vector prior to launch. The drag force of the wind on the balloon will tilt it about its tether point prior to release, and, upon release, will accelerate it in the direction of the wind. As its horizontal velocity approaches the horizontal velocity of the wind, the horizontal component of the relative wind vector $(\vec{v}_B - \vec{v}_a)$ approaches zero and the horizontal component of the drag also approaches zero. The remaining drag then is a vertical force which opposes the vertical motion of the balloon.

If the balloon rises or descends through a stratum in the atmosphere in which the vertical wind shear is significant, the horizontal component of $(\vec{v}_B - \vec{v}_a)$ will not be zero, and the balloon will be accelerated horizontally. Likewise, if $\vec{v}_a$ changes in a stratum in which the balloon has been floating and in which $(\vec{v}_B - \vec{v}_a)$ was zero prior to the change of $\vec{v}_a$, the balloon will be accelerated.

Figure 4 suggests that a balloon may develop lift when the wind blows upon it, but the lift coefficient is quite sensitive to the shape of the airfoil. Therefore, the data of Fig. 4 cannot be applied directly to a real balloon which is distorted by the wind. In launch system design work, the designer usually assumes a small positive value for C_L to assure that his launch equipment is designed with adequate safety margins. The operations crew may assume a small negative value to assure that it has enough free lift in the balloon to guarantee lift-off. No use has been made of the concept of trying to predict the motion of a balloon system in flight.

At this point it is useful to introduce some additional symbols. Let $M_a/M_g = \sigma$, $m_g/m_G = \mu$, and $T_a/T_g = \tau$. Then Eq. (36) may be written

$$\frac{m_g}{m_G} = \frac{1 + f'}{\sigma - 1} = \mu \tag{37}$$

and

$$\frac{m_a}{m_G} = \mu\sigma\tau^{-1} \tag{37a}$$

These permit Eq. (33) to be written in the following form if $\Pi = 0$:

$$\left\{ -\vec{k}gm_G \left[1 + \mu \ (1 - \sigma\tau^{-1}) \right] \right\}_1 - \left\{ \tfrac{1}{2} \rho_a C_D A_D \left| \vec{v}_B - \vec{v}_a \right| (\vec{v}_B - \vec{v}_a) \right\}_2$$

$$+ \left\{ \tfrac{1}{2} \rho_a \vec{k} \ C_L A_L \left| \vec{v}_B - \vec{v}_a \right|^2 \right\}_3 = \left\{ m_G \left[1 + \mu(1 + C_B\sigma\tau^{-1}) \right] \frac{d\vec{v}_B}{dt} \right\}_4 \tag{38}$$

The number subscripts outside the braces are used to identify the terms.

For a balloon system in flight μ will change only if gas is gained or lost or the gross mass m_G of the system is changed. These changes are usually made deliberately and the amount of change is known. The values of σ and C_B may be considered constant, and for a balloon in steady state flight g, C_D, A_D, C_L, and A_L are all essentially constant. Air density ρ_a is an atmospheric variable which may be expressed in terms of p_a and T_a or, approximately, as a function of height.

The variable τ is important, but is difficult to measure during flight and equally difficult to estimate realistically. Experience in ballooning shows that it may take values ranging from 0.8 to 1.2. Balloonists usually consider it to have a value of 1.0 when they make calculations. They then make whatever qualitative corrections they feel are appropriate to account for deviations from 1.0. The relationship between τ and Θ is given by the equation, $\tau = T_a/(T_a + \Theta)$, so that for $\Theta > 0$, $\tau < 1$, and for $\Theta < 0$, $\tau > 1$.

Equation (38) is equivalent to Eq. (34). Neither is as general as Eq. (33) because in both the superpressure is assumed to be zero.

I. ZERO-PRESSURE BALLOON FLIGHT

1. Inflation and Release

A balloon is usually inflated rapidly to minimize the duration of exposure of the partially inflated shape to the elements prior to release. It is inflated sufficiently to provide the desired nominal free lift. During inflation the lift gas expands from cylinders, where it is under high pressure, into the balloon at essentially atmospheric pressure. It cools below atmospheric temperature in the process. Therefore, unless the balloon bubble is left standing in its atmospheric environment for some

time, $\tau > 1$, and the actual free lift is less than the nominal free lift.

At the instant a restrained balloon is released, it accelerates away from the release point. This is often of great concern because of the sensitivity of the payload to acceleration. Therefore, accelerations immediately after release will be reviewed in some detail.

If the aerodynamic lift on a balloon is negligible as suggested earlier, the only vertical forces on it at the time of release when $\vec{k}v_B = 0$ are the buoyant and gravitational forces. The acceleration which a balloon system will experience if it is being acted upon only by buoyant and gravitational forces is, from Eq. (38)

$$\left(\frac{dv_B}{dt}\right)_1 = -\vec{k}g\left[1 + \mu\ (1 - \sigma\tau^{-1})\right]_1\left[1 + \mu\ (1 + C_B\sigma\tau^{-1})\right]_4^{-1} \qquad (39)$$

where the number subscripts identify the terms which are used from Eq. (38). The subscript used with $(d\vec{v}_B/dt)$, is intended to show that the acceleration is due only to the forces associated with the first term of Eq. (38).

If $\mu = 0$, indicating that there is no lift gas in the balloon, the system will have a free lift acceleration of $-\vec{k}g$. It is then a freely falling body. On the other hand, if μ is positive and μ and τ^{-1} are both very

large, the system acceleration will approach $+\vec{k}g/C_B$ as a limit. For a spherical balloon system this is 2 g upward, and that is the maximum acceleration a spherical balloon can have.

It is instructive to examine Eq. (39) for the special case when $\tau = 1$ and $f' > 0$ and also for the case when $f' = 0$ and $\tau \neq 1$. For $\tau = 1$ and $f' > 0$, one may write Eq. (39) in the following form:

$$\left(\frac{d\vec{v}_B}{dt}\right) = \vec{k}gf'\left[1 + \mu\ (1 + C_B\sigma)\right]^{-1} \qquad (40)$$

Since μ, C_B, and σ are all greater than zero for all practical balloon systems, $\left[1 + \mu\ (1 + C_B\sigma)\right]^{-1} < 1.0$; therefore, the acceleration of a practical balloon system cannot exceed gf'. In fact, $\left[1 + \mu\ (1 + C_B\sigma)\right]^{-1}$ is maximum when $f' = 0$; it then has a value of approximately 0.57 for a helium inflated balloon in air and 0.62 for a hydrogen inflated balloon. It decreases with increasing value of f', approaching $(\sigma - 1)/f'(1 + C_B\sigma)$ for very large values of f'.

An unenclosed gas bubble rising in the atmosphere may be compared to a balloon for which f' is very large. Therefore, a spherical gas bubble for which $\tau = 1$ would be expected to have an acceleration of $(\sigma - 1)g/(1 + C_B\sigma)$ which is approximately 1.35 g for helium in the atmosphere.

When $f' = 0$ and τ is not specified, Eq. (39) becomes

$$\left(\frac{d\vec{v}}{dt}\right)_1 = \vec{k}g\left(\frac{1-\tau}{C_B+\tau}\right) \qquad (41)$$

For very small values of τ, i.e., for very hot lift gas in a cold atmosphere, this approaches $\vec{k}g/C_B$ the same limit as when μ was very large and τ very small. Note that Eq. (41) does not contain a term which is a function of the type of gas used in the balloon, but the condition that $f' = 0$ implies that the balloon system must be in a state of neutral equilibrium when $\tau = 1$. An unenclosed bubble of air would meet this criterion.

Incidentally, the acceleration of a massless body which nonetheless displaces a mass of air is also $\vec{k}g/C_B$. Therefore, a balloon could approach this limiting acceleration only if the lift gas were so hot that its density were negligible. The lift gas would then occupy an essentially infinite volume. No balloon system can be expected to approach the limit.

Figures 5 and 6 are graphs of Eq. (39) for a realistic range of values of f' and τ. It must be emphasized that all accelerations discussed thus far are those which a balloon system would experience if no aerodynamic drag or lift forces were acting on it. Further, the accelerations are those of the balloon system as a whole. The payload, because of the peculiarities

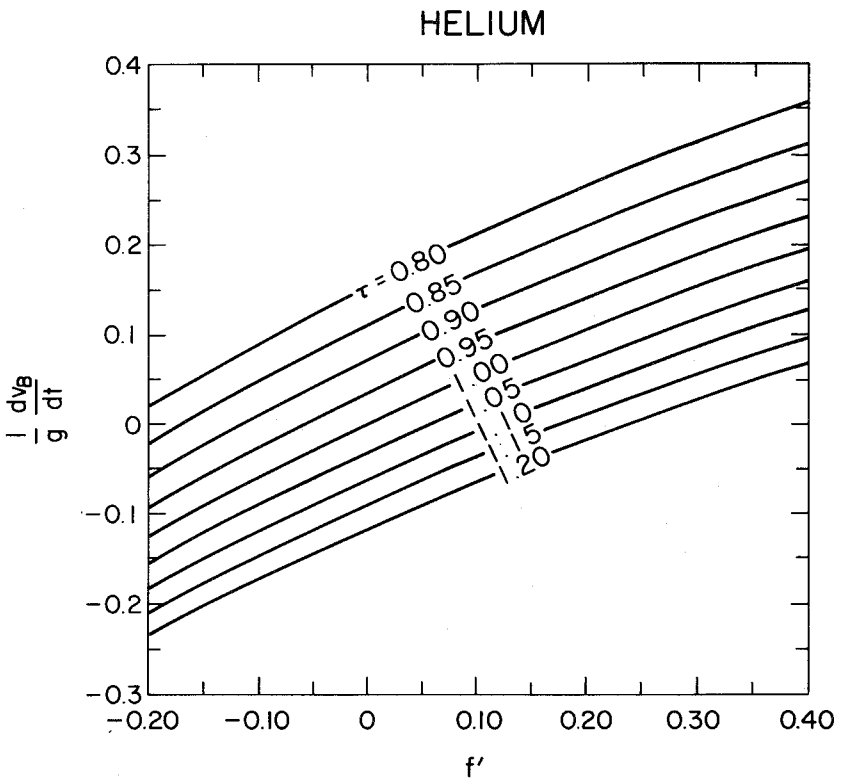

Fig. 5. Vertical acceleration for a helium filled balloon.

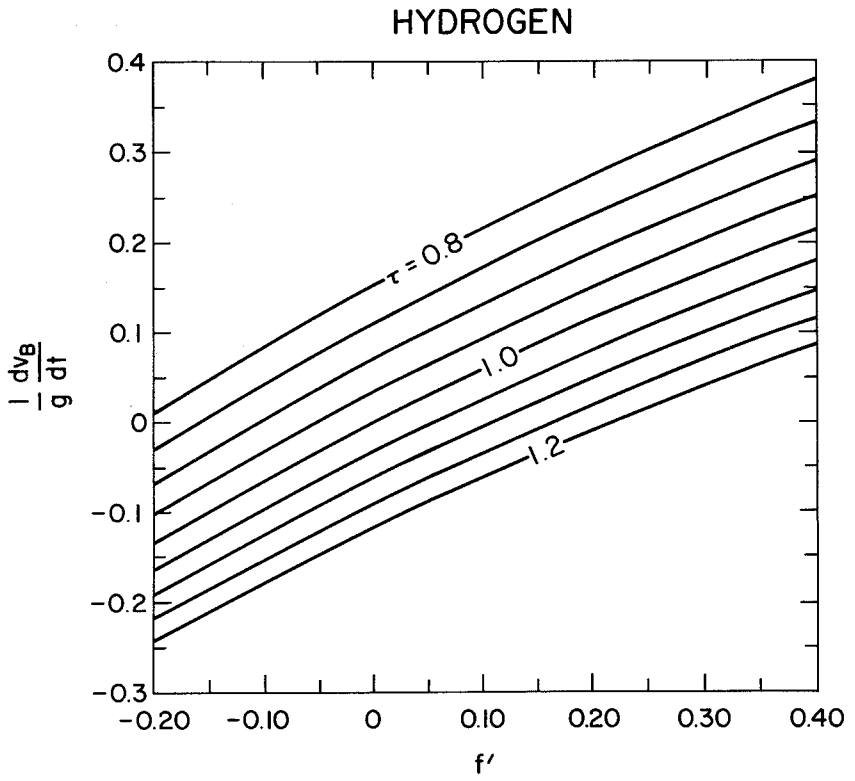

Fig. 6. Vertical acceleration for a hydrogen filled balloon.

of the suspension system, may experience transient or oscillatory accelerations which are quite different from the accelerations of the overall balloon system.

Aerodynamic drag contributes nothing to the vertical acceleration of the system at the moment of launch, because at that time $\vec{kv}_B = 0$ and $\vec{v}_a$ has no vertical component. It does, however, contribute to the horizontal acceleration of the system if $\vec{v}_B \neq \vec{v}_a$, and its contribution is given by

$$\left[\frac{dv_B}{dt}\right]_2 = \left[\tfrac{1}{2}\rho_a C_D A_D \left|\vec{v}_B - \vec{v}_a\right| (\vec{v}_B - \vec{v}_a)\right]_2 \div m_G\left[1 + \mu(1 + C_B\sigma\tau^{-1})\right]_4 \tag{42}$$

Now using the approximation $A_D = 4.66\ r^2$ (see Section XII.B, Fig. B-1 for $b = 90^\circ$ and $\theta = 20^\circ$) and $V_g = V_a = m_a/\rho_a = m_G\mu\sigma/\rho_a\tau$, and letting the coordinate system be oriented so that the x-axis is parallel to the wind permits us to write this in the form

$$\frac{dv_{B,x}}{dt} = \frac{0.56\ C_D(v_{B,x} - v_{a,x})^2}{[1 + \mu\ (1 + C_B\sigma\tau^{-1})]}\ \frac{\mu\sigma}{r\tau} \tag{43}$$

For $C_D = 0.4$, $f' = 0.1$, $C_B = 0.5$, $\tau = 1.0$, and $\sigma = 7.24$, this becomes $dv_{B,x}/dt \approx 0.16\ (v_{B,x} - v_{a,x})^2/r$. During a short period following launch,

r may be considered constant, and if $v_{a,x}$ is constant along the balloon's trajectory, integration between the limits $v_{B,x} = 0$ at time $= t_o$ and $v_{B,x} = v_{a,x} - v_r$ at time t_1 yields $(t_1 - t_o) \approx 6.2\ r\ (v_{a,x} - v_r)/v_{a,x}\ v_r$. Thus, the time required for the balloon to reach a speed which differs by an amount v_r from the wind speed is, subject to the simplifications assumed in this analysis, a linear function of the radius of the gas bubble. Also, according to this analysis, a balloon will accelerate rapidly to a speed near that of the wind, but it will require a very long time to reach wind speed. For example, a balloon system having a gas bubble radius of 5 m launched from rest in a 10 m sec^{-1} wind will reach a speed of 9 m sec^{-1} in about 28 sec, 9.5 m sec^{-1} in 59 sec, and 9.9 m sec^{-1} in 310 sec. Since v_r is the relative, horizontal wind blowing against the balloon, another way to view this analysis is that the relative, horizontal wind blowing on the balloon decreases rapidly when the balloon is freed to fly with the wind, but requires a long time to reach zero.

The maximum horizontal acceleration occurs when $\vec{v}_{B,x} - \vec{v}_{a,x}$ is greatest, i.e., at the moment of launch. For the rather extreme example given above in which at launch $v_B = 0$, $v_a = 10$ m sec^{-1} and r = 5 m, the horizontal acceleration immediately after release is 3.2 m sec^{-2} or $\sim$ 0.33 g. A 5 m sec^{-1} wind would be a more realistic wind in which to launch a balloon. In such a wind, a balloon with a radius of 5 m would accelerate horizontally at 0.8 m sec^{-2} or 0.08 g. From Eq. (40) or Fig.5, it can be determined that if $\tau = 1$ and $f' = 0.1$, a helium filled balloon system would accelerate vertically at 0.055 g. The initial vector acceleration would, therefore, have a magnitude $g\sqrt{0.08^2 + 0.055^2} \approx 0.1$ g and be directed at an angle of $\tan^{-1}\ (0.055/0.08) \approx 35^o$ above the horizon.

The drag force is exerted almost wholly on the balloon bubble and the balloon fabric immediately below it. The horizontal acceleration of the payload must then be due to a horizontal component of force exerted on it by the balloon train. To exert such a force the train must be tilted away from the vertical, and the amount of tilt is a function of the acceleration. The angle the train makes with the vertical is $\tan^{-1}\ (dv_{B,x}/dt)/g$. For the example used above with launch in a 10 m sec^{-1} wind, the maximum angle is $\sim \tan^{-1}\ 0.33$ or 18^o. Because a 10 m sec^{-1} wind is too strong for normal launches, most balloon systems will undergo less than 18^o tilt at launch; the tilt is nevertheless often quite discernible.

A flight as described thus far can be summarized by saying that sufficient gas is placed in the balloon to provide an upward acceleration upon release. At release, the lift due to the gas accelerates the balloon system upward. The temperature of the gas in the balloon at release is generally lower than that of the ambient atmosphere, and when it is, the balloon experiences a smaller vertical acceleration than if the gas and air temperatures were equal. The balloon is accelerated in the direction of the wind at release and rapidly reaches very nearly the horizontal velocity of the wind. Thus, a few minutes after release, the balloon is moving upward at a velocity such that the sum of the weight, the aerodynamic drag force, and the lift force is near zero, and it is moving horizontally with essentially the speed of the wind.

2. Free Flight

Equation (34) was developed in such a way as to make use of atmospheric properties which are normally measured directly, i.e., temperature and pressure. The distribution of these and other properties in the atmosphere is discussed in Section XI.

a. Ascent in a windless atmosphere. When a balloon is released, the free lift causes it to accelerate upward. Experience shows, however, that after a short time the upward acceleration ends and the balloon rises, at least for a time, at a nearly uniform rate. Then, except for unusual circumstances, the vector $(\vec{v}_B - \vec{v}_a) = \vec{k}v_{B,z}$ and $d\vec{v}_B/dt = 0$, and the vertical component of Eq. (38) may be written

$$|v_{B,z}|\, v_{B,z} = \frac{-2\, gm_G[1 + \mu\ (1 - \sigma\tau^{-1})]}{C_D\, \rho_a\, A_D} \tag{44}$$

Note that the aerodynamic lift term is not included because $C_L = 0$ when the relative wind on the balloon is a vertical wind.

Both ρ_a and A_D will change appreciably as a balloon ascends, and by comparison all other terms may be considered constant. For vertical motion, A_D is usually expressed as the area of a great circle of a sphere whose volume is that of the displaced air, and $\rho_a = m_a/V_a = m_G\mu\sigma/\tau V_a$. It follows that $\rho_a\, A_D = 3\, m_G\mu\sigma/4r\tau$.

Substituting in Eq. (44) yields

$$|v_{B,z}|\, v_{B,z} = \frac{8\, gr}{3\, C_D}\left(1 - \frac{\tau}{\sigma}\frac{\sigma + f'}{1 + f'}\right) \tag{45}$$

The magnitude of $v_{B,z}$ is the positive square root of the absolute value

of the right side of Eq. (45), and $v_{B,z}$ takes the algebraic sign of the term in parenthesis on the right side of the equation. From Eq. (45) it is apparent that if $\tau = \sigma(1 + f')/(\sigma + f')$, the supertemperature just counteracts the nominal free lift and $v_{B,z} = 0$. This is also the necessary condition for $dv_{B,z}/dt = 0$, and the relationship is shown graphically in Fig. 6. From Eq. (45) it is also evident that for $f' = 0$, the motion will be upward (positive) when $\tau < 1.0$ and downward (negative) when $\tau > 1.0$. If f' is very large compared to σ or if $\sigma = 1.0$, the motion will be upward when $\tau < \sigma$ and downward when $\tau > \sigma$. This is the basis for controlling a hot-air balloon for which $\sigma \approx 1.0$.

It should also be noted that for a given value of $\tau(\sigma + f')/\sigma(1 + f')$, the vertical speed of the balloon is a function of the radius of the balloon and is apparently independent of the air density. Therefore, a balloon at 20 km will rise at the same rate as a balloon at sea level if they both have the same radius and if the value of $\tau(\sigma + f')/\sigma(1 + f')$ is the same for both. On the other hand, as a zero-pressure balloon rises, the pressure decreases, causing the radius to increase. Therefore, if the balloon is to maintain a constant upward speed, as was assumed in deriving Eq. (45),

the value of $\tau(\sigma + f')/\sigma(1 + f')$ must increase to compensate for the increase in r.

The radius of a spherical balloon may be expressed in terms of the gross mass of the balloon system and the air density as follows:

$$r = \left(\frac{3\ m_a}{4\ \pi\rho_a}\right)^{1/3} = \left(\frac{3\ m_G\mu\sigma}{4\ \pi\rho_a\tau}\right)^{1/3}$$

Substituted in Eq. (45), this yields

$$|v_{B,z}|\ v_{B,z} = -\frac{8\ g}{3\ C_D}\left(\frac{3\ m_G\mu\sigma}{4\ \pi\rho_a\tau}\right)^{1/3}\left[1 - \frac{\tau}{\sigma}\frac{\sigma + f'}{1 + f'}\right] \tag{46}$$

or

$$|v_{B,z}|\ v_{B,z} = \frac{1.66\ g}{C_D}\left(\frac{m_g}{\rho_a}\right)^{1/3}\left[\frac{\sigma(1 + f') - \tau(\sigma + f')}{(1 + f')\sigma^{2/3}\ \tau^{1/3}}\right] \tag{47}$$

These equations show a dependence of upward speed on air density. Figure 7 is a graphical representation of Eq. (46) for $\rho_a = 1.225$ kg/m^3 and $\tau = 1.0$, conditions usually assumed for a sea level launch.

Equation (47) shows that if m_g, τ, f', and C_D were to remain unchanged during the ascent of a balloon system, the balance between buoyancy and aerodynamic drag could not be maintained unless the upward speed increased as the balloon gained height. Such an increase is not observed; therefore,

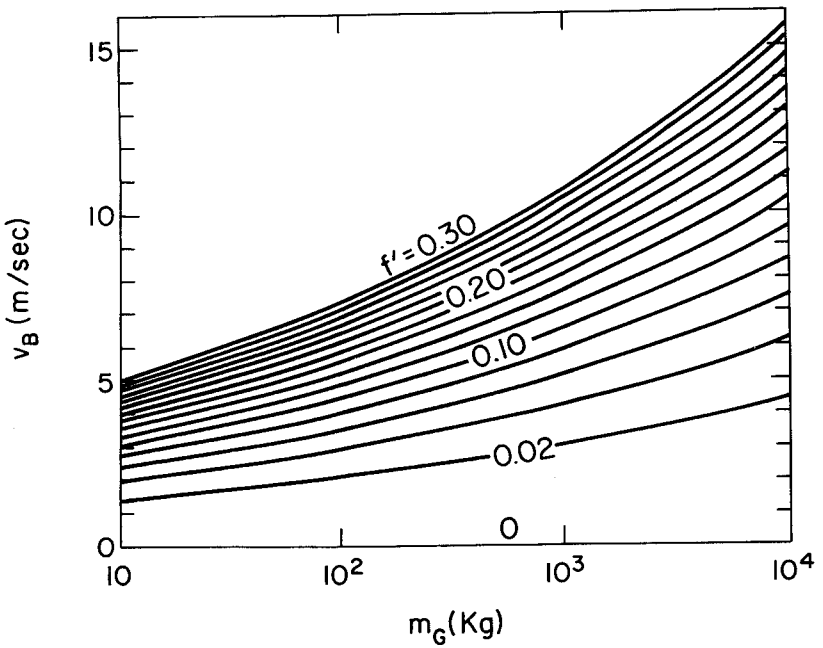

Fig. 7. Vertical velocity of a helium filled balloon ascending at sea level where $\rho_a = 1.225$ kg/m^3 and $g = 9.80665$ m/sec^2. It is assumed that $\tau = 1.0$ and $C_D = 0.3$.

compensatory changes in τ of C_D must occur during a normal ascent. The drag coefficient, C_D, is not believed to change significantly during ascent, but it will be shown that cooling by expansion of the gas in a balloon can readily cause adequate compensatory changes in τ.

A relationship may be expressed between τ, ρ_a, and f' which will maintain balance between aerodynamic drag and buoyancy during uniform vertical motion. Let Eq. (47) be written as follows for the level at which $\rho_a = \rho_{a,o}$ and $\tau = \tau_o$:

$$|v_{B,o}| v_{B,o} = \frac{1.66\ g}{C_{D,o}} \left(\frac{m_{g,o}}{\rho_{a,o}}\right)^{1/3} \left[\frac{\sigma(1 + f_o') - \tau_o(\sigma + f_o')}{(1 + f_o')\sigma^{2/3}\ \tau_o^{1/3}}\right]$$

Also, for all vertical motion, let $v_{B,z} = v_{B,o}$, $m_g = m_{g,o}$, $C_D = C_{D,o}$ and $f' = f_o'$. Then dividing this equation into Eq. (47) and rearranging gives

$$\frac{\rho_a}{\rho_{a,o}} = \frac{\tau_o}{\tau}\left[\frac{\sigma(1 + f_o') - \tau(\sigma + f_o')}{\sigma(1 + f_o') - \tau_o(\sigma + f_o')}\right]^3 \qquad (48)$$

Equation (48) is plotted in Fig. 8 (solid curves) for helium for select values of f' and τ_o. Note that τ must increase (i.e., the gas in the balloon must cool relative to the ambient air) for the motion to remain constant whether that motion be upward or downward. In motion toward lower density,

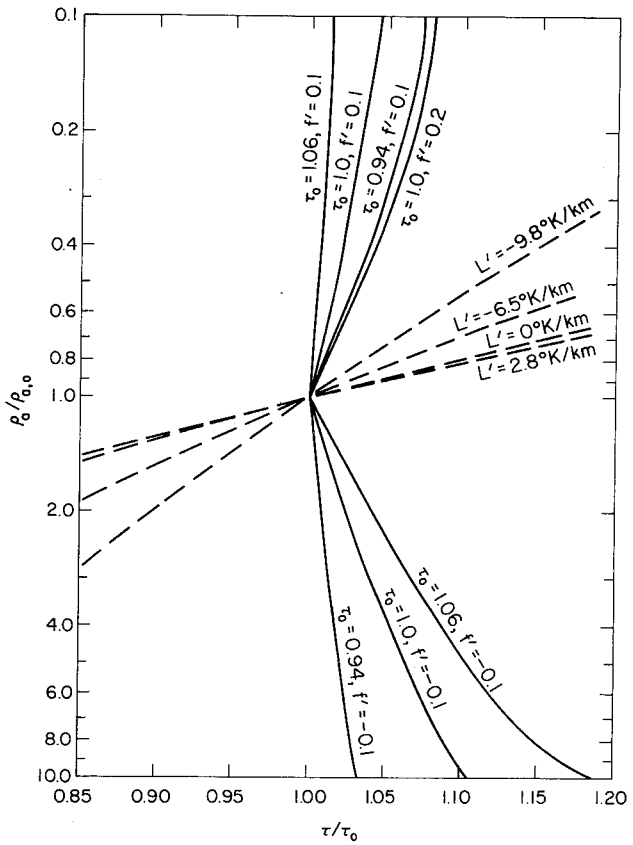

Fig. 8. The variation of τ with air density required to maintain constant vertical motion (solid curves) and variation of τ with air density for an adiabatic ascent (dashed curves) in four atmospheric lapse rates. The lift gas is helium.

the speed will increase unless τ increases. In motion toward higher density, the speed will decrease unless τ increases. Although each of the solid curves in Fig. 8 is an isoline of constant speed, the speed cannot be determined unless $\rho_{a,o}$ is assigned a value. The vertical line $\tau/\tau_o = 1.0$ is an isoline along which $v_{B,z} = 0$.

Cooling of the gas in a balloon because of expansion during ascent will be adiabatic unless the gas can exchange heat with its environment. Most standard texts on thermodynamics show that the pressure-volume relationship of an ideal gas undergoing an adiabatic volume change may be expressed as $p_g \alpha_g^{(C_p/C_v)} = \text{const}$ where α_g is the specific volume of the gas, and C_p and C_v are the specific heats of the gas at constant pressure and volume, respectively. By differentiating the pressure-volume relationship and making use the equation of state, Eq. (8), and the fact that $R/M_g = C_p - C_v$, it can be shown that

$$\frac{dT_g}{T_g} = \frac{R}{M_g C_p} \frac{dp_g}{p_g} \tag{49}$$

The gas pressure in a zero-pressure balloon is very nearly equal to the pressure of the ambient atmosphere at all times so that

$$\frac{dp_g}{p_g} = \frac{dp_a}{p_a}$$

From the hydrostatic equation and the equation of state

$$\frac{dp_a}{p_a} = -\frac{gM_a}{RT_a}\,dz$$

Combining this with Eq. (49) and solving for DT_g/dz gives

$$\frac{dT_g}{dz} = -\frac{g}{C_p}\frac{M_a}{M_g}\frac{T_g}{T_a} = -\frac{g\sigma}{C_p\tau} \tag{50}$$

Differentiating $\tau = T_a/T_g$ with respect to z yields

$$\frac{d\tau}{dz} = \frac{T_g\dfrac{dT_a}{dz} - T_a\dfrac{dT_g}{dz}}{T_g^2} \tag{51}$$

Let $dT_a/dz = L'$; this is the negative (additive inverse) of the lapse rate of the atmosphere. It is constant within each of the strata of the Standard Atmosphere, and it is often nearly constant through deep layers in the real atmosphere. It will be considered constant here. By combining Eqs. (50) and (51), substituting L' and rearranging, one may write

$$\frac{d\tau}{\tau} = \left(\frac{C_pL' + g\sigma}{C_p}\right)\frac{dz}{T_a} \tag{52}$$

Similarly, if the equation of state for air is differentiated with respect to z, the result may be written

$$\frac{M_a}{R}\frac{dp_a}{dz} = \rho_a\frac{dT_a}{dz} + T_a\frac{d\rho_a}{dz}$$

Substituting $-g\rho_a$ for dp_a/dz from the hydrostatic equation and L' for dT_a/dz and rearranging gives

$$\frac{dz}{T_a} = -\frac{R}{RL' + gM_a}\frac{d\rho_a}{\rho_a} \tag{53}$$

Combining Eqs. (52) and (53) yields

$$\frac{d\tau}{\tau} = -\frac{R(C_pL' + g\sigma)}{C_p(RL' + gM_a)}\frac{d\rho_a}{\rho_a} \tag{54}$$

which becomes

$$\frac{\tau}{\tau_o}\ (\text{adiabatic}) = \left(\frac{\rho_{a,o}}{\rho_a}\right)^{\dfrac{R(C_pL' + g\sigma)}{C_p(RL' + gM_a)}} \tag{55}$$

upon integration. This relationship is shown graphically by the dashed lines in Fig. 8 for helium for three Standard Atmosphere lapse rates and for $L' = -9.8^{\circ}$K/km, the adiabatic lapse rate for air.

If $L' = -g\sigma/C_p$, the exponent in Eq. (55) will be zero and τ will not change with density although density will vary with height. The combination

$g\sigma/C_p$ is the adiabatic lapse rate of the gas in the atmosphere. Thus, if a gas is ascending or descending adiabatically through the atmosphere, Eq. (56) shows that:

1) if $L' > -g\sigma/C_p$, τ will increase with movement toward lower density (ascent) and decrease during descent.

2) if $L' = -g\sigma/C_p$, τ will not change during ascent or descent.

3) if $L' < -g\sigma/C_p$, τ will decrease during ascent and increase during descent unless $L' \leq -g\, M_a/R$.

When $L' = -gM_a/R$, it is apparent from Eq. (53) that ρ_a is independent of height. If $L' < -gM_a/R$, more dense air overlies less dense air and overturning can be expected. Overturning will tend to restore the lapse rate to adiabatic. In fact, $-L'$ is rarely more than the adiabatic lapse rate for air except in thin strata or very near the ground; therefore, the case when $L' = -gM_a/R$ is of theoretical interest only. Incidentally, meteorologists call the lapse rate gM_a/R an autoconvective lapse rate because it is so unstable.

The numerical values of dT/dz for several gases undergoing adiabatic ascent or descent are shown in Table 2. When these are compared with the

Table 2

Molecular Weight, Specific Heat at Constant Pressure and

dT_g/dz for an Adiabatic Ascent or Descent for Various Lift Gases

Gas	M_g	C_p (joule/kg ^oK)	dT_g/dz (adiabatic) (^oK/km)
H_2	2.016	14,200	- 9.95
He	4.003	5,240	-13.5
NH_3	17.031	2,190	- 7.63
Air	28.964	1,003	- 9.8

In the U.S. Standard Atmosphere, 1962, $L' = 06.5^oK$/km in the troposphere and 0^oK/km in the lowest stratum of the stratosphere. See Section XI, Table 1 for other values.

temperature gradients of Table 1 of Section XI, two of which are given below Table 2, it is clear that in all strata in the Standard Atmosphere listed in Section XI, τ will increase during ascent and decrease during descent for the gases listed in Table 2 if the motion is adiabatic. Thus, when these gases are used in a balloon flown in an atmosphere like the Standard Atmosphere, vertical motion causes τ to change in such a way as to oppose the motion. The effect is more significant with helium than hydrogen and least significant with ammonia. Lapse rates in the troposphere of the real atmosphere will on occasion be greater than the adiabatic lapse rate of ammonia, but very rarely will they be greater than the adiabatic lapse rates of hydrogen or helium.

Comparison of the adiabatic curves in Fig. 8 with the curves plotted from Eq. (48) reveals that for helium an adiabatic change of τ is greater than is needed to compensate for the change of air density during uniform upward motion. During descent an adiabatic change of τ would augment the slowing due to the increase of density. Thus, for both ascent and descent the change of temperature of the gas in a helium inflated balloon caused by the change of pressure and volume serves as a brake, but if the motion were adiabatic, the braking action would be too severe. The same statement applies to a balloon inflated with hydrogen. It also applies to a balloon inflated with ammonia in most atmospheric strata, but occasionally an atmospheric stratum may exist in which the brake would fail. Thus, in most instances transfer of heat between the environment and the gas in a balloon is seen to be a requisite condition for uniform vertical motion.

Heat transfer processes include: radiation, convective exchange with the ambient air, and heat deliberately added to or subtracted from the lift gas by some means, such as chemical combustion. These are discussed more completely in Section III.

3. Wind Effects on a Balloon in Free Flight

A balloon in free flight moves with the air in which it is embedded, and, as was pointed out in I.1 of this section, it accelerates rapidly to nearly the speed of the wind immediately after it is released. It is common practice in calculating balloon trajectories to assume that throughout flight the horizontal velocity of the balloon is equal to the velocity of the air in which it is embedded. Interpreted strictly, this implies instant adjustment of the balloon's horizontal velocity as it moves from one stratum to another

where the air velocity is different. In fact, the accuracy with which the wind velocity is known as a function of time and place is not great enough to warrant more precise treatment for estimating trajectories.

For other reasons the difference between balloon and air velocities may be important. For example, it was shown earlier that the difference may cause the balloon system to tilt significantly from the vertical. Also, the uninflated portion of balloons have occasionally been observed to develop into huge spinnaker-like sails during ascent, and some observers have surmised that the wind forces on such sails may play a part in balloon bursts. Therefore, it is worthwhile to explore the possible magnitude of $(\vec{v}_B - \vec{v}_a)$ as a balloon ascends through atmospheric wind shear strata.

Consider a balloon system with the balloon envelope only partially inflated and rising at a constant rate through a deep stratum in the troposphere. Assume that the wind is blowing horizontally from the west at all levels and that its speed increases linearly with height. Assume also that the wind is invariant with time at all levels. Then the horizontal component of acceleration caused by aerodynamic drag in the stratum may be written

$$\frac{dv_{B,x}}{dt} = \tfrac{1}{2} \rho_a C_D A_D \left|\vec{v}_B - \vec{v}_a\right| (v_{B,x} - v_{a,x}) \div m_v \qquad (56)$$

where $(v_{B,x} - v_{a,x})$ is the horizontal component of the relative wind on the balloon. If, for the time being, interest is restricted to a shallow layer which will be penetrated in a short time, ρ_a, C_D, A_D, and m_v may all be considered constant. The drag coefficient and area, C_D and A_D, must take those values which will give the proper response of the balloon system to the overall vector wind acting on it. Therefore, A_D is not a vertical cross sectional area through the balloon system; on the contrary, if the vertical component of the relative wind is large compared with the horizontal component, A_D will be a nearly horizontal area.

Now, the successful practice of using the horizontal components of $\vec{v}_a$ as the horizontal components of $\vec{v}_B$ in calculating balloon trajectories suggests that the difference $(v_{B,x} - v_{a,x})$ must be small. On the other hand, there must be a difference. If at some level there were no difference, then as soon as the balloon had risen a short distance into the stronger winds above, a difference would develop. One reasonable solution to Eq. (56) is $v_{B,x} = v_{a,x} + v_{r,x}$, where $v_{r,x}$ is the constant horizontal relative wind on the bal-

loon. Then also $|\vec{v}_B - \vec{v}_a| = v_{r,x}/\sin b$ where b is the angle the vector relative wind makes with the vertical axis of the balloon. Differentiating $v_{B,x}$ with respect to time yields

$$\frac{dv_{B,x}}{dt} = \frac{dv_{a,x}}{dt} = \frac{dv_{a,x}}{dz}\frac{dz}{dt}$$

where $dv_{a,x}/dz$ is the vertical wind gradient and dz/dt is the rate of rise of the balloon. Substituting into Eq. (56) and rearranging gives

$$v_{r,x} = \left(\frac{2 \frac{dv_{a,x}}{dz} \frac{dz}{dt} m_v \sin b}{\rho_a C_D A_D} \right)^{\frac{1}{2}} \qquad (57)$$

This suggests that the relative horizontal wind on the balloon system would be significantly decreased if the uninflated portion of the balloon formed a spinnaker sail, because such a sail would increase C_D and A_D and decrease dz/dt without causing comparable changes in the other variables. It is not clear how b may change, but an example can provide some insight.

Data for the following example have been chosen to give larger values of $v_{r,x}$ than can be expected in the atmosphere during a flight except under an unusual combination of circumstances. Assume that a balloon at 8.0 km above sea level is ascending in an atmosphere which has the same density as

the Standard Atmosphere and that the wind shear is 40 m sec^{-1} km^{-1} or 4.0 x 10^{-2} sec^{-1}, a more extreme value than is likely to be encountered in the real atmosphere except in very thin strata. (See Section XI.D.4 or pages 5-41 of The Handbook of Geophysics (5).) Assume also that the balloon is ascending at a speed of 10 m sec^{-1}, a rate two or more times the desired rate for most flights. A balloon having a nominal volume of 3×10^5 m^3 could be expected to have a mass of 500 kg, and a gross mass for the system of 1500 kg is reasonable. At 8 km in the Standard Atmosphere, the air density is 0.525 kg m^{-3}, and if $f' = 0.2$ and $\tau = 1.03$, the balloon system would displace a volume of 3860 m^3. Let $b = 45^o$ as a first guess. Also, as a first estimate, let $A_D = 1.21\ V_g^{2/3} = 297\ m^2$, and $C_D = 0.35$.

Since the balloon is not accelerating relative to the fluid, the virtual mass is 1789 kg, the gross mass plus the mass of the gas. With these data $v_{r,x} \approx 4.3$ m sec^{-1}, and the estimated magnitude of the vector relative wind is 10.9 m sec^{-1}. A new estimate of b is $\sin^{-1}(4.3/10.9)$ which is $\approx 23^o$. Using the sphere-on-cone model (Section XII.B), one can make new estimates of A_D and C_D. After several iterations, using a half-cone-angle of 15^o for the balloon and 0.35 for C_D, the values of $v_{r,x}$ and b converge on 2.6 m sec^{-1}

and 15°, respectively.

When a balloon forms a spinnaker-like sail, the sail is shaped much like a hemispherical cup with the concave side facing into the wind (see Section XII.B). Assume for the present example that $C_D = 0.75$, and as a first estimate, that $b = 0$. Because a comparison is desired between the relative wind before and after the sail has formed, it will be necessary to estimate the value of dz/dt after sailing has occurred. By treating the vertical component of drag as if it were independent and assuming that the only essential differences between the system before and after the sail forms are the values of C_D and A_D, one can calculate the value of dz/dt after the sail has formed and the system has reached steady state. The following equation is used:

$$\left(\frac{dz}{dt}\right)_{after} = \left(\frac{dz}{dt}\right)_{before} \left[\frac{(C_D A_D)_{before}}{(C_D A_D)_{after}}\right]^{\frac{1}{2}}$$

It gives $(dz/dt)_{after} \approx 2.3$ m sec^{-1} for this example, and by an iterative solution of Eq.(57), $v_{r,x}$ and b are found to be 0.5 m sec^{-1} and 13°, respectively.

A relative, horizontal wind of 2.6 m sec^{-1} is not strong enough to create difficulty for a balloon, but it may be adequate to cause one to form a sail if other conditions are right. The magnitude of the relative wind vector is 10.3 m sec^{-1} under the conditions assumed for the ascending balloon before it sailed and 2.4 m sec^{-1} after the sail formed; consequently, the stresses during the transition period might conceivably be excessive.

The average aerodynamic pressure, $\bar{p}_r$, on the cross sectional area of a balloon normal to the relative wind on the balloon is

$$\bar{p}_r = \frac{m_v}{A_D} \frac{dv_B}{dt} = \tfrac{1}{2} \rho_a C_D v_r^2$$

The greatest pressure which might exist during the transition would occur immediately after the sail had formed and caused C_D to increase, but before v_r could be reduced by the increased drag. Thus, the maximum value which the mean aerodynamic pressure could have, using the data of the foregoing example, would be

$$\bar{p}_r \approx 0.5 \times 0.525 \times 0.75 \times 10.3^2 \approx 21 \text{ Nm}^{-2} \approx 3 \times 10^{-3} \text{ psi}$$

This pressure is not as large as the excess of gas pressure over atmospheric pressure at the top of the balloon, but the two may be additive, and it is

possible that local film stresses accompanying the transition might be great enough to cause damage.

In view of the rarity of situations in which a balloon will encounter relative winds as strong as the computed wind in the first part of this example and of the low aerodynamic pressures caused by such a wind, vertical wind shear does not loom as a very serious threat to balloons in flight.

A balloon in flight has an appreciable vertical dimension, and if the vertical wind shear is strong, the relative wind at the top may differ significantly from that at the bottom. The difference between the relative wind from top to bottom of a balloon system is the product of the length of the system and the vertical wind gradient.

If a balloon system 200 m long were ascending through a stratum in which the wind shear were 4×10^{-2} sec^{-1}, the relative wind at the top would be 8 m sec^{-1} greater than at the bottom. Thus, the top of the ascending balloon system in the foregoing example will be subject to a relative horizontal wind greater than the 2.6 m sec^{-1} estimated for the system as a whole. If the balloon system were long enough, the payload might experience a relative wind from the opposite direction to that experienced by the top of the balloon. This distribution of relative wind will cause the balloon system to tilt. This tilt has led to the suggestion that balloon systems in a stratum where wind shear exists may derive some aerodynamic lift from the relative winds. No quantitative measurements or estimates of the magnitude of lift are known to have been made.

4. Behavior at Float Altitude

In the following discussion frequent reference will be made to Fig. 9. Particular use will be made of the level numbers shown in the figure, often without otherwise referring to the figure.

As a balloon ascends into strata of lower pressure, the lift gas expands and the gas density decreases. The density of the balloon system, ρ_B, at any level is $(m_G + m_g)/V_g$ if the volume of the gondola, rigging, etc. are very small compared with V_g. This may also be written $m_G(1 + \mu)/V_g$. The density of the displaced air is m_a/V_g, which may be expressed as $m_G\mu\sigma/\tau V_g$. Thus the ratio of the density of the balloon system to that of the air is $\rho_B/\rho_a = \tau(1 + \mu)/\mu\sigma = \tau(\sigma + f')/\sigma(1 + f')$. But $\tau(\sigma + f')/\sigma(1 + f') = 1$ is the condition from Eq. (39) that the sum of buoyant and gravitational forces on the balloon be zero. Therefore, if ρ_B/ρ_a should become one during ascent or des-

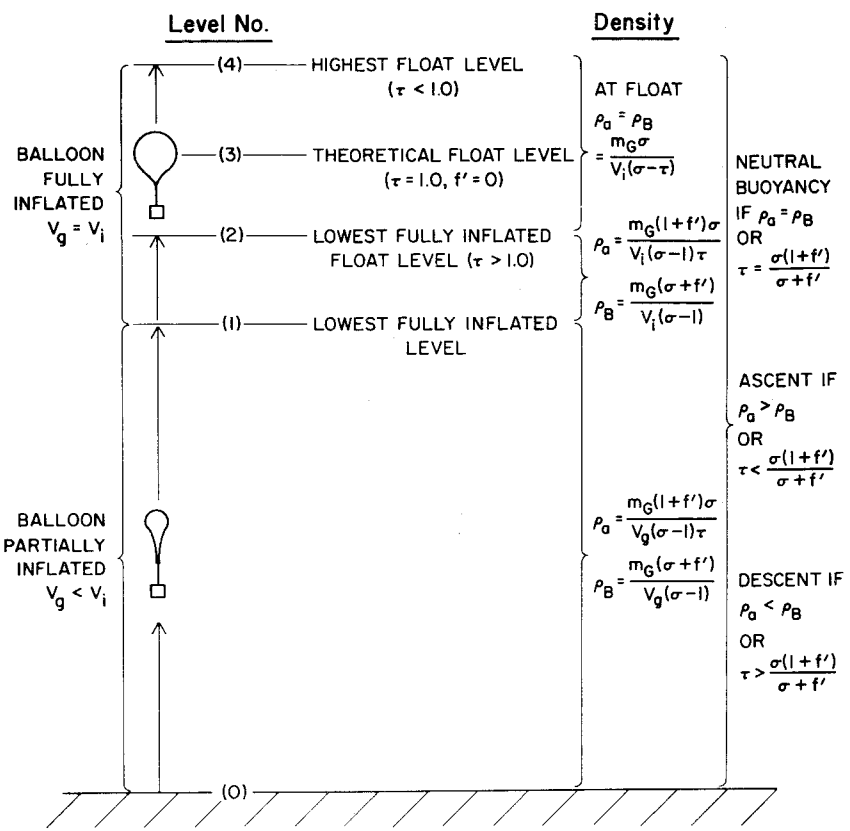

Fig. 9. Diagram showing relationship between air density and balloon system density. Level numbers are used in the text. Vertical distances on the diagram are not proportional to vertical heights in the atmosphere.

cent, aerodynamic drag would soon reduce the motion of the balloon to near zero.

The combination of f' and τ required to make $\rho_B/\rho_a = 1.0$ may be realized at any level during ascent or descent, but one combination has special significance. Clearly if $f' = 0$ and $\tau = 1.0$, $\rho_B/\rho_a = 1.0$. Under these circumstances, $\rho_B = \rho_a = m_G\sigma/V_g(\sigma - 1)$. Now if $V_g = V_i$ where V_i is the fully inflated volume of the balloon, ρ_a is the air density at which a fully inflated balloon should just be in hydrostatic equilibrium. The level (level 3) at which $\rho_a = m_G\sigma/V_i(\sigma - 1)$ is therefore called the "theoretical float altitude" of the balloon.

As f' is defined by Eq. (37), it is possible to change it during flight by changing m_G, m_g, or σ. The gross mass may be decreased by dropping ballast; such a change would increase f'. Gas may be exhausted from the balloon, thereby decreasing m_g; this would decrease f'. Also it is possible to change σ, and in fact when balloons were open at the lower end so that air could enter while a balloon was ascending, σ usually decreased rapidly near the end of ascent, accompanied by an increase in m_g. In modern scientific ballooning σ is kept constant throughout flight, but the possibility of changing it

should not be overlooked if special requirements occur.

Typically, when a balloon reaches level 1 (i.e., when the gas in an ascending balloon has expanded to just fill the balloon) $f' > 0$ and $\tau > 1.0$. It is usual also that $\rho_B/\rho_a < 1$ at level 1. Consequently, the balloon will continue to rise past level 1 and become superpressured or expel gas through its ducts or both. If the balloon is a closed vessel, its behavior above level 1 will be quite different from that of a balloon which can freely lose gas to avoid excessive overpressure. Only the latter, the zero-pressure balloon, will be discussed here at levels above level 1. The superpressure balloon is discussed in Section VIII.

A loss of gas will decrease m_g, thereby decreasing f'. Unless this change in f' is compensated by a change in τ, the buoyant force on the balloon will decrease and the vertical speed of the balloon system will dwindle. Since expansion of the gas results from vertical motion and is a cause for τ remaining above its equilibrium value (i.e., the value it would reach if its vertical motion were restrained long enough for it to come into thermal equilibrium with its environment) during ascent, reduced upward speed usually allows τ to decrease. Nonetheless, when an ascending balloon reaches level 2,

the lowest level at which $V_g = V_i$ and $\rho_B/\rho_a = 1.0$, $\tau > 1.0$ normally, and $f' > 0$. If $\tau = 1.0$ at level 2, levels 2 and 3 will coincide.

An ascending balloon will not usually have lost all of its vertical motion when it reaches level 2, and its inertia will cause it to overshoot. At this time the pressure of the gas must exceed ambient air pressure slightly because gas is being forced into the atmosphere from the balloon at its base. With such overpressure and continued cooling due to the decrease in pressure, the rising balloon system will soon become more dense than the ambient air and so be subject to a downward force, which will increase with distance above level 2. This force will ultimately stop the upward motion and initiate downward motion. It is not unusual for balloons with small ducts to oscillate up and down through several cycles before the motion is damped out (see Fig. 10). The equation of motion of the cycle is complicated since f', τ, and p_g are all simultaneously adjusting to the new environment and undergoing changes which are dependent on the phase of the cycle of oscillation. A numerical solution of the equation of motion (see Section III) can take all of these into account realistically. In a very simplified model which assumes the vertical motion of the gas to be adiabatic and $df'/dt = 0$, the period in

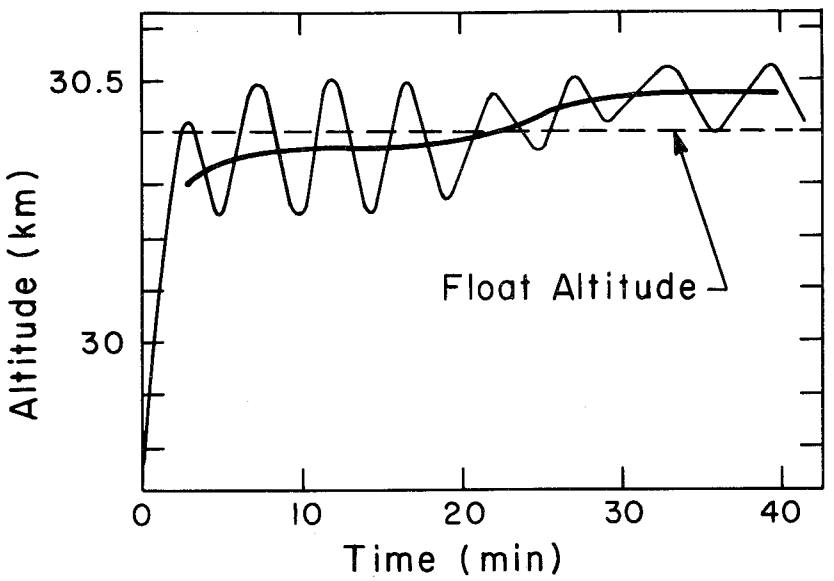

Fig. 10. Vertical oscillation of a balloon system on reaching float altitude. Not all balloon systems oscillate in this manner; many appear to approach float altitude in a nearly asymptotic manner.

seconds of the oscillation, t(osc), is given by

$$t(osc) = 2\sqrt{\frac{T_a}{\frac{g\sigma}{C_p} + L'}} \tag{59}$$

for a zero-pressure balloon. A derivation of a similar equation applicable to superpressure balloons in given in Section VIII. Equation (59) suggests that if $L' = -g\sigma/C_p$, i.e., if the lapse rate of the atmosphere is equal to the adiabatic lapse rate of the gas in the atmosphere, the period will be infinitely long. In the isothermal stratum of the Standard Atmosphere where $T_a \approx 217^{\circ}$ and $L' = 0$, a helium filled balloon becoming fully inflated would be expected from Eq. (59) to have a period of 253 sec (4.2 min). The record plotted in Fig. 10 shows that the average period of the first three cycles was 4.5 min and that the period increased with elapsed time.

Figure 10 shows another characteristic of many flights. The heavy curve is a hand-smoothed average of the oscillating curve. The dashed curve represents the theoretical float altitude. The balloon appears to have oscillated about a float level which gained height as time passed. It can be shown that the ratio of the density of a balloon system floating in the stratum above level 2 to the density of the air at the theoretical float altitude

is $\rho_{B,2}/\rho_{a,3} = (\sigma - 1)/(\sigma - \tau_2) = (\sigma + f_2')/\sigma$. If $\tau_2 > 1.0$, the density of the balloon system will be greater than air density at the theoretical float level, and the balloon will float at a level lower than the theoretical float level. Similarly, if $\tau < 1.0$ at the actual float level, balloon system density will be less than air density at the theoretical float level, and hence the actual float level will be higher than the theoretical. It is normal for a balloon to start floating at a level below the theoretical float level and to ascend slowly to a level above the theoretical level as the gas in the balloon warms.

In the stratosphere where most scientific balloon systems float, the temperature is nearly independent of height. Therefore, Eq. (10) may be integrated to yield the following relationship between the geopotential height (see Section XI.C.1) of two pressure levels:

$$H_2 - H_1 = \frac{RT_a}{M_a g_0} \ln \frac{p_{a,1}}{p_{a,2}} \tag{60}$$

Also, if temperature is independent of height and thus of pressure, $\rho_{a,1}/\rho_{a,2} = p_1/p_2$; therefore,

$$H_2 - H_1 = \frac{RT_a}{M_a g_0} \ln \frac{\rho_{a,1}}{\rho_{a,2}} \tag{61}$$

and

$$H_3 - H_2 = \frac{RT_a}{M_a g_0} \ln \left(\frac{\sigma - 1}{\sigma - \tau_2}\right) = \frac{RT_a}{M_a g_0} \ln \left(\frac{\sigma + f_2'}{\sigma}\right) \tag{62}$$

Equations (60) and (61) are applicable in any stratum in the atmosphere in which $L' = 0$ or the stratum is thin enough that the variation of T_a is not significant. Subject to these restrictions, the numerical subscripts may take any values. Equation (62) is valid only when level 3 is the theoretical float level and level 2 is any other float level at which $\rho_{B,2} = \rho_{a,2}$.

An example is useful. The value of $R/M_a g_0$ is 29.27 m/°K. At 40 km in the Standard Atmosphere $T_a = 251$°K, $\rho_a = 3.85 \times 10^{-3}$ kg/m^3 and $p_a = 277.5$ N/m^2. Assume that a fully inflated balloon system first reaches float at that level (now designated level 2) and that $\tau_2 = 1.08$. Substituting τ_2 in the relationship $p_{a,2}/p_{a,3} = \rho_{a,2}/\rho_{a,3} = (\sigma - 1)/(\sigma - \tau_2)$ yields $p_{a,2}/p_{a,3} = 1.013$; therefore, $p_{a,3} = 274$ N/m^2 and $\rho_{a,3} = 3.80 \times 10^{-3}$ kg/m^3. Also, from Eq. (62), $(H_3 - H_2) = 95$ m. The initial float level is not far from the theoretical in this example.

It should be noted that the theoretical float level as used here is that level at which the density of the air is equal to the density of the balloon system when $\tau = 1.0$, $f' = 0$, and the balloon is fully inflated. To calculate

that density, one must know the mass of the system and the volume of the fully inflated balloon under existing conditions. If they are not known precisely, the calculated theoretical float level density will probably be in error, and deviations of the actual float level from the calculated theoretical float level may greatly exceed the deviation of the example above. The distinction between the actual theoretical float level and the calculated theoretical float level is not always kept in mind in the practice of ballooning.

If a balloon system reaches initial float altitude below the theoretical float level and the gas starts to warm relative to ambient air temperature, gas will continue to be lost through the ducts, and f' will decrease. A sound balloon system will then gain height slowly as long as warming continues. If a gas leak should develop which removes gas faster than is necessary just to compensate for the warming, f' will become less than $\sigma(1 - \tau)/(\tau - \sigma)$, and the balloon will start to descend. Similarly, if for any reason the gas in a floating balloon should cool relative to the air, τ will increase and unless f' can be increased to maintain the condition for no acceleration, the balloon will descend. Thus a balloon at float altitude is in a rather precarious state of equilibrium. The only satisfactory way that has

been found to maintain that equilibrium is to control f', and that is done by dropping ballast and hence by decreasing m_G.

a. Ballasting and valving to maintain a float condition. It has been pointed out that dropping ballast and valving gas are the primary means of controlling the action of a balloon in flight. Theoretically, if the time rate of change of τ and f' are known, control can be precise.

The condition for zero acceleration of a balloon which is floating is that $1 + \mu(1 - \sigma\tau^{-1}) = 0$. Because T_a is nearly constant when a balloon is floating and because controls change m_G and m_g directly, the condition of zero acceleration for a floating balloon system is more convenient if written as

$$m_G = m_g(\sigma\tau^{-1} - 1) = m_g\left(\frac{\sigma T_g}{T_a} - 1\right) \tag{63}$$

A graphical solution of Eq. (63) is shown in Fig. 11 for helium. This graph and one similar to it for hydrogen are both given in Section XII in a more useful size. On the graphs, the numerical values on the ordinate may be multiplied by any constant and the validity of the chart will be preserved if the m_g values on the slanting lines are also multiplied by the same con-

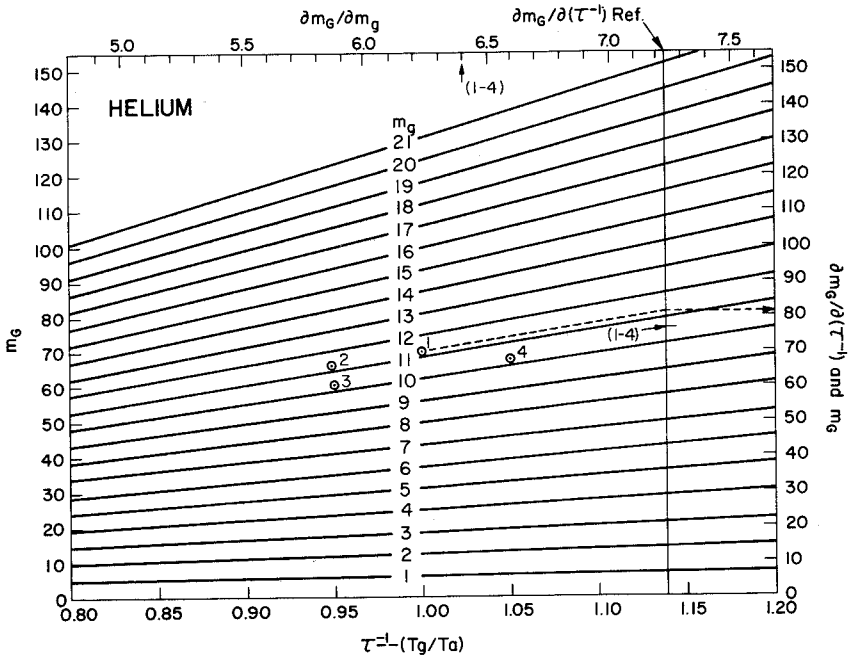

Fig. 11. Graphical solution of the equation of buoyant equilibrium for a helium-filled balloon.

stant, e.g., a multiple of 10. The values on the abscissa should not be changed. The chart thus serves for any range of values of m_G and m_g. With it, solving for any one of the three variables is simple if the other two are known. For example, point 1 on Fig. 11 may be interpreted as meaning that if $T_g/T_a = 1.0$, it will require 11.2 (or 112) units of mass of helium to support 70 (or 700) units of mass of balloon, scientific equipment, rigging ballast, etc. Any unit of mass may be used, but the gross mass and the mass of the gas must be measured in the same units.

The m_g lines are straight and their slope is

$$\frac{\partial m_G}{\partial (\tau^{-1})} = m_g \sigma = m_G \left(\frac{\sigma}{\sigma\tau^{-1} - 1} \right)$$

Therefore, when $\sigma/[\sigma\tau^{-1} - 1] = 1$, $\partial m_G/\partial(\tau^{-1}) = m_G$. This occurs for helium when $\tau^{-1} = 1.138$, and so by erecting a vertical reference line on the right side of the chart at $\tau^{-1} = 1.138$, one can read the slope of each of the m_g lines directly from the m_G coordinate at the point where the m_g lines cross the reference line. A scale of $\partial m_G/\partial m_g$ for constant values of τ^{-1} has been added along the abscissa at the top of the chart.

The following examples will illustrate the use of the chart: Assume that a stably floating balloon system has a gross mass of 700 kg and that $T_g = T_a = 250^{\circ}K$. Then $\tau^{-1} = T_g/T_a = 1.0$, and point 1 on the graph is a plot of m_G vs T_g/T_a. Note that the ordinate must be multiplied by 10. The mass of helium in the balloon as read from the slanting m_g lines is 11.2, and this must also be multiplied by 10, giving 112 kg. Following up the m_g line through point 1 to the reference line on the right shows the $\partial m_G/\partial(\tau^{-1})$ value to be 810 kg. Along the top scale $\partial m_G/\partial m_g$ is seen to have a value of 6.24 where T_g/T_a has a value of 1.0.

Assume further that the gas in the balloon is cooling uniformly at a rate of $12.5^{\circ}K/hr$ and that the air temperature is not changing. Then $\partial(\tau^{-1})/\partial t = (1/T_a)(\partial T_g/\partial t) = -0.05\ hr^{-1}$. At what rate should ballast be dropped to maintain the balloon system at float altitude without loss of gas, i.e., what should be the value of $\partial m_G/\partial t$? It is

$$\frac{\partial m_G}{\partial t} = \frac{\partial m_G}{\partial(\tau^{-1})}\frac{\partial(\tau^{-1})}{\partial t} = -810 \times 0.05 = -40.5 \text{ kg/hr}$$

The same result can be obtained in another way. By noting that a change of -0.05 in the value of T_g/T_a would reduce it to 0.95 in an hour

and then plotting point 2 at $T_g/T_a = 0.95$ and $m_g = 112$, one finds the value of m_G to be 660 kg. The difference (700 - 660) is 40. Since this change will have occurred in an hour, the average rate is 40 kg/hr.

Using the same data, assume that 100 kg of ballast (an excess of 60 kg) was dropped at a uniform rate during the hour. How much gas was lost due to the excessive ballasting? Point 3, plotted at $m_G = 600$, and $T_g/T_a = 0.95$, shows the status of the balloon system at the end of the hour. The value of m_g is 102. Therefore, 10 kg (112 - 102) of gas and 60 kg of ballast will have been wasted.

Again using the same initial conditions for the balloon system and assuming that gas is leaking at a rate of 10^{-4}kg/sec, and that the air and gas temperatures are not changing, at what rate should ballast be dropped to maintain constant float altitude? The value of $\partial m_G/\partial t$ is desired when $\partial m_g/\partial t = -10^{-4}$ and $T_g/T_a = 1.0 = \text{const}$. Then

$$\frac{\partial m_G}{\partial t} = \frac{\partial m_G}{\partial m_g}\frac{\partial m_g}{\partial t} = -6.24 \times 10^{-4}\text{kg/sec} = -2.25 \text{ kg/hr}$$

As a final example, starting with the initial conditions represented by point 1 and assuming that the balloon is leaking at a rate of 10 kg/hr

while the gas temperature is warming at a rate of 12.5°K/hr and the air temperature is remaining constant, what must the ballast rate be to maintain float? In an hour the mass of the gas will be 102 kg; the value of T_g/T_a will be 1.05. Using these, point 4 may be plotted. At point 4, m_G is 675 kg; therefore, during the hour ballast must have been dropped at the rate of 25 kg/hr to maintain float. Within the accuracy of the chart the same result may be obtained by using the rates of change in the total derivative as follows:

$$\frac{dm_G}{dt} = \frac{\partial m_G}{\partial m_g}\frac{dm_g}{dt} + \frac{\partial m_G}{\partial(\tau^{-1})}\frac{d(\tau^{-1})}{dt}$$

$$\frac{dm_G}{dt} = 6.4\times(-10) + 770 \times 0.05 = -25.5 \text{ kg/hr}$$

The values of $\partial m_G/\partial m_g$ and $\partial m_G/\partial(\tau^{-1})$ must be mean values for the process through which the balloon system is going as its state changes from that of point 1 to that of point 4. They are identified by arrows and the notation (1-4) along the $\partial m_G/\partial m_g$ scale at the top of the chart and on the $\partial m_G/\partial(\tau^{-1})$ reference line.

5. Excursions from Float and Valved Descent

A balloon system may depart from its theoretical float altitude for a

number of reasons. If a flight is to be terminated by bringing the balloon system down intact, gas may be valved from the balloon. Also, unplanned departures from the theoretical float altitude may occur because of a leak which decreases f′ without producing compensatory decreases of τ or because of warming or cooling of the gas relative to the air, which changes τ but leaves f′ unchanged. Large excursions from the theoretical float altitude are always downward, and it is these which are the principal topic of discussion in the remainder of this section.

Balloon system descent, either planned or unplanned, can be controlled if f′ can be controlled through the necessary range. In general, the discussion of I.2 of this section is applicable. Ballast can be dropped to increase f′, and gas can be valved to decrease it. The rate at which ballast or gas should be released is a complicated function of the desired rate of descent, the atmospheric lapse rate, the radiation environment of the balloon, the absorptivity and emissivity of the balloon, and a host of other things. The most important of these can be considered quantitatively in a numerical model (see Section III). It is possible, however, to gain a qualitative understanding of many of the reactions of a balloon system to the en-

vironment and to controls by studying them in reference to the equilibrium value of τ, called τ_e here.

The equilibrium value of τ is defined as that value which τ would ultimately reach in a balloon system floating stably for a long enough period to enable it to come into thermal equilibrium with its environment. Thus, it is the ratio of the thermal equilibrium temperature of the ambient air to the thermal equilibrium temperature of the gas in a balloon, and it is determined by the thermal characteristics of the balloon and its gas as well as by the environment (6, 7). Typical day and night curves of τ_e as a function of altitude for a helium-filled, polyethylene balloon in the middle latitude, summer atmosphere are shown in Fig. 12. Although τ_e is a function of many variables, the gross shape of the τ_e vs altitude curves may be explained by a greatly simplified model of the balloon-environment system.

The equilibrium temperature of a stably floating balloon is controlled essentially by convective heat exchange between the balloon and the ambient air and by radiative exchange between the balloon and its environment. The radiation environment of a balloon floating in the stratosphere at night consists of the relatively warm earth and atmosphere on one side and cold

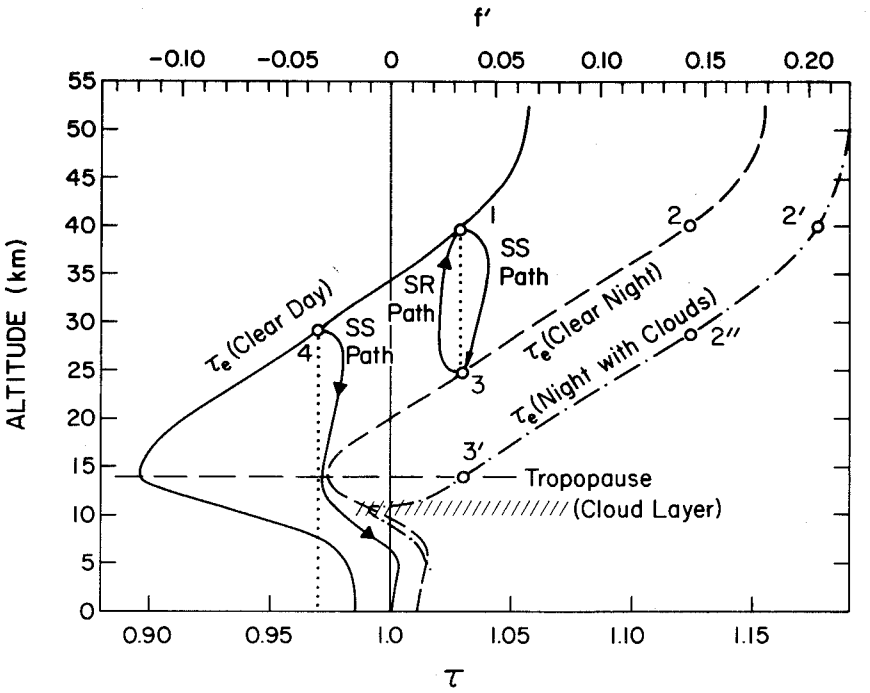

Fig. 12. Diurnal excursions of a gas-tight, helium-inflated, polyethylene balloon in a typical summer, mid-latitude, continental atmosphere.

space on the other. Convective exchange between the balloon and the air is normally small because of the low density of the air, but it can be significant if the air and balloon temperatures differ greatly. The temperature which the balloon gas would assume if it could come into thermal equilibrium with its radiation environment alone is colder than the air temperature in the stratosphere. Therefore, the actual equilibrium temperature of the lift gas will be below the air temperature, and τ_e will be greater than one.

A balloon in the lower troposphere will have a warmer radiation environment than a balloon in the stratosphere principally because it will be embedded in warmer air which is richer in water vapor and so can radiate well in certain bands of the infrared. Convective heat exchange will also be more important in the denser, tropospheric air. Even near the earth's surface at night, however, the radiation equilibrium temperature will be lower than air temperature in most instances, and the value of τ_e will be greater than one.

In the vicinity of the tropopause, a balloon will feel the influence of cold space slightly less and the warm earth and lower tropospheric air slightly more than in the high stratosphere. Consequently, the radiation equilibrium temperature of the gas in the balloon will be greater than at

higher levels, though not as large as near the earth's surface. Air temperature at the tropopause is lower than in either the stratosphere or the troposphere, and it is not unusual even at night for the radiation equilibrium temperature of a balloon to exceed the air temperature. When it does, equilibrium temperature of the balloon gas will be greater than air temperature and τ_e will be less than one.

During the day when the sun is shining, a balloon at any level will receive heat from the sun; hence its radiation equilibrium temperature will be greater than it would be under otherwise comparable conditions at night. The air may also be warmed by the sun, but air is much more transparent to the sun's radiation than a balloon and does not warm nearly as much as the balloon gas. Thus, the τ_e curve for daytime is shifted toward lower values of τ_e but retains much the same shape as the nighttime curve. During the sunrise and sunset periods, τ_e undergoes a marked change at all levels. A much slower change must occur thoughout both the day and night periods with the minimum value at each level being reached sometime after noon and the maximum value occurring after midnight. Except for the changes brought about by clouds, however, it will be assumed here that all changes in τ_e occur in a

period of a few hours near sunrise and sunset.

A cloud layer in the atmosphere will change τ_e at all levels, but the most marked change will occur above a cloud which is much colder than the earth. The value of τ_e above a cloud will be greater with the cloud than without it, and the change will be greater at night than in daytime. Below a cloud at night τ_e will have a slightly lower value than if the cloud were not present. A cirrus cloud layer which is so thin that it cannot be seen at night can produce a drastic change in τ_e above the layer. This change, which is illustrated by the difference in the τ_e curves in Fig. 12 for a clear night and a night with clouds, can occur rapidly.

From the definition of τ_e it is apparent that if τ for a balloon in flight differs from τ_e for any reason, the heat exchange between the balloon and its environment will be in the direction which will move τ toward τ_e. Warming or cooling due to pressure changes during ascent or descent may prevent τ from reaching τ_e, however.

An f' scale has been plotted across the top of the chart. This scale has been arranged so that for any point on the chart $f' = \sigma(1 - \tau)/(\tau - \sigma)$. Since this is the condition relating f' and τ when the sum of the gravitational

and buoyant forces is zero, both the f' and τ values of a stably floating balloon system can be represented by a single point on the chart. If the f' and τ values for a balloon system do not plot as a single point on the chart, the balloon system will have a non-zero free lift. That free lift will be upward (+) if the τ,H point lies to the left of the f',H point and downward (-) if the τ,H point lies to the right of the f',H point. Further, its magnitude will vary as the distance between the two points.

An excursion from a stable float level must be expected each evening as the sunset effect increases τ_e unless compensatory ballast is dropped. For example, a balloon floating stably during the day at 45 km can be represented by point 1 in Fig. 12. At that point τ_e is 1.029 and f' is +0.033. As the sun approaches the horizon at sunset, the τ_e curve will start to migrate to the right, and as it does, τ for the balloon will increase. If ballast is dropped at precisely the right rate during the sunset transition, the points representing both the τ,H and f',H status of the balloon system can be made to move horizontally together from point 1 to point 2 on Fig. 12. Since at point 2, $f' = +0.145$, enough ballast must have been dropped to change f' from 0.033 to 0.145; any less ballast will not let the balloon reach its nighttime

value of τ_e without losing altitude. The following morning as sunrise causes the τ_e curve to migrate back toward its day value, the τ,H point representing the balloon will move leftward also, lagging the τ_e curve slightly. As the gas warms, it will be expelled through the ducts, thereby automatically causing the f',H point to move coincidentally with the τ,H point. The balloon system will be less massive than it was the previous day due to the loss of ballast and gas; consequently, it will climb slowly as it warms and occupy a slightly higher position on the day τ_e curve than it had occupied the previous day.

If no ballast is dropped at sunset, the τ,H point representing the balloon will move toward the right in an effort to follow the τ_e curve as it migrates. As soon as τ changes, however, without a compensating change of f', the balance of hydrostatic and gravitational forces will be disturbed and the balloon will start descending. Descent will be accompanied by an increase in pressure and warming of the gas, which will tend to move τ to the left on the chart. The point representing the τ,H state of the balloon cannot cross the vertical dotted line below point 1, however, because if it did so the combination of τ and f' would cause an upward resultant force on the balloon

system. This would stop the downward motion until the gas could cool enough to initiate it again. The nighttime τ_e curve and the f',H curve of the balloon then serve as boundaries which the τ,H point, moving along its sunset (SS) path, cannot cross. Ultimately, the τ,H point of the balloon will reach point 3 and since it cannot cross the τ_e and f',H curves, the balloon will have again reached a stable float condition, where it will remain until sunrise causes the τ_e curve to start migrating leftward. The balloon will then rise and the τ,H point will follow the sunrise (SR) path back to point 1. The maximum nighttime excursion, if no ballast is used and no gas is lost, is just the vertical distance between the day and night τ_e curves.

A balloon floating stably at point 4 during the day would have a lower f' value than the lowest possible f' value of any point on the night τ_e curve. Therefore, the τ,H curve of such a balloon descending at sunset might reach all the way to the surface, as shown by the trace marked SS path below point 4, without encountering an intersection of the nighttime τ_e and the balloon's f',H curves. Only if the balloon were to descend so slowly during the sunset and night that it were caught by the τ_e curve as that curve migrates leftward at sunrise would it not descend all the way to the surface. Any balloon

floating lower during the day than the level represented by point 4 should be expected to descend to the surface at night under conditions such as those depicted by Fig. 12.

The τ_e curve for a cloudy night can be used in conjunction with the other τ_e curves to illustrate the effect of a cold cloud layer. Assume that a balloon at point 1 has been maintained at 40 km through sunset by ballasting and is floating stably at night at point 2 when a cloud layer forms under it. More ballast, dropped at the right rate, will force it to maintain its altitude and move its τ,H point to point 2′. If no additional ballast is dropped, the balloon will descend and its τ,H point will move to point 2′′. In either event, sunrise the following day will cause it to move back to a point slightly above point 1 on the clear day τ_e curve if the cloud layer has disappeared or to an equivalent point on a cloudy day τ_e curve (not shown).

If a balloon is floating stably at point 3 at night when a cloud layer forms under it, it will immediately start moving downward, its τ,H point moving along a path similar to that followed from point 1 to point 3 at sunset. Unless ballast is dropped, the balloon will descend to the level marked 3′ and float there until further adjustment of the τ_e curve occurs. If the

cloud remains unchanged, no adjustment will occur before sunrise the following day, but if the cloud should disappear before sunrise, the τ_e curve will lift up to the clear night τ_e curve and the balloon will rise toward level 3 again. Thus, it is quite conceivable that with variable cloudiness, a balloon may descend and ascend through short distances several times during a day or night period.

Another possible effect of a cold cloud layer is to open wider the "trap door" through which the balloon may descend all the way to earth at night. In Fig. 12, for example, any balloon floating stably on a clear day below an altitude of 30 km would have a good chance of descending all the way to earth on the following clear night. If a cloud should appear at night as shown in the figure, any balloon floating during the day below 33 km could conceivably descend all the way to earth.

It is often not necessary to maintain an unvarying float level throughout a flight; yet the magnitude of the excursions which would occur from day to night without ballast may be too large to be tolerated. In a situation like that depicted by Fig. 12, any ballasting which results in an increase in f′ will decrease the magnitude of the excursion. A balloon at point 1 prior

to sunset can, for example, be ballasted at such a rate that it will maintain level float until f′ reaches +0.10. If ballasting is then stopped, the balloon system will start descending, but it can descend only to the point where the night τ_e curve crosses the f′ = +0.10 line. Since that occurs at about 34 km, the nighttime excursion will be 6 km instead of the 15 km which would occur without any ballasting. It does not matter when the ballast is dropped as long as the drop occurs far enough about the 34 km level to enable the balloon system to stop there and provided that the drop does not occur so early that it forces the balloon above its fully-inflated float level and causes it to vent gas. If gas is vented, f′ will be decreased by the gas loss and the ballast will not have been fully effective. It is also pertinent to note that at the following sunrise, a balloon from which ballast has been dropped at night to limit its excursion will vent gas. Then the excursion the following night will again be the vertical distance between the day and night τ_e curves unless additional ballast is dropped to limit it.

Figure 13 is a τ,H diagram showing the same clear day and night τ_e curves as Fig. 12. The dotted line segment leading from point 1 to point 2 represents the path followed by the f′,H point of a slowly leaking balloon.

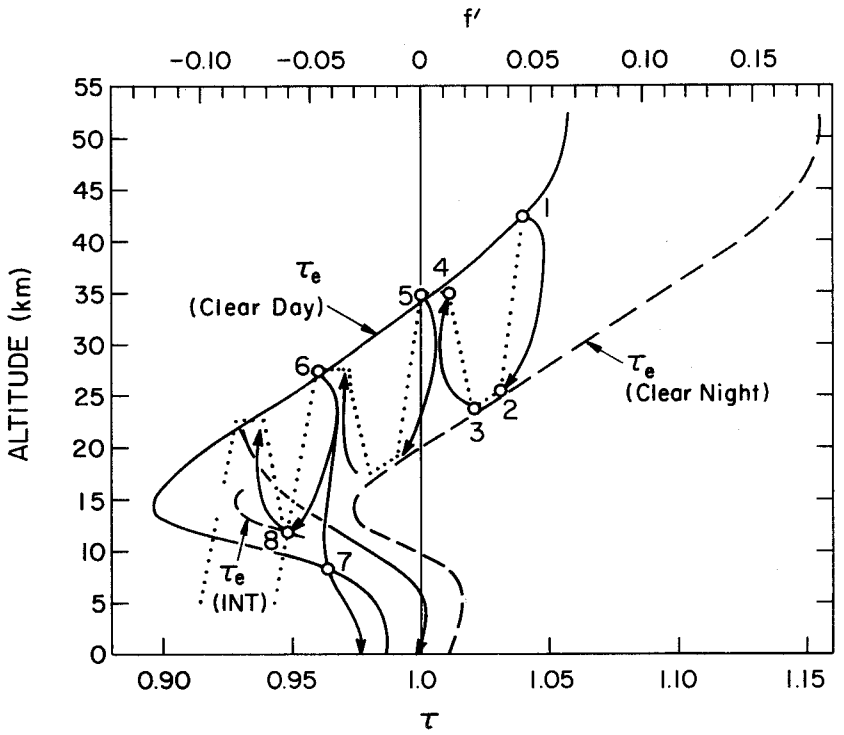

Fig. 13. Diurnal excursions of a slowly leaking, helium-inflated, polyethylene balloon in a typical summer, mid-latitude, continental atmosphere.

The τ,H point of the balloon will follow the solid curve from point 1 to point 2. Both curves are approximate; the important thing to bear in mind is that the f',H curve should show a decreasing value of f' and that during descent the τ,H curve should be to the right of the f',H curve. This assures negative buoyancy, which is essential to continued downward motion.

When the balloon reaches point 2, downward motion would cease if there were no leak. Because there is a leak, the downward motion must continue and the compressive heating will cause τ to be slightly lower than τ_e. Thus, the balloon will continue to descend along characteristic f',H and τ,H curves which are nearly identical and a little to the left of the night τ_e curve on the graph. As sunrise starts to influence the balloon at point 3, it will rise, eventually reaching its highest level at point 4, a point near the day τ_e curve. Because of the leak it will then start to descend, warming because of the increase in pressure so that is τ,H curve will cross the day τ_e curve. As the f',H and τ,H curves reach point 5, the effects of sunset overtake the balloon and start it on a second descent.

If the diurnal cycle of τ_e does not change at any level while the leaking balloon is flying, the balloon will descend further each night than it will

ascend on the following day. Its τ,H and f',H paths will progress leftward and downward on the chart in a series of up and down motions until one night the balloon's f',H curve will not intersect the τ_e curve during descent and the balloon will descend all the way to the surface. In Fig. 13, two possibilities are shown. One possibility is that after the balloon leaves point 6 it will descend past the day position of the τ_e curve at point 7 before the following sunrise can influence it. If it does, it will descend to the surface, even though it may not reach ground until well after sunrise. The second possibility is that sunrise will influence the balloon in its descent from point 6 before it has reached the position of the day τ_e curve. If the τ_e curve as it is migrating leftward at sunrise catches the balloon as shown by the τ_e(int) curve segment at point 8, the balloon will go through another ascent before it starts its final descent.

In the example of a leaking balloon discussed above, it was assumed that the leak was slow and continuous. A larger leak would have permitted the balloon to undergo fewer diurnal oscillations before bringing it to the surface. A leak large enough to decrease f' faster than compensatory changes in τ can be produced by sunrise will prevent the balloon from ascending, though

the descent rate will vary from day to night. Gas may leak or be valved rapidly enough to produce descent in a few hours. Figures 14 and 15 show the approximate form of some possible valved descent curves.

The A and A′ curves of Fig. 14 are the f′,H and τ,H curves respectively of a balloon which has descended to the surface during the daytime from level 1, where it was floating stably. The A curve shows that gas was valved rapidly for a short time to initiate descent and then subsequently left unchanged. Initially, since the vertical velocity of the balloon was zero, the loss of lift caused rapid downward acceleration. As the balloon moved downward, the increasing pressure warmed the gas above its equilibrium temperature, causing the balloon's τ,H curve to shift away from the τ_e curve toward lower values of τ. Also, as the downward velocity increased, aerodynamic drag built up. As descent continued above level 2, the τ,H curve moved closer to the f′,H curve and downward velocity decreased until at level 2 the balloon was barely descending. Only a little less gas loss due to valving would have caused the balloon to reach a state of stable, level flight just above level 2. As the balloon descended below level 2, however, it entered an environment in which the value of τ_e increased rapidly as height decreased. Its own τ adjusted

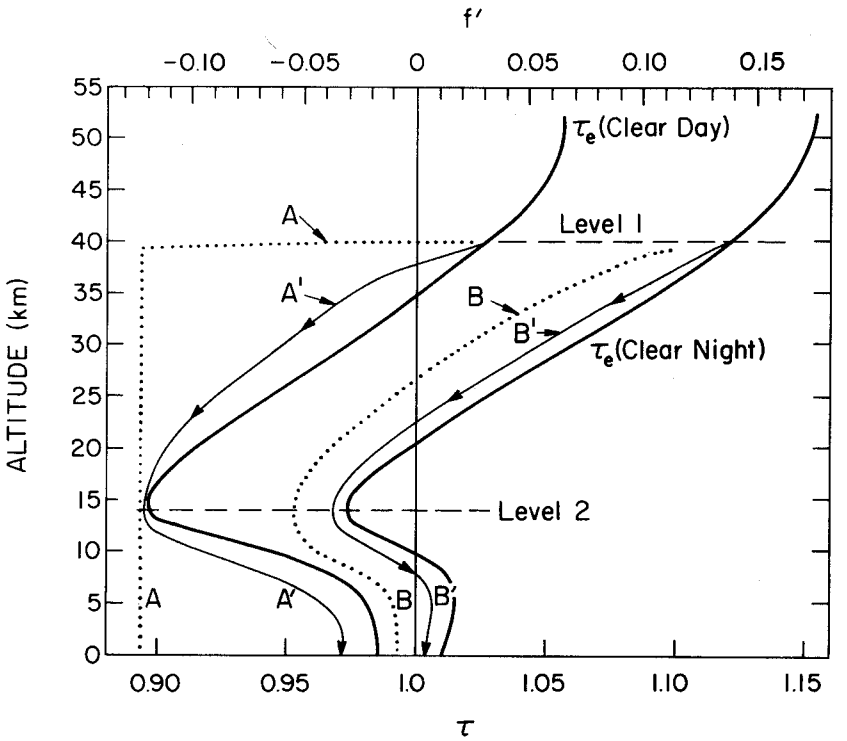

Fig. 14. Valved descent of a helium-inflated polyethylene balloon in a typical summer, mid-latitude, continental atmosphere.

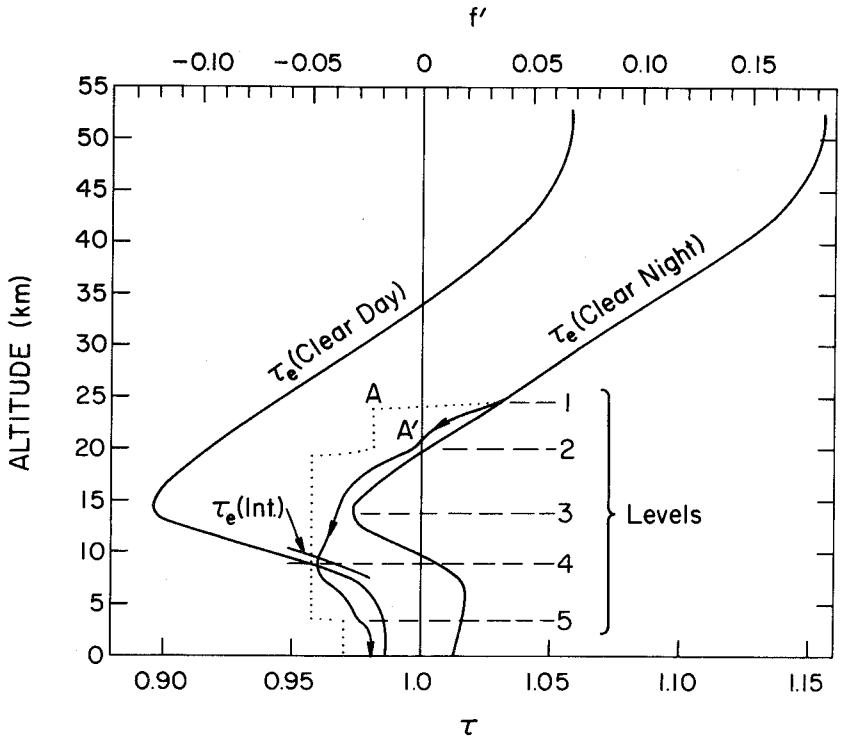

Fig. 15. Stepwise valved descent of a helium-inflated, polyethylene balloon in a typical summer, mid-latitude, continental atmosphere.

upward in response to the higher τ_e, and as its f′,H and τ,H curves moved apart it accelerated downward again, reaching a high but nearly constant speed just a little way above the surface.

A nighttime descent is shown by the B and B′ curves in Fig. 14. In this case continuous control was exercised during descent. As shown by the curves, gas was valved at a rate which kept the B and B′ curves separated by a nearly constant distance down to level 2, and ballast was dropped at the proper rate to maintain the constant separation below level 2. This resulted in an approximately constant descent rate, and because of the constant descent, the displacement of the B′ curve from the night τ_e curve was also approximately constant.

The simple broad brush treatment of a day and night descent given in the last two paragraphs is not meant to imply that one valving technique is a daytime technique while the other is a nighttime technique. Either can be applied at any time, in principle, but in practice neither is used. In one, only initial valving is used; in the other, either valving or ballasting is being used continuously. Practical limitations in a real flight, including limited knowledge about how a balloon system will react to a change in f′,

prompts most flight directors to valve or ballast in what amounts to small increments. In Fig. 15 and the next paragraphs, steps are outlined by which a more complicated descent may be accomplished using stepwise valving or ballasting. The purpose is to illustrate the behavior of a balloon system in a relatively complex situation, without getting caught up in attempts to answer quantitative questions of timing, etc.; therefore, the treatment is again highly simplified.

The problem is to bring a balloon system which is floating stably at level 1 at night to the surface intact using a minimum of ballast. Gas is valved rapidly for a short time to start the descent from level 1 as shown by the f′,H trace, curve A. As the downward speed increases the τ,H trace of the balloon, curve A′, separates from the night τ_e curve, but as the τ,H trace approaches the first constant portion of the f′,H trace, vertical velocity slows and the τ,H curve swings back toward the τ_e curve. At level 2, gas is valved again in a short burst causing the τ,H curve to increase its distance from the τ_e curve again.

The valving which was done at level 2 was enough to cause the balloon to descend past level 3, and indeed all the way to the surface if it does not get

caught by the migrating τ_e curve at sunrise. Thus the minimum gas which must be ejected is that will will cause the τ,H curve to cross the daytime position of the τ_e curve just short of the intersection of that curve with the f′,H curve just before the τ_e curve reaches that position. A short section of an interim τ_e curve as it is approaching the day position of the τ_e curve is shown as τ_e(int) in Fig. 15. Incidentally, the τ,H point representative of the balloon will stay ahead of the migrating τ_e curve as long as the balloon is descending and the atmospheric lapse rate is less than the adiabatic lapse rate of the gas in the atmosphere. Thus, the τ,H point as it traces out curve A′ from level 3 to level 4 does not move away from the τ_e curve; it actually moves nearer the interim τ_e curve as it approaches the f′,H curve. If the τ,H point should intercept the f′,H curve as it moves leftward and downward ahead of the migrating τ_e curve, the balloon's downward motion will stop; it will be overtaken by the τ_e curve and, unless additional gas is valved, it will start ascending again.

Once the balloon system has descended below the day position of the τ_e curve, it will gain speed as it descends, if left to its own devices, until it reaches approximately the 3 km level. From there down the speed will be

nearly constant. If that speed is too great for a proper landing, ballast can be dropped as shown at level 5 to slow the descent. The key to making a descent such as this with minimum ballast is to have the balloon system penetrate the position of the day τ_e curve position with near zero speed just before the τ_e curve reaches that position.

REFERENCES

(1) Streeter, V. L., 1961: Handbook of Fluid Dynamics, McGraw-Hill, New York, Sections 4 and 13.

(2) Hoerner, S. F., 1965: Fluid-Dynamic Drag, published by author, 148 Busteed Drive, Midland Park, N. J. 07432.

(3) Sherburne, Paul A., 1968: Wind Tunnel Tests of a Natural Shape Balloon Model, AD 667563, Goodyear Aerospace Corp.

(4) Peters, Penn A., Shojiro Shindo, Hilton H. Lysons, 1972: personal communication with Mr. Peters. Forest Engineering Research, U.S. Forest Service, Seattle.

(5) Anonymous, 1961: Handbook of Geophysics, Rev. Ed., The MacMillan Co., New York, 5-41.

(6) Staff, Dept. of Physics, Univ. of Minnesota, 1953: Progress Report on High Altitude Balloons, Vol. IX, Office of Naval Research Contract NONR-710(01).

(7) Gergen, John L., 1957: Atmospheric Infrared Radiation over Minneapolis to 30 Millibars, Journal of Meteorology, Vol. 14, December 1957, 495-504.

SECTION III

ENERGY BALANCE AND A FLIGHT MODEL

by

Frank Kreith

LIST OF SYMBOLS

Symbol	Description	Dimensions
a	absorptance	
a	subscript identifying its symbol with air or atmosphere	
a_z	the angle measured from the south meridian of the projection on the earth's surface of the normal to a tilted surface	deg
A	area	L^2
A_z	azimuth of the sun from the south meridian	deg
b	film thickness	L
b	subscript identifying its symbol with ballast	
B	subscript identifying its symbol with the balloon	
c	subscript identifying its symbol with convection	
c_f	specific heat of film	$L^2T^{-2}\theta^{-1}$
c_v	specific heat at constant volume	$L^2T^{-2}\theta^{-1}$
C_D	drag coefficient	
C_M	virtual displacement coefficient	
d	subscript identifying its symbol with ducting	
D	diameter, used as a primary symbol and as a subscript	L
e	emittance	
e	subscript identifying its symbol with earth	
$\dot{E}_d$	volumetric gas flow rate through the ducts	L^3T^{-1}
$\dot{E}_v$	volumetric gas flow rate through valves	L^3T^{-1}

f	subscript identifying its symbol with the balloon film or fabric	
f′	fractional, nominal free lift	
F	force	MLT^{-2}
F	subscript identifying its symbol with free lift	
g	acceleration due to gravity	LT^{-2}
g	subscript identifying its symbol with the lift gas	
G	radiation incident on a unit surface in unit time (W/m^2)	MT^{-3}
G	subscript identifying its symbol with gross lift	
G_s	solar constant (1395 W/m^2)	MT^{-3}
GHA	Greenwich hour angle	deg
h	local hour angle	deg
h_c	heat transfer coefficient	$MT^{-3}\theta^{-1}$
i	the plane angle which measures the dihedral angle between a tilted plane and a horizontal plane	deg
i	subscript identifying its symbol with infrared	
I	intensity of radiation (W/steradian)	ML^2T^{-3}
J	joule	ML^2T^{-2}
k_a	thermal conductivity of air	$MLT^{-3}\theta^{-1}$
k_g	thermal conductivity of lift gas	$MLT^{-3}\theta^{-1}$
ℓ	length dimension	L
ℓ	subscript identifying its symbol with the payload	
ℓ'	equivalent length dimension selected by Börner to correlate free convection for several shapes with one equation; also used as a subscript	L

L	length dimension	L
L′	lapse rate (-dT/dz) of a stratum in the atmosphere	θL^{-1}
L_F	free lift	MLT^{-2}
L_G	gross lift	MLT^{-2}
m	mass	M
m	optical air mass; also used as a subscript	
M	molecular weight	$M(M\text{-mol})^{-1}$
o	subscript identifying its symbol with a base state, e.g., z_o is zero height	
p_a	pressure of ambient air	$ML^{-1}T^{-2}$
p_g	pressure of lift gas	$ML^{-1}T^{-2}$
$\dot{P}$	power dissipation	ML^2T^{-4}
q	rate of heat transfer	ML^2T^{-3}
r	radial distance	L
r	reflectance	
R	universal gas constant (8314.32 J/Kg-mol°K or 1.9859 BTU/lb-mol°R)	$L^2T^{-2}\theta^{-1}$
s	subscript identifying its symbol with the sun	
S	surface area	L^2
t	time	T
t	thickness of cloud; also used as a subscript to indicate that its symbol is a function of thickness	L
T	temperature	θ
v	subscript identifying its symbol with a valve or valving	

v	specific volume	L^3M^{-1}
V	volume	L^3
V_a	volume of air	L^3
V_g	volume of gas	L^3
x	ratio of a horizontal and vertical distance (Fig. 8)	
y	see x above	
z	altitude (frequently given as a geopotential height)	L
z	subscript identifying its symbol with height	

Greek letters

α	absorptance	
β	temperature coefficient of volume expansion [$1/T(^\circ K)$] for an ideal gas	θ^{-1}
δ_s	solar declination	deg
ζ	zenith angle of the sun	deg
θ	polar angle (see Fig. 9)	deg
λ	wave length of radiation	L
λ_1	latitude	deg
μ	micron (standard abbreviation for 10^{-6} m)	L
ρ	mass density	ML^{-3}
ρ	bidirectional reflectance	
σ	Stefan-Boltzman constant	$MT^{-3}\theta^{-4}$
σ_s	solar declination	deg
τ	transmittance	
τ	angle between a tilted surface and the horizontal	deg

ϕ	angle between the normal to a tilted surface and the bearing of the sun	deg
φ_1	longitude	deg
ψ	azimuth angle (see Fig. 9)	deg

List of Figures

List of Tables

ENERGY BALANCE AND A FLIGHT MODEL

A. INTRODUCTION

The vertical motion of balloon systems depends critically on the heat transfer to and from the gas inside, because the temperature and the pressure of the gas determine the lift of the balloon. In the past the thermal design of high altitude balloons has largely been based on a combination of experience, empirical data, and approximate calculations (1, 2). Recent advances in heat transfer research make it feasible, however, to calculate the temperature of the lifting gas as a function of altitude and to predict the vertical motion of the balloon system with the aid of high speed computers (3, 4).

There are three general problem areas in which thermal design can improve balloon operation. The first involves rapid variations in internal energy, which occur when clouds cause sudden changes in the radiation incident on the balloon. This type of change in the heat transfer rate is usually sensed only after the altimeter registers a change. After an altitude change is registered, altitude is maintained by dropping ballast or

exhausting gas. If one could control altitude by reacting rapidly and precisely to a change in radiation, the loss of ballast or gas could be reduced. The second area of thermal design is concerned with changes in heat loss during a complete day. More accurate predictions of heat loss and the use of appropriate materials or surface coatings could increase the payload or the float altitude for a given balloon system. The third area of thermal design involves long-range planning for balloon flights, such as those currently envisioned in the equatorial zone over new routes.

This section reviews recent advances in heat transfer experimentation and theory pertinent to the processes which affect the calculation of balloon performance and the thermal design of balloon instrument packages. Finally, the pertinent equations of fluid mechanics, heat transfer, and thermodynamics are combined to predict analytically the vertical motion of balloons.

B. THE ENERGY EQUATIONS

The conservation equation for the gas inside the skin of a balloon can be obtained by applying the First Law of Thermodynamics (Fig. 1). The rate of change of the internal energy of the gas equals the rate at which heat is

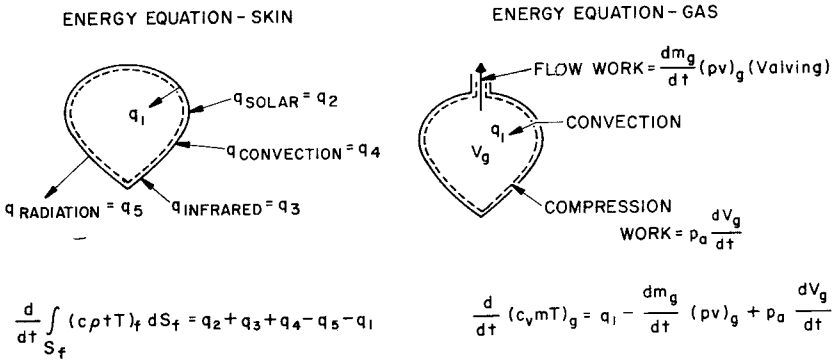

Fig. 1. Schematic illustrating energy balance for lifting gas and balloon skin.

transferred to the gas (q_1) minus both the rate at which net work is done by the gas and the rate at which internal energy is lost by valving. Assuming that the equation of state of the gas can be approximated by the ideal gas law and that the temperature and pressure of the gas inside the balloon are uniform, one obtains

$$\frac{d}{dt}(C_v m \bar{T})_g = q_1 + \frac{RT_g}{M_g}\frac{dm_g}{dt} - p_a \frac{dV_g}{dt} + (C_v T)_g \frac{dm_g}{dt} \qquad (1)$$

where the term on the left-hand side of Eq. (1) is the rate of change in internal energy of the balloon gas; the first term on the right-hand represents the rate of heat transfer by free convection from the interior surface of the balloon skin to the gas; the second term, the flow work done during gas release; the third term, the work done on the external pressure when the balloon volume changes because of a change in gas temperature or because of valving; and the last term the loss of internal energy by valving. If the pressure inside the balloon is uniform and equal to the atmospheric pressure, the flow work done during valving in the absence of heat transfer equals the work done by the atmosphere on the balloon, and the second and third terms cancel.

The assumption that the temperature of the gas inside the balloon is uniform may lead to serious error when short-term transients occur, and the gas adjacent to the balloon skin undergoes temperature variations while the gas in the interior does not. When this situation prevails, the term on the left-hand side of the energy equation should be replaced by

$$\frac{d}{dt}\iiint_{V_g} C_{vg}\rho_g T_g dV_g$$

A similar analysis can be performed on the balloon skin. The internal energy of the skin will change only because of heat transfer to and from its surfaces. The skin is so thin that one can neglect the temperature drop across it at any location, but since the heat transfer over the skin is not uniform, its temperature will vary. This variation cannot, however, be expressed analytically, and when it becomes important, only a numerical analysis can yield a satisfactory approximation of the physical reality.

To simplify the thermodynamic analysis, it will be assumed that an averaged skin temperature can be used. A First Law analysis (Fig. 1) then gives

$$\frac{d}{dt}\iint_{S_f} C_f\rho_f t_f T_f dS_f = C_f m_f \frac{d\bar{T}_f}{dt} = q_2 + q_3 + q_4 - q_5 - q_1 \qquad (2)$$

where C_f is specific heat of skin, m_f is mass of skin, $\bar{T}_f$ is average skin temperature, ρ_f is density of the balloon skin, q_2 is rate of absorption of solar radiation = ($q_{2,\,\text{direct}} + q_{2,\,\text{reflected}}$), q_3 is rate of absorption of infrared radiation, q_4 is rate of heat transfer by convection from the atmosphere to the skin, q_5 is rate of radiant heat transfer from the skin, t_f is thickness of film, S_f is surface area of balloon, and q_1 is rate of heat transfer by convection from the skin to the lift gas.

The energy equations for the balloon gas and the skin fabric can be treated analytically if one assumes that all of the gas is at one temperature and the entire skin is at one temperature (these two temperatures may or may not be identical). This assumption is quite good at night, but can introduce appreciable errors during the day when solar energy heats the skin unevenly. Modifications for non-uniform heating could be made in the analysis (5) for the exterior of the fabric skin by numerical means, but the convection process inside a non-uniformly heated, balloon-shaped container is very complex. At this time the process is not well enough understood to be modeled analytically; thus, an accurate calculation of the heat transfer in the interior is not possible. Fortunately, during normal flight, balloons

rotate so all parts of their skins are exposed equally (on the average) to the sun and the balloon gas is mixed. This makes the assumption of uniform gas and skin temperatures valid for thermal analyses performed for times ranging from hours to days.

In the following three sub-sections, the heat transfer phenomena in balloon systems will be examined in the light of recent advances in heat transfer research. Sub-sections C and D will deal with convection and Sub-section E with radiation phenomena. The final objective will be the evaluation of the five heat transfer terms in Eq. (2).

C. CONVECTION BETWEEN THE ATMOSPHERE AND THE BALLOON SYSTEM [q_4 in Eq. (2)]

Convective heat transfer between balloon systems and the atmosphere occurs over wide ranges of the convectional parameters used to describe the process. Heat is transferred between the atmosphere and the balloon by forced convection or free convection, or both, at Reynolds numbers from 0 to 10^7 and Grashof numbers from 0 to 10^{11}. Depending on the circumstances, the flow can be laminar or turbulent. The shapes of superpressure balloons resemble a sphere, those of zero-pressure balloons resemble an onion, but instrument packages come in a variety of shapes, such as cubes,

cylinders, and plates. Balloon diameters may range from one to 100 m (3 to 330 ft), ascent velocities from near zero to 12 m/sec (0 to 40 ft/sec), and temperature differences (between the skin and gas) from zero to $30C^o$ (0 to $55F^o$).

Although convective heat transfer to and from an object in air has been studied extensively, few investigations extend into the extreme Reynolds- and Grashof-number ranges encountered by balloons and none have specifically treated the onion shape typical of zero-pressure balloons. Therefore, approximations and extrapolations of existing data are unavoidable.

Heat transfer from spherical shapes in forced convection has recently been investigated experimentally by Yuge (6) and Vliet and Leppert (7). Local values of the heat transfer coefficient in flow over a sphere in the neighborhood of the stagnation point have been calculated by Merk (8). The pressure distribution for flow over spheres has been investigated by Fage(9), who also measured the separation point. He found that at a Reynolds number of 1.6×10^5, separation occurred at a polar angle ϕ of 70^o and moved toward the rear with increasing Reynolds number. At the highest Reynolds number of his tests, $Re_D = 4.2 \times 10^5$, separation occurred at a polar angle

of 100°. The subscript D indicates that the diameter of the sphere was used in calculating the Reynolds number.

Extensive correlations of experimental data indicate that in forced convection the average Nusselt number, Nu, of the entire surface of a sphere of diameter D in air can be obtained from the relation

$$Nu_{D,m} = \frac{\bar{h}_c D}{k_a} = 2 + 0.30\ Re_{D,m}^{0.57} \qquad (3)$$

for Reynolds numbers between 1.8×10^3 and 1.4×10^5 (6) or from the relation

$$Nu_{D,m} = \frac{\bar{h}_c D}{k_a} = 2 + 0.41\ Re_{D,m}^{0.55} \qquad (4)$$

for Reynolds numbers between 0.4 and 2×10^5 (7). In both of the above equations, the subscript m indicates that all physical properties should be evaluated at the mean temperature between the skin and the atmospheric temperatures.

Using Eq. (4), the rate of heat transfer by convection to or from the surface of the balloon skin during ascent or descent can be written in the form

$$q_4 = 3.9\ V_g^{1/3}\ k_a(T_a - \bar{T}_f)\left(2 + 0.472\ V_g^{0.183}\left[\rho_a \frac{|dz/dt|}{\mu_a}\right]^{0.55}\right) \qquad (5)$$

Krause and Schenk (10) investigated thermal free convection from a warmer surrounding fluid to a cooler spherical body at uniform surface temperature in the range of Rayleigh numbers ($Gr_D \times Pr$) between 6×10^2 and 5×10^8. The experimental results for the local heat transfer coefficient agree reasonably well with a theoretical analysis of Merk (11) up to the hydrodynamic separation point, which for the narrow Grashof-number range of this investigation occurred at a polar angle of about 145° from the vertical axis. Since Merk's theory applies equally well for laminar free convection from a heated sphere, it also seems reasonable to use it to calculate heat transfer from the upper hemispherical surface of heated balloons. No theory or data exist at present, however, to predict the influence of the non-uniform azimuthal temperature distribution, which is always present when the balloon is heated by the sun.

Experimental evidence is contradictory regarding the influence of the Grashof number on the separation point in laminar free convection to or from a sphere. Garner, et al. (12, 13) found a shift in separation point from 155 to 100° between mass transfer Rayleigh numbers ($Gr_D \times Sc$) from 1.5×10^8 to 5.5×10^8 for different fluids with $800 < Sc < 2{,}200$, whereas

Schütz (14) found a much weaker dependency in the region $2 \times 10^8 < Gr_D \times Sc < 2 \times 10^{10}$ (170 to 135°) for a fluid with Sc = 1,800. According to conventional boundary layer theory, the separation point should shift toward the stagnation point with increasing Grashof numbers and the heat transfer coefficient in the region of the free convection plume, where the flow is turbulent, will be larger than in the laminar flow regions. The results agree qualitatively with observations of free convection about a horizontal cylinder.

The point of transition from laminar to turbulent flow in the free convection regime is not presently known. Schlieren patterns (10) show that purely laminar flow prevails over a sphere between the stagnation point and the equator at Grashof numbers as high as 6×10^8 and that some disturbances exist between 100° and separation (190 to 150°), but real turbulence was observed only in the plume at a Grashof number of about 10^9. Perhaps the stability analysis of Gebhart (15) could be applied to natural convection over a balloon-shaped body (idealized as a sphere) to analytically predict the point of transition. Gebhart's analysis for a flat plate predicts that

turbulent instabilities could amplify at local Grashof numbers of the same order of magnitude as have been observed on balloons.

If the designer can use averaged values of the heat transfer coefficient over the entire surface of the sphere, available data can be correlated (10) by a relation of the type

$$\overline{Nu}_{D,m} = \frac{\overline{h}_c D}{k_a} = 2 + 0.6\ (Gr_D \times Pr)_m^{\frac{1}{4}} \qquad (6)$$

for Rayleigh numbers between 10^5 and 2×10^{10}. The constant value of 2 applies in the limit as the Grashof number approaches zero and the heat transfer mechanism approaches pure conduction. The theoretical convergence of the Nusselt number at small Grashof numbers has recently been elegantly verified by Fendell (16).

The influence of vibration on the heat transfer from spheres has been investigated in free and forced convection (17), and the influence of rotation about a vertical axis has been studied experimentally for free convection (18, 19). The results of these investigations indicate that under flight conditions neither vibration nor rotation will influence balloon heat transfer characteristics.

Using Eq. (6), the rate of heat transfer by free convection to or from a balloon at float altitude can be written in the form

$$q_4 = 7.79\, V_g^{1/3} k_a (T_a - \bar{T}_f) \left[1 + 0.322 \left(\frac{\rho_a^2 g \,|T_a - \bar{T}_f|\, V_g}{T_a \mu_a^2}\right)^{1/4}\right] \qquad (7)$$

For computational purposes a very convenient correlation of averaged experimental convection data has recently been provided by Börner (20), who reviewed 70 previous investigations of heat and mass transfer by free convection or forced convection, or both, in flow over single bodies, and who also conducted additional tests. One convenience of Börner's correlation is that data for bodies of different shapes can be handled (21) by choosing a pertinent length dimension, ℓ', defined in Table 1 for several shapes.

Reference (20) presents correlations of free convection data for horizontal and vertical plates, spheres, and horizontal and vertical cylinders as plots of $\overline{Nu}_{\ell'} = \bar{h}_c \ell'/k$ vs $(Gr_{\ell'} \times Pr) = (g\rho^2 \beta \Delta T \ell'^3/\mu^2) \times (C_p \mu/k)$ and of forced convection data in the form $\overline{Nu}_{\ell'}$ vs $Re_{\ell'}$. A combined free and forced convection correlation was obtained by defining an equivalent Reynolds number for free convection $Re_{\ell'}^*$

$$Re_{\ell'}^* = f(Pr)(Gr_{\ell'})^{1/2} \qquad (8)$$

Table 1

Equivalent Length Dimensions of Convection Correlation

Shape of Body	Equivalent Length ℓ'
Very wide plate with surface parallel to the flow in forced convection with length ℓ in direction of flow	$\ell' = \ell$
Sphere or long cylinder of diameter D with axis perpendicular to the flow in forced and free convection	$\ell' = (\pi/2)D$
Long rectangular bar of width a* and height b* with its long axis perpendicular to the flow in forced convection	$\ell' = a^* + b^*$
Vertical plate (surface parallel to gravity) of height ℓ in free convection	$\ell' = \ell$
Long horizontal plate (surface perpendicular to gravity) of width ℓ in free convection	$\ell' = \ell/2$

where the function f(Pr) for air, which is dependent upon the Prandtl number, should be taken equal to $\sqrt{\frac{1}{2}}$ for a "best fit correlation," compared to 0.64 predicted by analysis. With the definition of an equivalent Reynolds number for free convection given in Eq. (8), free convection dominates when $Re_{\ell'} < 2.4\ Re_{\ell'}^*$ and forced convection dominates when $Re_{\ell'}^* < 2.4 Re_{\ell'}$. A transition region, where both free and forced convection are appreciable, exists between these limits. It has been shown that in this transition region free convection aids the forced convection transfer when the motion caused by buoyance is in the same direction as the forced flow and retards it (22, 23) when buoyancy opposed the flow. In order to bridge the gap between forced and free convection Börner (20) defines a third Reynolds number, $Re'_{\ell'}$, as

$$Re'_{\ell'} = \sqrt{Re^2_{\ell'} + (Gr_{\ell'}/2)} \qquad (9)$$

and then plots $Nu_{\ell'}$ vs $Re'_{\ell'}$. Figure 2 shows the results of this correlation for a sphere with downward forced convection. Under these circumstances free convection will oppose the forced convection flow, but visualization studies for this condition (20) have shown that the existence of a

free convection field will produce turbulence at low velocities and will also cause separation of the boundary layer. These effects tend to offset any decrease in the heat transfer, as predicted for purely laminar flow (22). The correlation function shown in Fig. 2 was also found to be applicable for upward flow. Sharma and Sukhatme (24) have recently published experimental results concerning the interaction between free and forced convection in flow over a horizontal cylinder for Reynolds numbers from 10 to 5,000 and Grashof numbers from 3×10^3 to 7×10^6. These results indicate chat the Reynolds number exponent n in the parameter Gr/Re^n is affected by turbulence and separation pehnomena and that a value of 3.25 is most suitable when free convection dominates, whereas a value of 1.8 is more suitable at the forced convection end. An average value of 2.5 was found to give a reasonably good correlation in the transition region.

Börner's correlation does not give insight into local variations of the heat transfer coefficient, but it is convenient. By computing $Re_{\ell'}$ and $Re_{\ell'}^*$ simultaneously and continuously from the time of launch until the balloon has reached the float altitude, a smooth transition between the

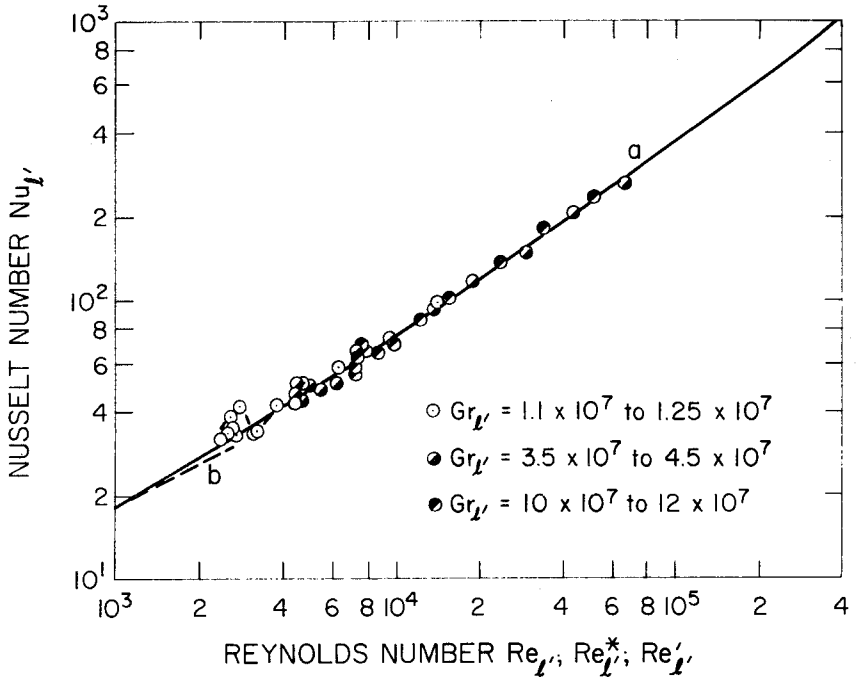

Fig. 2. Average Nusselt number for sphere in combined free and forced convective flow.

forced and free convection regions can be made and the influence of radiation can be superimposed directly.

In general, only the equilibrium temperature at float altitude is important to the thermal design of balloon instrument packages. During ascent forced convective heat transfer is quite effective (25) in maintaining a small instrument package at a temperature close to that of the ambient air, but when the balloon has reached its float altitude only free convection can transfer heat directly between the package and the surrounding air. The relative magnitude of the radiation to and from the surfaces of the package dominates the thermal transfer during the day, but convection enters prominently at night.

In certain specialized instrument packages, in addition to the averaged heat transfer coefficient, local values at the top and bottom surfaces are also sometimes of interest. The numerical study of Suriano and Yang (26) provides some insight into the flow and temperature field in the vicinity of a heated horizontal square plate at small Rayleigh numbers. Table 2 shows averaged Nusselt numbers obtained by their calculations for both the top and bottom surfaces. The temperature field over a horizontal plate at

Table 2

Average Nusselt Numbers for a Horizontal Plate in Free Convection

Ra	Pr = 0.72			Buznik and Bezlomtsev[1]
	x = 0-	x = 0+	Average	
0.	1.049	1.047	1.048	1.00
0.10	1.052	1.045	1.048	1.28
5.0	1.201	0.946	1.074	1.77
10.0	1.406	0.932	1.169	1.91
50.0	2.879	1.259	2.069	2.38
100.0	4.041	1.330	2.685	2.64
200.0	6.166	1.492	3.829	2.96
250.0	7.194	1.594	4.394	3.00
300.0	7.620	1.678	4.469	3.03

[1] Buznik, V. M. and K. A. Bezlomtsev, 1960: A generalized equation for the heat exchange of natural and forced convection during external flow about bodies. Izv. Uyssh. Ucheb. Zaved 2, 68-74; 1961: Ref. Zh. Meckl. 6, Rev. 6V506.

a Rayleigh number of 50 (Fig. 3) suggests boundary layer behavior on the lower surface but not on the upper. However, the analysis of Stewartson (27), as modified by Gill et al. (28), indicates that a boundary layer also forms over the upper surface of a heated horizontal strip and that the average Nusselt number for a strip of width L in air can be predicted from the relation

$$\overline{Nu}_L = \frac{\bar{h}_c L}{k_a} = 0.79\ Gr_L^{1/5} \qquad (10)$$

in the laminar flow region. This result is not in complete agreement with experimental data for the upper surface of a heated square plate of side L in air (29). These data give larger heat transfer coefficients that are correlated empirically by the relations

$$\overline{Nu}_L = 0.50\ Gr_L^{1/4} \quad (10^5 < Gr_L < 2 \times 10^7\text{, laminar}) \qquad (11)$$

$$\overline{Nu}_L = 0.125\ Gr_L^{1/3} \quad (2 \times 10^7 < Gr_L < 3 \times 10^9\text{, turbulent}) \qquad (12)$$

Heat transfer by free convection from the lower surface of finite heated plates (or to the upper surface of cooled plates) has recently been studied by Singh et al. (30) and Kimbadi et al. (31) for square and circular plates and a long strip. Local heat transfer coefficients are lowest in the

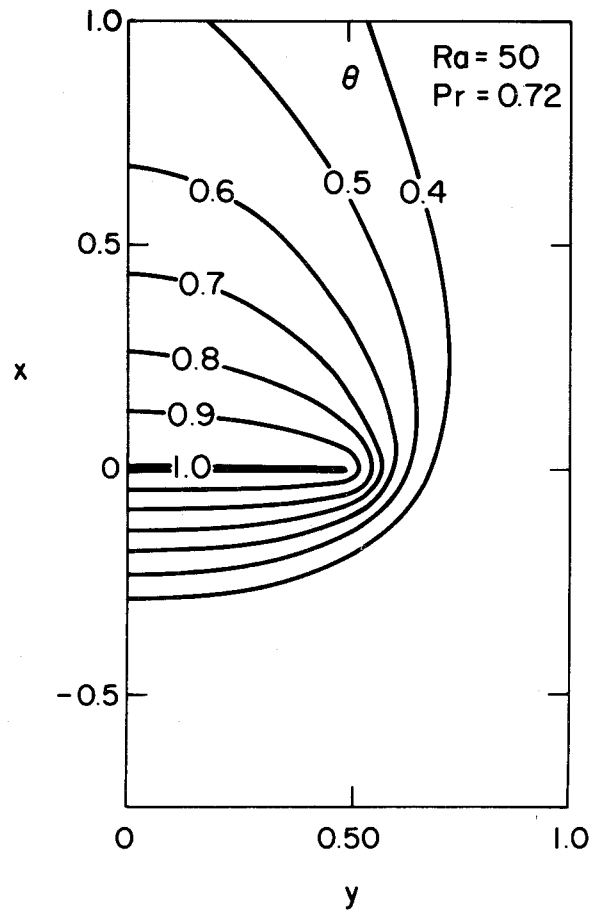

Fig. 3. Temperature field about a heated horizontal flat plate at a Rayleigh number of 50.

center and increase toward the edges. For a square plate of side L the local Nusselt number at a distance x from the center is

$$\frac{h(x)L}{k_a} = 0.58\ Ra_L^{1/5} \Bigg/ \left\{ \left[1 - \left(\frac{2x}{L}\right)^2 \right] + 0.271 \left[1 - \left(\frac{2x}{L}\right)^2 \right]^4 + \ldots \right\}^{1/4} \qquad (13)$$

The average Nusselt number for square plates, as well as for circular plates and long strips, is given by the relation

$$\overline{Nu}_L = \frac{\bar{h}\, L}{k_a} = C\ Gr_L^n \qquad (14)$$

where constants C and n are given in Table 3.

Flow-visualization experiments with a number of other shapes, with heated surface facing upward, have been reported by Husar and Sparrow (32), but information regarding the interaction between the boundary layer flow over vertical surfaces and the flow developing over horizontal surfaces (i.e., the top and bottom of boxes or vertical cylinders) is still lacking.

D. CONVECTION INSIDE THE BALLOON [q_1 in Eqs. (1) and (2)]

The convection process inside the balloon is important because it determines the temperature, the pressure, and the volume of the lift gas (usually helium). Little research has been done on convection inside a

Table 3

Constants for the Free Convection Equation (Eq. 14).

Reference Numbers		Constants	
		C	n
35 (analytical) 34 (experimental)	Square Plate[1] (L is length of side)	0.89 1.00	0.2 0.2
35 (analytical) 36 (experimental)	Circular Plate[1] (L is the diameter)	0.79 1.0	0.2 0.2
32 and 33 (analytical)	Long Strip[1] (L is the width)	0.80	0.2

[1] Heated surface facing downward, influence of side walls neglected.

sphere (33, 34) and none has been done on convection inside cavities resembling the shapes of high altitude balloons.

The heat transfer process is free convection. Hellums and Churchill showed as early as 1961 (35, 36) that the partial differential equations for the conservation of mass, momentum, and energy can be solved for laminar natural convection under many different conditions, but so far no solution for the heat transfer inside a balloon has been obtained. Investigations of natural convection in annuli (37) suggest that several types of flow patterns will exist as the temperature difference between the surface and the gas varies during a 24-hr period. It seems likely that in the daytime, when the balloon skin is warmer than the gas inside, there would be an upward flow near the balloon skin and downward flow in the interior. The reverse would be expected at night. But there could also be situations during the day when gas ascends on the side heated by the sun and descends on the cooler side. As a first approximation, one could use existing solutions for flow in a rectangular cavity heated on two sides as long as the flow is laminar. But the tremendous size of a balloon makes

it very likely that the flow will be turbulent, except for very small temperature differences.

A semi-empirical analysis (38) suggests that for turbulent free convection over a vertical plate the Nusselt number fits the relationship

$$\frac{\bar{h}_c L}{k_g} = 0.021 \, (Gr_L \times Pr)^{2/5} \tag{15}$$

at Grashof numbers of the order of 10^{12}, but Clark (39) suggests using a relationship of the type

$$\frac{\bar{h}_c D_g}{k_g} = C \left[\frac{\rho_g^2 \, g(\bar{T}_f - \bar{T}_g) D_g^3}{T_g \mu_g^2} \times Pr_g \right]^n \tag{16}$$

with the constants C and n selected from Table 4, and with all physical properties of the gas evaluated at the skin temperature.

Table 4

Free Convection in a Sphere
(Constant C and Exponent n for Eq. 16)

Gr x Pr	C	n	Type of Flow
10^4 - 10^9	0.59	1/4	Laminar
10^9 - 10^{12}	0.13	1/3	Turbulent

In the absence of more concrete information, Dingwell et al. (40) used Eq. (16) for their balloon study, with C and n equal to 0.13 and 1/3, respectively. Equation (16) can then be used to write the rate of heat transfer from the skin to the gas in the form

$$\begin{aligned} q_t &= \iint_{A_i} \bar{h}_c (T_f - T_g) \, dA_i = h_c \pi D_g^2 \, (T_f - T_g)_{ave} \\ &= 4.83 \, \bar{h}_c \, V_g^{2/3} \, (T_f - T_g)_{ave} \\ &= 0.628 \, V_g^{2/3} \, k_g \, (\bar{T}_f - \bar{T}_g) \left[\frac{\rho_g^2 \, g(\bar{T}_f - \bar{T}_g)}{\mu_g^2 \, T_g} Pr_g \right]^{1/3} \end{aligned} \tag{17}$$

Experimental data supporting the form of Eq. (16) have recently been reported by Ulrich et al. (41) for the transient condition encountered in filling a cylindrical tank with air at Grashof numbers between 10^8 and 10^{13}. The length-to-diameter ratio of their tanks varied between 0.5 and and 2.0, so their results should indicate what might occur inside a sphere. The experiments showed that during the initial stages of the process the heat transfer coefficients were significantly higher than those predicted by turbulent free convection, but agreement with the heat transfer rate predicted by Eq. (17) was achieved after a few seconds. Available information

on the transient free convection heat transfer characteristics of vertical surfaces in the laminar region is extensive and has been summarized by Gebhart et al. (42); little information is available for the turbulent flow region (41).

E. RADIATION HEAT TRANSFER

The radiation heat transfer to and from balloons strongly influences their performance and determines their short-term stability. Balloon skins absorb direct and reflected solar radiation and radiation emitted by the earth and the atmosphere. Over 99% of the solar radiation is in the wavelength range between 0.2 and 4.0 μ, whereas the earth and atmospheric radiation is in the infrared range between 6 and 100 μ, with about 70% below 20 μ. Balloon skins are usually at temperatures of about 210-260°K (380-470°R) and thus emit infrared radiation. For approximate calculations the sun and earth can be considered to be blackbodies at 5550 and 300°K (10,000 and 540°R), respectively. The direct radiation from the earth and the clouds can be as high as 475 W/m^2 (150 BTU/ft^2 hr) (3). However, the direct solar radiation is collimated and, therefore, the effective receiving area is the projected area, which in the case of a

30,000 m^3 (1.06 million ft^3) spherical balloon is about 1170 m^2 (12,600 ft^2). Reflected solar radiation, on the other hand, impinges on the lower half of the total surface area of the balloon, which is about 2340 m^2. Earth and atmosphere radiation impinges on the total area of the balloon (about 4670 m^2) during ascent through the atmosphere, but only on the lower half of the balloon surface after it has risen to an altitude of 21 km, where less than 5% of the total air mass remains above. Thus, the total direct solar radiation is about 1.58×10^6 W (5.4×10^6 BTU/hr), and the reflected radiation is about 1.06×10^6 W. Infrared radiation from the earth and the atmosphere can amount to as much as 2.11×10^6 W, but at float altitude will be of the order of 0.59×10^6 W. The balloon emits radiation at a rate of $1.41 \times \bar{e}_f \times 10^6$ W, where the effective emissivity $\bar{e}_f$ may vary between 0.2 and 0.7 for different skin materials. In comparison, convection contributes only about 0.59×10^6 W to the heat transfer over the exterior balloon surface, but it is the only heat transfer mechanism in the interior because helium is transparent to radiation.

Since the actual amount of radiation absorbed depends critically on the radiation properties of the receiving and emitting surfaces, a know-

ledge of these properties is very important to the designer. The two most common materials for balloon skins are polyethylene and Mylar, which have--according to available data (43)--an effective absorptance to solar radiation of about 0.12 and 0.17, respectively. The absorptance to infrared earth radiation, which is also approximately the emittance of the skin, is 0.21 for polyethylene and 0.63 for scrim Mylar (0.5 mil Mylar on dacron scrim). A Mylar balloon absorbs, therefore, a much smaller percentage of its total radiation load from the sun than does a polyethylene balloon, and since it also emits more radiation by virtue of its higher emittance, a Mylar balloon will be cooler than a polyethylene balloon. At the same time, however, because of its high emittance a change in environmental conditions (e.g., setting of the sun) will reduce the gas temperature in a Mylar balloon more quickly than in a polyethylene balloon. A Mylar balloon, therefore, has less altitude stability than a polyethlene balloon.

In the evaluation of the radiant contribution to the total heat load on balloons and their instrument packages, engineers are faced with a lack of experimental data for the pertinent surface radiation characteristics of balloon materials. To calculate accurately the percentage of direct

solar incident radiation absorbed by a surface, one must know its monochromatic absorptance for radiation of wavelengths between 0.2 and 4.0 μ at various angles of incident radiation (44). The absorptance of thin films has a strong angular variation; radiation perpendicular to the surface passes through more readily than does radiation at a grazing angle. This angle variation can become particularly important in a balloon system where the radiation incidence angle is zero at sunrise, rises to a maximum at noon, and then decreases again to zero at sunset. For passive temperature control, i.e., the use of surfaces with very different solar absorptances and infrared emittances, the influence of the average incident angle of radiation cannot be ignored.

The difficulty of determining radiation properties for balloon skins is exacerbated by the transparency of these skins, and the transmittance has to be considered (45). As will be shown, to calculate accurately the radiation heat load on a balloon, one needs to know the total hemispherical emittance of the skin at its temperature, the directional and the angular hemispherical absorptance in the solar spectrum (since surfaces are irradiated directly and indirectly by the sun), the directional reflectances of

clouds and terrestrial surfaces in the solar spectrum, and the hemispherical absorptance in the infrared (for the surfaces exposed to the earth or clouds).

In 1969 Edwards (46) summarized our knowledge of the radiative transfer characteristics of materials and surveyed techniques available to measure surface properties (47). It does not seem feasible to measure spectral-angular surface properties for all potentially useful materials. The amount of data would be unmanageable, and the cost with present equipment would be unreasonably high. It would, therefore, be desirable to classify materials according to their physical surface properties and to develop working relationships to estimate "effective" angular properties from measurements of a few select properties. One should also know the influence on the radiation surface properties of launch procedures, aging, solar radiation, and atmospheric phenomena so thermal predictions can be made not only for idealized laboratory samples but also for actual operational systems.

The flight lifetime of a balloon depends critically on the relationship between the amount of radiant energy absorbed during the day and the amount of radiant energy lost at night. In the morning the balloon is

usually at the lowest float altitude because the gas is at its lowest temperature. After sunrise the gas is warmed by transient free convection from the skin after the skin has been warmed by the absorption of solar radiation. The part of the skin exposed to the sun transfers heat by transmission and internal emission to the rest of the skin. As the temperature of the gas increases, the buoyancy of the balloon also increases and the system begins to rise. This rise will continue until shortly after sunset, whereupon the net loss of energy exceeds the net input of energy, and the balloon begins to sink. At present the total balloon heat balance over a 24-hr period shows a small loss in internal energy. One of the long-range objectives of balloon designers is a system which will passively maintain its average float altitude, i.e., the altitude for which the net change in lift-gas energy over a 24-hr period is zero.

Various schemes to achieve a zero net change have been tried without success. But even if a "permanent balloon" is not possible, increased balloon lifetime and altitude stability would materially contribute to programs aimed at permitting long-term weather prediction and eventual weather control.

At altitudes below 21 km the radiation incident on a balloon is subject to considerable variation, and quantitative estimates are uncertain. The amounts of infrared radiation from below and above will differ and will both depend on the weather and cloud cover. The incident solar radiation will also depend on the altitude and the clouds. At altitudes over 21 km a balloon is above the weather and receives nearly all of its infrared radiation from below. Under these conditions the infrared radiation heat load can be estimated with considerably more confidence. Fortunately, large balloons are generally launched in good weather so that changes in cloud cover during ascent are minimized.

Although measurements of upward and downward radiation in the atmosphere have been made for many years, accurate evaluation of rapid changes in radiation flux are unreliable because it is not possible to predict the critical local weather changes in advance. One could, however, modify the radiation heat flux calculations to include observed weather data, such as the types of clouds and their altitudes. Calculations based on recent observations made at NOAA by Kuhn (48) clearly correlate changes in the radiation flux with cloud cover. Application of available knowledge of

atmospheric radiation to balloon performance will, however, require the close cooperation of meteorologists, cloud physicists, and ballooning engineers.

For small packages used on superpressure balloons at intermediate altitudes, an engineering analysis of the thermal control problem and a summary of the experience gained in several flights by NCAR have been presented by Lichfield and Carlson (25). The basic problems of temperature control at float altitude are quite similar to those encountered in spacecraft. In space, where only radiation can transfer heat, the equilibrium temperature T developed by an opaque body subjected only to direct solar radiation at the rate G_s over a projected surface area S_s normal to the sun, having an averaged directional absorptance per unit projected area $\bar{a}_{s,ave}$ and a surface area S with an average hemispherical emittance in the infrared $\bar{e}_{H,i}$ is

$$T = \left(\frac{\bar{a}_{s,ave} G_s S_s}{\sigma \bar{e}_{H,i} S} \right)^{1/4} \tag{18}$$

Equation (18) shows that in this case the ratio of the absorptance in the solar spectrum to the emittance in the infrared controls the equilibrium temperature.

In the balloon packages the heat transfer problem is more complicated because of the addition of reflected solar radiation, convection, and the influence of the atmospheric radiation, all of which depend strongly on the cloud cover and weather. In daytime flights, the temperature can be controlled by proper treatment of the surface of the package. The properties of a number of materials and surface coatings for such use are presented in references (49-52); Table 5 presents a typical selection. Silver sulfide, which has an average infrared emittance of only 0.03 and an average solar absorptance of 0.60, has been used successfully in balloon packages for which a temperature between 7 and 16°C was desirable. A further increase in temperature during the day was achieved by covering the package with a thin film of material such as Mylar, which is transparent to radiation only in the solar spectrum between 0.2 and 3.0 μ, but has a large reflectance for infrared radiation. This method of trapping the

Table 5

Radiation Characteristics of Surfaces

Material	IR Emissivity	Solar Absorption	Ratio
Silver (polished)	0.02	0.07	3.50
Platinum	0.05	0.10	2.00
Aluminum	0.08	0.15	1.88
Nickel	0.12	0.15	1.25
Stellite	0.18	0.30	1.67
Aluminum paint	0.55	0.55	1.00
White lead paint	0.95	0.25	0.26
Zinc oxide paint	0.95	0.30	0.32
Gray paint	0.95	0.75	0.79
Black paint	0.95	0.95	1.00
Lamp black	0.95	0.97	1.02
Silver sulfide[1]	0.03	0.60	20.00
Nickel black[1,2]	0.10	0.90	9.00
Cupric oxide[1,2]	0.15	0.90	6.00

[1] These are special surfaces where a metal is covered with a very thin layer of absorbing material. The layer is so thin that it is a fraction of a wavelength thick in the infrared and is, therefore, almost transparent to IR. The result is that the IR emissivity is nearly that of the underlying metal. However, the thickness is large compared to the wavelength of the maximum solar spectrum so the absorptivity is large for solar radiation.

[2] H. Tabor, 1961: Solar Energy.

radiation, using the so-called greenhouse effect, should be used cautiously to avoid an excessive temperature rise during the middle of the day.

For nighttime balloon flights, energy must be stored to maintain the internal temperature of the flight package. A simple heat reservoir is water. When a kilogram of water freezes, 3.34×10^5 J of energy are released. In addition, 4184 J of energy are released for each kg of water cooled $1C^{o}$. Table 6 compares the energy storage capacity of water with that of various batteries. The zinc-air and silver-zinc batteries have greater energy storage capacity than water, but zinc-air batteries require a supply of oxygen at balloon float altitude, and water is cheaper and easier to handle.

Table 6

Energy Storage Capabilities of Water and Batteries

	W-hr/lb	W-hr/kg	W-hr/in.^{3}
Water (heat of fusion)	42.0	92.6	1.52
Water (per ^{o}C)	0.528	1.16	0.019
Zinc-air	80.0	176.	5.0
Lead-acid	11.0	24.2	1.2
Nickel-cadmium	8.0	17.6	0.4
Silver-cadmium	35.0	77.0	3.5
Silver-zinc	55.0	121.0	4.5

For flights lasting several days, the package must be able to absorb as much heat during the day as it loses during the night. With suitable black paint, daytime surface temperatures of -15 to -12^{o}C can be attained, but since a typical nighttime surface temperature is -55^{o}C, it is necessary to achieve a daytime surface temperature of about 55^{o}C (131^{o}F) to maintain temperature equilibrium in the water. This requires the use of special coatings, such as silver sulfide, or the use of one or more greenhouse covers. One can also use solar cells to generate energy within the package during the day, but this adds weight and complicates the system.

F. EMITTED RADIATION [q_5 in Eq. (2)]

The balloon fabric, polyethylene or Mylar, transfers heat to the atmosphere by infrared radiation. A typical Mylar balloon fabric (9 μ thick Mylar with dacron scrim, 160 x 240 strands per meter) has at its operating temperature an average transmittance of about 0.55, an average reflectance of about 0.20, and an average absorptance of 0.25. A typical poly-

ethylene film has an average transmittance of 0.75, an average reflectance of only 0.05, and an average absorptance of 0.20. However, the monochromatic properties of fabric materials vary considerably. Mylar, for example, has radiation windows with transmittances as high as 0.80 for wavelengths between 3 and 6 μ and opaque ranges with transmittances as low as 0.10 for wavelengths between 13 and 15 μ (53).

To calculate the emitted radiation it is necessary to know the spectrally averaged hemispherical emittance in the infrared region. The evaluation of an average hemispherical emittance for a given wavelength range or a given temperature offers no difficulties for an opaque surface (46, 50, 54). As shown in Fig. 4, however, a surface element of a balloon skin dS radiates not only directly into space, but also into the interior where radiation can pass through the fabric into space, can be reflected from the interior surface of the balloon fabric, or can be absorbed by the fabric. To calculate accurately the "effective emittance" of a balloon from data on the surface radiation properties of its fabric skin, bidirectional values of the monochromatic emittance, absorptivity, and reflectivity of the interior surface would have to be known for the infrared wavelengths between

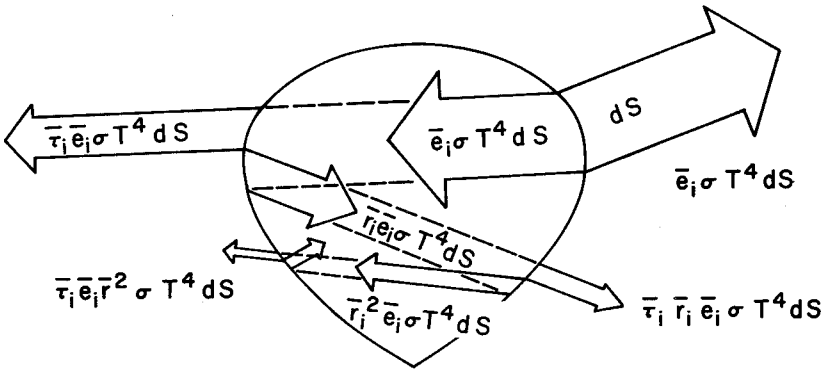

$$E_f = \int_S \int_0^\infty e_i(\lambda)\, \sigma\, T_f^4\, dS d\lambda \simeq \bar{e}_i\, \pi D_g^2\, \sigma\, T_f^4$$

$$Q_{total} \simeq \bar{e}_i\, \pi\, D_g\, \sigma\, T_f^4 \left[1 + \bar{\tau}_i (1 + \bar{r}_i + \bar{r}_i^2 + \cdots\cdots)\right]$$

Fig. 4. Emission of radiation from a balloon skin--the effective emittance.

6 and 100 μ (46). Such measurements are difficult and are generally too expensive. For balloon design it would actually be much more desirable to measure the actual emittance of a spherical sample of the fabric material filled with helium. However, no such data have as yet been taken, and calculations have been based on a model proposed by Germeles (55). This model assumes that the inner fabric surface obeys Lambert's law, i.e., it emits and refects diffusely. It also assumes that average values can replace the spectrum of values for the emittance, absorptivity, and reflectivity of the inner surface over the wavelength range (between 6 and 20 μ) for which data are available (48). The net rate of emission from the entire balloon is then equal to the radiation directly emitted from the outer surface, $\bar{e}_i \pi D_g^2 \sigma T_f^4$, plus that portion of the radiation emitted by the interior surface which eventually passes through the fabric, $\bar{e}_i \bar{\tau}_i \pi D_g^2 \sigma T_f^4 (1 + \bar{r}_i + \bar{r}_i^2 + \ldots)$. By summing the series, one obtains the effective emissivity of the fabric

$$\bar{e}_{eff} = \bar{e}_i \left[1 + \bar{\tau}_i (1 + \bar{r}_i + \bar{r}_i^2 \ldots)\right] \qquad (19)$$

$$= \bar{e}_i \left(1 + \frac{\bar{\tau}_i}{1-\bar{r}_i}\right) = \bar{e}_i \left(2 - \frac{\bar{a}_i}{1-\bar{r}_i}\right)$$

where

$$\bar{a}_i = \int_6^{100} a(\lambda)\, I\,(\lambda)\, d\lambda \Big/ \int_6^{100} I\,(\lambda)\, d\lambda \qquad (20)$$

$$\bar{r}_i = \int_6^{100} r(\lambda)\, I\,(\lambda)\, d\lambda \Big/ \int_6^{100} I\,(\lambda)\, d\lambda \qquad (21)$$

$$\bar{\tau}_i = 1 - \bar{r}_i - \bar{a}_i \qquad (22)$$

$$\bar{e}_i\,(T_f) = \bar{a}_i\,(T_f) \qquad (23)$$

Use of the effective emissivity gives the rate of heat transfer from the balloon fabric in the form

$$q_s = 4.83\, \bar{e}_{eff}\, V_g^{2/3}\, \sigma \bar{T}_f^4 \qquad (24)$$

where $\bar{T}_f^4$ is the average of the fourth power of the absolute temperature of the balloon fabric.

The infrared hemispherical emittance of the surface of an opaque body can be measured easily, so the determination of radiation emitted by the surface of a balloon instrument package generally offers no problem.

G. DIRECT SOLAR RADIATION [$q_{s,\,direct}$ in Eq. (2)]

The solar radiation spectrum has been investigated in great detail, and summaries of the current state of knowledge are presented in references

(49) and (57). Figure 5 shows the solar spectrum at the outer fringes of the atmosphere and at the surface of the earth after attenuation and absorption by the atmosphere. Over 99% of the solar energy is contained within a narrow wavelength band between 0.2 and 4 μ, and for most engineering heat transfer calculations the sun's spectrum can be approximated by that of a blackbody at 5550°K (10,000°R). The solar constant, i.e., the radiation received by a surface placed perpendicular to the rays of the sun outside the earth's atmosphere, is 1395 W/m^2 (2.0 g cal/cm^2 min or 442 BTU/ft^2 hr). The solar radiation per unit area on a horizontal surface outside the earth's atmosphere depends only on the solar constant and zenith angle, i.e., the angle between a line normal to the surface and the rays of the sun. This angle, ζ, can be determined from the relationship

$$\cos \zeta = \sin \lambda_1 \sin \delta_s + \cos \lambda_1 \cos \delta_s \cos h \qquad (25)$$

As shown in detail in references (54) and (56), the radiation per unit area on a surface tilted at an angle i to the horizontal is

$$\overline{G} = \overline{G}_s \cos \phi \qquad (26)$$

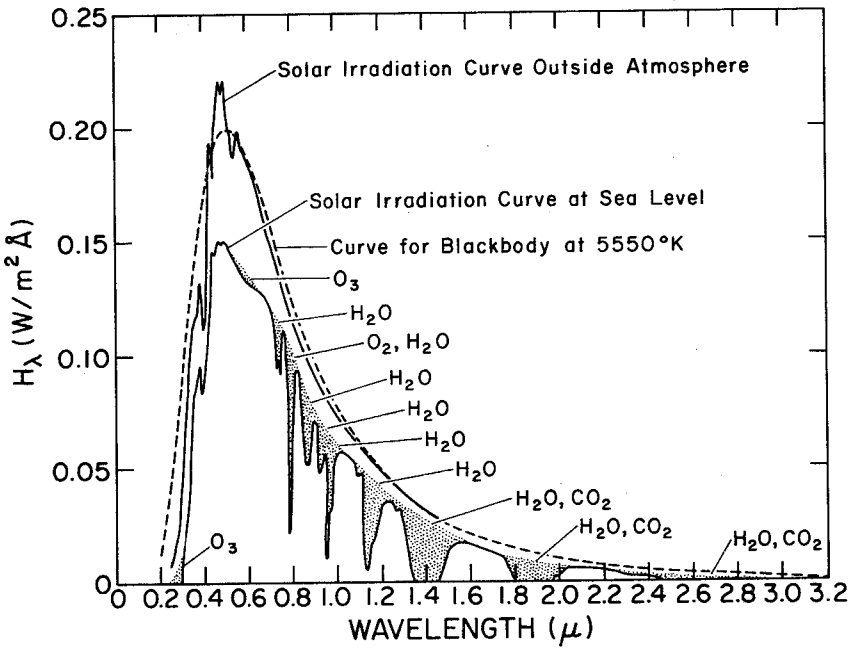

Fig. 5. Spectral distribution of solar radiation in space and at sea level.

where λ_l is latitude, δ_s is solar declination, h is local hour angle, i is angle between the local vertical and the normal to the tilted surface, $\bar{G}_s$ is average incident solar radiation, ϕ is angle between the normal to the tilted surface and the bearing of the sun, A_z is azimuth of the sun measured westward from the south meridian, a_z is the angle measured from the south meridian of the projection on the earth's surface of the normal to the tilted surface, and $\cos \phi = \cos (A_z - a_z) \sin \zeta \sin i + \cos \zeta \times \cos i$.

The zenith angle can be defined in a time coordinate system related to the flight of the balloon. If the Greenwich hour angle at the time of launch is GHA, then at any subsequent time t, the local hour angle at the balloon is

$$h = GHA - \varphi_l + \frac{t}{240} \tag{27}$$

where GHA and the longitude φ_l of the balloon are in degrees and t is in seconds.

Once ϕ is known the solar radiation absorbed by a surface outside the atmosphere is simply $\bar{a}_s(\phi)\bar{G}_s$, where $\bar{a}_s(\phi)$ is the effective directional absorptance for that angle.

In passing through the atmosphere, the intensity and spectrum of the solar energy are altered by absorption and scattering (58). Therefore, the radiation on an object is strongly dependent on the atmospheric path length of the solar rays, usually expressed in terms of the "optical air mass." Exact calculations of the attenuated spectrum are quite cumbersome (58, 59), and for engineering purposes such calculations are only useful when the directional absorptances of the receiving surfaces are known (60, 61). Figure 6 shows the distribution of direct solar radiation incident at sea level on a horizontal surface, as a function of wavelength, for several short paths corresponding to optical air masses between 1.0 and 8.0. The optical air mass, m, is unity when the sun is directly overhead and the body receiving radiation is on the earth's surface. When m = 1.0 the fraction of the solar constant received at sea level ranges from 0.62 to 0.81. A mean value of 0.7 is generally considered acceptable for most purposes. For other values of m, the fraction of solar radiation received may be expressed (55) by the empirical relation

$$\frac{\bar{G}_{s,m}}{\bar{G}_s} = 0.5 \quad (e^{-0.65m} + e^{-0.095m}) \tag{28}$$

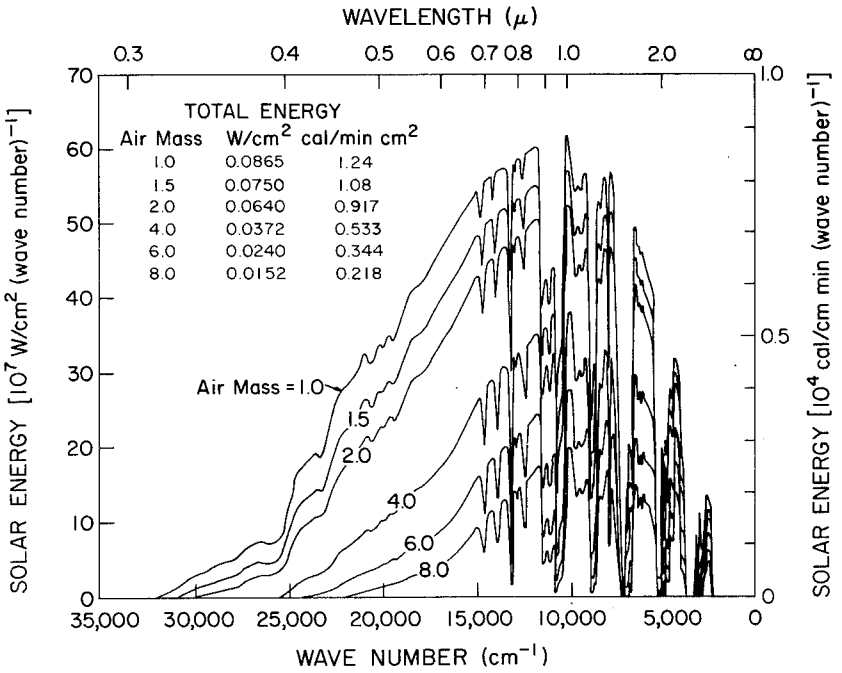

Fig. 6. Spectral distribution of solar radiation incident at sea level for air masses 1.0 to 8.0.

where optical air mass depends on the altitude and the sun's zenith angle, ζ . The variation of the optical air mass at sea level with zenith angle, $m(o,\zeta)$, is given in Tables 16-18 of reference (57) and can be closely approximated (55) by the relationship

$$m(o,\zeta) = [1229 + (614 \cos \zeta)^2]^{\frac{1}{2}} - 614 \cos \zeta \qquad (29)$$

for $0 < \zeta < 90^o$. Since the attenuation is proportional to the number of air molecules in the path, for a given zenith angle the optical air mass at altitude z can be related approximately to the air mass at sea level by the relationship

$$m(z,\zeta) = m(o,\zeta)\,[p(z)/p(o)] \qquad (30)$$

Using Eqs. (25)-(30)one can determine radiation on a surface at any altitude, geographical location, and time between sunset and sunrise. There are two short periods

$$90^o < \zeta \leq 90^o + \cos^{-1}\left(\frac{D_{earth}}{D_{earth} + 2z}\right)$$

before sea-level sunrise and after sea-level sunset during which a balloon also receives solar radiation. A method for determining the air mass during these periods is presented in reference (55), but for most purposes

it is sufficiently accurate to double the value of the air mass calculated at sea-level sunrise or sunset.

The portion of the solar radiation absorbed at the surface of an opaque body, such as an instrument package, can be calculated once the orientation of the surface relative to the sun is known. The amount of incident radiation absorbed per unit area is

$$q_{absorbed} = \int_{0.2}^{4} a\,(\phi, \lambda)\, \bar{G}\,(\lambda, m)\, d\lambda = \bar{a}_s\,(\phi)\, \bar{G}(z) \qquad (31)$$

However, as mentioned previously, the problem is more complicated for the balloon because the skin is transparent, and a portion of the incident solar radiation is absorbed, a portion reflected, and the rest transmitted into the interior where some of the radiation transmitted on the first pass will be absorbed as a result of internal reflection and absorption.

Except for occasional measurements in connection with basic investigation of radiation (46, 60), only Dingwell (43) has attempted to make systematic measurements of the radiation properties of balloon fabrics. Since balloon skins are transparent, absorptances are difficult to measure

directly. Therefore, Dingwell measured the monochromatic transmittance of solar radiation using a Beckman D.K. spectrophotometer. The reflectance was then estimated by observing interference fringes caused by internal reflections and applying Fresnel's formula for normal incidence. Finally, the monochromatic absorptance for incident radiation, presumably normal to the surface, was calculated from the relationship

$$a\,(\lambda) = 1 - r(\lambda) - t(\lambda) \qquad (32)$$

and the integrated normal absorptance of the fabric over the solar spectrum was determined by numerical integration of the relationship

$$\bar{a}_s\ (\text{normal}) = \int_{0.2}^{4.0} a(\lambda)\ I\ (\lambda)\ d\lambda \Big/ \int_{0.2}^{4.0} I\ (\lambda)\ d\lambda \qquad (33)$$

No measurements have yet been made of the effect on the radiation properties of balloon films of the solar radiation angle of incidence. Edwards (61) has shown, however, that predicted equilibrium temperatures can be as much as $22C^{o}$ ($40F^{o}$) in error if the angular dependence of radiation characteristics is neglected, and it would be desirable to measure the directional absorptance for some typical materials.

To estimate from available information the percentage of the solar radiation actually absorbed by the skin of a balloon, it will be assumed that the absorptance of the skin is independent of the angle of incidence and that radiation transmitted through the skin emerges diffusely from the interior surface. Furthermore, the shape of the balloon will be idealized as a sphere so that the projected area is $\pi D_g^2/4$. The fraction of the incident solar energy absorbed on the first pass is $\bar{\alpha}_s G(m) \pi D_g^2/4$, and the fraction transmitted is $\bar{\tau}_s G(m) \pi D_g^2/4$. Of the fraction transmitted, $\bar{\alpha}_s$ will be absorbed by the fabric and $\bar{r}_s$ will again be reflected. The total amount of the incident solar radiation eventually absorbed, obtained by summing this series of interreflections, will be

$$q_{\ell,d} = G(m) \left(\pi D_g^2/4\right) \bar{a}_s \left(1 + \frac{\bar{\tau}_s}{1 - \bar{r}_s}\right) \tag{34}$$

or in terms of the gas volume in the balloon

$$q_{\ell,d} = G(m)\ 1.21\ V_g^{2/3}\ \bar{a}_s \left(1 + \frac{\bar{\tau}_s}{1 - \bar{r}_s}\right) \tag{35}$$

H. REFLECTED SOLAR RADIATION [$q_{\ell,\ \text{reflected}}$ in Eq. (2)]

Until recently, the heat load of greatest uncertainty in Eq. (2)

was the reflected solar radiation. It was known from an overall heat balance that the portion of the solar radiation reflected by the earth and its atmosphere (the albedo), when averaged over time and space, was about 34% (62). It was also known from balloon and aircraft observations that the albedo can vary widely, but no accurate long-term measurements could be made without an observation station outside the atmosphere. The early measurements of Explorer VII and several Tiros satellites resulted in data for only part of the globe because these satellites were not in polar orbits. In 1967 and 1968, however, the meteorological satellite Nimbus II measured the incoming and outgoing radiation over the entire globe for several weeks, and Raschke of the Goddard Space Flight Center correlated the results and presented them in convenient graphs (62). These results are very useful for estimates of the reflected solar radiation above the atmosphere at the geographic locations scanned by Nimbus II, but they cover only a limited period and do not indicate variations with weather or direction.

The works of Houghton (63) and Fritz (64) are, therefore, still very useful for engineering design. Houghton established a convenient graph

for the approximate albedo as a function of latitude for clear, partially overcast, and completely overcast skies (Fig. 7). Although these curves were designed for conditions above the atmosphere, they also will give approximate results for balloons in the atmosphere as long as the sky above is not completely overcast. The accuracy of the method, which is very good for altitudes above 18 km (60,000 ft), depends upon the altitude and the amount of cloud cover. From the work of Fritz (64) and Coulson (65) an estimate of the spectrum of the reflected solar radiation can be made. Table 7 presents the results (49) as the ratio of the solar radiation received from below at a wavelength λ to the radiation at the wavelength of maximum intensity for three sky conditions. The reflected solar radiation incident on a satellite or a balloon from a surface element of the earth-atmosphere dS_e is

$$dG_s = (\pi D_g^2/4)\, G_s r_s(\theta,\zeta) \cos\theta \cos\zeta\, (dS_e/l_{s-B}^2) \qquad (36)$$

where $r_s(\theta,\zeta)$ is the bidirectional reflectance of dS_e for a solar zenith angle ζ in the direction of the balloon, θ (see Fig. 9); and l_{s-B} is the distance between the balloon and dS_e. For a known geographical distribution of $r_s(\theta,\zeta)$, the reflected radiation can be calculated numerically.

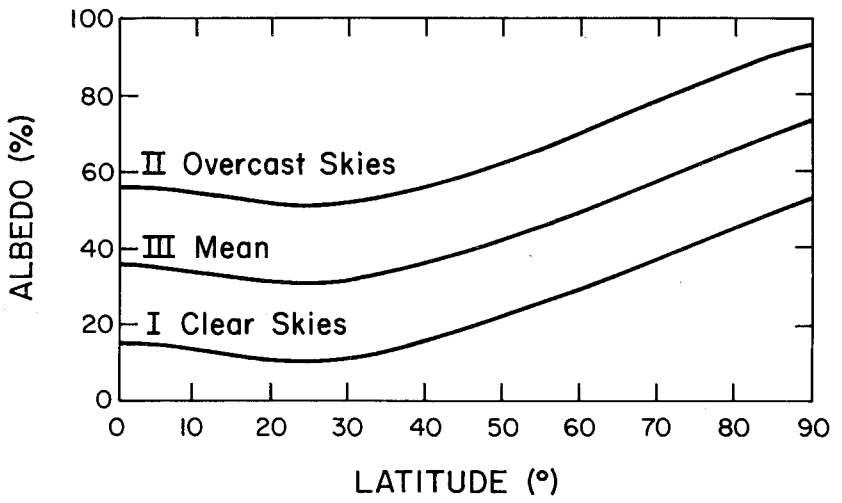

Fig. 7. Albedo as a function of latitude under various sky conditions.

Table 7

Relative Spectral Distribution of Solar Radiation under Various Sky Conditions

	R_λ[1]				R_λ[1]		
λ (μ)	Clear Skies	Mean	Overcast Skies	λ (μ)	Clear Skies	Mean	Overcast Skies
0.29	0.	0.	0.				
0.30	0.882	0.721	0.477	0.55	0.333	0.637	0.795
0.31	0.892	0.761	0.534	0.56	0.312	0.615	0.770
0.32	0.848	0.749	0.553	0.57	0.288	0.590	0.752
0.33	1.000	0.920	0.705	0.58	0.276	0.581	0.748
0.34	0.858	0.813	0.648	0.59	0.262	0.563	0.734
0.35	0.815	0.802	0.661				
0.36	0.744	0.746	0.634	0.60	0.241	0.541	0.717
0.37	0.768	0.796	0.700	0.70	0.134	0.396	0.554
0.38	0.671	0.714	0.632	0.80	0.084	0.293	0.425
0.39	0.575	0.624	0.570	0.90	0.057	0.224	0.331
0.40	0.758	0.840	0.772	1.00	0.042	0.179	0.266
0.41	0.781	1.000	0.950	1.10	0.028	0.149	0.219
0.42	0.790	0.937	0.925	1.20	0.019	0.118	0.181
0.43	0.675	0.835	0.835	1.30	0.017	0.095	0.145
0.44	0.708	0.908	0.934	1.40	0.015	0.076	0.115
0.45	0.734	0.958	1.000	1.50	0.013	0.063	0.093
0.46	0.649	0.892	0.960	1.60	0.010	0.051	0.078
0.47	0.713	0.864	0.954	1.70	0.008	0.042	0.063
0.48	0.563	0.834	0.935	1.80	0.006	0.034	0.052
0.49	0.487	0.749	0.853	1.90	0.005	0.029	0.045
0.50	0.524	0.727	0.840	2.00	0.005	0.025	0.037
0.51	0.422	0.697	0.825				
0.52	0.378	0.650	0.780	4.00	0.000	0.002	0.028
0.53	0.378	0.668	0.807				
0.54	0.252	0.663	0.812				

[1] R_λ = the ratio of the solar radiation at wavelength λ to the solar radiation at the wavelength of maximum intensity.

If one assumes that the earth-atmosphere system reflects uniformly and diffusely, Eq. (36) can be approximately integrated (66) over the portion of the earth visible from the balloon, and the radiation heat load resulting from albedo reflection $q_{z,r}$ becomes

$$q_{z,r} = 1.21\, V_g^{2/3}\, \bar{a}_s\, G_s \left[2\, \bar{r}_{s,a} \left(1 - \sqrt{z/D_e} \right) \cos \zeta \right] \qquad (37)$$

where G_s is solar constant (1395 W/m^2 or 442 BTU/ft^2 hr), $\bar{a}_s$ is average effective absorptance of the skin in the solar spectrum, $\bar{r}_{s,a}$ is average hemispherical albedo of the earth-atmosphere for a given zenith angle, z is altitude of the balloon, D_e is earth diameter (12,756 km), and ζ is zenith angle of the sun at the balloon.

When the atmosphere below a balloon is partially covered by clouds, the reflection from below will not be uniform. In such a situation one can improve the accuracy of the calculations by dividing the visible earth-atmosphere system into areas of uniform, but not equal, reflection. Assuming that each area reflects diffusely, one can approach this problem by means of shape-factor algebra (54, 66, 67, 68) just as in calculations of radiation between two diffuse surfaces.

Although the atmospheric layers are curved, one can approximate the atmosphere below the balloon by a flat surface without introducing an appreciable error. The shape factor between a small sphere dA_1 and a plane rectangle A_2 when the sphere is located at one corner of a second rectangle having a common side with A_2 (Fig. 8) is

$$F_{dA_1 - A_2} = \frac{1}{4\pi} \tan^{-1} \frac{xy}{\sqrt{1 + x^2 + y^2}} \tag{38}$$

where $x = b/c$ and $y = a/c$.

An approximate method, sufficiently accurate for most purposes, is to assume that: (a) the atmosphere ends at the intersection of a straight line between the balloon and the horizon, and (b) the atmospheric surface below the balloon is flat.

As x and y approach infinity, the shape factor for radiation between a sphere and an infinitely large plane approaches $\pi D_g^2/2$, which is larger by a factor of $\left(1 - \sqrt{4\ z/D_{earth}}\right)$ than the correct value between a small and a large sphere. At an altitude of 32 km (20 mi), the error would be about 10%. A calculation taking the curvature into account is presented by Cunningham (69).

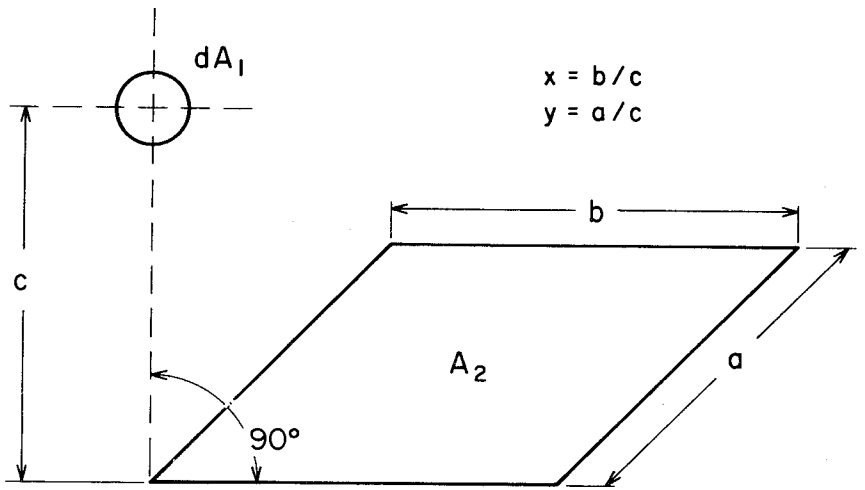

$$F_{dA_1 - A_2} = \frac{1}{4\pi} \tan^{-1} \left(\frac{x\ y}{\sqrt{1 + x^2 + y^2}} \right)$$

Fig. 8. Shape factor for a small sphere and rectangular area.

The reflectance of various types of clouds can be estimated from Table 8 in conjunction with the relationship (70)

$$r_t = r_\infty \left(1 - e^{-b_1 t}\right) \tag{39}$$

where r_t is reflectance of cloud of thickness t, r_∞ is reflectance of cloud of infinite depth, t is cloud thickness in meters, and b_1 is constant whose value depends on liquid water content or cloud type.

Data from which the geographic distribution of reflected solar radiation above the atmosphere can be calculated were gathered by the Nimlus II meteorological satellite, which was launched 16 May 1966 and remained in a polar, synchronous, circular orbit at a mean altitude of 1140 km (707 mi) until 28 July 1966. Its orbital period was 108.6 min, and during its 13 daily orbits the entire globe could be observed day and night. Reflected solar radiation in the wavelength range between 0.2 and 4 μ and the earth-emitted long-wave radiation between 5 and 30 μ were measured with a radiometer. Details of the data reduction and instrumentation are presented by Raschke (62). In the following, only the application of the averaged data to the evaluation of the reflected solar radiation will be discussed.

Table 8[1]

Mean Values of Thickness, Reflectance, and Absorptance as Well as Constants b_1 and b_2 for Various Cloud Types

	Mean Reflectance $\bar{r}_t$ [2]	Mean Absorptance $\bar{a}_t$ [3]	Mean Thickness t (m)	$b_1 \times 10^4$ (m^{-1})	$b_2 \times 10^4$ (m^{-1})
Low cloud	0.60	0.07	450	21.9	4.5
Middle cloud	0.48	0.04	600	10.5	1.8
High cloud	0.21	0.01	1700	1.2	0.15
Nimbostratus	0.70	0.10	4000	4.2	0.78
Cumulonimbus	0.70	0.10	6000	2.8	0.52
Stratus	0.69	0.06	100	155.0	16.8

[1] Adopted from Yamamoto (70).

[2] $\bar{r}_t = r_\infty \left(1 - e^{-b_1 t}\right)$; value of $\bar{r}_t$ corresponds to mean thickness.

[3] $\bar{a}_t = a_\infty \left(1 - e^{-b_2 t}\right)$; value of $\bar{a}_t$ corresponds to mean thickness.

Using the parameters defined in Fig. 9, the solar radiation reflected from a surface element dS_e depends on the location of dS_e on the globe, the time of year, the weather conditions (primarily the cloud cover), and the zenith angle of the sun. The total hemispherical radiation reflected from dS_e will be

$$q_{reflected} = \int_0^{2\pi} \int_0^{\pi/2} \bar{I}_s (\psi,\theta) \sin\theta \cos\theta \, d\theta d\psi \qquad (40)$$

where $\bar{I}_s$ is the intensity of the reflected solar radiation and θ and ψ are the zenith and azimuth angles of measurement, respectively. Since the intensity of radiation reflected from the earth-atmosphere system depends on θ, ψ, and ζ^1 (the instantaneous zenith angle of the sun), ρ^1, the instantaneous bidirectional reflectance of the area element dS_e at longitude λ_1 and latitude φ_1 can be defined as

$$\rho^1 (\theta,\psi,\zeta^1,\lambda_1,\varphi_1) = \frac{\bar{I}_s (\lambda_1,\varphi_1)}{\cos\zeta^1 \; I_s^+} \qquad (41)$$

where I_s^+ is the instantaneous direct intensity of the direct solar radiation incident on dS_e.

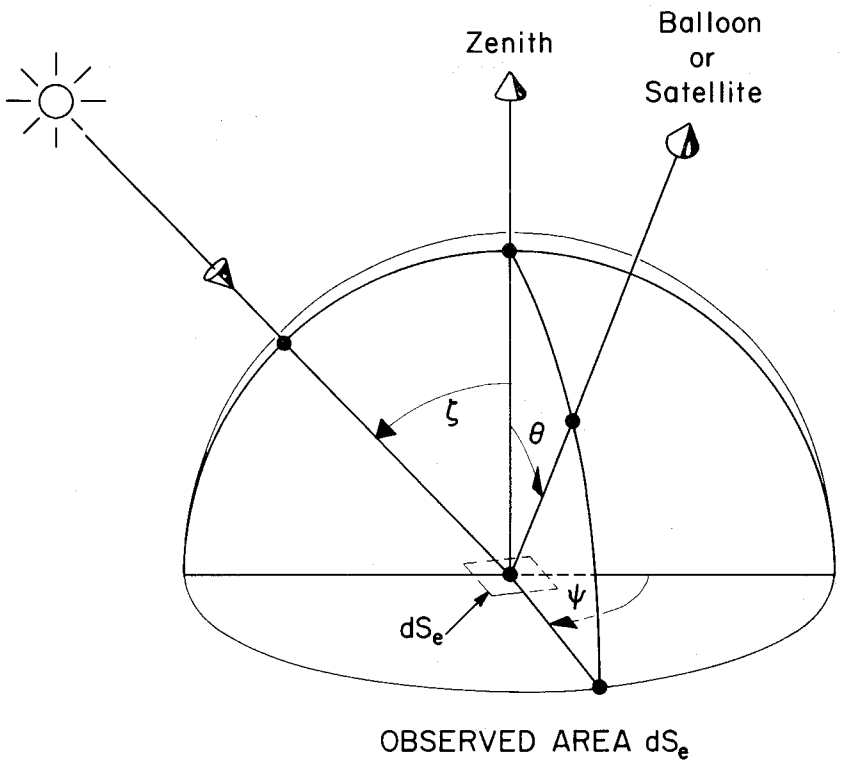

Fig. 9. Satellite- or balloon-to-earth geometric configuration.

The hemispherical directional reflectance $r(\zeta)$ is the ratio of the total reflected solar radiation (as would be received by a black hemisphere placed over dS_e) to the incoming solar radiation. It depends only on the zenith angle ζ and the time of year. From airplane and balloon measurements Raschke prepared diagrams relating the ratio between the directional hemispherical reflectance $r(\zeta)$ and the bidirectional reflectance ($\rho^1 = \rho/\pi$) at various azimuth angles within relatively narrow ranges of the zenith angle. Figure 10 shows one of these diagrams in which isolines of $x = r/\rho$ are drawn as functions of θ and ψ for a range of solar zenith angles between 60 and 80°. With the aid of these intermediate approximations, Raschke calculated the hemispherical directional reflectance from the Nimbus II data and presented his results as maps of the average albedo of the earth-atmosphere system during a two-week period (62). Figure 11 shows such a map for the northern hemisphere during the period 16-28 July 1966. The albedo varies from 20 to 30% over coastal parts of the North American continent to 80% over Greenland.

In addition to the albedo maps, Raschke also presented a correlation of available data showing the variation of the directional hemispherical

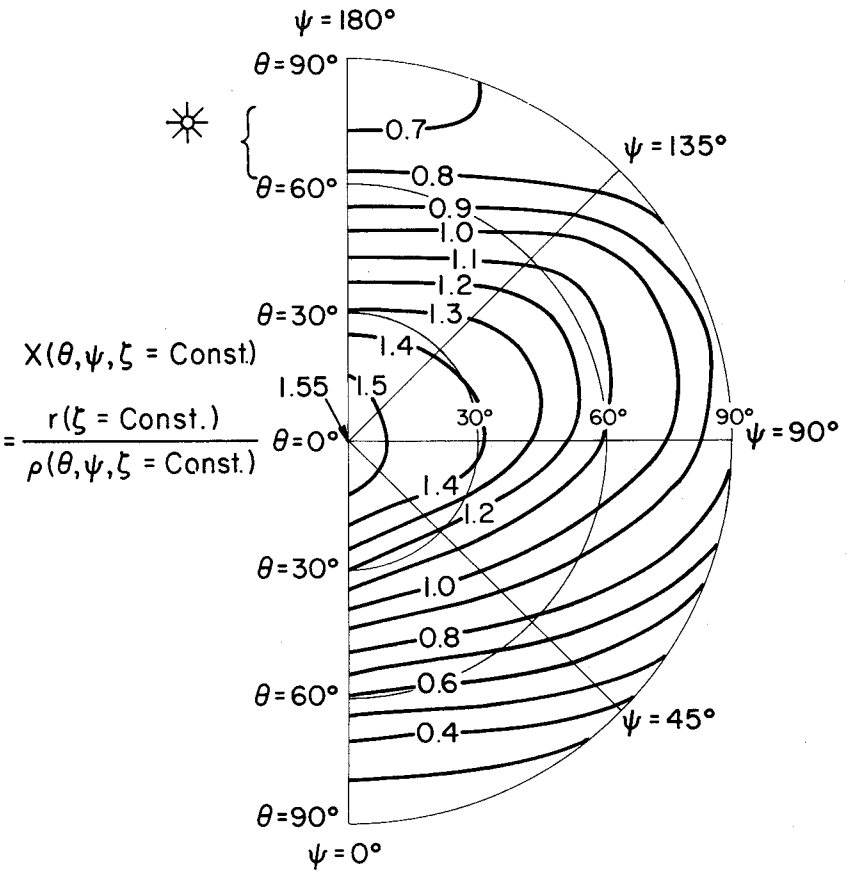

Fig. 10. Variation of directional solar reflectance with zenith angle ($60^\circ < \zeta \leq 80^\circ$).

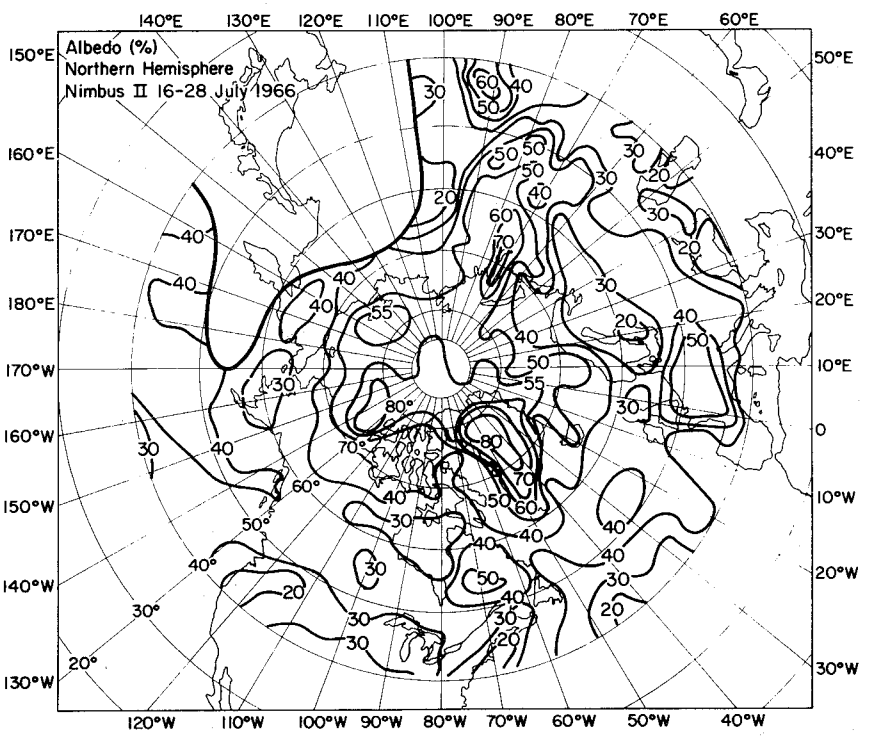

Fig. 11. Albedo map for the northern hemisphere during the period 16-28 July 1966.

reflectance with zenith angle (Fig. 12) and the ratio between the directional hemospherical reflectance and the bidirectional reflectance at various azimuth angles for snow, stratocumulus clouds, and cloudless ocean areas. With the aid of these diagrams one can make predictions of the reflection at altitudes above 18 km (60,000 ft). Such predictions are quite accurate except when there are changes in cloud cover. For engineering design it is usually satisfactory, however, to use Eq. (37) in combination with the graph in Fig. 12 relating the average hemispherical reflectance to the zenith angle, which can be calculated, using Eqs. (25) and (27) in a time-coordinate system related to a balloon flight.

I. INFRARED RADIATION FROM THE EARTH AND THE ATMOSPHERE [q_3 in Eq. (2)]

The contribution to the total heat load on a balloon by the radiation from the earth and the atmosphere is an important variable in the energy balance formulated by Eq. (2). Unfortunately, the quantitative prediction of this portion of the total heat load is subject to some uncertainty because it depends on several factors difficult to specify.

The infrared radiation from the earth and the atmosphere varies as the balloon ascends. Immediately after its launch, the balloon receives

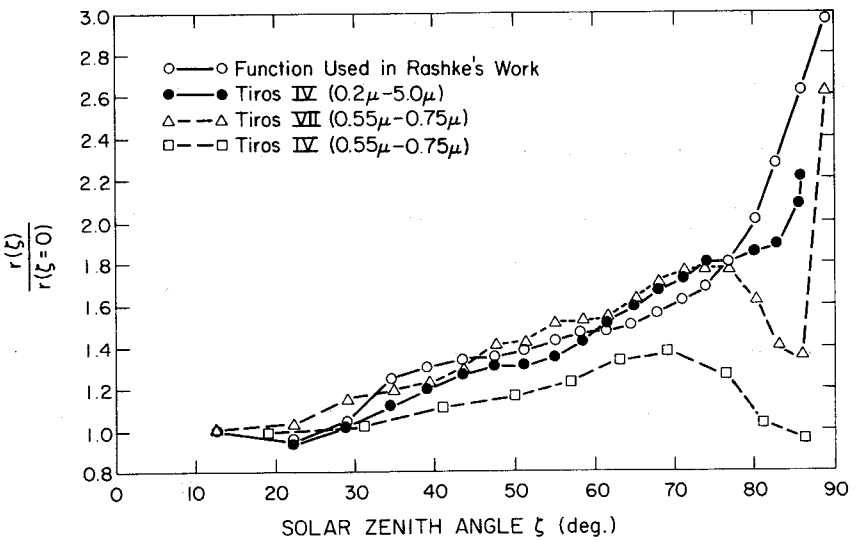

Fig. 12. Variation of directional hemispherical reflectance with zenith angle.

radiation from the atmosphere over its entire surface, but as it ascends the amount of air above the balloon continuously decreases. Eventually, only the lower part of the balloon receives radiation from the atmosphere. This infrared radiation is dependent on the altitude and cloud cover, and since the cloud cover often changes rapidly, a balloon can experience unexpected and unpredictable fluctuations in the radiation from the earth-atmosphere. The situation improves considerably, however, as the balloon ascends; once it has risen above the clouds and the weather to an altitude of about 18 km, the contribution of radiation from the earth and the atmosphere can be predicted with a considerable degree of accuracy.

Radiation from the earth and the atmosphere is of considerable interest to meteorologists. Comprehensive treatises on the radiation characteristics of the atmosphere have been published during the past decade by outstanding meteorologists such as Goody (71), Feigelson (59), Budyko (72), and Kondratyev (73). The radiation characteristics have been investigated and reduced to convenient graphs and charts by Simpson (74), Yamamoto (70), and Elsasser and Culbertson (75). Using Nimbus II data Raschke also prepared infrared radiation maps. Figure 13 shows the infrared radiation

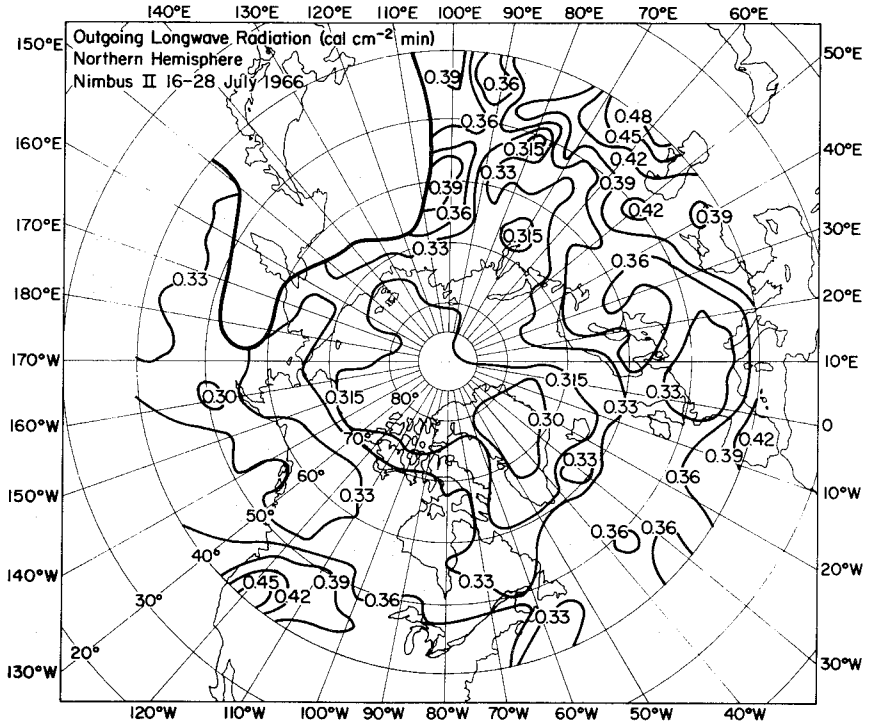

Fig. 13. Infrared radiation map for the Northern Hemisphere during the period 16-28 July 1966. Multiply radiation values by 697.35 to obtain radiation in W/m^2.

emitted by the earth and the atmosphere into space over the northern hemisphere during the period 16-28 July 1966.

In connection with efforts to construct a general circulation model of the atmosphere, several researchers including Houghton (63), London (76), Manabe and Möller (77), and Davis (78) have studied theoretical aspects of atmospheric radiation, but most of them calculated the meridional distribution and seasonal variation of the radiation balance and not its global distribution. From a practical point of view, Simpson's simple model (74, 79) is still very useful for estimating radiation heat loads, although Budyko (72) presents more accurate heat balance calculations at the earth's surface. Neither of them, however, considers the radiation within the atmosphere. Recently, Katayama (80) has made valuable calculations of the radiation budget of the troposphere over the northern hemisphere, and Sasamori (81) has developed a method for calculating the upward and downward radiation flux in a cloudless atmosphere. Sasamori's calculations are based on empirical formulas for the spectral variations of the absorptances of water vapor, carbon dioxide, and ozone (the constituents of the atmosphere with absorption bands in the infrared range) and on the assumption

that the surface of the earth is perfectly black. A summary of his results is shown for various latitudes in Fig. 14, in which the upward and downward radiation fluxes are plotted as a function of altitude. The spectral characteristics of the radiation are not shown but can be calculated from the empirical relations in reference (81).

It should be noted that the atmosphere is almost transparent to wavelengths between 8 and 12 μ. Consequently, a balloon will receive such radiation directly from the earth. At longer and shorter wavelengths the atmospheric water vapor and carbon dioxide have strong absorption bands, and in those parts of the spectrum the infrared radiation received by a balloon is emitted by the atmosphere, usually at a temperature lower than that of the earth. Some balloon materials exhibit considerable variations in the monochromatic absorptance in the infrared, and to estimate reliably the infrared radiation absorbed by the skin, integrations over the spectrum between 6 and 100 μ, as shown by Eq. (20), are necessary (54, 82). For these integrations, simplified models of the variations in the monochromatic radiation of the atmosphere, such as those given in references (83) or (54), are quite satisfactory.

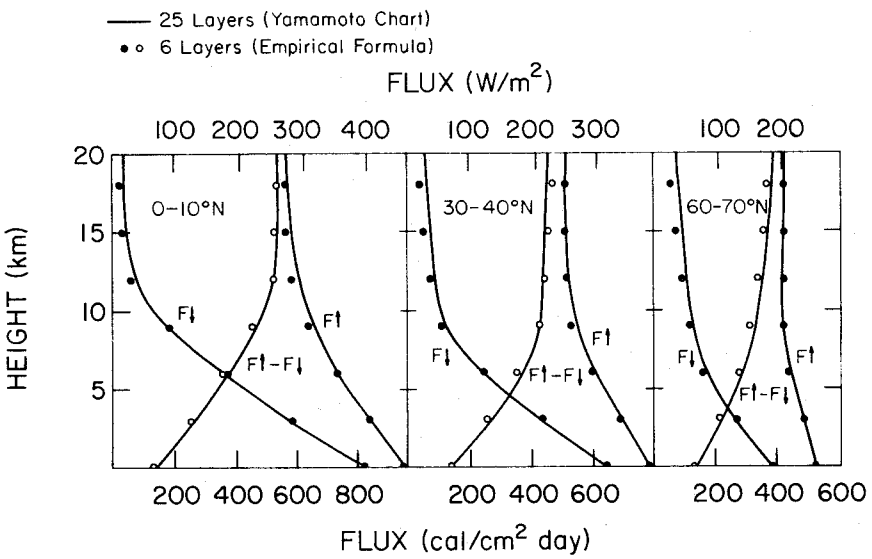

Fig. 14. Upward and downward radiation flux as a function of altitude.

In view of these complicated conditions it is not surprising that several approaches have been taken to calculate the radiation from the earth and its atmosphere which is absorbed by a balloon. Lally (3), dealing only with superpressure balloons, divided the incoming infrared radiation into four parts: from below, from above, and from two sides, each illuminating an area of $\pi D_g^2/4$. The radiation environment is then estimated using the following simplified assumptions:

1. Downward radiation.
   a. If clouds above: downward flux equals blackbody radiation from a source at the temperature of the cloud base.
   b. If clear above: balloon above 15 km (9 mi)--10 W/m^2 (3.2 BTU/ft^2 hr); balloon between 10-15 km (6-9 mi)--20 W/m^2 (6.3 BTU/ft^2 hr); balloon below 10 km (6 mi)--40 W/m^2 (12.7 BTU/ft^2 hr).
2. Upward radiation.
   a. If clouds below: upward flux equals blackbody radiation from a source at the temperature of the cloud tops.

   b. If clear below: upward radiation will vary from 150 W/m^2 to 450 W/m^2 (48 to 144 BTU/ft^2 hr) depending on altitude and air mass. Table 9 provides estimates of the effect of upward flux for several altitudes and air masses.
3. The radiation from the sides can be estimated as equal to blackbody radiation from a source at the temperature of the air at balloon altitude.

London (82) considered only the upward and downward fluxes. The advantage of this approach is that theoretical analyses and measurements of atmospheric radiation usually provide the upward and downward, but not horizontal, radiation fluxes. An instrument which has been widely used at NOAA to obtain measurements of the upward and downward atmospheric radiation was developed by Suomi and Kuhn (84). This instrument (Fig. 15) is basically a double-faced, hemispherical bolometer with broad-response, blackened sensing surfaces shielded from convection currents by thin membranes of polyethylene. The upward and downward radiation flux can be calculated from the temperatures, measuredwith tiny thermistors, of the sensor surfaces and the air. A flight test of this instrument, also called an "economical

Table 9

Radiation Environment for Superpressure Balloons[1]

Altitude	Season[2]	Air	Av. nighttime clear sky balloon super temperature		Mylar balloon (α_o = 0.05)		
		Temperature (°C)	Mylar balloon (°C)	Metallized top balloon (°C)	Temperature increase per W/m² increment (°C)	Maximum added solar flux (W/m²)	Maximum daytime temperature increase (°C)
3 km (700 mb)	Winter	-10	0	5	0.24	35	8
	Summer	5	- 3	2	0.21	35	8
	Tropic	10	- 5	0	0.20	35	8
6 km (500 mb)	Winter	-30	0	8	0.30	35	10
	Summer	-15	- 5	5	0.27	35	9
	Tropic	- 5	-10	2	0.25	35	9
9 km (300 mb)	Winter	-50	5	15	0.36	40	14
	Summer	-35	- 5	7	0.34	40	13
	Tropic	-30	-10	2	0.34	40	13
12 km (200 mb)	Winter	-55	10	20	0.36	45	16
	Summer	-55	10	20	0.36	45	16
	Tropic	-50	5	15	0.36	45	17
16 km (100 mb)	Winter	-60	5		0.42	45	19
	Summer	-65	10		0.42	45	21
	Tropic	-80	15		0.47	45	21
24 km (30 mb)	Winter	-55	- 5		0.45	45	20
	Summer	-55	- 5		0.45	45	20
	Tropic	-55	- 5		0.45	45	20

[1] Adapted from Lally (3).
[2] Winter and summer seasons in temperate latitudes and all seasons in the tropics.

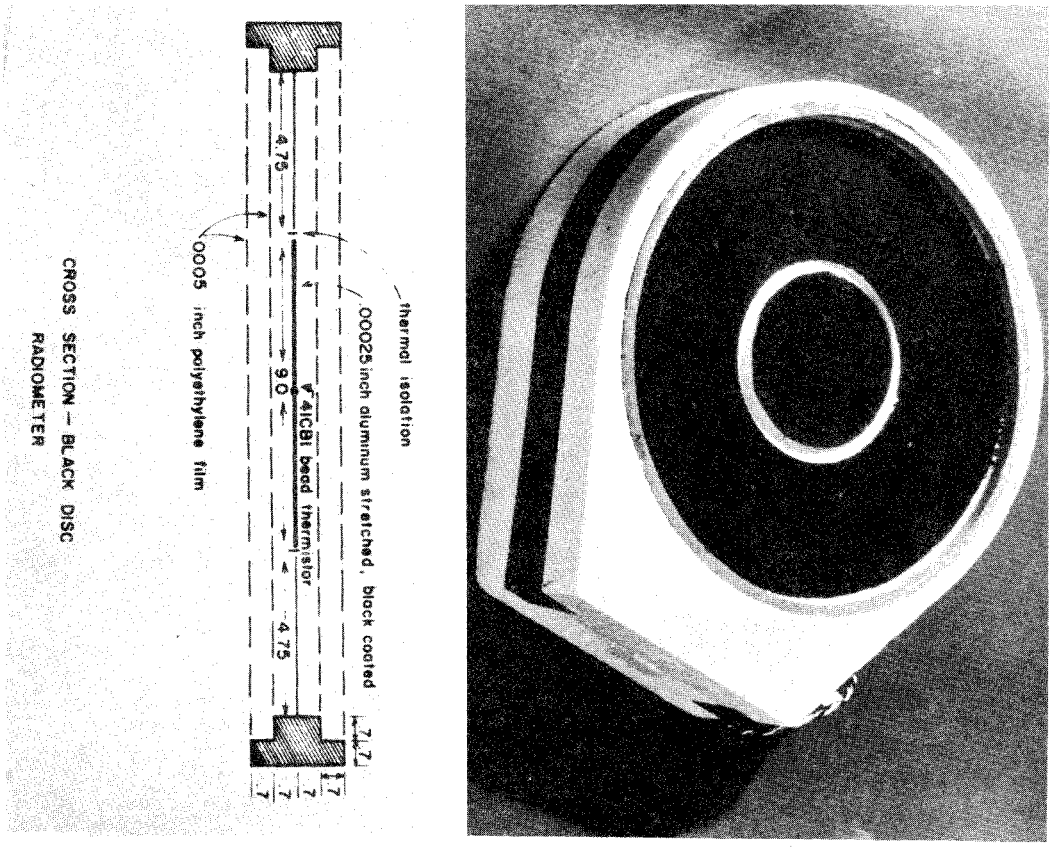

Fig. 15. Suomi-Kuhn flat plate radiometer.

net-radiometer," is reported in reference (85). Data taken during several balloon flights have been published [e.g., (85-89)], but data from other flights are still being processed at NOAA (48). Whenever the spectra of the upward and downward infrared radiation are known, the rate at which infrared radiation is transferred to the balloon skin can be calculated from the relationship

$$q_B = (\pi D_g^2/2) \int_4^{100} \left[\bar{a}_{eff}(\lambda)\, G_{i,up}(\lambda) + \bar{a}_{eff}(\lambda)\, G_{i,down}(\lambda) \right] d\lambda \qquad (42)$$

where $\bar{a}_{eff}(\lambda)$ is the effective monochromatic absorptance of the balloon film, which can be approximated from Eq. (34) by

$$a(\lambda)\left[1 + \frac{1 - a(\lambda) - r(\lambda)}{1 - r(\lambda)}\right]$$

and where $G_{i,up}(\lambda)$ is the upward monochromatic radiation as measured by a hemispherical flat surface radiometer, and $G_{i,down}(\lambda)$ is the downward monochromatic radiation, measured likewise.

Unfortunately, only the total average radiation over all wavelengths is usually measured. Typical data from meteorological measurements are illustrated in the graphs of Figs. 16, 17, and 18. In all three figures

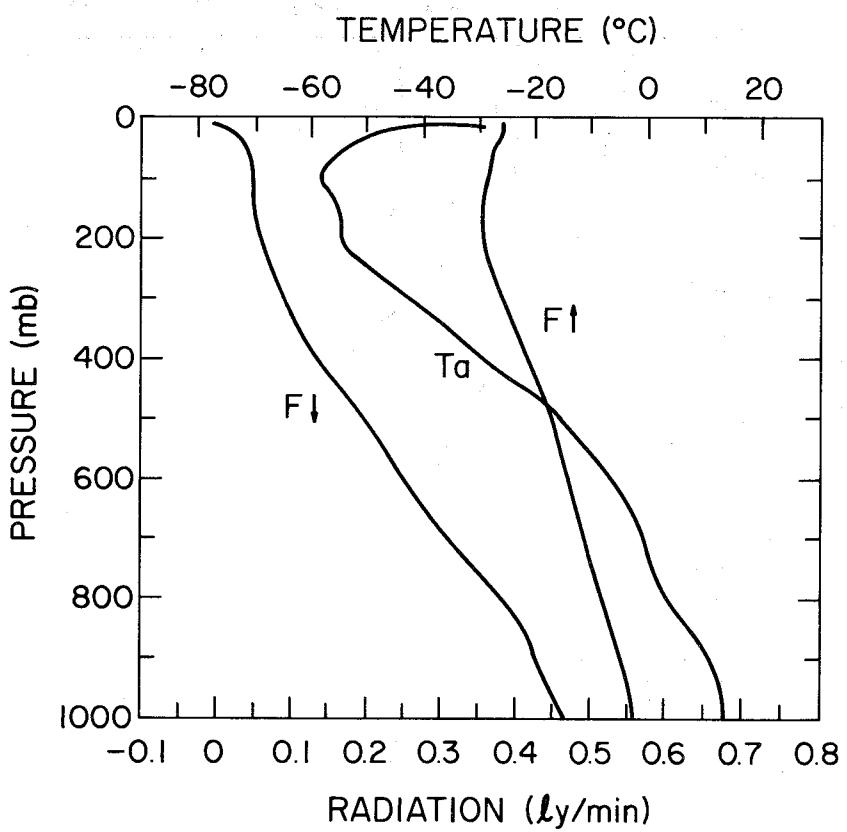

Fig. 16. Radiation environment at Green Bay, Wisconsin, in the summer.

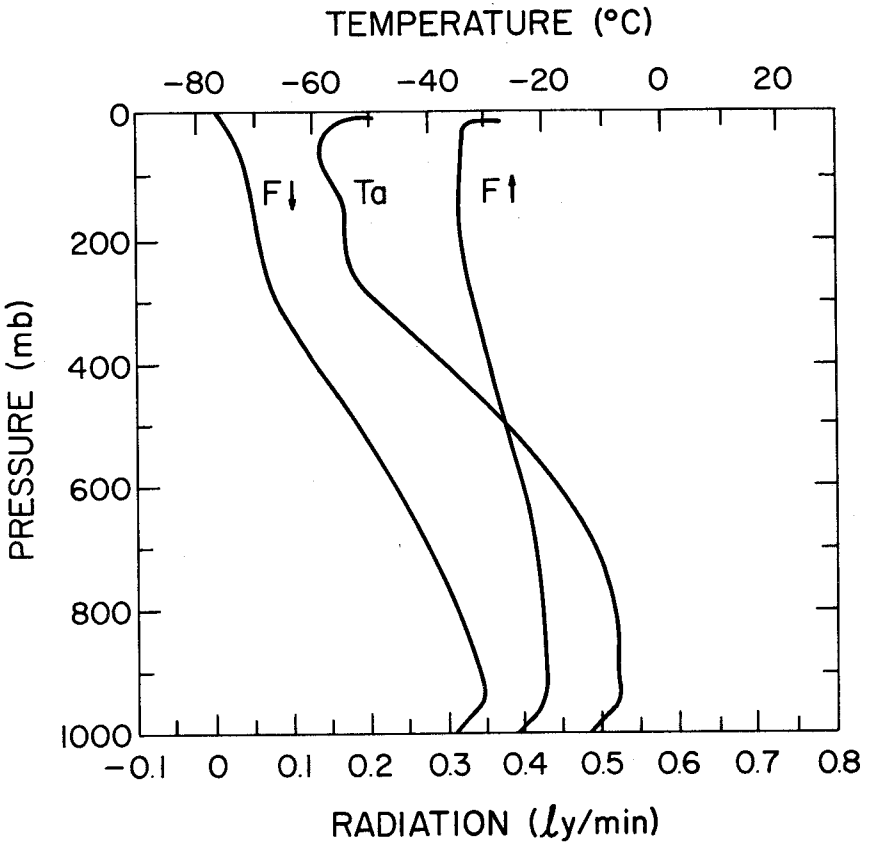

Fig. 17. Radiation environment at Green Bay, Wisconsin, in the winter.

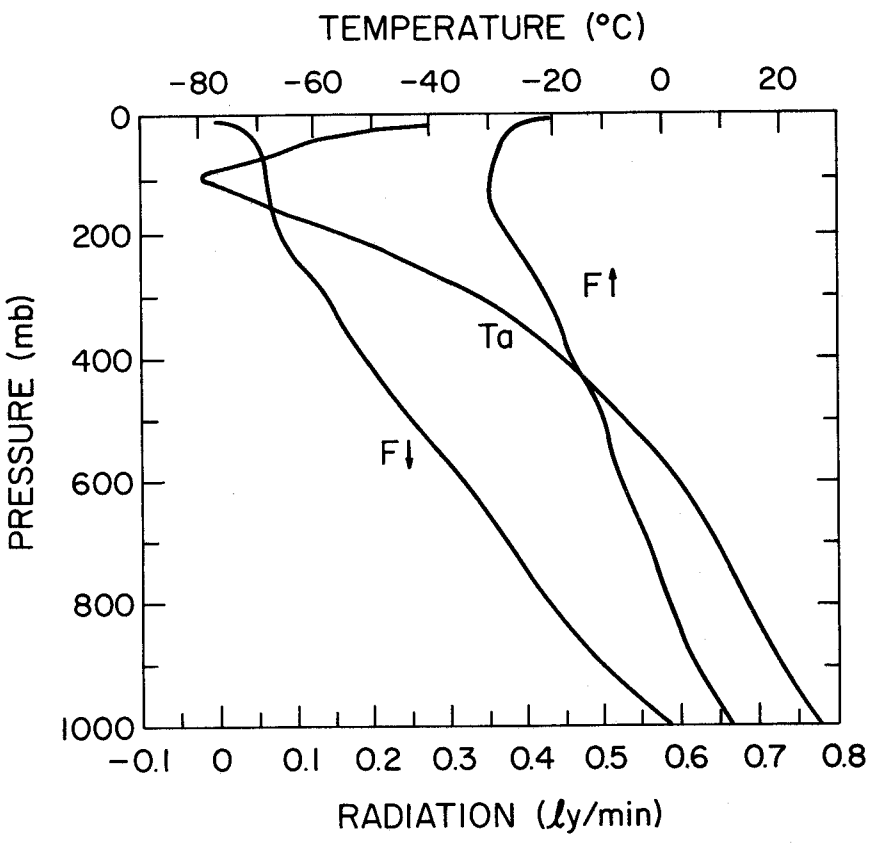

Fig. 18. Radiation environment at a desert island, 2^{o}S.

To obtain W/m^2 multiply ly/min by 697.35.

the air temperature and the total radiation on a horizontal surface from above and below are plotted as a function of altitude. Also shown are the net radiation flux (i.e., the difference between the radiation from above and from below) and the atmospheric cooling rate--quantities which are of meteorological interest only.

Figures 16 and 17 show the average radiation environment at Green Bay, Wisconsin, during summer and winter, and Fig. 18 shows the radiation environment of a desert island at $2^{o}S$. The downward radiation increases markedly with decreasing altitude, whereas the upward radiation decreases slowly with increase in altitude. In winter, when the atmospheric temperature variation with altitude is less than in summer, the changes in radiation are also smaller. Near the equator where variation in the atmospheric temperature with altitude is even larger than at Green Bay during the summer, the changes in the infrared radiation environment are also more pronounced. It should be noted that the infrared radiation graphs in Figs. 16, 17, and 18 represent averages of the total hemispherical radiation over all wavelengths. When the spectrum is not known, an average absorptance must be estimated to calculate the rate of absorption of infrared radiation from

Eq. (42). There will, of course, always be variations with changes in weather conditions, and the amount of radiation absorbed by a balloon skin or an instrument package will depend not only on the spectrum of the incoming radiation but also on the variation with wavelength, as yet not known, of the directional hemispherical absorptance of the receiving surface.

A third method of estimating the infrared heat load has been proposed by Germeles (13). It uses the measurements obtained by a "black-ball" radiometer (Fig. 19), an instrument widely used by meteorologists to measure the radiation in the atmosphere. The instrument, developed by Gergen (90), consists essentially of a small balsa dodecahedron painted black and surrounded by a convection shield. A thermistor imbedded in the center is used to measure T_r, the "equilibrium radiation temperature" of the device. From this measurement, the radiation is then calculated from the relationship (90)

$$G_i = \sigma T_r^4 \tag{43}$$

Measurements with this device are carried out during the night so the detector is not affected by the sun. It is claimed that the temperature recorded by the black ball is representative of the total radiation field

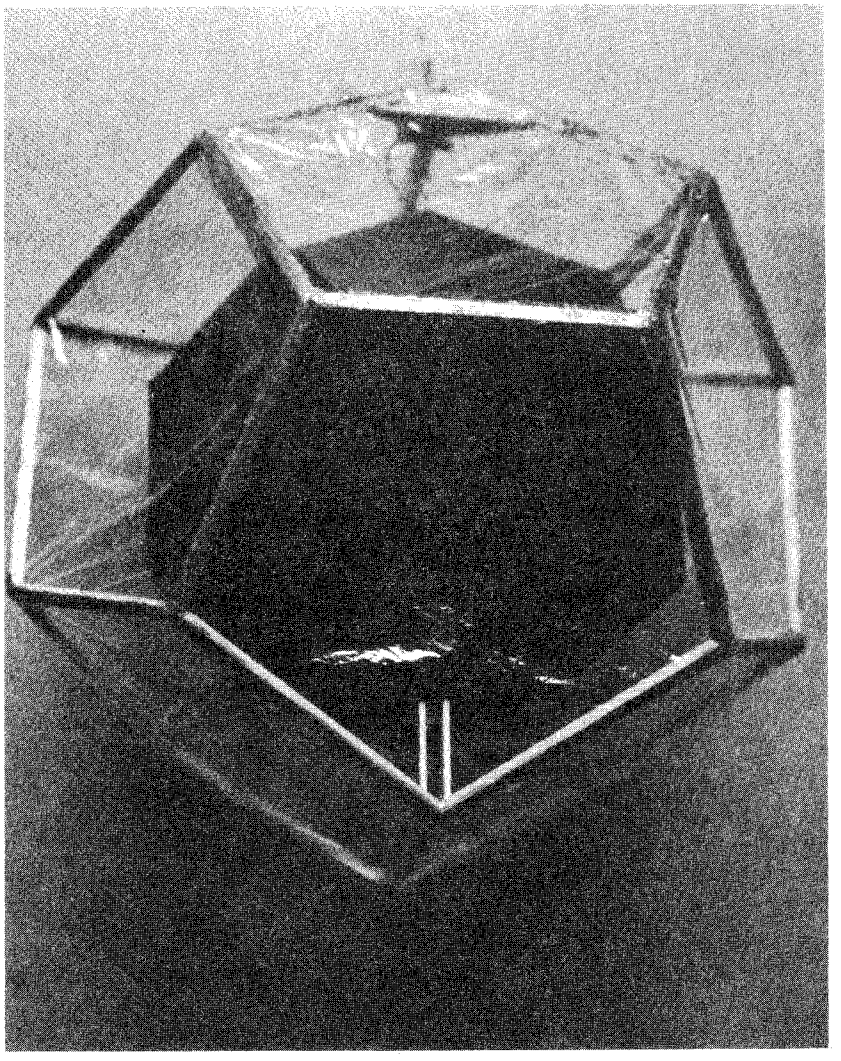

Fig. 19. Gergen "Black-Ball" radiometer.

to which it is exposed. Black-ball equilibrium temperatures have been recorded as a function of altitude at different geographic locations, and it has been observed that large changes in the black-ball temperature profile occur within days at the same location. The results of these measurements support the following approximate, simple, general rule. At ground level, the radiation temperature is usually less than the air temperature, and the deviation is about $5^{\circ}C$ ($10^{\circ}F$). The equivalent radiation temperature decreases almost linearly with altitude up to the tropopause, where it becomes about 75% of its ground value. From there to higher altitudes the radiation temperature remains approximately constant, indicating that most of the radiation is received from below.

Germeles (13) used data obtained by means of a black-ball radiometer to calculate the infrared radiation on a balloon. He assumed that the black-ball temperature profile is known. Since the black ball has a shape similar to that of a balloon, the radiation absorbed by the balloon can be obtained from the relationship

$$q_B = 4.83\ \bar{a}_{eff}\ \sigma\ V_g^{2/3}\ T_r^4 \qquad (44)$$

It is apparent that the estimates of radiation emitted by the atmosphere and the earth require considerable improvement and elaboration. It may well be that such improvement has not been made because the properties of balloon fabrics are not precisely known, so that even if the heat load could be calculated with considerably higher accuracy, the uncertainty in the absorption load would remain.

At this juncture, the following is recommended: (a) use black-ball radiometer data, when available, or (b) calculate the heat load from above and below, making use of measurements obtained with an instrument such as the Suomi-Kuhn radiometer, and calculate the actual amount of radiation with a simple model of the atmosphere such as that proposed by Simpson (74), which considers only water and carbon dioxide absorption. This approach, described in reference (53) for use in spacecraft design, is also directly applicable to calculations on balloon and instrument packages. For calculations of heat loads in areas where the Suomi-Kuhn instrument has not been flown, the Nimbus II data may be used. They are similar to albedo data in that they include the total radiation flux emitted by the earth's atmosphere. This approach, of course, will only be useful for altitudes

above 18 km since satellite data are taken far outside the atmosphere. An aid to further improvement of the calculation of the heat load would be to fly several balloons instrumented to measure gas temperature, the radiation heat load, and air temperature simultaneously. Although such measurements have not been made, they are feasible with existing instrumentation.

J. GAS EXPANSION AND LIFT AND LOAD ADJUSTMENTS

The variation of the gas volume in the balloon with time is

$$\frac{dV_g}{dt} = \frac{d}{dt}\left(\frac{Rm_g T_g}{M_g P_g}\right) = \frac{Rm_g}{M_g P_g}\frac{dT_g}{dt} + \frac{RT_g}{M_g P_g}\frac{dm_g}{dt} - \frac{Rm_g T_g}{M_g P_g^2}\frac{dP_g}{dt} \tag{45}$$

If the relation between atmospheric pressure and altitude from Eq. (5), Section XI, is used and superpressure is neglected, the above equation can be written in the form

$$\frac{dV_g}{dt} = \frac{R}{M_g P_a}\left(m_g \frac{dT_g}{dt} + T_g \frac{dm_g}{dt} + \frac{gm_g T_g M_a}{RT_a}\frac{dz}{dt}\right) \tag{46}$$

As mentioned in Section II, the lift of a balloon system can be reduced by exhausting helium automatically through the gas expulsion duct when float altitude is reached, or by valving to maintain float altitude, to

reduce the rate of ascent, or to cause the balloon to descend. If $\dot{E}_d$ is the volumetric gas flow rate through the expulsion duct (required to stabilize the balloon at ceiling) and $\dot{E}_v$ is the flow rate through the exhaust valve, the net change in balloon mass due to loss of gas is

$$\frac{dm_g}{dt} = \rho_{gd}\dot{E}_d + \rho_{gv}\dot{E}_v \tag{47}$$

The mass of the balloon system can be reduced by dropping ballast or part of the payload. This change in mass of the balloon system during a time increment $\Delta t = t_2 - t_1$ is

$$\int_{t_1}^{t_2} \frac{dm_G}{dt} = \int_{t_1}^{t_2} \frac{dm_b}{dt} + \Delta m_\ell \tag{48}$$

where Δm_ℓ represents the amount of payload mass or increments of ballast which may be dropped during the time interval $(t_2 - t_1)$.

K. A VERTICAL MOTION MODEL

The vertical component of Eq. (33) of Section II, the energy balance equations of this section, equations from Section XI which describe the atmosphere, and miscellaneous equations for calculating parameters such as Reynolds numbers may be combined into a set of equations which constitute

a mathematical model of the vertical motion of a balloon in the atmosphere. One such set is listed here with a minimum of explanatory material, but a reference to the source of each equation is given.

$$-g\left[m_G + m_g\left(1 - \frac{M_a}{M_g}\frac{p_a}{p_g}\frac{T_g}{T_a}\right)\right] - \tfrac{1}{2}\rho_a C_D A_D \left|\frac{dz}{dt}\right| \frac{dz}{dt} = \left[m_G + m_g\left(1 + C_B\frac{M_a}{M_g}\frac{p_a}{p_g}\frac{T_g}{T_a}\right)\right]\frac{d^2z}{dt^2} \qquad \text{II,Eq. (33)}$$

$$\frac{d}{dt}\left(C_v m \bar{T}\right)_g = q_1 + \frac{RT_g}{M_g}\frac{dm_g}{dt} - p_a\frac{dV_g}{dt} + \left(C_v T\right)_g \frac{dm_g}{dt} \qquad \text{III,Eq. (1)}$$

$$\frac{d}{dt}\iint_{S_f} C_f \rho_f t_f T_f dS_f = C_f m_f \frac{d\bar{T}_f}{dt} = q_2 + q_3 + q_4 - q_5 - q_1 \qquad \text{III,Eq. (2)}$$

$$q_1 = 0.628\, V_g^{2/3}\, k_g\,(\bar{T}_f - \bar{T}_g)\left[\frac{\rho_g^2\, g\,(\bar{T}_f - \bar{T}_g)}{\mu_g^2\, T_g}\,Pr_g\right]^{1/3} \qquad \text{III,Eq. (17)}$$

$$q_2 = q_{2,\text{direct}} + q_{2,\text{reflected}}$$

$$q_{2,\text{direct}} = 1.21\, G(m)\, V_g^{2/3}\,\bar{a}_s\left(1 + \frac{\bar{T}_s}{1 - \bar{r}_s}\right) \qquad \text{III,Eq. (35)}$$

$$q_{2,\text{reflected}} = 1.21\, V_g^{2/3}\,\bar{a}_s G_s\left[2\bar{r}_{s,a}\left(1 - \sqrt{z/D_e}\right)\cos\zeta\right] \qquad \text{III,Eq. (37)}$$

$$q_3 = 4.83\,\bar{a}_{eff}\,\sigma\, V_g^{2/3}\, T_r^4 \qquad \text{III,Eq. (44)}$$

$$q_4 = 7.79\, V_g^{1/3} k_a (T_a - \bar{T}_f)\left[1 + 0.322\left(\frac{\rho_a^2\, g\left(\left|T_a - \bar{T}_f\right|\right) V_g}{T_a \mu_a^2}\right)^{1/4}\right] \qquad \text{III,Eq. (7)}$$

if $Re_{\ell'} \leq 1.697\ (Gr_{\ell'})^{\frac{1}{2}}$ III.C.

or $$q_4 = 3.9\ V_g^{1/3}\ k_a(T_a - \bar{T}_f)\left[2 + 0.472\ V_g^{0.183}\left(\rho_a \frac{|dz/dt|}{\mu_a}\right)^{0.55}\right]$$ III,Eq. (5)

if $Re_{\ell'} > 1.697\ (Gr_{\ell'})^{\frac{1}{2}}$ III.C.

$$q_5 = 4.83\ \bar{e}_{eff}\ V_g^{2/3}\ \sigma\ \bar{T}_f^4$$ III,Eq. (24)

$$m_G = m_B + m_\ell + m_b$$ II.D.

$$\int_{t_1}^{t_2} \frac{dm_G}{dt} = \int_{t_1}^{t_2} \frac{dm_b}{dt} + \Delta m_\ell$$ III,Eq. (48)

$$m_g = \frac{m_G\ (1 + f')}{\left(\frac{M_a}{M_g} - 1\right)}$$ II,Eq. (36)

$$\frac{dm_g}{dt} = \rho_{g,d}\left(\frac{dV_g}{dt}\right)_d + \rho_{g,v}\left(\frac{dV_g}{dt}\right)_v$$ III,Eq. (47)

$$V_g = M_g/\rho_g$$

$$\rho = \frac{PM}{RT}$$ for either gas or air II,Eq. (8)

Gas will flow from a valve at the top of a balloon at a rate

$$\left(\frac{dV_g}{dt}\right)_v = -1.58\ CA\sqrt{g\frac{\rho_a - \rho_g}{\rho_g}\left(\frac{m_g}{\rho_g}\right)^{1/3}}$$ XII,Eq. (E-5)

where C is a dimensionless coefficient which must be determined empirically for each valve and A is the nominal area of the valve.

$$\frac{dV_g}{dt} = \frac{R}{M_g p_a}\ m_g \frac{dT_g}{dt} + T_g \frac{dm_g}{dt} + \frac{g m_g T_g M_a}{R T_a}\ \frac{dz}{dt}$$ III,Eq. (46)

If $V_g \geq V_B$ (the nominal volume of the loaded balloon at float),

$$\left(\frac{dV_g}{dt}\right)_d = \frac{dV_g}{dt} - \left(\frac{dV_g}{dt}\right)_v$$

where the subscripts d and v indicate loss of gas through the ducts and valves, respectively.

$$\bar{G} = \bar{G}_{s,m}\left[\cos\ (A_z - a_z)\ \sin\ \zeta\ \sin\ i\ + \cos\ \zeta\ \cos\ i\right]$$ III,Eq. (26)

$$\zeta = \cos^{-1}\left[\sin\ \lambda_1\ \sin\ \delta_s + \cos\ \lambda_1\ \cos\ \delta_s\ \cos\ h\right]$$ III,Eq. (25)

$$h = GHA\ (\text{at launch}) - \varphi_1 + [t(\text{sec})/240]$$ III.G.

$$\bar{G}_{s,m} = 0.5\ \bar{G}_s\ (e^{-0.65m} + e^{-0.095m})$$ III,Eq. (28)

$$m(o,\zeta) = \left[1229 + (614\ \cos\ \zeta)^2\right]^{\frac{1}{2}} - 614\ \cos\ \zeta$$ III,Eq. (29)

and $$m(z,\zeta) = m(o,\zeta)\left[p_a(z)/p_a(o)\right]$$ III,Eq. (30)

for $0 < \zeta < 90^o$

$m(z,\zeta) \approx 70$ III.G.

for $z > 20$ km and $90^{o} < \zeta \leq 90^{o} + \cos^{-1}\left(\frac{D_{earth}}{D_{earth} + 2z}\right)$

$G_s = 1395\ W/m^2 = 442\ BTU/ft^2\ hr$

$$\frac{dz}{dt} = -\frac{1}{g\,\rho_a}\frac{dp_a}{dt}$$ XI,Eq. (1)

$$\ln\frac{p_{a,2}}{p_{a,1}} = -\frac{gM_a}{R}\int_{z_1}^{z_2}\frac{dz}{T_a}$$ XI,Eq. (5)

In a stratum in which the lapse rate $L'\ (=-dT_a/dz)$ is constant but not zero

$$T_{a,2} = T_{a,1} + L'\,(z_2 - z_1)$$ XI,Eq. (6)

and $$\frac{p_{a,1}}{p_{a,2}} = \left(\frac{T_{a,2}}{T_{a,1}}\right)^{\frac{gM_a}{RL'}} \quad \text{and} \quad \frac{\rho_{a,1}}{\rho_{a,2}} = \left(\frac{T_{a,2}}{T_{a,1}}\right)^{\frac{gM_a + RL'}{RL'}}$$ XI,Eqs. (15) and (16)

if $L' = 0$

$$\frac{p_{a,1}}{p_{a,2}} = \frac{\rho_{a,1}}{\rho_{a,2}} = e^{\frac{gM_a}{RT_{a,1}}(z_2 - z_1)}$$ XI,Eqs. (9) and (18)

$A_D = 1.209\ V_g^{2/3}$ (Area of great circle of a sphere)

$$C_D = 0.47 + \frac{24}{Re + 0.01} \quad \text{for } Re \leq 4.5 \times 10^5$$ II,Eq. (30)

or $C_D = 0.3$ for $Re > 4.5 \times 10^5$

are simple approximations for drag coefficient.

$$Re = \frac{\rho_a D_B |dz/dt|}{\mu_a}$$ II,Eq. (29)

$$\mu_a = \frac{1.458 \times 10^{-6}\ T_a^{1.5}}{T_a + 110.4}$$ kg/m sec; T_a in ^{o}K XII,(Eq. J-4)

or $$\mu_a = \frac{7.30248 \times 10^{-7}\ T_a^{1.5}}{T_a + 198.72}$$ lbm/ft sec; T_a in ^{o}R XII,(Eq. J-4)

$$\mu\ (helium) = 1.895 \times 10^{-5}\left(\frac{T_g}{273.15}\right)^{0.647}$$ XII,(Eq. J-7)

kg/m sec; T_a in ^{o}K

$$\mu\ (helium) = 1.273 \times 10^{-5}\left(\frac{T_g}{491.67}\right)^{0.647}$$ XII,(Eq. J-7)

lbm/ft sec; T_g in ^{o}R

$$\mu\ (hydrogen) = 386.9 \times 10^{-6}\left(\frac{T_g}{273.15}\right)^{1.5}\frac{T_g + 650.4}{(T_g + 19.6)(T_g + 1176)}$$

kg/m sec; T_g in ^{o}K XII,(Eq. J-6)

$$\mu\ (hydrogen) = 467.2 \times 10^{-5}\left(\frac{T_g}{491.67}\right)^{1.5}\frac{T_g + 1170.7}{(T_g + 35.3)(T_g + 2116.8)}$$

lbm/ft sec; T_g in ^{o}R XII,(Eq. J-6)

$$Gr_L = \frac{\rho^2 g\,(T_f - T)\,L^3}{T\,\mu^2}$$ Kreith (5)

where T is the temperature of the air or gas at a distance sufficiently far from the film surface that it is not directly influenced by the surface. The length L must be a length appropriate to the correlating equation in which Gr is used; e.g., in Eq. (8), Section III.C. $L = \ell' = \pi D_g/2$ for a sphere or long cylinder while in Eq. (15), $L = D_g$.

$$Pr = \frac{C_p \mu}{k} \qquad \text{XII, (Eq. J-8)}$$

Also Pr may be approximated by

$$Pr = a + b \times 10^{-4} T \qquad \text{XII, (Eq. J-9)}$$

where a and b are functions of the gas and T is gas temperature in ^{o}K. See Section XII for values of a and b.

$$k = k_o \left(\frac{T}{T_o}\right)^n \qquad \text{XII, (Eq. J-2)}$$

See Section XII for values of k_o and n.

$$C_p = R\left[a + b \times 10^{-2} T + c \times 10^{-5} T^2\right] \qquad \text{XII, (Eq. J-1)}$$

See Section XII for values of R, a, b, and c.

L. EXPERIMENTAL RESULTS

Coordinated measurements of the thermal and aerodynamic characteristics of large balloons have been published for two flights conducted with

7000m^3 (250,000 ft^3) balloons designed to float at 24 km (80,000 ft) (91, 92). The skins of both balloons were 1.5 mil polyethylene. During both flights the air temperature, the altitude, and the balloon helium temperature were measured continuously. During one flight the temperature of the balloon fabric was also measured at two locations, and the black-ball radiation temperature 90 m (300 ft) below the balloon was determined. These flights were conducted by NCAR from its launch site in Page, Arizona, in October 1966 and January 1968. During the first flight, two of the five thermistors inside the balloon failed during launch, and the system measuring the air temperature malfunctioned after the balloon reached its ceiling.

The thermistors used to measure the helium temperature inside the balloon have a diameter of 0.023 cm (9 mils), roughly 20 times the mean free path of helium at its pressure at 24 km. Such small thermistors were used to maximize the ratio q_c/q_r of heat loss by conduction or convection to heat loss by radiation (93). As shown by Ney et al. (94), for a spherical sensor this ratio is

$$q_c/q_r = 2\, k_g/eD\, \sigma\, T^3$$

The error caused by incident radiation and self heating is given by the equation

$$T - T_g = (D_a \bar{a}_i G/k_g) + (\dot{P}/2\pi D k_g)$$

where T is sensor temperature; T_g, the true gas temperature; D, the sensor diameter; k_g, the gas conductivity; $\bar{a}_i$, the absorptance for incident radiation; G, the incident radiation flux per unit surface area; and $\dot{P}$, the internal power dissipation. The estimated temperature error in the tests is less than $0.1C^{\circ}$.

Uncertainties in the data reduction resulted from the difference between the value of the air temperature measured by a standard radiosonde and the value indicated by the thermistor suspended 90 m below the payload. Approximately 1.5 hr after launch, at an altitude of about 24 km (65,000 ft), the air temperature indicated by the radiosonde was $22^{\circ}C$ higher than the air temperature indicated by the thermistor.

The internal balloon temperatures measured during the flight were compared with the temperature computed using equations very similar to those representing the model presented in this section. The results of the comparison between the computed and measured temperatures are shown in Fig. 20 for the first flight. The relationship between the temperature of each

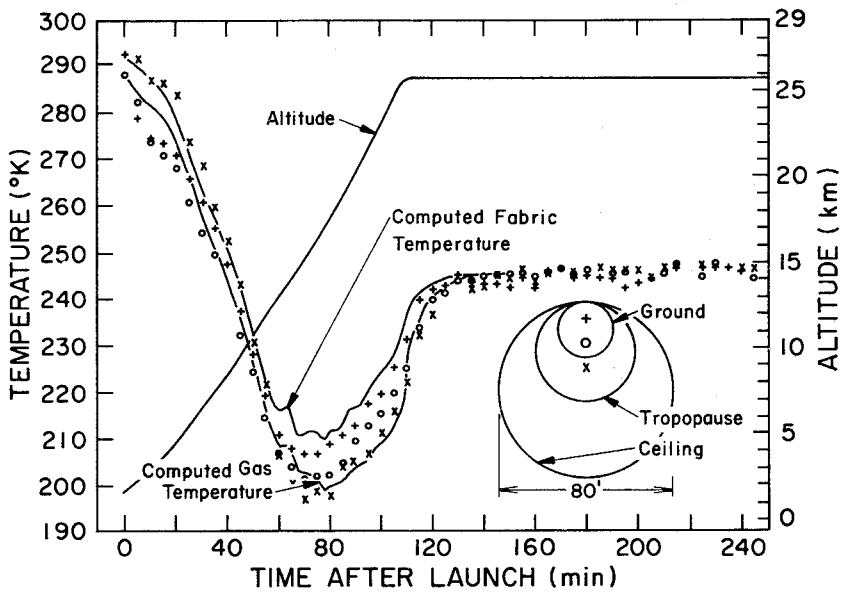

Fig. 20. Experimental results of balloon flight, October 1966; comparison of predicted and measured gas temperatures.

thermistor and the average temperature of the gas and fabric depends on the position of the thermistor in the balloon. In Fig. 20 the rough position of each thermistor during the flight is indicated on the sketch in the lower right-hand corner, in which the balloon is approximated by a sphere. The diameter of the balloon was about 8, 14, and 24 m at ground, tropopause, and ceiling, respectively. The lowest thermistor was buried in the loose fabric at ground level and became exposed to the helium only after the tropopause was reached.

An examination of the experimental data shows that there was considerable temperature stratification in the helium, but the averaged gas temperature followed closely the prediction of the idealized model. The computed gas temperature initially followed the upper thermistor, but just before reaching the tropopause it approached more closely the temperature record of the middle thermistor. At float altitude, the thermistor in the center of the balloon agreed most closely with the average temperature prediction. After about an hour, the temperature of the top thermistor followed closely the temperature predicted for the fabric of the balloon.

On the basis of the scant evidence available so far, it appears that the basic method outlined in this section can, with some additional measurements, be refined to the point where it can be used with confidence to predict the performance of high altitude balloons and to design instrument packages. The current rapid pace of research in heat transfer, meteorology, and atmospheric physics insures that those areas where knowledge is insufficient will be studied and the information needed for thermal design will become available in the near future. However, close cooperation between researcher and designer will be necessary to interpret and relate the results of research so they will be accessible to the people designing and operating scientific balloons.

REFERENCES

(1) Gibbs-Smith, C. H., 1948: Ballooning. Penguin Books, London, 40 pp.

(2) Dollfus, C., 1961: The Orion Book of Balloons. The Orion Press, New York, N.Y., 108 pp.

(3) Lally, V. E., 1967: Superpressure Balloons for Horizontal Soundings of the Atmosphere. NCAR Technical Note TN-28, Boulder, Colo., 25 pp.

(4) Kreith, F. and J. C. Warren, 1970) Thermal Analysis of Balloonborne Instrument Packages. NCAR Technical Note TN-45, Boulder, Colo., 25 pp.

(5) Kreith, F., 1965: Principles of Heat Transfer, 2nd ed., International Textbook Co., Scranton, Pa., 620 pp.

(6) Yuge, T., 1960: Experiments on heat transfer from spheres including combined natural and forced convection. J. Heat Trans. C-82, 214-220.

(7) Vliet, G. C. and G. Leppert, 1961: Forced convection heat transfer from an isothermal sphere to water. J. Heat Trans. C-83, 163-175. (See also discussions by R. M. Drake, J. Kestin, and P. D. Richardson.)

(8) Merk, H. J., 1959: Rapid calculations for boundary-layer transfer using wedge solutions and asymptotic expansions. J. Fluid Mech. 5, 460-480.

(9) Fage, A., 1937: Pressure Distribution for Flow Past Spheres. Brit. Aeronaut. Res. Com. R. & M. No. 1766.

(10) Krause, A. A. and J. Schenk, 1965-66: Thermal free convection from a solid sphere. Appl. Sci. Res. A-15, 397-403.

(11) Merk, H. J. and J. A. Prins, 1954: Thermal convection in laminar boundary layers, Pts. I, II, and III. Appl. Sci. Res. A-4, 207-221.

(12) Garner, F. H. and R. B. Keey, 1958: Mass transfer from single solid spheres, Pt. I. Chem. Eng. Sci. 9(2 & 3), 119-129; also Garner, F. H. and R. B. Keey, 1959: Mass transfer from single solid spheres, Pt. II. Chem. Eng. Sci. 9(4), 218-224.

(13) Garner, F. H. and J. M. Hoffman, 1961: Mass transfer from single solid spheres by free convection. AIChE J. 7, 148-152.

(14) Schütz, G., 1963: Natural convection mass-transfer measurements on spheres and horizontal cylinders by an electrochemical method. Int. J. Heat Mass Trans. 6, 873-879.

(15) Gebhart, B., 1969: Natural convection flow, instability, and transition. J. Heat Trans. C-91, 293-309.

(16) Fendell, F. E., 1968: Laminar natural convection about an isothermally heated sphere at small Grashof number. J. Fluid Mech. 34, 163-176.

(17) Boxi, C. B. and A. Ramachundran, 1969: Effect of vibration on heat transfer from spheres. J. Heat Trans. C-91, 337-344.

(18) Kreith, F., L. G. Roberts, J. A. Sullivan, S. N. Singh, 1963: Convection heat transfer and flow phenomena of rotating spheres. Int. J. Heat Mass Trans. 6, 881-895.

(19) Nordlie, R. L. and F. Kreith, 1961: Convection from a rotating sphere. Int. Dev. in Heat Transfer, ASME, New York, N.Y., 461-467.

(20) Börner, H., 1965: Uber den Wärme-und Stoffübergang an umspülten Einzelnkörpern bei Überlagerung von freier und erzwungener Strömung. VDI-Forschungsheft 512, VDI-Verlag, Düsseldorf, West Germany.

(21) Krischer, O. and G. Loos, 1958: Wärme und Stoffaustausch bei erzwungener Strömung an Körpern verschiedener Form-Teilung. Chem. Ing. Techn. 30, 31-39.

(22) Acrivos, A., 1958: Combined laminar free and forced convection heat transfer in external flows. AIChE J. 4, 285-289.

(23) Mori, Y., 1961: Buoyance effects in forced laminar convection flow over a horizontal flat plate. J. Heat Trans. C-83, 479-482.

(24) Sharma, G. K. and S. P. Sukhatme, 1969: Combined free and forced convection heat transfer from a heated tube to a transverse air stream. J. Heat Trans. C-91, 457-459.

(25) Lichfield, E. W. and N. E. Carlson, 1967: Temperature Control of Balloon Packages. NCAR Technical Note TN-32, Boulder, Colo., 38 pp.

(26) Suriano, F. J. and K.-T. Yang, 1968: Laminar free convection about vertical and horizontal plates at small and moderate Grashof numbers. Int. J. Heat Mass Trans. 11(3), 473-490.

(27) Stewartson, K., 1958: On the free convection from a horizontal plate. Z. Angew. Math. Phys. 9, Ser. A, 276-282.

(28) Gill, W. N., D. W. Zeh, and E. D. Casal, 1965: Free convection on a horizontal plate. Z. Angew. Math. Phys. 16(4), 539-541.

(29) Saunders, O. and M. Fischenden, 1935: Some measurements of convection by an optical method. Engineering, 483-485.

(30) Singh, S. N., R. C. Birkebak, and R. M. Drake, 1969: Laminar free convection heat transfer from downward facing horizontal surfaces of finite dimensions. In Progress in Heat and Mass Transfer, Vol. 2, Pergamon Press, Oxford.

(31) Kimbadi, V. and R. M. Drake, 1960: Free surfaces for prescribed variations in surface temperature and mass flow through the surface.

T. R. Mech. Eng. HT-1, Princeton University, 17 pp.

(32) Husar, R. B. and E. M. Sparrow, 1968: Patterns of free convection flow adjacent to horizontal heated surfaces. Int. J. Heat Mass Trans. 11(7), 1206-1208.

(33) Tyler, B. J. and A. F. Tuck, 1967: Heat transfer to a gas from a spherical enclosure: measurements and mechanisms. Int. J. Heat Mass Trans. 10(21), 251-253.

(34) Sherman, M. and S. Ostrach, 1967: Lower bounds to the critical Rayleigh number in completely confined regions. J. Appl. Mech. 39(2), 308-312.

(35) Hellums, J. D. and S. W. Churchill, 1961: Computation of natural convection by finite difference methods, Pt. I. Int. Dev. in Heat Transfer, ASME, New York, N.Y., 984-994.

(36) _____ and _____, 1962: Transient and steady state, free and natural convection, numerical solutions, Pts. I and II. AIChE J. 8, 690-693, 719.

(37) Powe, E. R., C. T. Carley, and E. H. Bishop, 1969: Free convective flow patterns in cylindrical annuli. J. Heat Trans. C-91, 310-314.

(38) Eckert, E. R. G. and T. W. Jackson, 1950: Analysis of Free Convection Boundary Layer on a Flat Plate. NACA Rept. No. 1015, 7 pp.

(39) Clark, A. J., 1968: Cryogenic heat transfer. Advances in Heat Transfer 5, Academic Press, Inc., New York, N.Y., 325-517.

(40) Dingwell, I. W., W. K. Sepetoski, and R. M. Lucas, 1963: Vertical Motions of High Altitude Balloons. Tech. Rept. II, prepared for Office of Naval Research by A. D. Little, Inc., Cambridge, Mass., 119 pp.

(41) Ulrich, R. D., D. P. Wirtz, and R. H. Nunn, 1969: Transient heat transfer in closed containers after gas injection. J. Heat Trans. C-91, 461-463.

(42) Gebhart, B., R. P. Dring, C. E. Polymeropoulos, 1967: Natural convection from vertical surfaces, the convection transient regime. J. Heat Trans. C-89, 53-59.

(43) Dingwell, I. W., 1967: Thermal Radiation Properties of Some Polymer Balloon Fabrics. Tech. Rept. VI, prepared for Office of Naval Research by A. D. Little, Inc., Cambridge, Mass., 43 pp.

(44) Dunkle, R. V., 1963: Thermal radiation characteristics of surfaces. In Fundamental Research in Heat Transfer, J.A. Clark, Ed., MacMillan Co., New York, N.Y , 1-31.

(45) Hartnett, J. P., E. R. G. Eckert, and R. Birkebak, 1959: The emissivity and absorptivity of parachute fabrics. J. Heat Trans. C-81, 195-201.

(46) Edwards, D. K., 1969: Radiative characteristics of materials. J. Heat Trans. C-91, 1-15.

(47) _____, 1969: Thermal Radiation Measurements. Measuring Techniques in Heat Transfer. E. R. G. Eckert and R. J. Goldstein, Eds., Advisory Group for Aeronautical Research and Development.

(48) Kuhn, P. M., 1969: Environmental Science Services Administration, Boulder, Colo., private communication.

(49) Goetzel, C. G., J. B. Rittenhouse, J. B. Singletary, Eds., 1965: Space Materials Handbook, 2nd ed., TORML 64-40 Air Force Materials Lab., Wright-Patterson Air Force Base, Ohio, 712 pp.

(50) Camack, W. G. and D. K. Edwards, 1960: Effect of surface thermal radiation characteristics on the temperature control problem in satellites.

In Surface Effects on Spacecraft Materials, F. J. Clauss, Ed. John Wiley and Sons, Inc., New York, N.Y., 3-54.

(51) Gaumer, R. C. and L. A. McKellar, 1961: Thermal Radiative Control Surfaces for Spacecraft. Lockheed Tech. Rept. LMSD-704014, Lockheed Aircraft Corp., Sunnyvale, Calif., 198 pp.

(52) Blau, H. H. and H. Fischer, Eds., 1962: Radiative Transfer from Solid Materials, MacMillan Co., New York, N.Y., 257 pp.

(53) Wiebelt, John A., 1966: Engineering Radiation Heat Transfer. Holt, Rinehart and Winston, New York, N.Y., 278 pp.

(54) Kreith, F., 1962: Radiation Heat Transfer for Spacecraft and Solar Power Plant Design, International Textbook Co., Scranton, Pa., 236 pp.

(55) Germeles, A. E., 1966: Vertical Motion of High Altitude Balloons. Tech. Rept. No. 4 prepared for Office of Naval Research by A. D. Little, Inc., Cambridge, Mass., 88 pp.

(56) Zarem, A. M. and D. D. Erway, Eds., 1963: Introduction to the Utilization of Solar Energy, McGraw-Hill, New York, N.Y., 398 pp.

(57) Valley, S. L., Ed., 1965: Handbook of Geophysics and Space Environments, McGraw-Hill, New York, N.Y.

(58) Gates, D. M., 1966: Spectral distribution of solar radiation at the Earth's surface. Science 151(3710), 523-529.

(59) Feigelson, E. M., 1966: Light and Heat Radiation in Stratus Clouds, U.S. Dept. of Commerce, Springfield, Va., 245 pp.

(60) Dunkle, R. V., D. K. Edwards, J. T. Gier, K. E. Nelson, and R. D. Roddick, 1961: Heated cavity reflectometer for angular reflectance measurements. In Proc. Int. Heat Trans. Conf., ASME-AIChE, New York, N.Y., 541-562.

(61) Edwards, D. K., 1961: Directional solar reflectances in the space vehicle temperature control problem. ARS Journal, 1548-1553.

(62) Raschke, E., 1968: The Radiation Balance of the Earth-Atmosphere System from Radiation Measurements of the Nimbus II Meteorological Satellite. NASA Tech. Note TN D-4589, Washington, D.C., 81 pp.

(63) Houghton, H. G., 1954: On the annual heat balance of the northern hemisphere. J. Meteorol. 11(1), 1-9.

(64) Fritz, S., 1949: The albedo of the planet Earth and of clouds. J. Meteorol. 6, 277-282.

(65) Coulson, K. L., 1959: Characteristics of the radiation emerging from the top of a Rayleigh atmosphere: total upward flux and albedo. Planet, Space. Sci. 1(1), Pergamon Press, London, 277-284.

(66) Hibbs, A. R., 1956: The Temperature of an Orbiting Missile. Progress Rept. No. 20-294, Jet Propulsion Laboratory, Pasadena, Calif., 20 pp.

(67) Hottel, H. C. and A. F. Sarofim, 1967: Radiative Transfer, McGraw-Hill, New York, N.Y., 520 pp.

(68) Sparrow, E. M. and R. D. Cess, 1966: Radiation Heat Transfer, Brooks Cole Publ. Co., Belmont, Calif., 322 pp.

(69) Cunningham, F. E., 1961: Power Input to a Small Flat Plate from a Diffusely Radiating Sphere. NASA Tech. Note TN D-710, Washington, D.C., 15 pp.

(70) Yamamoto, G., 1952: On a radiation chart. Sci. Rept. Tohoku Univ., Ser. 5, Geophys., 4, 9-23.

(71) Goody, R. M., 1964: Atmospheric Radiation. Vol. I. Theoretical Basis. Oxford Monogr. on Meteorol., Clarendon Press, Oxford, 436 pp.

(72) Budyko, M. I., 1956: The Heat Balance of the Earth's Surface. Hydrometeorological Publ. House, Leningrad (trans. by U.S. Weather Bureau, 1958), 259 pp.

(73) Kondratyev, K. Y., 1965: Radiative Heat Exchange in the Atmosphere (trans. by O. Tedder). Pergamon Press, Oxford, 411 pp.

(74) Simpson, G. C., 1928: Some studies in terrestrial radiation. Mem. Roy. Meteorol. Soc. 2.

(75) Elsasser, W. M. and M. F. Culbertson, 1960: Atmospheric radiation tables. Meteorol. Monogr. 4(23), Amer. Meteorological Soc., Boston, Mass., 43 pp.

(76) London, J., 1957: A Study of the Atmospheric Heat Balance. Final Rept. AF19, New York Univ., 122-165.

(77) Manabe, F. and F. Möller, 1961: On the radiative equilibrium and heat balance of the atmosphere. Mon. Wea. Rev. 89, 503-532.

(78) Davis, P. A., 1963: An analysis of the atmospheric heat budget. J. Atmos. Sci. 20(1), 5-22.

(79) Simpson, G. C., 1929: The distribution of terrestrial radiation. Mem. Roy. Meteorol. Soc. 3.

(80) Katayama, A., 1966: On the radiation budget of the troposphere over the northern hemisphere, Pt. I. J. Meteorol. Soc. Japan 44(6), 381-401; also Katayama, A., 1967: On the radiation budget of the troposphere over the northern hemisphere, Pts. II and III. J. Meteorol. Soc. Japan 44(1), 1-38.

(81) Sasamori, T., 1968: The radiative cooling calculations for application to general circulation experiments. J. Appl. Meteorol. 7(5), 721-729.

(82) London, J., 1965: The heat-load on a balloon. Unpublished notes, University of Colo., Boulder, Colo.

(83) Valley, S. L., Ed., 1965: Handbook of Geophysics and Space Environments, McGraw-Hill, New York, N.Y.

(84) Suomi, V. E. and P. M. Kuhn, 1958: An economical net radiometer. Tellus 10(1), 160-163.

(85) Bushnell, R. H. and V. E. Suomi, 1961: Experimental flight varification of the economical net radiometer. J. Geophys. Res. 66(9), 2843-2848.

(86) Suomi, V. E., D. O. Staley, and P. M. Kuhn, 1958: A direct measurement of infrared radiation divergence to 160 mb. Quart. J. Roy. Met. Soc. 84(360), 134-141.

(87) Kuhn, P. M., 1963: Measured effective long-wave emissivity of clouds. Mon. Wea. Rev. 91, 635-640.

(88) _____ and D. R. Johnson, 1966: Improved radiometersonde observations of atmospheric infrared irradiance. J. Geophys. Res. 71(2), 367-373.

(89) Kuhn, P. M., L. P. Stearns, and J. R. Stremkis, 1967: Atmospheric Infrared Radiation Over the Antarctic. ESSA Tech. Rept. ER55-IAS2, Boulder, Colo.

(90) Gergen, J. L., 1956: "Black ball": A device for measuring atmospheric infrared radiation. Rev. Sci. Instr. 27(7), 453-460.

(91) Lucas, R. M. and G. H. Hall, 1960: The Measurement of High Altitude Balloon Gas Temperature. Tech. Rept. V, prepared for Office of Naval Research by A. D. Little, Inc., Cambridge, Mass., 30 pp.

(92) Dingwell, I. W. and R. Lucas, 1968: Recent Theoretical and Experimental Studies of High Altitude Balloon Vertical Trajectories. AIAA

Paper 68-940, presented at AIAA 2nd Aerodynamic Deceleration Systems Conference, El Centro, Calif., Sept. 1968.

(93) Gabron, F., I. Dingwell, B. Allen, D. Comstock, 1968: A Study of Balloon-Borne Instrumentation (Radiometers) to Detect Thermal Radiation Transients. NCAR Subcontract 84-68, prepared by A. D. Little, Inc., Cambridge, Mass., 63 pp.

(94) Ney, E. P., R. W. Maas, and W. F. Huch, 1961: The measurement of atmospheric temperature. J. Meteorol. 18, 60-80.

SECTION IV

LIFT GASES

by

Alvin L. Morris

LIST OF SYMBOLS

Symbol	Description	Dimensions
a	subscript identifying its symbol with air	
b	subscript indicating that its symbol has a base or standard value	
B	magnitude of buoyant force	MLT^{-2}
$\vec{B}$	buoyant force vector	MLT^{-2}
c	subscript used with pressure or temperature symbols to indicate that they are cutoff values, i.e., values at which gas flow from a container is stopped	
C_p	specific heat of a gas at constant pressure	$L^2T^{-2}\theta^{-1}$
C_v	specific heat of a gas at constant volume	$L^2T^{-2}\theta^{-1}$
e	linear coefficient of thermal expansion	θ^{-1}
E	Young's modulus	$ML^{-1}T^{-2}$
f	subscript used with pressure or temperature symbols to indicate that they are final values, i.e., values to which the gas in a container returns after some gas has been withdrawn and the remaining gas returns to thermal equilibrium with its environment	
F_t	factor to be multiplied by the base volume of a container to correct its volume for deviations of temperature from base temperature	
F_p	factor to be multiplied by the base volume of a container to correct its volume for deviations of pressure from base pressure	

F_v	factor which is a function of p and T which may be multiplied by the base volume (water volume) of a container to yield the volume of gas in the container reduced to a specified base temperature and pressure	
g	subscript identifying its symbol with a gas as contrasted to air	
g	acceleration due to gravity	LT^{-2}
g_o	standard sea level acceleration due to gravity at 45° N	LT^{-2}
i	subscript used with pressure or temperature symbols to indicate that they are initial values, i.e., values applicable to the gas in a container immediately prior to the withdrawal of gas	
k	exponent of pressure used to indicate the relation between pressure and temperature in a polytropic expansion of gas in a container, e.g., $T_1/T_2 = (p_1/p_2)^k$	
$\vec{k}$	unit vector directed upward	
L	internal length of a cylinder	L
m	mass; subscripts used with it make it specific, e.g., m_c is mass of a cylinder and m_g is mass of gas	M
M	molecular weight; subscripts used with it make it specific. Its dimensions are mass per mass mole, e.g., for air M_a = 28.9644 kilograms per kilogram mole	M/M-Mol
o	subscript indicating that its symbol is at the base datum level, e.g., V_o is the volume of a cylinder containing gas at the base temperature and pressure	

p	absolute pressure; subscripts used with it make specific, e.g., p_a is pressure of air	$ML^{-1}T^{-2}$
p*	gage pressure; subscripts used with it make it specific, e.g., p_g* is gage pressure of gas	$ML^{-1}T^{-2}$
R	universal gas constant	$L^2T^{-2}\theta^{-1}$
R_i	internal radius of a cylinder	L
R_e	external radius of a cylinder	L
s	subscript indicating that its symbol is associated with the stretched condition of a container, e.g., p_s is the pressure of a gas in a container whose dimensions are increased (stretched) by the excess of internal over external pressure or by a temperature different from the base temperature	
T	absolute temperature in °K or °R	θ
T*	temperature in °F	θ
V	volume	L^3
V_o	volume of a gas container at base temperature and pressure. Also called water volume of a container	L^3
y	Poisson's ratio	
Z	gas compressibility = $pM/R\rho T$	

Greek letters

γ	ratio of specific heats of gas ($\gamma = C_p/C_v$)	
β_v	mass which a unit volume of gas will lift in air when air and gas are both at the same base conditions of p and T	ML^{-3}

List of Figures

List of Tables

LIFT GASES

A. EQUATION OF BUOYANCY

The buoyant force $\vec{B}$ exerted on a volume of gas V_g displacing a volume of air V_a is (see Sect. II, Eq. [1])

$$\vec{B} = \vec{k}\left(\rho_a V_a - \rho_g V_g\right)g \tag{1}$$

where ρ_a and ρ_g are the density of air and lift gas, respectively, g is the acceleration due to gravity, and $\vec{k}$ is a unit vector directed upward. (For a description of the coordinate system used here, see Sec. II.C.) Only the buoyant force will be considered in this section; therefore, the vector notation will be dropped. If $B > 0$, it is a force directed upward. If $B < 0$ it is directed downward. Also, except for the small volume occupied by the balloon film, the rigging, and the payload, $V_a = V_g$. With these simplifications, Eq. (1) may be written

$$B = \rho_a V_a g\left(1 - \frac{\rho_g}{\rho_a}\right) \tag{2}$$

Although some potentially useful lift gases, such as ammonia, may be readily liquified, most gases will be used in balloons only under conditions of pressure and temperature which are enough above critical

to be considered to be ideal gases. Then

$$\rho_a = \frac{p_a M_a}{R T_a} \text{ and } \rho_g = \frac{p_g M_g}{R T_g} \tag{3}$$

and

$$\frac{\rho_g}{\rho_a} = \frac{p_g M_g T_a}{p_a M_a T_g}$$

where p, M, and T are pressure, molecular weight, and temperature, respectively; the subscripts a and g identify their symbols with air and gas, respectively; R is the universal gas constant.

Normally $p_g > p_a$. The difference is only slight in the so-called zero-pressure balloon, but it may be appreciable in a fully inflated superpressure balloon. Also frequently $T_a \approx T_g$, although the difference may be quite significant at times. In fact, the hot air balloon relies on that difference to obtain lift. In searching for gases which may be used to provide lift, however, one may assume that $p_g T_a / p_a T_g \approx 1$ as a first approximation, so that

$$\frac{\rho_g}{\rho_a} = \frac{M_g}{M_a} \tag{4}$$

Then from Eq. (2)

$$\frac{B}{\rho_a V_a g} = \left(1 - \frac{M_g}{M_a}\right) = (1 - \sigma^{-1}) \tag{5}$$

where σ is substituted for the ratio M_a/M_g for convenience. Since $\rho_a V_a g$ is the weight of the displaced air, its alebraic sign is positive. Equation (5) then indicates that any gas having a molecular weight less than the molecular weight of air, so that $(1 - \sigma^{-1}) > 0$, is a potentially useful gas for ballooning. Also the term $(1 - \sigma^{-1})$ may be interpreted as the lift of the gas per unit weight of displaced air. Thus it serves as a useful index for selecting lift gases, although other characteristics, such as inflammability and toxicity, must also be considered.

B. LIFT GAS CHARACTERISTICS

Table 1 from Morris (1) lists several gases having molecular weights less than air and provides some other pertinent data about each. No effort is made to provide an exhaustive list of potentially useful lift gases. On the other hand most such gases are listed, and the table can be used to illustrate some useful information about gases for ballooning.

Table 1

Lift Gas Comparison

Gas	Chemical formula	Molecular weight	Lift index $(1-M_g/M_a)$	Flammable limits in air (%)	Comments
Perfect lift gas		0.	1.000	Inert	Does not exist; vacuum is weightless, but difficult to contain
Hydrogen	H_2	2.0159	0.930	4 - 75	Readily available, inexpensive
Helium	He	4.0032[(a)]	0.862	Inert	Readily available in U.S., moderately expensive
Deuterium	D_2	4.032	0.861	5 - 75	Very rare
Decomposed ammonia	N_2+3H_2	8.515	0.706	7 - 73	Readily generated in small quantities
Methane	CH_4	16.04	0.446	5.3-14	Major constituent of natural gas
Ammonia	NH_3	17.03	0.412	15-28	Toxic only in high concentrations, liquifies readily
Water vapor	H_2O	18.01	0.378	Non-flammable	Liquifies too readily
Air	Mixture of N_2, O_2, etc.	28.96	0.000	--	Provides lift only if density of the air inside balloon is less than that outside

(a) Molecular weight of helium supplied for ballooning in the U.S. in 1972.

1. Hydrogen and Helium

Hydrogen forms a molecule by combining two atoms; helium does not. Therefore, the molecular weight of helium is only twice that of hydrogen, and a given volume of hydrogen produces only 1.08 (0.930/0.862) times the lift of a like volume of helium in the atmosphere. The value of $(1 - \sigma^{-1})$ is 0.930 for hydrogen and 0.862 for helium. A vacuum would produce the maximum possible lift if it could be contained by the same balloon film used for the gases. It cannot, of course, but hydrogen and helium both produce a very high fraction of the maximum possible lift.

The adiabatic lapse rate of hydrogen in the atmosphere is much nearer the normal tropospheric lapse rate than is the lapse rate of helium (see Sect. II, Table 3). Therefore, a hydrogen filled balloon is less stable, i.e., its vertical movement is more difficult to control than that of a helium filled balloon. Hydrogen is highly flammable in air; helium is inert. Neither gas is toxic. If helium is available at reasonable cost, it is preferred for ballooning. Hydrogen is satisfactory, however, if adequate precautions are taken. Other gases are generally less satisfactory, but some may have properties which make them useful under some circumstances.

2. Ammonia as a Lift Gas and Source of Hydrogen

Ammonia is an interesting gas. Its critical temperature is 132.9° C and it may readily be liquified at normal atmospheric temperatures. In fact, it is usually stored and transported as a liquid under its own vapor pressure, which equals 2.032×10^6 N/m² (294.8 psia) at a temperature of 50° C (122° F). The liquid boils readily under normal atmospheric conditions, providing a gas. It is toxic in high concentrations, but it is so offensive that a person using it is not likely to suffer more than temporary discomfort if exposed to it unless he cannot escape. Its adiabatic lapse rate in the atmosphere is even closer to the normal tropospheric temperature lapse rate than that of hydrogen.

Ammonia can be decomposed into nitrogen and hydrogen according to the following formula:

$$2NH_3 + \text{heat} \rightleftharpoons N_2 + 3H_2$$

The decomposition is endothermic, i.e., it requires heat. The reaction can proceed in either direction, but if nitrogen and hydrogen are mixed at normal atmospheric temperatures, the combination reaction is extremely slow. Further, at atmospheric pressures, the amount of ammonia in an

equilibrium mixture of ammonia, nitrogen, and hydrogen is very low. Therefore, if decomposition of ammonia can be accomplished, the hydrogen and nitrogen mixture can be used as a ballooning lift gas. Interestingly, because two volumes of ammonia when completely decomposed produce one volume of nitrogen and three volumes of hydrogen, the decomposed gas provides greater lift than the original ammonia. This can be demonstrated quantitatively by comparing molecular weights.

The molecular weight of this mixture of gases, M_m, may be calculated as follows:

$$M_m = \frac{\left(\text{Vol of } N_2\right)\left(M_{N_2}\right) + \left(\text{Vol of } H_2\right)\left(M_{H_2}\right)}{\left(\text{Vol of } N_2\right) + \left(\text{Vol of } H_2\right)}$$

$$M_m = \frac{1 \times 28.013 + 3 \times 2.016}{4}$$

$$M_m = 8.515$$

A given volume of the decomposed mixture then provides 1.7 times the lift of a like volume of ammonia and 0.82 times the lift of a like volume of helium. At least one lift gas generator makes use of this property of ammonia, using a catalyst to aid in the decomposition. Unfortunately, the decomposition is not complete, and the mixture contains a small amount of

ammonia, which decreases its effectiveness somewhat. Using this method and present equipment, the rate at which lift gas can be generated at the launch site is great enough to provide gas for small meteorological sounding balloons but not for large scientific balloons. This same statement applies to most methods of generating hydrogen at the launch site. When hydrogen is needed in large quantities for ballooning, it is usually transported to the launch site in high pressure cylinders or as a cryogen in large dewars.

3. Special Characteristics

Several of the light gases are flammable, helium and neon are inert, and water vapor and nitrogen are nonflammable. Ammonia, hydrogen fluoride, diborane, and carbon monoxide are toxic. Methane, a major constituent of natural gas, is usually thought of as a toxic gas. However, while one will suffocate in a methane atmosphere, it is not toxic. Hydrogen fluoride and diborane are so corrosive or so unstable that they are not useful as lift gases.

Water vapor condenses so readily under atmospheric temperature and pressure conditions that it is not useful except perhaps for very special purposes.

C. GAS STORAGE AND MEASUREMENT

By following a series of steps like that used in deriving Eq. (5), one can derive the following equivalent form:

$$\frac{B}{g} = \rho_g V_g (\sigma - 1) \qquad (6)$$

This form is more convenient as a starting point for measuring the buoyant lift of gas in a balloon. The product $\rho_g V_g$ is the mass of gas required to provide lift of magnitude B when the local acceleration due to gravity is g and the conditions assumed in deriving Eq. (5) are fulfilled. Thus, under these conditions, the mass which can be lifted is a function only of the mass of gas placed in the balloon and the ratio of the molecular weight of that gas to the molecular weight of air. Normally, at the time of inflation of either zero-pressure or superpressure balloons, conditions approximate the assumed conditions well enough that Eq. (6) may be used to determine the mass of gas required to lift the mass B/g.

The mass of gas may be measured directly by means of a set of balances or indirectly by measuring the volume and density and taking the product. It can be, and sometimes is, measured by measuring the lift of the balloon, but to measure the lift of very large balloon systems in the turbulent

atmosphere is difficult enough that it does not often serve as the primary means of determining how much gas to put into a balloon. Most often the volume and density of the gas are measured.

Lift gases are stored in either the gaseous state under high pressure or as cryogens. A flowmeter has been described by Kubara (2) which can provide a sufficiently accurate measure of gas volume to serve the needs of scientific ballooning. Flowmeters can measure gas flow from any source, but if cryogenic storage is used, the gas must be warmed to a temperature which is within the operating limits of the meter. Their use is not yet commonplace, but cryogenic storage and transport are likely to increase in the future and to be accompanied by increased use of flowmeters.

Flowmeters must indicate both volume and density to be useful or they must provide volume reduced to some acceptable base temperature and pressure, often called standard temperature and pressure (STP). When volume is reduced to a given set of base conditions, the density is also determined for that set of conditions. That this is true when the base conditions permit the gas to be considered an ideal gas is apparent from Eq. (3), and base conditions are usually chosen so that Eq. (3) is applicable.

From Eq. (6) it is evident that if the product $\rho_g V_g$ of gas in a pressurized container can be ascertained, the mass which that gas will lift can also be determined. For conditions of temperature and pressure for which Eq. (3) serves as an acceptable equation of state, the product $\rho_g V_g$ is easily expressed in terms of the measurable quantities p_g, T_g, and V_g, where V_g is the nominal volume of the container, henceforth designated V_o. The nominal volume (also called water volume) of a container is usually determined by weighing the container empty and then when filled with water having a known temperature. The difference in weight divided by the known specific weight of the water yields the water volume of the container.

The actual (stretched) volume of a container is a function of the temperature of the container and the pressure exerted against its walls by the fluid it contains. Also the equation of state for a gas becomes much more complicated than Eq. (3) when the pressure is greater than a few atmospheres. Therefore, the product $\rho_g V_g$ of an actual gas contained under high pressure is not a simple function of p_g, T_g, and V_o.

1. Pressure and Temperature Measurement

Precision bourdon tube pressure gages which are carefully handled and checked are accurate to ±0.5%, and gas pressure, measured when no gas is flowing from the container, is representative. To obtain a temperature which is representative of the gas in a container is more difficult. The practice of the U.S. Bureau of Mines and of most scientific ballooning crews is to place a mercury-in-glass thermometer in contact with the outside of the container and read it when it has come to equilibrium with the container. This is nothing more than the usual practice in measuring any temperature with a glass thermometer, but the temperature obtained is that of the container and not of the gas. Precautions must be taken, therefore, to assure that the temperature is representative of the gas inside the container. The best measurements are probably made at night when the temperature of the ambient air is at a minimum. Then air temperature does not change rapidly, and if air circulation is maintained about the container, the container and the gas in it are likely to be in thermal equilibrium with the air, and the temperature shown by the thermometer will be representative of the gas temperature. A temperature taken during the day when

ambient air temperature is at a maximum is likely to be all right also if the container is shaded from the sun and is well ventilated. Temperature measurements made when the temperature of the ambient air is changing rapidly or when the sun is shining on the container are not likely to be accurate.

In scientific ballooning a single tube rarely contains enough gas to inflate a balloon. Therefore, computations must be made of the lift of the gas in a number of individual tubes or several must be joined together by a manifold. The pressure of all tubes is then equal and may be read by a single gage. The temperature may also be determined by a single thermometer if the cylinders are close together and are in thermal equilibrium with the ambient air. The nominal volume of the entire container is the sum of the nominal volumes of the individual cylinders.

It is usually possible to exercise proper care in determining the lift in one or many cylinders before balloon inflation starts. A trailer such as the one shown in Fig. 1 is used to transport the gas to the launch site. The tubes on the trailer are interconnected at the rear by a manifold as shown in the picture, but each is usually sealed separately to minimize

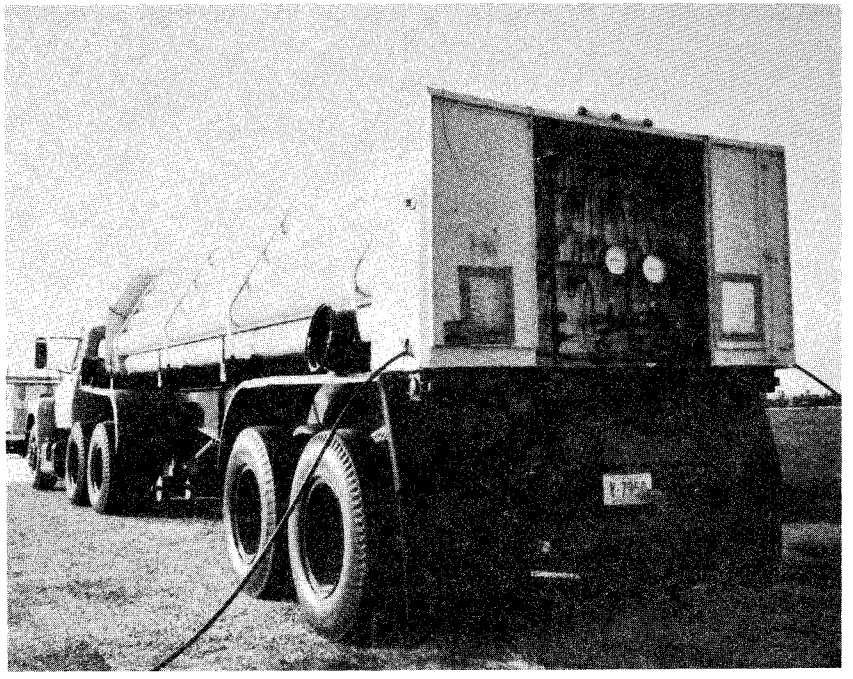

Fig. 1. Lift gases for ballooning are usually transported in cylinders mounted on trailers as shown here. The cylinders are connected at the rear by a manifold in such a way that gas may be taken from any one or any combination of them simultaneously. Each tube normally has its water volume stamped on it.

leakage. Thus, the pressure and temperature of the gas in just those tubes needed for inflation may be determined under optimum conditions some time before inflation starts.

2. Stretched Volume of Steel Cylinders

It has been pointed out that the actual volume of a container is a function of its temperature and of the pressure of the fluid it contains. Equation (7), taken from Kalman (3), expresses the stretched volume of a cylindrical steel tube as a function of its nominal volume, its temperature, and the pressure of the gas it contains.

$$V_s = V_o \left[1 + 1.89 \times 10^{-5} \ (T^* - 70)\right] \left[1 + 7.4 \times 10^{-7} p_g^*\right] \qquad (7)$$

where V_s is the stretched volume, T^* is the temperature of the tube in degrees Farenheit, and p_g^* is the gage pressure of the gas in pounds per square inch.

A number of assumptions were made in deriving Eq. (7). For example, since the coefficient of the temperature in the first bracket is actually three times the linear coefficient of thermal expansion of steel, it is clear that all products of small quantities of second and higher order have been neglected in accounting for thermal expansion. The pressure stretch

coefficient, given as 7.4×10^{-7}, is an unweighted average between a value obtained by testing helium tank-car cylinders hydrostatically and a value computed from the characteristics of the steel and the physical dimensions of the cylinders. The two values were in reasonable agreement and both were apparently believed to be equally well founded; therefore, their average was used as a "best" estimate of the coefficient. Another assumption which is made in applying Eq. (7) is that the temperature of the gas is equal to the temperature of the cylinder. Finally, if one expression is used for all steel cylinders, the assumption is made that all have essentially the same characteristics, in this case the characteristics of the helium tank-car cylinders used in the U.S. during and prior to 1968.

The assumptions made in deriving Eq. (7) have not caused problems in calculating lift for ballooning even when steel cylinders much smaller and much larger than tank-car cylinders were used. Nonetheless, if cylindrical containers are to be used which are significantly different from the helium tank-car cylinders used in the U.S. prior to 1968, new coefficients for Eq. (7) may be computed.

The first term in brackets in Eq. (7) may be expressed more generally as

$$F_T = \left[1 + 3e(T - T_b)\right] \tag{8}$$

where F_T is a factor which can be multiplied by the volume of the cylinder at its base temperature T_b to correct the volume to temperature T, and e is the linear coefficient of thermal expansion of the material from which the cylinder is made. F_T is dimensionless; e must have the dimensions of T^{-1}. A more general expression for the second bracketed term of Eq. (7) is

$$F_p = \left[1 + \frac{2dR_i}{R_i} + \frac{dL}{L}\right]_p \tag{9}$$

where F_p is a dimensionless factor which may be multiplied by the volume of the cylinder at its base pressure to correct the volume to pressure p. R_i is the internal radius of the unstretched cylinder and L is its unstretched internal length. Also

$$\frac{dR_i}{R_i} = \frac{p_g^*}{E}\left[\frac{R_e^2 + R_i^2}{R_e^2 - R_i^2} - y\left(\frac{R_i^2}{R_e^2 - R_i^2} - 1\right)\right] \tag{10}$$

$$\frac{dL}{L} = \frac{p_g^*}{E}\left[\frac{R_i^2}{R_e^2 - R_i^2} - y\left(\frac{R_e^2 + R_i^2}{R_e^2 - R_i^2} - 1\right)\right] \tag{11}$$

In Eqs. (10) and (11) R_e is the unstretched external radius, E is Young's modulus, and y is Poisson's ratio.

The external diameter and length of a cylinder may be measured, but the internal diameter and length cannot be determined directly. An average value of the internal radius of a tube may be approximated from its mass, length, and external radius by means of the formula

$$R_i = \left(R_e^2 - \frac{m_c}{\pi L \rho_c}\right)^{\frac{1}{2}} \tag{12}$$

or from its nominal volume and length by the formula

$$R_i = \left(\frac{V_o}{\pi L}\right)^{\frac{1}{2}} \tag{13}$$

where m_c is the mass of the cylinder and ρ_c is the density of the material from which it is made. In using Eq. (12) an average of several measurements of R_e taken along the tube should be employed. All measurements should be made when the tubes are in an unstretched condition and L should be measured so that the value obtained approximates as nearly as possible the internal length of the tube. This involves making allowance for the forming of the ends of the tubes.

3. Equations of Lift for Helium

Any of several equations of state might serve for measuring helium which is stored under high pressure. The form which has the best foundation in theory is the virial form, but the form most commonly used for engineering purposes is Eq. (3) with a compressibility factor Z included to account for deviations of the real gas from an ideal gas. The equation of state using Z is

$$\rho_g = \frac{P_g M_g}{Z_g R T_g} \tag{14}$$

The compressibility, Z_g, is a function of pressure and temperature; therefore, the very simple appearance of Eq. (14) is deceptive.

Generalized charts of Z can be found in most engineering handbooks (e.g., Eshbach [4]). Tables also exist, and a set taken from Lydersen et al. (5) is reproduced in readily usable form by Reid and Sherwood (6). These tables and charts provide values of Z which may be used for hand calculations, but for the machine calculation of lift tables, an equation relating Z, p, and T is preferable.

For computing the volume of helium in cylindrical steel containers, Kalman (3) used the empirical expression

$$Z_g = 1 + \left[10.2297 \times 10^{-5} - 19.2998 \times 10^{-8} T_g + 1.1836 \times 10^{-10} T_g^2\right] P_g - 2.217 \times 10^{-10} P_g^2 \quad (15)$$

which was developed by Miller et al. (7). Temperature must be entered in degrees Rankine and pressure in pounds per square inch. Angevine (8), who compared values given by several equations of state with available experimental data, also elected to use an equation of the form of Eq. (14) with Z_g given by Eq. (15) to compute lift tables for helium.

Equations (6) and (14) may be combined as follows:

$$\frac{B}{g} = \frac{M_g (\sigma - 1)}{R} \frac{p_{g,s} V_{g,s}}{T_{g,s} Z_{g,s}} \quad (16)$$

where the subscript pair g,s indicates identification with the lift gas in the stretched cylinder. Equation (16) is applicable to any gas. If it is written specifically for the helium available in 1969 from the U.S. Bureau of Mines (M_g = 4.0032), it and Eqs. (7) and (15) provide a set of equations suitable for helium lift calculations. For convenience the equations are given for direct calculations in Système International and English Engineering

Units (lb m, lb f, ft °R, sec).

$$\text{SI units } \left(\frac{B}{gV_o}\right)_{g,s} = \frac{3.0022 \times 10^{-3}\ p_{g,s}}{T_{g,s} Z_{g,s}} \frac{V_{g,s}}{V_o} \text{ (kg/m}^3\text{)} \quad (17)$$

$$\text{Eng units } = \frac{2.3260\ p_{g,s}}{T_{g,s} Z_{g,s}} \frac{V_{g,s}}{V_o} \text{ (lb m/ft}^3 \quad (17a)$$

$$\text{SI units } \frac{V_{g,s}}{V_o} = \left[1 + 3.40 \times 10^{-5} (T_{g,s} - T_b)\right] \left[1 + 1.07 \times 10^{-10} (p_{g,s} - p_b)\right] \quad (18)$$

$$\text{Eng units } = \left[1 + 1.89 \times 10^{-5} (T_{g,s} - T_b)\right] \left[1 + 7.4 \times 10^{-7} (p_{g,s} - p_b)\right] \quad (18a)$$

$$\text{SI units } Z_{g,s} = 1 + (1.48369 - 5.03856 \times 10^{-3} T_{g,s} + 5.5620 \times 10^{-6} T_{g,s}^2) p_{g,s} \times 10^{-8} - 4.664 \times 10^{-18} p_{g,s}^2 \quad (19)$$

$$\text{Eng units } = 1 + (10.2297 - 19.2998 \times 10^{-3} T_{g,s} + 1.1836 \times 10^{-5} T_{g,s}^2) p_{g,s} \times 10^{-5} - 2.217 \times 10^{-10} p_{g,s}^2 \quad (19a)$$

Equation (17) gives the lift of each unit of nominal volume of helium in a cylinder at absolute temperature $T_{g,s}$ and absolute pressure $p_{g,s}$. Kalman (3) claims that volume factors based on Eqs. (7), (14), and (15) are accurate to within ±0.05% and that accuracy in measuring the volume of helium in cylindrical steel containers depends primarily on the accuracy of the pressure and temperature measurements. Tables I-1 and I-2 of Sect. XII are short helium lift tables in which linear interpolation is possible. More complete tables which avoid the need for interpolation can easily be generated from Eqs. (17)-(19) by anyone having access to a computer.

4. Practical Helium Measurement During Balloon Inflation

Unfortunately, one never finds precisely the amount of lift desired in any set of tubes, and some gas (enough to provide lift equal to the total initial lift in the set less the lift to be placed in the balloon) must be left in at least one of them when balloon inflation is completed. Also, removing all gas from a container is such a slow process that ballooning crews frequently prefer to maintain a high gas flow rate throughout inflation by withdrawing gas simultaneously from a container composed of enough cylinders so that when inflation is completed the pressure in the

container is still quite high. Neither gas pressure nor temperature can be measured accurately while gas is being withdrawn from the container. The pressure of the flowing gas will be lower than the static pressure of the gas in the container due to the Bernoulli effect, and the temperature of the gas is likely to be less than the temperature of the container because of the cooling of the expanding gas. It is a simple matter to close off the flow momentarily during inflation to check the static pressure, and this is what is normally done. (The usual precautions of waiting until transients have died out and tapping the gage prior to the reading must be taken.) There is no equally simple way, however, to measure the gas temperature during inflation and to be certain the measurement is representative. However, the container can be placed in a well ventilated, shady location and, when the ambient air temperature is steady, and air, container, and gas have all reached thermal equilibrium, both temperature and pressure can be read. This is not practical, but the concept is useful as an introduction to the reasoning behind the method which is developed here.

As stated before, when gas is being withdrawn from a container and withdrawal is stopped, the pressure can be readily determined but the

temperature cannot. Except under unusual circumstances, the temperature of the gas falls below the temperature of its container during withdrawal; therefore, gas temperatures may be expected to increase when the container is closed and withdrawal is ended. But the lift remaining in a closed container is constant, and any change in temperature of the enclosed gas must also be accompanied by a change in pressure. Any combination of temperature and pressure which satisfied Eqs. (17)-(19) when $\left(B/gV_o\right)_{g,s}$ is assigned the proper value and held constant is, in principle, an acceptable combination. Tables I-1 and I-2 of Sect. XII generated from these equations provide a means of solving for p, T, or $\left(B/gV_o\right)_{g,s}$ if any two of the three are known. $\left(B/gV_o\right)_{g,s}$ is constant for a closed container, and if the changes in p and T are small, then changes in $V_{g,s}/V_o$ and $Z_{g,s}$ are negligible, and approximately

$$\frac{P}{T} = \text{Const} \tag{20}$$

Thus, if one acceptable combination of p and T can be found for a closed container, other combinations may be readily determined from Eq. (20).

Let p_c and T_c be the cutoff pressure and temperature of gas in a container at the time immediately after withdrawal is stopped when the container retains precisely the desired amount of lift gas. T_c will be less than T_i, the temperature of the gas when inflation was begun. Assume also that $T_i = T_a = \text{Const}$ for the period of inflation and long enough after inflation is completed to let the gas "recover" its temperature--i.e., to let the gas temperature warm up to T_a, the temperature of the ambient air. Also let p_f be the "final" gas pressure, the pressure after the gas has recovered its initial temperature. Then if $\left(T_i - T_c\right)$ is not too large, Eq. (20) may be used to establish a relationship between p_c, T_c, p_f, and T_i. It is

$$\frac{p_c}{T_c} = \frac{p_f}{T_i} \tag{21}$$

The polytropic process is frequently assumed in gas compression and expansion work (e.g., Gill [9] or Streeter [10]). It is expressed in a form which relates the pressure and temperature of an expanding gas by Eq. (22)

$$\frac{T_c}{T_i} = \left(\frac{p_c}{p_i}\right)^k \tag{22}$$

For an adiabatic process, $k = \left(C_p - C_v\right)/C_p = (1 - \gamma^{-1})$ where C_p and C_v are the specific heats of the gas at a constant pressure and volume, respectively, and $\gamma = C_p/C_v$. For an isothermal process, $k = 0$.

During the withdrawal of gas, heat can readily flow from the container to the gas. Also the container is a good thermal conductor which will transfer heat from the ambient air to the gas if the gas temperature is lower than the air temperature. Therefore, the gas in the container cannot expand adiabatically as gas is withdrawn. Since it is observed to cool appreciably during balloon inflations, it clearly does not expand isothermally. For short periods it probably expands in such a way that Eq. (22) with k = Const and $0 < k < (1 - \gamma^{-1})$ provides a good approximation to the expansion process. If withdrawal is rapid and $T_i = T_a$, little heat will flow into the gas during the first few seconds, and $k \approx (1 - \gamma^{-1})$. As withdrawal continues and $\left(T_a - T_g\right)$ increases, however, heat will flow more rapidly to the gas until, if withdrawal continues long enough, the process will become essentially isothermal.

This reasoning suggests that if Eq. (22) is to be used to relate T_i, T_c, p_i, and p_c, the value of k must vary during withdrawal. It is possible, nonetheless, to calculate a mean value of k for the entire withdrawal if T_i, T_c, p_i, and p_c are all known. Further, if gas is withdrawn at a constant, rapid rate, the mean value should be near $(1 - \gamma^{-1})$ for very small withdrawals and near zero for very large ones. This reasoning has been confirmed by test data reported by Gildenberg (11), which show k to correlate well with $\left(p_f/p_i\right)$.

Now Eqs. (21) and (22) can be combined to yield

$$\frac{p_c}{p_f} = \left(\frac{p_c}{p_i}\right)^k$$

from which

$$p_c = p_f \left(\frac{p_f}{p_i}\right)^{\frac{k}{1-k}} \tag{23}$$

Equation (23) makes use of p_f, p_i, and k to calculate p_c without making explicit use of the gas temperature, although T_i must be used to calculate p_f. The exponent $k/(1 - k)$ must be determined, and since k correlates with p_f/p_i, the ratio $k/(1 - k)$ might also be expected to do so. In fact, the data from 14 inflation tests reported by Gildenberg show that $k/(1 - k)$

correlates linearly with $\left(p_f/p_i\right)^3$ with a coefficient of correlation of 0.966, and $k/(1 - k)$ may be estimated by means of the regression equation

$$\left(\frac{k}{1 - k}\right) = 0.038 + 0.23\left(\frac{p_f}{p_i}\right)^3 \qquad (24)$$

Either Table I-1 or I-2 of Sect. XII may be used to determine p_f from p_i, T_i, and the residual lift. Then p_f and p_i may be entered into Eq. (24) to determine $k/(1 - k)$. Finally, Eq. (23) enables one to compute the pressure at which the gas in the container should be left immediately after withdrawal is ended to assure that the container retains the proper residual lift. Figure 2 is a graph of $\left(p_f/p_i\right)^{k/(1 - k)}$ (shown as p_c/p_f) as a function of p_f/p_i. The graph may be used to determine a factor p_c/p_f which can be multiplied by p_f to yield p_c.

The method developed here to calculate p_c gives values which are comparable to the values one may obtain from the much used General Mills Inflation Tables (General Mills, Inc. [12]). Unfortunately, the basis of the General Mills Tables was never published as far as can be determined, but their successful use over the years leaves little doubt that they give acceptable values. With both methods, the best measurements occur when p_f

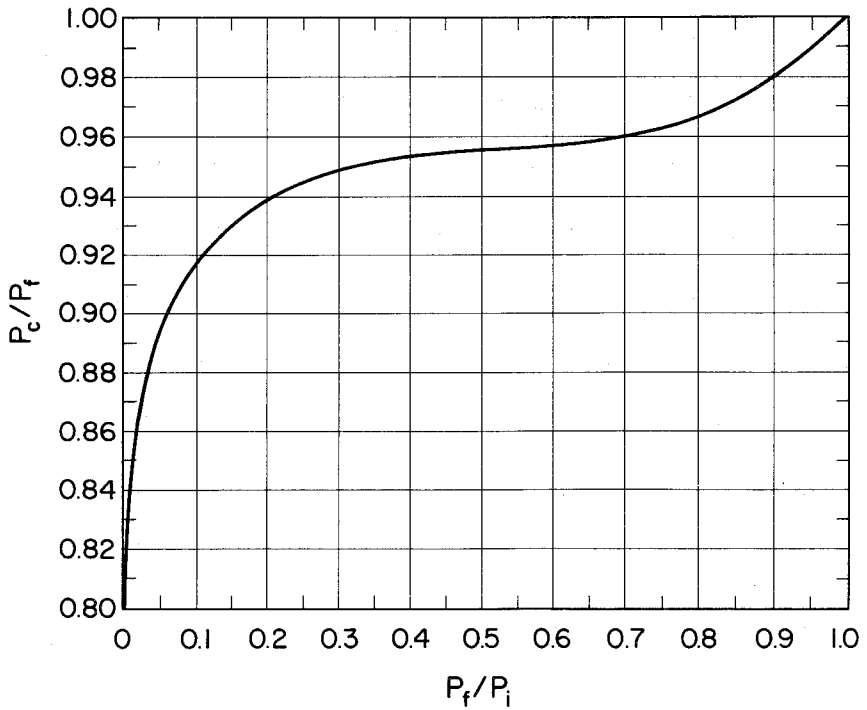

Fig. 2. Graph of Eq. (23) where $k/(1 - k)$ was determined from Eq. (24).

is very small, i.e., when essentially all the gas is removed from the container. Either method may result in a large percentage error when a very small fraction of the gas in a container is withdrawn. It is recommended that withdrawals resulting in $\left(p_f/p_i\right) > 0.75$ should be avoided if possible. This may be done by using fewer or smaller cylinders.

5. Hydrogen Contained in Steel Cylinders

The foregoing discussion has covered most of what can or needs to be said about measuring any gas for balloon inflation aside from the safety aspects and the need for an accurate equation of state for the gas if it is stored under high pressure.

The following set of equations is the counterpart for hydrogen of Eqs. (17) and (19) for helium. No counterparts of Eqs. (17a) and (19a) are given:

$$\left(\frac{B}{gV_o}\right)_{g,s} = \frac{3.2412 \times 10^{-3} p_{g,s}}{T_{g,s} Z_{g,s}} \frac{V_{g,s}}{V_o} \ (kg/m^3) \qquad (25)$$

$$Z_{g,s} = \exp\left[\frac{1}{T_{g,s}^{1.25}}\left(B_1 T_{g,s} - B_2 T_{g,s}^{\frac{1}{2}} - B_3\right)\frac{\rho_{g,s}}{\rho_o} + \frac{1}{T_{g,s}^{2}}\left(C_1 T_{g,s}^{\frac{1}{2}} - C_2\right)\left(\frac{\rho_{g,s}}{\rho_o}\right)^2\right] \qquad (26)$$

where $B_1 = 5.5478 \times 10^{-3}$, $B_2 = 3.6877 \times 10^{-2}$, $B_3 = 2.2004 \times 10^{-1}$,

$C_1 = 4.788 \times 10^{-3}$, $C_2 = 4.053 \times 10^{-2}$ and $\rho_o = 8.9886 \times 10^{-2}$ kg/m^3.

Equation (26) is a modified form of an equation by Wooley et al. (13).

Since Eq. (18) is a mathematical description of certain aspects of a steel cylindrical tube and is independent of the fluid the tube may contain, it applies also to hydrogen. Equations (18), (25), and (26) were used to generate Table I-3 of Sect. XII. They were also used with suitable conversion of units to generate Table I-4 of Sect. XII.

Equation (23) is essentially an empirical equation derived for helium withdrawals, but the reasoning leading to its form is as valid for hydrogen as for helium. The value of γ for hydrogen is 1.41 compared to 1.66 for helium, so that the limits for k are different, being 0 to 0.40 for helium and 0 to 0.29 for hydrogen. Further, the thermal conductivity for hydrogen is greater than for helium; the ratio of the two being approximately 1.2. These differences suggest that k is likely to be smaller for hydrogen than for helium when comparable withdrawals result in identical values of p_f/p_i; consequently, k/(1 - k) will be smaller and $\left(p_f/p_i\right)^{k/(1-k)}$ will be larger. Using a value of $\left(p_f/p_i\right)^{k/(1-k)}$ for helium taken from Fig. 2

or Fig. I-1 of Sect. XII will result in a value of p_c which is slightly small for hydrogen, but a value which is too small will cause too much gas to be placed in a balloon rather than too little. Therefore, Fig. I-1 of Sect. XII is considered acceptable, but slightly conservative, for use with hydrogen.

6. Determining Lift from STP Volume

Gas used in commerce is usually measured in terms of volume reduced to a set of base conditions. Knowing the base conditions permits one to calculate the density corresponding to that volume also. Therefore, the product, $\rho_g V_g$, may be calculated, and from Eq. (6) lift may be determined. If Eq. (6) is written in the form

$$\frac{B}{g} = \rho_{g,b} (\sigma - 1) V_{g,b} \tag{27}$$

where the subscript b indicates that the variables ρ_g and V_g are both reduced to base conditions, it is apparent that

$$\rho_{g,b} (\sigma - 1) = \beta_v = \text{Const} \tag{28}$$

Table 2 lists values of β_v and β_v^{-1} for helium and hydrogen for some of the most frequently used base conditions. β_v may be viewed as the mass which a unit volume of gas under base conditions will lift in air under those same base conditions. It has the units of density. Its reciprocal is useful when one needs to calculate the volume of gas needed to lift a given mass. For example, the number 15.5 ($\sim \beta_v^{-1}$ for helium at $T_b = 70^\circ$F and $p_b = 14.7$ psia) is often multiplied by the mass in pounds to be lifted to give the volume of helium in cubic feet required to lift that mass.

The volume under base conditions may be determined in many ways, but for scientific ballooning purposes gas is usually delivered in cylinders at high pressure, and tables are used to determine $V_{g,b}$ in the cylinders prior to and after withdrawal. The difference is the amount delivered. This is exactly parallel to the method of computing lift which was developed in C.4. of this section. Therefore, a volume table for the container in which a lift gas is delivered may be readily used to compute lift.

Kalman's (3) table for computing the volume of helium in cylindrical steel tubes gives tabulated values of what he calls a volume factor, F_v,

Table 2

Values of β_v and β_v^{-1} for Helium and Hydrogen for SI and English Units

Units and Base Condition	Value of $\rho_{g,b}(\sigma - 1) = \beta_v$			
	Helium		Hydrogen	
	β_v	β_v^{-1}	β_v	β_v^{-1}
SI Units T_b = 288.15°K (15°C) p_b = 101325 N/m^2	1.0557	0.9472	1.1397	0.8774
Mass - lb m Vol - ft^3 T_b = 518.67°R (59°F) p_b = 14.6959 psia	0.06590	15.174	0.07115	14.055
Mass - lb m Vol - ft^3 T_b = 529.67°R (70°F) p_b = 14.7 psia	0.06455	15.492	0.06969	14.349

which is a function of the temperature and pressure of the gas and which is defined by the following equation:

$$V_{g,b} = F_v V_o \tag{29}$$

Combining Eqs. (27, (28), and (29) yields

$$\left(\frac{B}{gV_o}\right) = \beta_v F_v \tag{30}$$

which shows that multiplying each of the entries of Kalman's table by β_v converts that table into a lift table comparable to Tables I-2 and I-4 of Sect. XII.

D. PRECAUTIONS IN HANDLING GAS

The individual characteristics of a gas must be considered when using it as a lift gas in a balloon, and anyone using toxic or flammable gas should acquaint himself with those characteristics. Only those precautions which are generally necessary when handling any gas stored under high pressure and those which are peculiar to ballooning are covered here.

1. High Pressure Containers

Any container filled with gas under high pressure constitutes a potential hazard; care should be taken to protect the container. It should not be struck violently or dropped. It should be stored in a dry area where

the temperatures are not excessively high; 125° F (~ 50° C) is usually stated as a maximum for compressed gas cylinders in the U.S. Flame should never be allowed to touch a cylinder, and a cylinder should never be allowed to become part of an electrical circuit. In particular, an electrical welding arc should never be struck against a cylinder containing pressurized gas. Cylinders should never be dragged or rolled. Small cylinders should be moved short distances on a hand cart, and when they are moved in a truck, care should be taken to assure that they do not strike each other violently. One should never tamper with safety devices in valves or cylinders, and the cap should be left in place until a cylinder has been securely fixed in place and is ready to be used.

Gas is frequently carried through high pressure hoses from the container to the balloon inflation tubes. Care should be taken to avoid kinking these hoses, because kinks may cause invisible weaknesses in them. All hoses, valves, gages, and other equipment used with the inflation system should be inspected regularly, and high pressure hoses should be replaced periodically, the period depending on the use and handling they receive, whether or not they show evidence of damage.

Some additional precautions should be taken with flammable or toxic gases. Flammable gases should not be stored with oxygen or other oxidizing materials, and special care should be taken to avoid open flames or sparks in an area where flammable gases are being stored or used. Only explosion-proof equipment and spark-proof tools should be used where such gases are being stored or used. All equipment should be grounded. People working with flammable gases should also keep themselves electrically grounded.

2. Cryogenic Containers

Gas is being transported increasingly as a cryogen because of the lower transport cost, and cryogenic hydrogen has been used to inflate balloons. The large dewars used to transport cryogenic gases must receive special care to avoid damage that will break the vacuum. They should be stored in an open, well-ventilated place, and all the precautions against flame, sparks, etc. which must be taken with compressed, flammable gas must also be taken with flammable cryogens. Even the best dewars leak heat to the cryogen, and eventually some gas will have to be removed to prevent excessive pressure buildup. Periodic use may take care of this buildup, but a safety valve will release gas if necessary. The gas may

be released at any hour of the day or night, and precautions must be adequate to assure that it does not create a hazard. Placing the dewar in an open field where it will not be molested is desirable. Lift gases, if expelled into the atmosphere, rise and so do not create a hazard at the surface for very long unless they are trapped. The very cold gases coming from a dewar may not rise immediately, however, so it is possible for them to flow along the surface and become trapped at some distance from the dewar.

Another danger associated with cryogens occurs when they are used in large quantities, as in scientific ballooning. As the cryogen is removed from the dewar, air condenses on the outside of the pipes and tubes carrying the cryogen. This liquid air drips off and may collect in sizeable quantities. The boiling point of nitrogen is lower than oxygen and as the nitrogen boils off, the liquid which remains becomes increasingly rich in oxygen. Then any material which will oxidize constitutes a danger if it comes in contact with this liquid. The usual precautions include catching the liquid air in an aluminum trough and being very careful to keep other materials away from it. This problem is associated with extreme cold and so any cryogenic gas, including the inert ones, will create it.

3. Helium Inflation

Helium, being an inert gas, is quite safe to handle during inflation. The hoses leading from the container to the balloon inflation tubes should be high pressure hoses which will not kink. If precautions are taken to assure that the helium containers are adequately protected and the pressure in the hoses is adequately provided for, no other special precautions are necessary.

4. Inflation with Flammable Gases

When a balloon is being inflated with a flammable gas, great care must be exercised by everyone in the vicinity. All possible preparations incident to the flight should be made away from the site of inflation or before inflation begins. In particular, no electrical testing should be done in the vicinity of the balloon or gas source during inflation. Also, all equipment should be grounded before any gas is released from its container. If it should be necessary to connect two pieces of equipment where there may be gas, they should first be connected by a wire either prior to the presence of the gas or outside of the area where gas may exist. No car or truck engine should be started or left running anywhere where gas

may reach it or where sparks from it may reach the gas. Even the handling of the balloon or work at the base of the bubble should be kept to an absolute minimum.

All who are handling inflation hoses or who must go near the sources of the gas should wear heavy flame-proof clothing and a conducting strip which makes contact with the leg and extends under the shoe. Anyone who must work under or near the gas bubble of the inflating balloon should also wear a hood--one with a small hole in the top to allow gas to escape. Each such person should also be in constant communication with someone who is well outside the area of danger and who is watching for fire. Because hydrogen burns with an invisible flame, the first warning anyone has of a fire may be the heat radiating from it, or the start of collapse of the balloon. The two events will occur nearly simultaneously, and a person working near the balloon will be in far more danger from the molten plastic of the balloon which may rain down under and downwind of the bubble than from the burning gas which will rise. Therefore, on receiving a warning, a man working near the balloon should retreat along the shortest path to a safe area. It is a good idea to have the danger area marked prior to the

start of inflation and to have each person constantly aware of his optimum route of retreat. In general, the area of danger may be visualized as an oval area oriented with its long dimension (major axis) parallel to the wind and with the balloon bubble near the upwind end. Anyone upwind of the balloon should move into the wind if he receives a warning; from all other locations it is usually best to move cross wind away from the major axis of the oval. Except in very unusual circumstances, one should never move toward or across the major axis if he perceives danger.

Any balloon which has contained a flammable gas and is lying on the ground constitutes a hazard. It may contain small pockets of gas which are nonetheless large enough to inflict serious burns if they are ignited. Consequently, it should not be left unattended until all pockets can be opened and the gas allowed to escape, and it should be handled with care by everyone working with it.

Anyone using flammable gases should study carefully the safety standards for handling hazardous gases, including local standards.

REFERENCES

(1) Morris, Alvin L., 1969: Buoyancy of Gases in Air. Helium Symposia Proc. in 1968 -- A Hundred Years of Helium, U.S. Dept. of Interior, Bureau of Mines Information Circular 8417, 9-16.

(2) Kubara, Robert S., 1968: A Liquid Hydrogen Inflation System. In Proc. Fifth ARCRL Scientific Balloon Symposium, U.S. Air Force Cambridge Research Laboratories Special Report No. 85, 217-221.

(3) Kalman, H.S., 1968: Computing Volume of Helium in Cylindrical Steel Containers at 10 to 10,000 PSIA. U.S. Dept. of Interior, Bureau of Mines Information Circular 8367.

(4) Eshbach, Ovid W., 1952: Handbook of Engineering Fundamentals, 2nd ed., John Wiley and Sons, New York.

(5) Lydersen, A. L., R. A. Greenkorn and O. A. Hougen, 1955: Generalized Thermodynamic Properties of Pure Liquids, Univ. of Wisconsin Coll. Eng. Rept.

(6) Reid, Robert C. and Thomas K. Sherwood, 1966: The Properties of Gases and Liquids, 2nd ed., McGraw-Hill, New York.

(7) Miller, J. E., L. W. Brandt and L. Stroud, 1961: Compressibility Factors for Helium and Helium-Nitrogen Mixtures, Bureau of Mines Report of Investigation 5845, p. 3.

(8) Angevine, J. M., 1970: A Listing of Computer Programs Available at NCAR for Solving Recurring Problems in Ballooning. In Proc. Sixth AFCRL Scientific Balloon Symposium, U.S. Air Force Cambridge Research Laboratories Special Report No. 105, 198-203.

(9) Gill, Thomas T., 1941: Air and Gas Compression, John Wiley and Sons, New York, 15-16.

(10) Streeter, Victor L., 1962: Fluid Mechanics, 3rd ed., McGraw-Hill, New York, p. 249.

(11) Gildenberg, Bernard D., 1954: Investigation of Inflation Techniques for Nonextensible Balloons, Holloman Air Force Base, New Mexico.

(12) General Mills, Inc., Mechanical Division, Minneapolis, Minn., Helium Inflation Tables.

(13) Wooley, Harold W., Russell B. Scott and F. G. Brickwedde, 1948: Compilation of Thermal Properties of Hydrogen in its Various Isotopic and Ortho-Para Modifications, U.S. Dept. of Commerce, NBS Research Paper R P 1932, Vol. 41, 426-427.

SECTION V

BALLOON DESIGN CONSIDERATIONS

by

Justin H. Smalley

LIST OF SYMBOLS

Symbol	Description	Dimensions
a	distance of zero-pressure level below the bottom of a balloon	L
$\bar{a}$	a/λ	
A	surface area of a balloon	L^2
b	specific buoyancy of a lifting gas	$ML^{-2}T^{-2}$
B	buoyant force	MLT^{-2}
c	dimensionless constant used to relate meridional and circumferential stresses	
c	subscript identifying its symbol with a circumference of a balloon which lies in a plane normal to the axis of symmetry	
C	circumference	
d	subscript identifying its symbol with the design condition	
es	subscript identifying its symbol with end section	
f	subscript identifying its symbol with the balloon film	
F	force; subscripts are used to make it specific	MLT^{-2}
G	gross weight of a balloon system exclusive of the lift gas; G = W + P	MLT^{-2}
GI	gross inflation force	MLT^{-2}
h	pressure head	L
k	dimensionless constant; $k = (2\pi)^{-1/3}$	
K	dimensionless parameter which is a function of ϕ	
L	load carried at the bottom of a balloon	MLT^{-2}

L	subscript identifying its symbol with lower	
m	subscript identifying its symbol with a meridian of a balloon; i.e., the circumference which lies in a plane that contains the axis of symmetry	
o	subscript identifying its symbol with a base value	
p	pressure	$ML^{-1}T^{-2}$
p	subscript identifying its symbol with pressure	
P	total payload carried on a balloon	MLT^{-2}
r	radius of the intersection of a balloon's skin with a plane which cuts the balloon normal to its axis of symmetry	L
$\bar{r}$	r/λ	
R	maximum radius of a balloon, i.e., the maximum value which r may have	L
s	distance measured along a gore	L
$\bar{s}$	s/λ	
S	gore length	L
t	subscript identifying its symbol with seams or load tapes	
T	force caused by film stress; subscripts c and m identify it with the circumferential and meridional directions, respectively	MLT^{-2}
U	subscript identifying its symbol with upper	
v	subscript identifying its symbol with vertical	
V	volume	L^3
w	weight of a unit area of balloon film	$ML^{-1}T^{-2}$
w	subscript identifying its symbol with weight	
W	balloon weight	MLT^{-2}

W_t	seam weight	MLT^{-2}
z	height	L
$\bar{z}$	z/λ	

Greek letters

θ	angle the balloon skin makes with the vertical in a plane which includes the vertical axis of symmetry	deg
λ	a length unit defined so that λ^3 is the volume of gas required to lift the payload alone	L
σ	film stress per unit of film width; subscripts c and m identify it with the circumferential and meridional directions, respectively	MT^{-2}
$\bar{\sigma}_c$	$\sigma_c/b\,\lambda^2$	
$\bar{\sigma}_m$	$\sigma_m/b\,\lambda^2$	
Σ	non-dimensional film weight parameter; $\Sigma = (2\pi)^{1/3}(w/b\,\lambda)$	
ϕ	angular coordinate (latitude) of points on a sphere--positive above the equator	deg
ψ	dihedral angle between two planes, both of which contain the axis of symmetry of a balloon	deg

List of Figures

List of Tables

BALLOON DESIGN CONSIDERATIONS

A. DERIVATION OF EQUATIONS

The purpose of this section is to derive a set of differential equations which, with the proper boundary conditions, can be integrated to determine the characteristics of various balloon shapes.

The simplest development of the equations considers the balance of forces on an elemental surface area of the balloon. The top and bottom of this element are defined by two parallel planes normal to the axis of symmetry and located a distance Δz apart. The intersection of such planes with the balloon surface defines the circumferential direction. The sides of the element are defined by two planes containing the axis of symmetry and separated by an angle ψ. The intersection of such planes with the balloon surface defines the meridional direction. The tangents to the meridional and circumferential directions and the normal to the surface form an orthogonal set. The relationship of the surface element to the balloon is shown in Fig. 1. The element and the forces on it are shown in detail in Fig. 2.

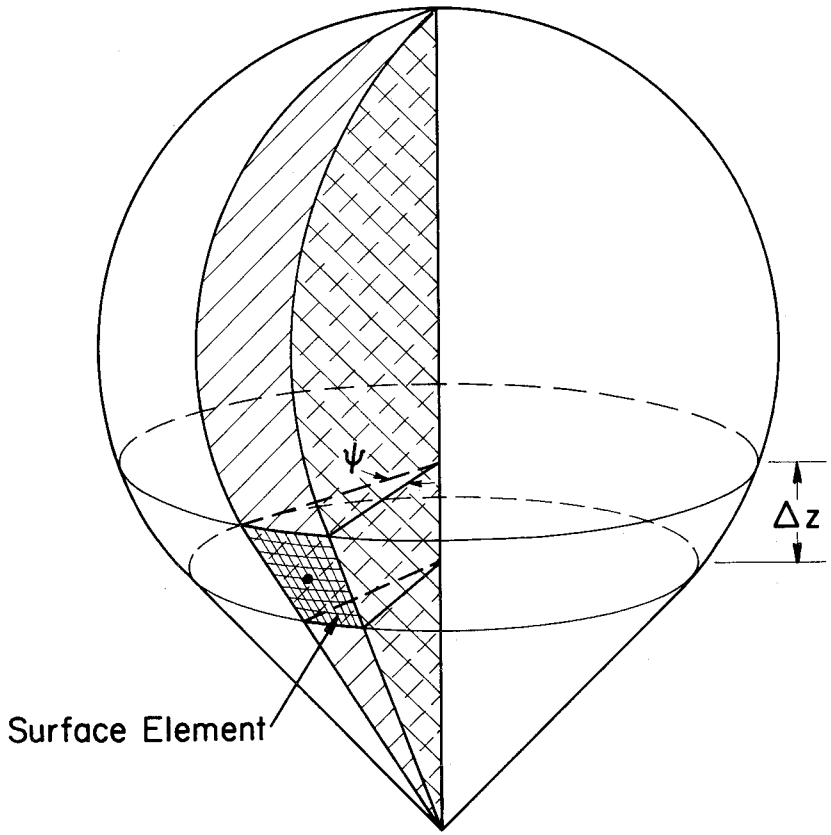

Fig. 1. Sketch showing relation of a surface element to a balloon.

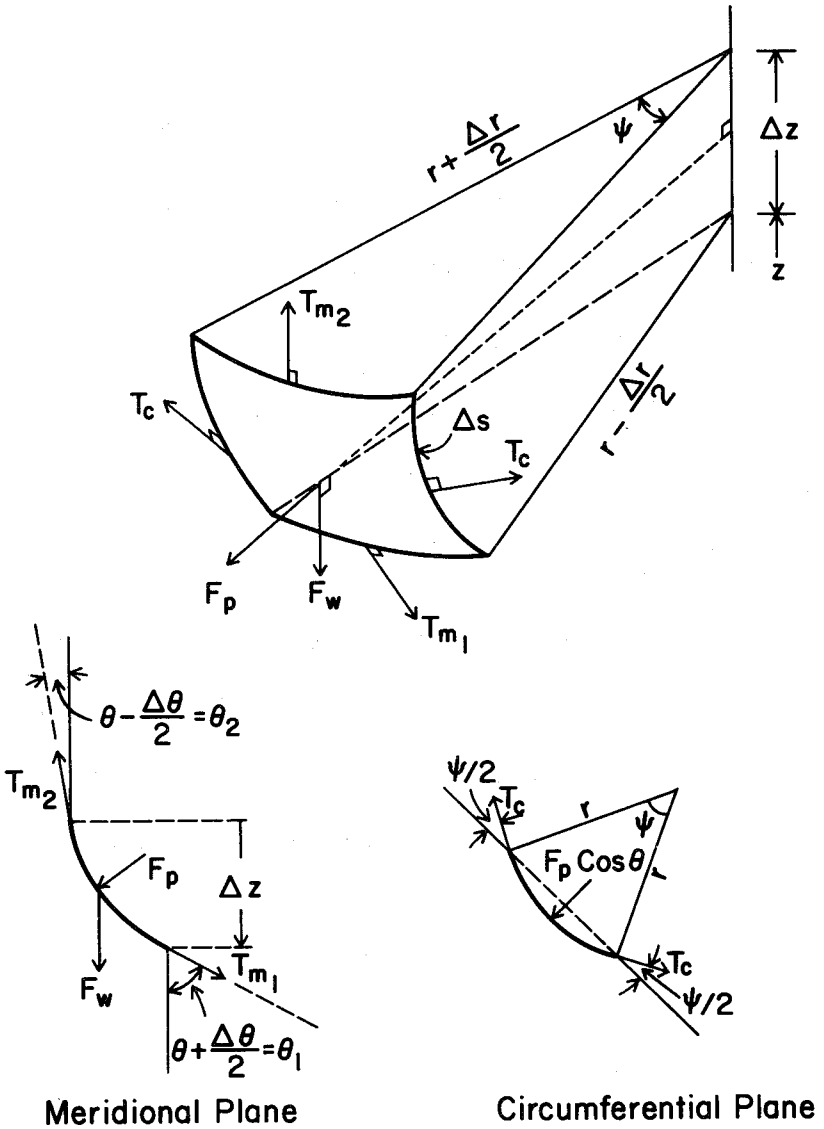

Fig. 2. Sketch of surface element.

The forces shown are: F_p, the pressure force on the element; F_w, the weight of the element; T_c, the circumferential force; and T_m, the meridional force. Using a very small element (i.e., $\Delta z \ll 1$ and $\psi \ll 1$) we can state to first-order accuracy

$$F_p = p\ (\psi\ r\ \Delta s)$$

$$F_w = w\ (\psi\ r\ \Delta s)$$

where p is the differential pressure across the balloon film, w is the weight of the balloon film per unit area, and $(\psi\ r\ \Delta s)$ is the area of the element. Also,

$$T_c = \sigma_c\ \Delta s$$

$$T_{m_1} = \left(\sigma_m - \frac{\Delta\sigma_m}{2}\right)\psi\left(r - \frac{\Delta r}{2}\right)$$

$$T_{m_2} = \left(\sigma_m + \frac{\Delta\sigma_m}{2}\right)\psi\left(r + \frac{\Delta r}{2}\right)$$

where σ_c and σ_m are the film stresses per unit length in the circumferential and meridional directions, respectively. From Fig. 2,

$$\theta_1 = \theta + \Delta\theta/2$$

$$\theta_2 = \theta - \Delta\theta/2$$

Summing forces vertically and horizontally, respectively, in the meridional plane we obtain

$$T_{m_2} \cos \theta_2 - T_{m_1} \cos \theta_1 - F_p \sin \theta - F_w = 0$$

$$T_{m_2} \sin \theta_2 - T_{m_1} \sin \theta_1 + F_p \cos \theta - 2T_c \sin \frac{\psi}{2} = 0$$

It can be shown that when higher order infinitisimals are omitted,

$$T_{m_2} \cos \theta_2 - T_{m_1} \cos \theta_1 = \psi \, \Delta(r \sigma_m \cos \theta)$$

$$T_{m_2} \sin \theta_2 - T_{m_1} \sin \theta_1 = \psi \, \Delta(r \sigma_m \sin \theta)$$

and then, substituting further, assuming $\sin \psi/2 = \psi/2$, we obtain

$$\Delta(r \sigma_m \cos \theta) - rw \, \Delta s - pr \sin \theta \, \Delta s = 0$$

$$\Delta(r \sigma_m \sin \theta) - \sigma_c \, \Delta s + pr \cos \theta \, \Delta s = 0$$

Dividing by Δs and taking the limit as Δs approaches zero, we obtain

$$\frac{d}{ds} (r \sigma_m \cos \theta) - rw - pr \sin \theta = 0$$

$$\frac{d}{ds} (r \sigma_m \sin \theta) - \sigma_c + pr \cos \theta = 0$$

Another form of these equations is more convenient for integration. When the indicated differentiation is carried out

$$\frac{d}{ds}(r \sigma_m) \cos \theta - (r\sigma_m) \sin \theta \frac{d\theta}{ds} - rw - pr \sin \theta = 0$$

$$\frac{d}{ds}(r \sigma_m) \sin \theta + (r\sigma_m) \cos \theta \frac{d\theta}{ds} - \sigma_c + pr \cos \theta = 0$$

Eliminating $d(r\sigma_m)/ds$ and substituting $p = b\,(z + a)$, where a is the distance the zero-pressure level is below the bottom of the balloon and b is the specific buoyancy of the lifting gas, gives

$$(r\sigma_m) \frac{d\theta}{ds} = \sigma_c \cos \theta - rw \sin \theta - br\,(z + a) \qquad (1)$$

then eliminating p gives

$$\frac{d}{ds} (r\sigma_m) = \sigma_c \sin \theta + rw \cos \theta \qquad (2)$$

These equations represent the balance of forces normal and parallel, respectively, to the surface element. They could have been derived directly, but the geometry is not straightforward, particularly regarding the force T_c. To complete the set of equations necessary to define a balloon it is noted that

$$\frac{dr}{ds} = \sin \theta$$

$$\frac{dz}{ds} = \cos \theta$$

and by definition, where A and V are surface area and volume, respectively,

of the balloon

$$\frac{dA}{ds} = 2\pi r$$

$$\frac{dV}{ds} = \pi r^2 \cos\theta$$

The total film load in the meridional direction is

$$T = 2\pi (r\sigma_m)$$

Observe that there are three factors in the above which may be independently specified. They are σ_c, w, and a. When σ_c is set equal to zero everywhere, the very important natural-shape balloon results. If a is zero, the balloon is known as the zero-pressure type. If w is held constant, the resulting balloon will be fully tailored. If the term rw is constant, the balloon will be a cylinder type.

Various boundary conditions are of interest. In the usual case, $0 < \theta < \pi/2$ at the bottom of the balloon and $\theta = -\pi/2$ at the top (i.e., flat-topped). If $\theta = \pi/2$ at the bottom this means that there is no payload there and it must be carried elsewhere. If $\theta < -\pi/2$ at the top of the balloon, an additional lift force is being applied there.

If at either the top or the bottom of the balloon, rw is zero and $\sigma_c \neq \sigma_m$, then σ_m will be infinite. Although σ_m may diverge, the total film load will not. If there is a load L at the bottom of the balloon, the initial value of the total film load is $T = L/\cos\theta$.

B. NON-DIMENSIONAL EQUATIONS

In general it is convenient to work with a non-dimensional form of the equations. Equations (1) and (2) are repeated here in rearranged form

$$(r\sigma_m)\frac{d\theta}{ds} = \sigma_c \cos\theta - rw \sin\theta - br(z + a)$$

$$(r\sigma_m) = \int_0^s (\sigma_c \sin\theta + rw \cos\theta)\, ds + \frac{L}{2\pi \cos\theta}$$

The non-dimensionalizing force and length are somewhat arbitrary. Certainly the payload L is a logical choice for the force. Dividing through by L yields the term b/L, which has the units of $(\text{length})^{-3}$. The cube root of L/b has been chosen as the length. These are not the only terms that could have been used, but are related to ones chosen by the University of Minnesota in their pioneering work and are continued here. Since it is not necessary that all the payload be at the bottom, it is convenient to use P rather than L in the length unit, where P is the total payload. Finally, $\lambda = (P/b)^{1/3}$,

which is a length. At float altitude, the equation of balloon equilibrium for a balloon of weight W and volume V is $bV = W + P = G$, or $V/\lambda^3 = (W/P) + 1 = G/P$. This simple expression shows the value of λ as the length unit. An interpretation of λ is that λ^3 is the volume of gas required to lift the payload alone. Another common and useful unit is the gore length. However, at the outset of a design, P and b and, therefore, λ are more apt to be known than the gore length.

The University of Minnesota defined the non-dimensional film weight parameter as

$$\Sigma = (2\pi/1)^{1/3} \ (V/G)^{2/3} w$$

This is identical to

$$\Sigma = (2\pi)^{1/3} (w/b\lambda)$$

which will be retained in the further work. With the following definitions: $\bar{a} = a/\lambda$, $\bar{r} = r/\lambda$, $\bar{s} = s/\lambda$, $\bar{z} = z/\lambda$, $k\Sigma = (2\pi)^{-1/3} \Sigma = w/b\lambda$, $\bar{\sigma}_c = \sigma_c/b\lambda^2$, and $\bar{\sigma}_m = \sigma_m/b\lambda^2$, the final non-dimensionless differential equations of the shape and stresses in the balloon are

$$(\bar{r}\,\bar{\sigma}_m)\,\theta' = \bar{\sigma}_c\,\bar{z}' - k\,\Sigma\,\bar{r}\,\bar{r}' - \bar{r}\,(\bar{z} + \bar{a}) \tag{3}$$

$$(\bar{r}\,\bar{\sigma}_m)' = \bar{\sigma}_c\,\bar{r}' + k\,\Sigma\,\bar{r}\,\bar{z}' \tag{4}$$

$$\bar{r}' = \sin\theta \tag{5}$$

$$\bar{z}' = \cos\theta \tag{6}$$

$$(A/\lambda^2)' = 2\pi\,\bar{r} \tag{7}$$

$$(V/\lambda^3)' = \pi\,\bar{r}^2\,\bar{z}' \tag{8}$$

where the prime denotes differentiation with respect to the gore length variable, $\bar{s}$. The independent variables are $\bar{\sigma}_c$, Σ, and $\bar{a}$. If two are fixed, the third then uniquely defines a family of balloon shapes. The famous Σ tables define a family of shapes for $\sigma_c = a = 0$. A version of these tables is presented as Table L-1 in Section XII.

From a practical standpoint, a real balloon is not tailored to zero gore width at the nadir and zenith as in the Σ tables. A sketch of a gore pattern illustrating cylinder-end, taper-tangent, and full-cylinder designs is presented in Fig. 3. Data for end-section radii of ¼, ½, and 3/4 times the maximum radius and for a full-cylinder design as well as portions of the data from Table L-1 of Section XII have been plotted in Figs. 4 through 10.

C. PRELIMINARY DESIGN

In the absence of a computer to solve Eqs. 3 through 8, a preliminary design using the data in Table L-1 of Section XII and Figs. 4 through 10 is as

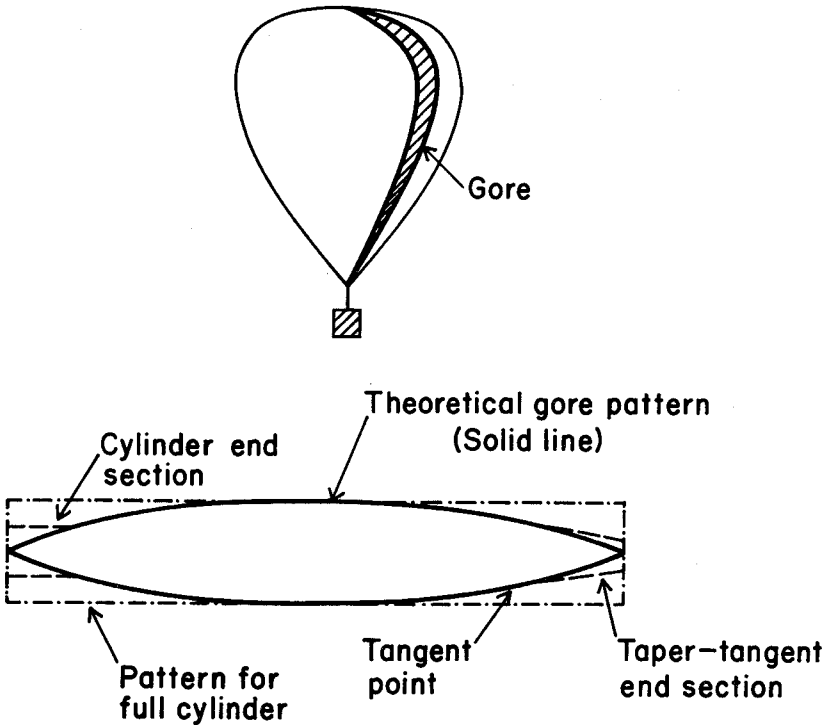

Fig. 3. Sketch illustrating various end sections and gore patterns.

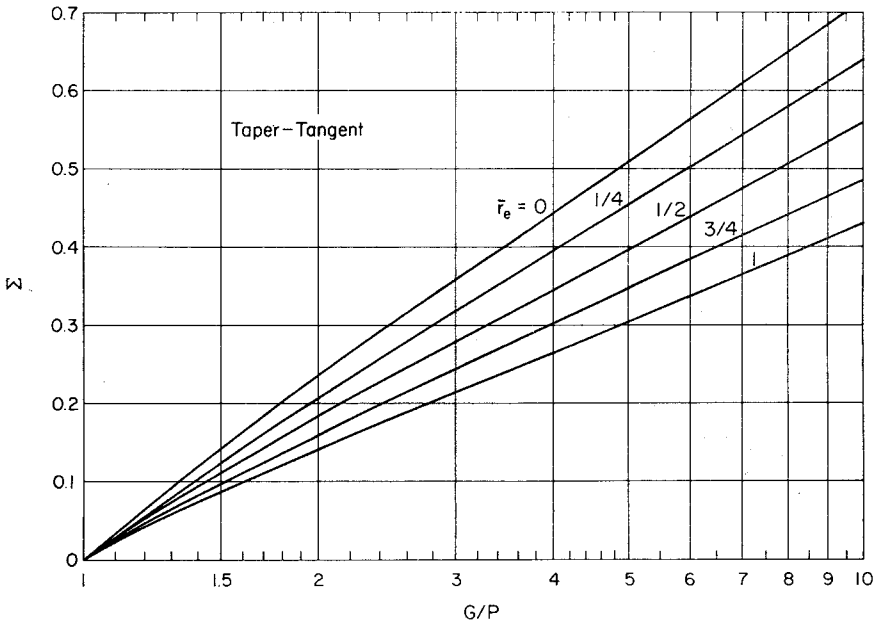

Fig. 4a. Effect of film weight on gross weight for zero-pressure, natural-shape, flat-top balloons with taper-tangent end sections. $\bar{r}_e$ is the ratio of end section radius to maximum balloon radius.

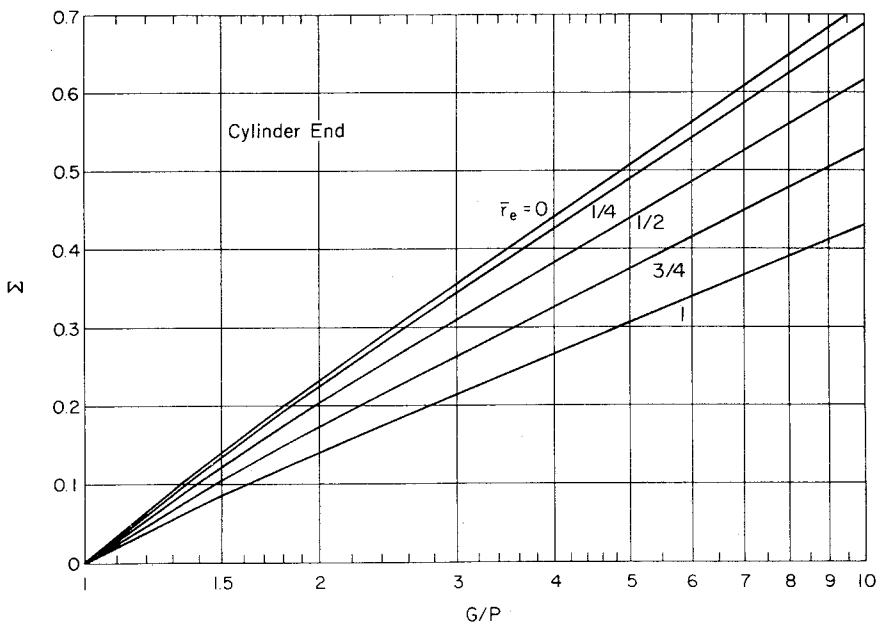

Fig. 4b. Effect of film weight on gross weight for zero-pressure, natural-shape, flat-top balloons with cylinder end sections. $\bar{r}_e$ is the ratio of the end section radius to the maximum balloon radius.

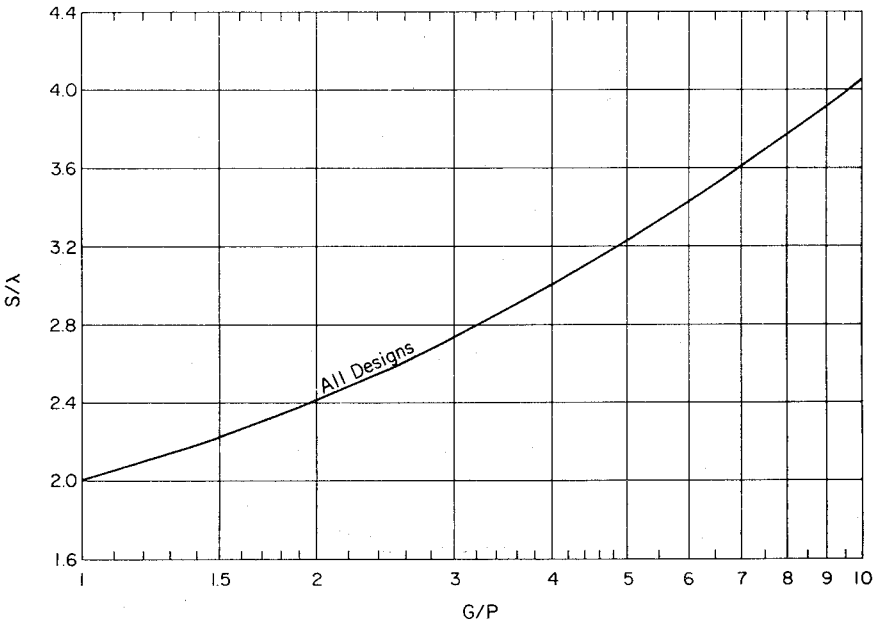

Fig. 5. Gore length of zero-pressure, natural-shape, flat-top balloons.

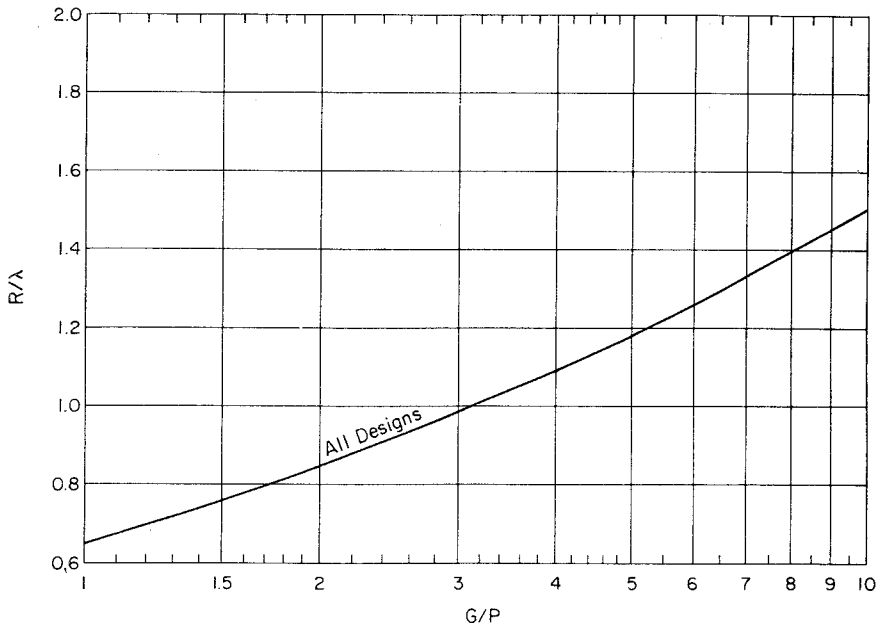

Fig. 6. Maximum radius of zero-pressure, natural-shape, flat-top balloons.

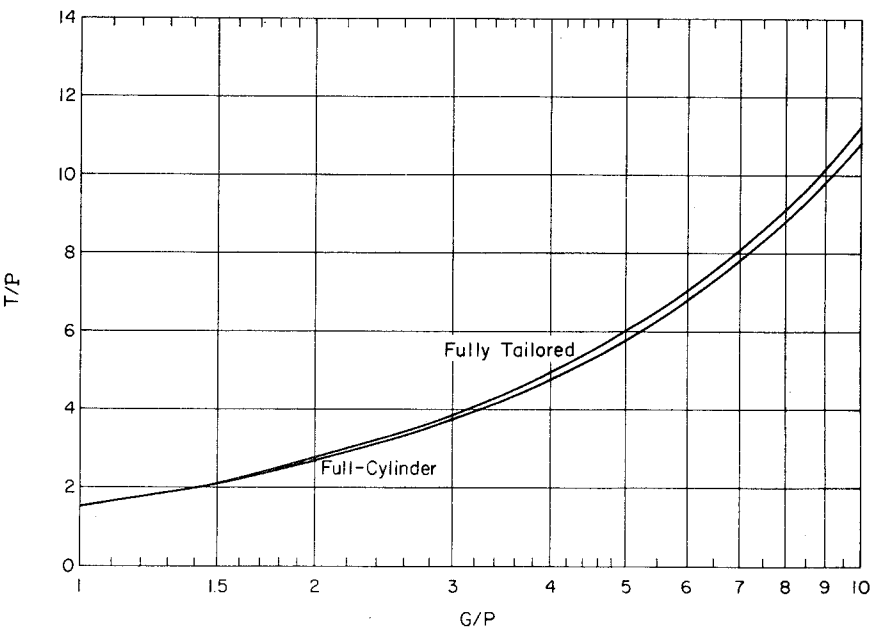

Fig. 7. Total meridional film load at the top of the two extreme zero-pressure, natural-shape, flat-top balloons.

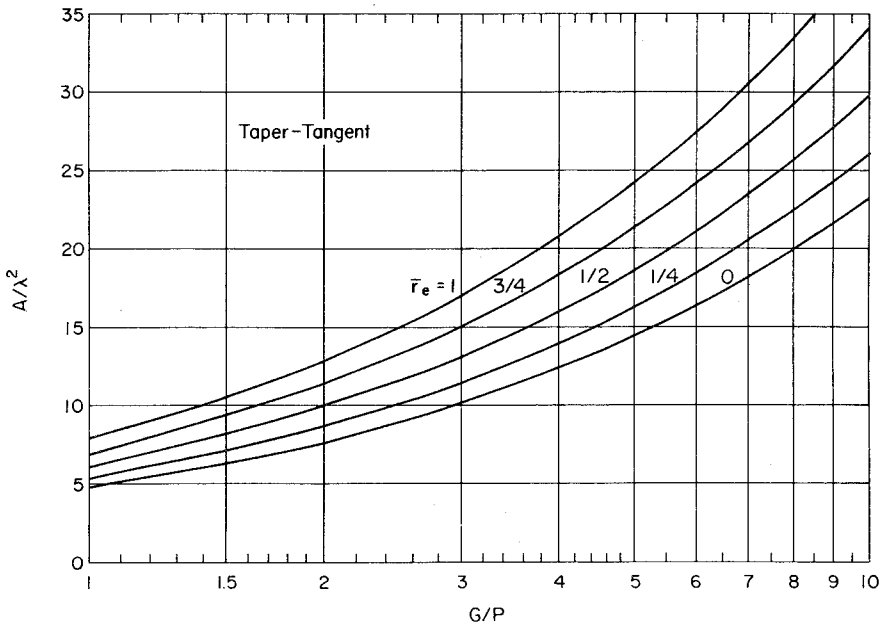

Fig. 8a. Surface area of zero-pressure, natural-shape, flat-top balloons with taper-tangent end sections; $\bar{r}_e$ is the ratio of end-section radius to maximum balloon radius.

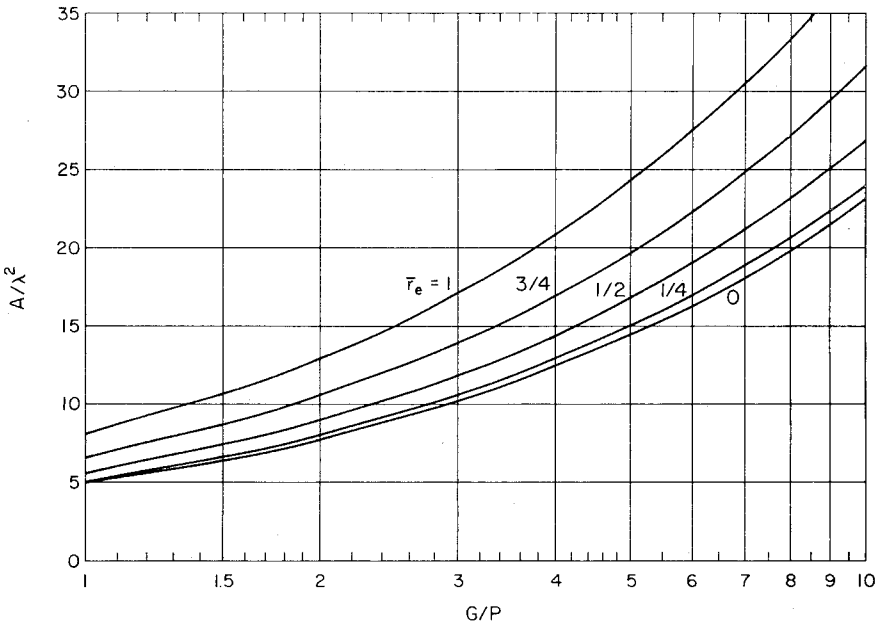

Fig. 8b. Surface area of zero-pressure, natural-shape, flat-top balloons with cylinder end sections; $\bar{r}_e$ is the ratio of end-section radius to maximum balloon radius.

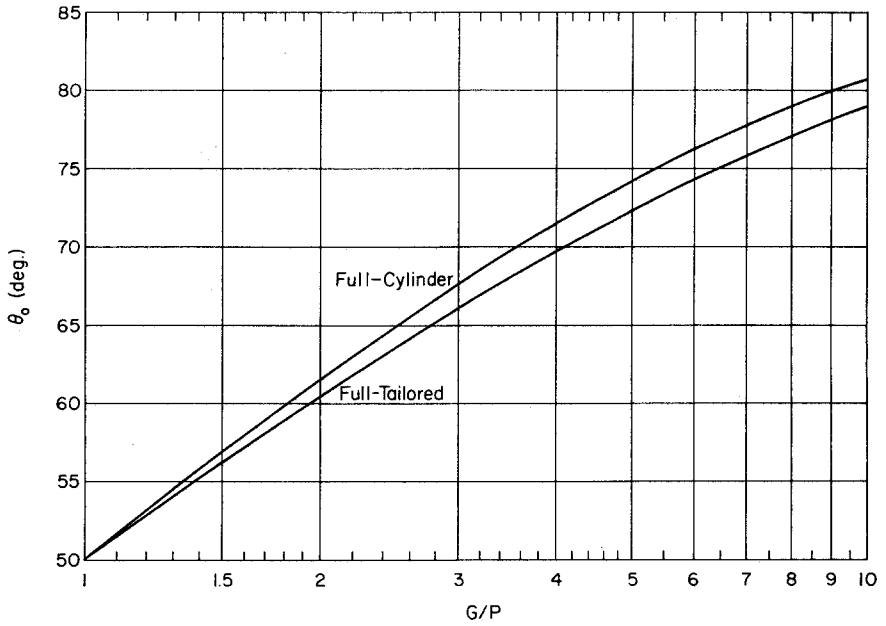

Fig. 9. Nadir angle of the two extreme zero-pressure, flat-top balloons.

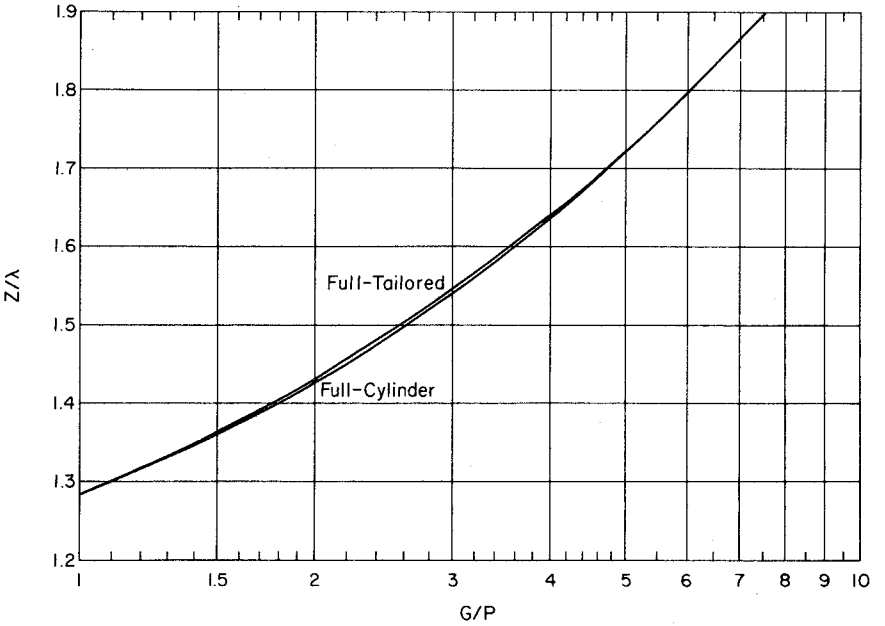

Fig. 10. Overall height of two extreme, zero-pressure, natural-shape, flat-top balloon designs.

follows:

1. Determine total payload P.

   a. The payload includes: the experimental apparatus; support structure and rigging; shock absorbers; balloon command and control electronics telemetry and antennas; parachute and radar reflector; bottom end fitting; top end fitting; valves and other top loads; and miscellaneous items, e.g., ducts, destruct device, warning lights, pennants, inflation tubes, and electrical wires.

The method that follows determines the balloon size for payload P. If it is desired to accommodate a range of payloads, the P used should be the minimum value.

   b. Find the characteristic length, $\lambda = (P/b)^{1/3}$.

The value of b as a function of altitude in the U.S. Standard Atmosphere, 1962, is given by Fig. 11 of this section and by Table K-1 of Section XII. For a range of altitudes, b should correspond to the highest altitude.

   c. Form the film weight parameter, $w/b\lambda$.

   d. Calculate Σ where $\Sigma = (2\pi)^{1/3}(w/b\lambda)$ and estimate G/P from

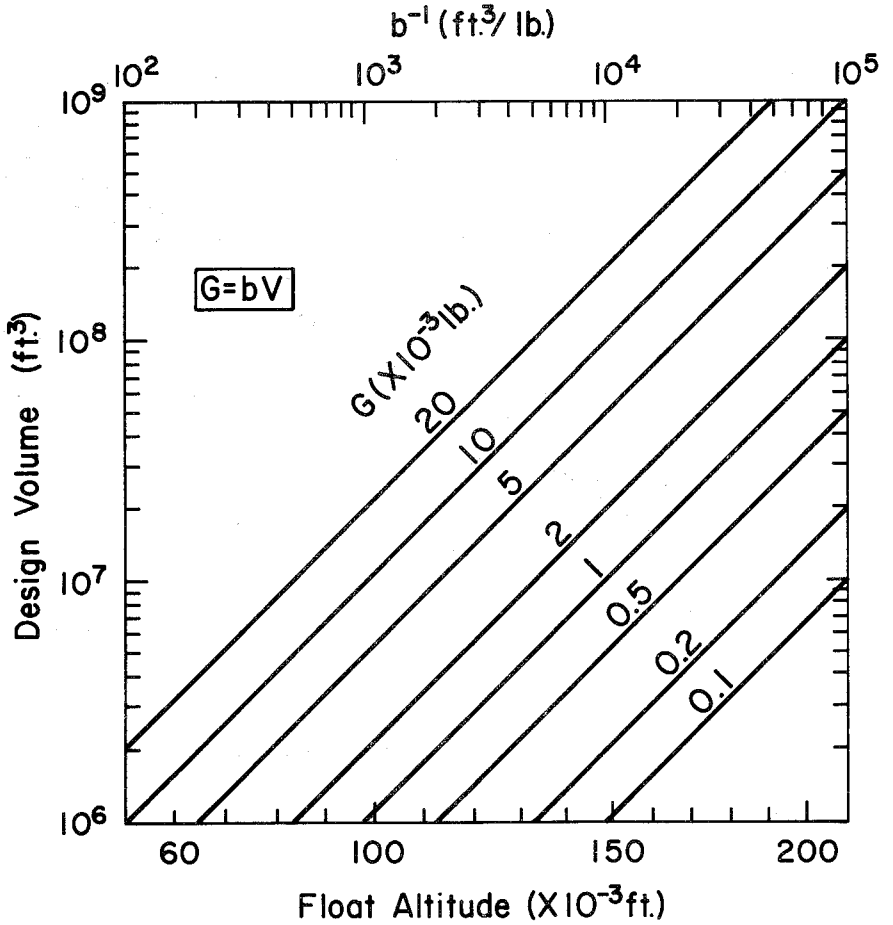

Fig. 11. Graphical solution to the equation G = bV. The graph also shows the relationship between specific buoyancy for helium and altitude in the U.S. Standard Atmosphere, 1962.

Fig. 4. Go to step 2b.

2. Determine balloon weight, W.

   a. Form the ratio, $G/P = (W + P)/P$.

   b. From Fig. 5, find the gore length (S/λ); from Fig. 6, find the radius (R/λ); from Fig. 7, find the total film load (T/P); and from Fig. 8, find the surface area (A/λ^2).

   c. Estimate the total film weight, $W_f/P = (A/\lambda^2)\ (w/b\lambda)$.

   d. Estimate the volume, $V/\lambda^3 = G/P$.

   e. Determine the total seam weight, W_t. The number of seams is $(2\pi R)$/(usable material width).

The seam length is the gore length. The seam weight should include the weight of load tapes if used. The strength needed per load tape at float altitude is (T/P) (Payload) (Safety Factor)/(Number of tapes).

A more critical condition is the load-tape tension at launch. The number of active load tapes is estimated to be (2π) (radius of launch bubble)/(local gore width at the radius). The strength needed in the load tapes at launch is (GI) (Safety Factor)/(Number of active tapes), where GI is the gross inflation for the heaviest payload, including the free lift.

   f. If a balloon needs fullness in the end sections (for manufacturing reasons or because it does not have load tapes), this excess material must be included in the balloon weight. The end-section weight W_{es} is estimated from consideration of its geometry and the film weight. For the specific designs of Fig. 8, the area includes the excess material of the end sections. At the bottom, where θ_o is the angle the film makes with the vertical (Fig. 9), the total load on the film is $L/\cos\theta_o$, and $(L/\cos\theta_o)$(Safety Factor)$/(2\pi r)$ must be less than the allowable film stress, where r is the radius of the bottom end section. At the top (P)(Safety Factor) (T/P)/$(2\pi r)$ must be less than the allowable film stress, where r is the radius of the top end section.

   g. The balloon weight is $W = W_f + W_t$.

   h. Repeat 2a through 2g until $bV = G$.

Then the preliminary design is complete. It may be necessary to make slight adjustments to the payload value P if the size estimates vary significantly.

3. Determine the gore pattern. The gore pattern can be calculated from the appropriate Σ table. The height of the balloon is found in Fig. 10.

4. Determine the "Load-Altitude" curve for a range of payloads.

   a. Using the value of W from the last iteration of 2g and a series of values of P, calculate corresponding values of G/P, where $G/P = (W + P)/P = V/\lambda^3$.

   b. From Fig. 5 determine S/λ for each value of G/P. Using these values of S/λ, the value of S from 2b, and the relationship $\lambda = S/(S/\lambda)$, calculate corresponding values of λ.

   c. From the definition of λ, the unit lift b is calculated, $b = P/(\lambda^3)$.

   d. Finally, from Table K-1 of Section XII, or Fig. 11, the altitude is determined. A plot of these results will be the desired load-altitude curve.

The curve in Fig. 5 is based on the assumption of a perfectly deployed balloon with no weight at the top and bottom end fittings and the assumption that all balloon fabric is evenly deployed over the surface. In real balloons

the ducts are the biggest departure from this latter assumption. For engineering purposes, the manufacturer's stated weight and gore length should be adequate for W and S. A slight increase in the precision would result if the bottom end fitting and material in the end fitting were considered as part of the payload. This also circumvents the problem when P = 0.

Note: The data in Table L-1 of Section XII and Figs. 4 through 10 are only for zero-pressure, flat-top, natural-shape balloons. The user will need to modify the procedure if his balloon has a cap or caps, is a multi-cell system, or otherwise deviates significantly from the above designs.

D. CALCULATION OF MERIDIONAL STRESS

A convenient method for calculating meridional stress at any level in the balloon is to consider the balloon as a free body cut at the level in question. Either the part above or below the cut may be considered--whichever is easier. Let the vertical component of the meridional film load be T_v. Then, above the cut, $T_v = B_U + p\pi r^2 - W_U$, and below the cut, $T_v = W_L + p\pi r^2 - B_L$, where B is the buoyant force of gas; W is the weight of balloon, payload, etc.; p is the gas pressure at the cut; r is the radius of the balloon at the cut; L is a subscript referring to the part below the cut; and U

is a subscript referring to the part above the cut.

If z is the vertical distance from the zero-pressure level to the cut, $p = bz$. The total meridional film load T is $T = T_v/\cos\theta$, and the meridional stress is $\sigma_m = T/C$, where C is circumference of the balloon film at the cut. If the cut is in an end section where there is excess material, C will exceed the local balloon circumference.

The buoyant force and weight of a portion of a balloon can be determined from the partial area and partial volume data given in Table L-1, Section XII.

E. BALLOONS BELOW THEIR FLOAT ALTITUDES

The gas is not fully expanded in a balloon which is below its design altitude. As a result, some of the balloon material has large vertical folds in it, the bottom apex angle is reduced, and the position of the zero-pressure level is somewhat above the base of the balloon. These effects are most obvious just after launch. The shapes and stresses in such balloons have been calculated for the ideal case in which the excess material along the gore is uniformly distributed around the circumference, Smalley (1). This is known to be unrealistic for an ascending balloon. The vertical distribution of pressure determined by these same calculations is, however, representative

of the real balloon. From Fig. 12 the pressure at the top of a balloon may be calculated at any altitude below the design altitude for all styles of natural-shape balloons from fully tailored to full cylinder, for $\Sigma < 1$. The pressure is given in terms of the distance from the zero-pressure level to the top of the balloon. This head h is readily converted to pressure units if desired by the following equation:

$$\frac{p}{b_d \lambda_d} = \frac{h}{S} \frac{S}{\lambda_d} \frac{b}{b_d}$$

where the subscript denotes a value at the design condition.

1. Cutting the Duct to Change Float Altitude

The data in reference 1 can be used to determine where to cut a valving duct to cause a balloon to float below its design altitude. At design conditions, b_d is the specific lift and (G/P_d) is the ratio of gross weight to design payload weight. With the specific lift b at the new float altitude, Fig. 13 can be used to find the position of the zero-pressure level in gore length units. Cutting the duct at this position will cause the balloon to level off at the new altitude when carrying the design payload. For heavier payloads a new load-altitude curve should be constructed along the lines of the method of sub-Section C.4.

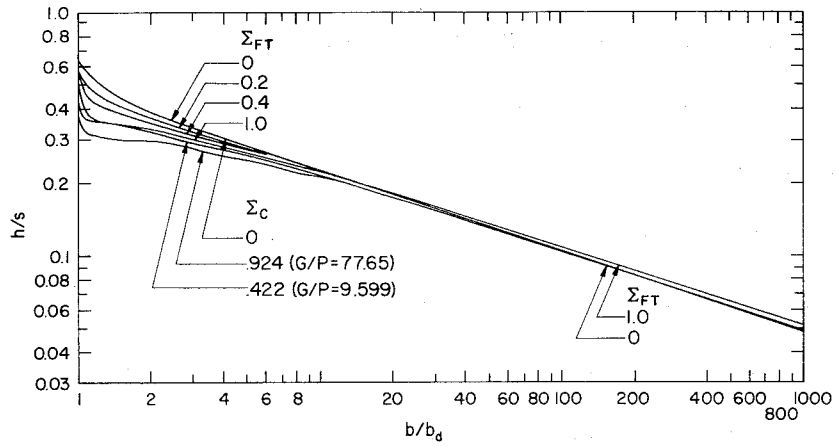

Fig. 12. Pressure heat at the top of various zero-pressure, natural-shape, flat-top balloons.

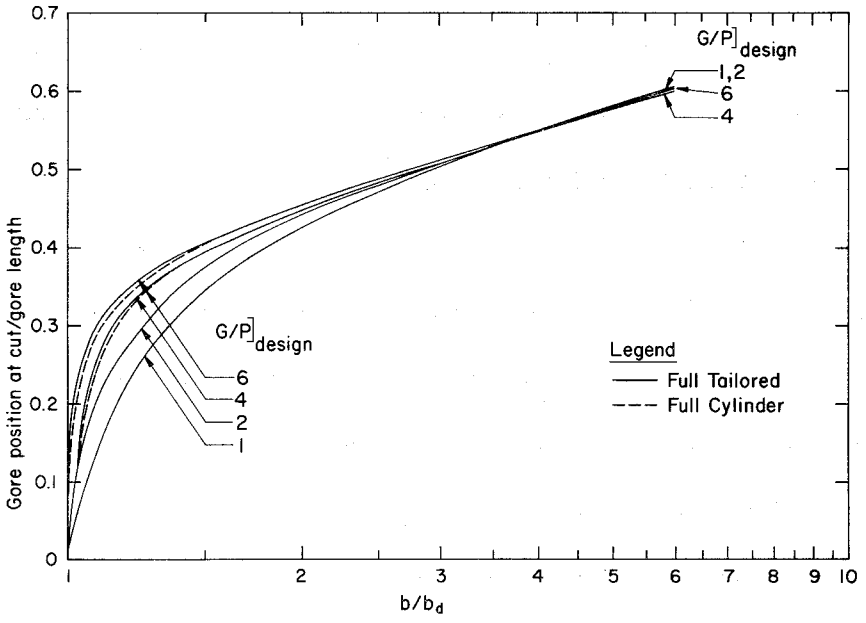

Fig. 13. Zero-pressure level in balloons below their design altitude as a basis for cutting the valving duct.

F. BALLOONS WITH CIRCUMFERENTIAL STRESS

A great amount of design work has been done (e.g., Table L-1 of Section XII and Figs. 4 through 10) and a great number of balloons have been built for which the circumferential stress was intentially held zero. However, when considering balloons for very high altitudes, it is found that the natural shape pays a weight penalty when compared to the ideal spherical balloon. This penalty can be reduced if the balloon is designed to have circumferential stress. With today's materials and sealing methods, such a step is feasible. Various styles have been investigated and are discussed in the following sub-section.

1. The Ideal (i.e., Spherical) Balloon

As a basis for comparison, the weight and stresses for buoyant spheres are given first. The assumptions are made that: the shape is perfectly spherical (regardless of the magnitudes of the stresses) and the payload is attached along a circumferential ring with a force resultant which is tangent to the balloon surface at the ring.

Let p_o be the internal pressure at the center, R the radius, and ϕ the angular coordinate of points on the sphere--positive above the equator. Integrating the internal pressure over the surface of the sphere,

we find the film stresses to be

$$\frac{\sigma_m}{bR^2} = \frac{p_o}{2bR} + \frac{P}{3bV} K_m + \frac{\sin\phi}{3} \tag{9}$$

$$\frac{\sigma_c}{bR^2} = \frac{p_o}{2bR} + \frac{P}{3bV} K_c + \frac{\sin\phi}{3} \tag{10}$$

where, above the payload attachment,

$$K_m = \frac{1}{1 + \sin\phi}$$

$$K_c = \sin\phi - \frac{1}{1 + \sin\phi}$$

and, below the payload attachment,

$$K_m = \frac{1}{\sin\phi - 1}$$

$$K_c = \sin\phi - \frac{1}{\sin\phi - 1}$$

The stresses for a weightless sphere (P/bV = 1) are given in Fig. 14.

Several points should be noted. Meridional and circumferential stresses are equal only at the poles. There are discontinuities in both stresses where the payload is attached. The changes in stresses are

$$(\Delta\sigma_m/bR^2) = -(\Delta\sigma_c/bR^2) = \frac{2P}{3bV\cos^2\phi}$$

These are minimum when $\phi = 0$. There is some value of p_o which will ensure

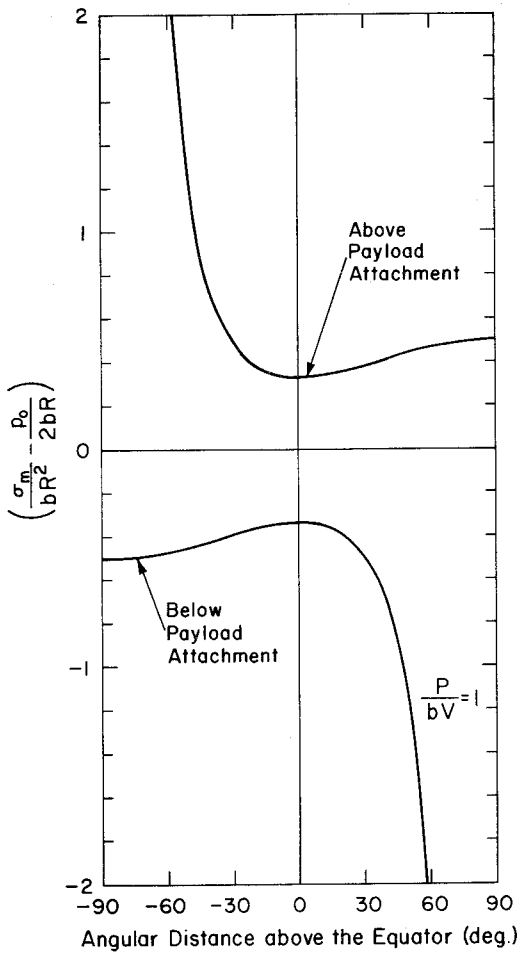

Fig. 14a. Meridional stress in an ideal, spherical, weightless, buoyant balloon.

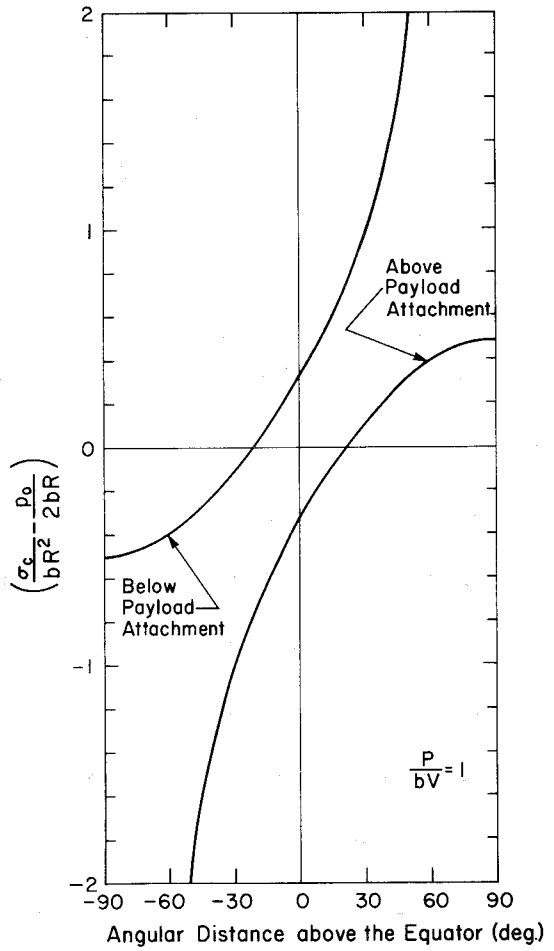

Fig. 14b. Circumferential stress in an ideal, spherical, weightless, buoyant balloon.

tension throughout the sphere no matter where the payload is attached (excepting the nadir). For example, if the payload is attached on the -30^{o} latitude line, $p_o/2bR$ must be at least 1.0 to assure that $\sigma_c \geq 0$ above the payload attachment. It can be seen from Eqs. (9) and (10) that only when the payload is negligible ($P/bV = 0$) are the stresses equal to each other everywhere on the sphere. The minimum permissible pressure to maintain a spherical shape is determined by the stresses at the bottom. Here $\sigma_m = \sigma_c$ and the minimum pressure value is

$$\frac{p_o}{2bR} = \frac{P}{6bV} + \frac{1}{3}$$

If the pressure at the base of the sphere is exactly zero, then $p_o = bR$ and the location of zero circumferential stress is

$$\phi = \arcsin \left[\frac{\sqrt{\left(20\,\frac{P}{bV} + 12\right)\frac{P}{bV} + 1} \; -5 \; -2\,\frac{P}{bV}}{4\left(\frac{P}{bV} + 1\right)} \right]$$

Example results are

$\frac{P}{bV}$	1	1/2	1/3	1/4	1/5
ϕ	-9.03	-25.00	-33.96	-39.92	-49.27

The payload attachment ring should not be lower on the balloon than these

angular positions.

For analysis purposes, it is desirable to know the volume of such ideal spheres as a function of film weight. If, as noted earlier,

$$\lambda^3 = P/b$$

$$\Sigma = (2\pi)^{1/3}(w/b\,\lambda)$$

$$V/\lambda^3 = bV/P = (W/P) - 1$$

then

$$V/\lambda^3 = 1 + 18^{1/3}\,(V/\lambda^3)^{2/3}\Sigma$$

This relationship has been solved in reference (2), and the results are presented in Table 1.

2. Round-Top Balloons

The ideal spherical balloons described in the sub-Section F.1 have the disadvantage that the payload must be applied at a circumferential ring. Such an attachment would be difficult to manufacture. Also, at this ring there are discontinuities in the stresses. From an efficiency standpoint, however, it would be desirable to approach closely the spherical shape. In the early days of plastic balloons a sphere-on-cone combination was used. This design suffered from the weak seam strength obtainable at that time.

Table 1

Non-dimensional Physical Parameters of Ideal Spherical Balloons

Σ	Radius	Gore Length	Area	Volume
0	0.62035	1.94889	4.83598	1.00000
0.1	0.67955	2.13487	5.80301	1.31448
0.2	0.74980	2.35556	7.06477	1.76572
0.3	0.83233	2.61485	8.70573	2.41536
0.4	0.92770	2.91446	10.81503	3.34438
0.5	1.03552	3.25319	13.47502	4.65123

It also had the disadvantage that there must be a discontinuity in circumferential stress at the juncture where the cone is tangent to the sphere.

It is possible, however, to match both the circumferential and meridional stresses by using a shape other than a cone. Figure 14b shows that, by proper choice of pressure, it is possible to obtain zero circumferential stress at any desired level on the sphere. It is probably simplest to match the stresses by using a natural shape below the zero stress level. The characteristics of such a design are given in Table 2. Table 2(a) gives results for round-top balloons with a fully tailored section. Table 2(b) gives results for full-cylinder bottom end sections. All other end-section designs fall between these two extremes.

As with all natural shapes, meridional stress is infinite at the nadir of the fully tailored bottom section. This must be accommodated by either tapes or fullness. No fullness is required at the top because the stresses are finite. However, caution should be exercised because stresses during inflation, launch, and ascent may exceed the design stresses at float. The results presented in Table 2 are only representative of the conditions at float.

Table 2

Non-Dimensional Physical Characteristics of Round-Top Balloons
(Zero superpressure, natural-shape bottom section, no load on top)

Σ	Base Angle	Radius	Height	Gore Length	Area	Volume	Sphere Size (deg)	Maximum Stress
				(a) Fully Tailored Bottom Section				
0	47.778	0.61055	1.48344	2.05815	4.88155	1.00000	137.78	0.453
0.1	51.446	0.67249	1.57653	2.22657	5.84775	1.31691	141.45	0.512
0.2	55.262	0.74496	1.69084	2.43039	7.10691	1.77028	145.26	0.589
0.3	59.099	0.82917	1.83030	2.67420	8.74356	2.42151	149.10	0.691
0.4	62.809	0.92572	1.99683	2.96031	10.847	3.35138	152.81	0.824
0.5	66.253	1.03431	2.19055	3.28788	13.501	4.65835	156.25	0.993
				(b) Full-Cylinder Bottom Section				
0	47.778	0.61055	1.48344	2.05815	6.35400	1.00000	137.78	0.453
0.1	53.314	0.69008	1.60959	2.27996	7.80485	1.42297	143.31	0.537
0.2	58.864	0.78201	1.76167	2.54417	9.67403	2.04852	148.86	0.646
0.3	64.093	0.88609	1.94044	2.85074	12.0415	2.95769	154.09	0.788
0.4	68.739	1.00128	2.14470	3.19647	14.9738	4.24588	158.74	0.965
0.5	72.672	1.12597	2.37163	3.57585	18.5179	6.01766	162.67	1.183

3. Constant Circumferential Stress

The effect of a constant amount of circumferential stress along the entire gore is illustrated by an example in Fig. 15. The maximum possible circumferential stress is approximately 0.325 because at that value the bottom apex angle is essentially zero. It would be possible to use greater values of circumferential stress only if the initial pressure were positive. This design is not considered a practical one since it saves very little weight over the natural-shape design and would be difficult to manufacture in the areas near the end fittings. Examination of the defining equations and the figure shows that this style balloon has a negative meridional radius of curvature at the bottom.

4. Circumferential Stress Proportional to Meridional Stress

From the standpoint of reducing manufacturing tolerances, it is desirable to have zero circumferential stress at the end fittings. Circumferential stress may then exist for intervening points on the balloon. One such design uses circumferential stress as $\sigma_c = c(\sigma_m - \sigma_{mo})$, where σ_m is the local meridional stress, σ_{mo} is the meridional stress at nadir, and c is a constant.

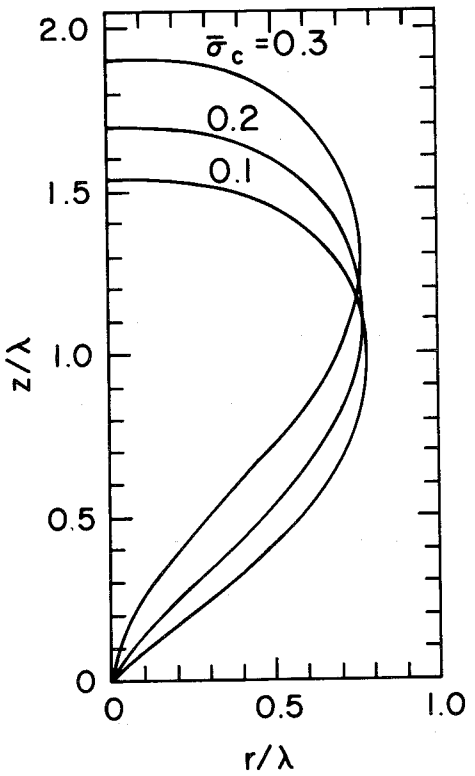

Fig. 15. Shapes of balloons with constant circumferential stress. The balloons are zero-pressure, and $\Sigma = 0.2$.

Three cases arise. First, if $c < 1$, circumferential stress diverges at the zenith. Second, when $c = 1$, the circumferential stress rises asymptotically to a maximum at the zenith. Interestingly, this results in the total meridional film load being equal at the nadir and the zenith. Third, if $c > 1$, the circumferential stress tends to zero at the zenith. A value to use for the constant in this last case is somewhat arbitrary. Solutions to the equations do not exist if c is too large. Manufacturing tolerances would probably have to be tight to achieve the stress distribution predicted. Data for the case when $c = 1$ is presented in Table 3.

Another possibility for a design with zero circumferential stress at the nadir and zenith would be to use $\sigma_c = c$ (radius). The value of the constant to use would depend upon permissible stress level. No general data have been generated for this design.

G. COMPARISON OF BALLOON DESIGNS

Most large balloons have been and will continue to be made with the natural-shape design, i.e., with zero circumferential stress. Such balloons are quite efficient, and their simplicity and demonstrated reliability recommend them for normal use.

Table 3

Non-Dimensional Physical Characteristics of Balloons with Circumferential Stress Equal to Net Meridional Stress
(Zero superpressure, fully-tailored, flat-top)

Σ	Base Angle	Radius	Height	Gore Length	Area	Volume	Maximum T/P*	Maximum $\bar{\sigma}_c$
0	50.159	0.65219	1.28421	1.99441	4.91628	1.00000	1.56056	0.00000
0.1	52.615	0.71479	1.39793	2.17142	5.89795	1.31963	1.89687	0.07509
0.2	55.620	0.78945	1.50544	2.37943	7.17588	1.77776	2.36045	0.18650
0.3	59.129	0.87764	1.63751	2.62241	8.83555	2.43646	3.00122	0.26585
0.4	63.001	0.98014	1.78457	2.90297	10.9696	3.37789	3.88355	0.38634
0.5	66.993	1.09670	1.94666	3.22156	13.6673	4.70332	5.08494	0.52729

* Maximum T/P does not occur at the top of the balloon. In fact, in this design, T/P at the top equals the value at the bottom.

In the comparison to follow, the ideal buoyant sphere is used as a standard. For a given altitude, payload, and gas-barrier material, balloons should all be compared at the same Σ value. The designs presented in the foregoing sub-sections are compared in Table 4.

All weightless balloons ($\Sigma = 0$) are 100% efficient. As the film weight parameter increases ($\Sigma > 0$), efficiency decreases. The exceptions are those balloons with circumferential stress at the zenith, because they are more spherical. Balloons with circumferential stress are more efficient than natural-shape balloons. The exception is a round-top balloon with a cylinder end; however, this is an extreme design and would not be used. It can be seen that end sections quickly reduce efficiency.

The data in Tables 1 through 3 can be plotted as in Figs. 4 through 10, and a preliminary design made as outlined in sub-Section C.

Table 4

Comparison of Balloon Designs on the Basis of Balloon Weight

Designs	$\Sigma = 0.2$	$\Sigma = 0.4$
Ideal Sphere	1.	1.
Natural-Shape		
fully-tailored	0.9769	0.9615
cylinder end*	0.9246	0.8921
taper-tangent end*	0.8300	0.7686
Circumferential Stress Equal to Net Meridional Stress	0.9845	0.9859
Round-Top		
fully-tailored	0.9941	0.9970
full-cylinder end	0.7303	0.7223

* These designs are listed as being more representative of real balloons. The ratio of end section radius to maximum radius os 0.25.

REFERENCES

(1) Smalley, J. H., 1966: Balloon Shapes and Stresses Below the Design Altitude. NCAR-TN-25, December 1966.

(2) Smalley, J. H., 1964: Determination of the Shape of a Free Balloon. AFCRL-65-68, Scientific Report No 4, November 1964.

SECTION VI

SCIENTIFIC BALLOON INSTRUMENTATION

by

Oscar L. Cooper

LIST OF SYMBOLS

Symbol	Description	Dimensions
a	subscript used to identify its symbol with antenna	
b	subscript used to identify its symbol with balloon	
B	bandwidth	T^{-1}
c	speed of light (3×10^8 m/sec)	LT^{-1}
C	capacitance	
d	distance from a point on the ground below a balloon system to the radio horizon	L
D	distance from an airborne balloon system to the radio horizon	L
DR	deviation ratio	
f_r	pulse repetition rate of radar	T^{-1}
F	noise factor	
F	maximum value of the data modulation frequency	T^{-1}
G	gain	
h	height of an airborne balloon system	L
k	Boltzmann constant ($1.38 \times 10^{-23} J^{o}K^{-1}$)	$ML^2T^{-2}\theta^{-1}$
L	transmission loss	
n	integer	
n	subscript used to identify its symbol with noise	
N	total noise power	
NF	noise figure (NF = 10 log F)	
o	subscript used to identify its symbol with a base or reference level	
R	range from balloon borne radio system to ground system	L
R	resistance	ohms
T	temperature	θ

Greek Letters

Δf	maximum frequency deviation of a subcarrier oscillator	T^{-1}
λ	wave length	L

List of Figures

List of Tables

SCIENTIFIC BALLOON INSTRUMENTATION

A. INTRODUCTION

The free balloon has provided science with a very useful means of reaching the upper levels of the earth's atmosphere. To take full advantage of the balloon's capability as a scientific platform, methods for determining the balloon's trajectory, recovering the scientific data, and controlling the scientific equipment and balloon system are needed. Several radio linkages are necessary for complete instrumentation between the ground station and the balloon system, as illustrated in Fig. 1. Some of the systems and techniques required to accomplish the necessary communication and control are discussed in this section.

B. TELEMETRY AND DATA RECOVERY

All scientific balloon experiments must have a means of retrieving the data for real-time and post-flight analysis. Earlier experiments relied upon on-board recording such as tape recorders, photographic film, charts, and emulsion plates. Since telemetry has been introduced to scientific ballooning, most data are recovered in real time through radio transmission and are

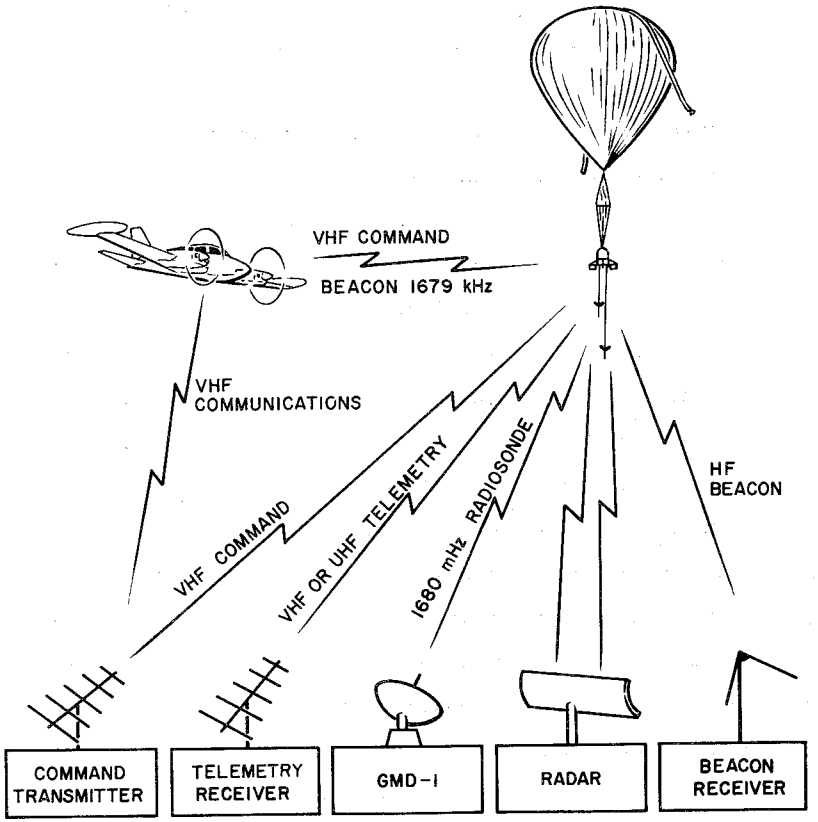

Fig. 1. Typical balloon instrumentation system.

recorded with graphic recorders, digital printers, or on magnetic tape for later computer analysis.

Telemetry may be defined as the science of transmitting data from inaccessible to accessible locations. Aerospace telemetry requires the transmitting of information from air and space vehicles to accessible (usually ground) locations. The source instruments of the system, sometimes called transducers, convert physical quantities, such as pressure, temperature, or strain into electrical signals, which can be transmitted to an accessible location, such as a balloon instrumentation ground station, where they are recorded for study, Stiltz (1).

1. Basic Techniques

The basic telemetry techniques in use today are FM/FM, PCM (pulse-code-modulation), PAM (pulse-amplitude-modulation), and PDM (pulse-duration-modulation). The first two are the most commonly used for general purpose data recovery from balloons and receive the most discussion here. Some balloon experiments include special purpose data encoders and use a coding technique which does not have a standard data format.

In order to establish standards for radio telemetry in the atmospheric

and space research fields, a standardization committee called the Inter-Range Instrumentation Group (IRIG) has established standards which are used by the telemetry industry to standardize telemetry techniques and equipment performance. The most recent compilation of the IRIG standards is found in IRIG Document 106-69 (2).

The subject of telemetry is extensive and is discussed only briefly in this section. A more complete discussion of the theory and application of telemetry may be found in Stiltz (1) and Gruenberg (3).

Radio telemetry systems are commonly classified in accordance with the methods employed to multiplex and modulate the RF carrier. The two basic methods for multiplexing are frequency division and time division. In frequency division the data signals from separate instruments are kept independent of each other by separate allocation of frequency channels, in time division separate periods of time are provided for each channel. The former is used in FM/FM telemetry, while the latter is used for pulse telemetry systems such as pulse-code-modulation (PCM).

a. FM/FM telemetry. The designation FM/FM refers to a frequency division technique of modulating a telemetry transmitter with the output of one

or more subcarrier oscillators which, in turn, are frequency modulated by data signals. One of the principal advantages of using FM/FM telemetry is the fact that a properly designed system will suppress noise caused by intermodulation, thermal agitation, and microphonics to a considerable degree. The ratio of the maximum deviation of a subcarrier oscillator Δf to the maximum value of the data modulation frequency F is called the deviation ratio.

$$DR = \frac{\Delta f}{F}$$

The greater this ratio the less noise the system will have. The same applies to the carrier deviation by the subcarriers. In practice, the system should be operated to make the best compromise between noise suppression and intelligence carrying capacity. The maximum data bandwidth of a channel has been defined by IRIG as that frequency which yields a deviation ratio of 5 when the subcarrier is deviated ± 7½% (or 15% in some cases) of the center frequency, Bendix (4).

Table 1 lists the IRIG proportional bandwidth subcarrier channels and the data bandwidth of each channel. The designation proportional-bandwidth channel indicates that the width of each channel is proportional to its

Table 1

Proportional Subcarrier Channels

Channel	Center Frequencies (Hz)	Lower Deviation Limit* (Hz)	Upper Deviation Limit* (Hz)	Nominal Frequency Response (Hz)	Nominal Rise Time (ms)	Maximum Frequency Response*** (Hz)*	Minimum Rise Time*** (ms)
	±7.5% Channels						
1	400	370	430	6	58	30	11.7
2	560	518	602	8	42	42	8.33
3	730	675	785	11	32	55	6.40
4	960	888	1,032	14	24	72	4.86
5	1,300	1,202	1,398	20	18	98	3.60
6	1,700	1,572	1,828	25	14	128	2.74
7	2,300	2,127	2,473	35	10	173	2.03
8	3,000	2,775	3,225	45	7.8	225	1.56
9	3,900	3,607	4,193	59	6.0	293	1.20
10	5,400	4,995	5,805	81	4.3	405	.864
11	7,350	6,799	7,901	110	3.2	551	.635
12	10,500	9,712	11,288	160	2.2	788	.444
13	14,500	13,412	15,588	220	1.6	1,088	.322
14	22,000	20,350	23,650	330	1.1	1,650	.212
15	30,000	27,750	32,250	450	.78	2,250	.156
16	40,000	37,000	43,000	600	.58	3,000	.117
17	52,500	48,562	56,438	790	.44	3,938	.089
18	70,000	64,750	75,250	1050	.33	5,250	.067
19	93,000	86,025	99,975	1395	.25	6,975	.050
20**	124,000	114,700	133,300	1860	.19	9,300	.038
21**	165,000	152,625	177,375	2475	.14	12,375	.029
	±15% Channels****						
A	22,000	18,700	25,300	660	.53	3,300	.106
B	30,000	25,500	34,500	900	.39	4,500	.078
C	40,000	34,000	46,000	1200	.29	6,000	.058
D	52,500	44,625	60,375	1575	.22	7,875	.044
E	70,000	59,500	80,500	2100	.17	10,500	.033
F	93,000	79,050	106,950	2790	.13	13,950	.025
G**	124,000	105,400	142,600	3720	.09	18,600	.018
H**	165,000	140,250	189,750	4950	.07	24,750	.014

* Rounded off to nearest Hz.

** Recommended for use in UHF transmission systems only.

*** The indicated maximum data frequency response and minimum rise time is based upon the maximum theoretical response that can be obtained in a bandwidth between the upper and lower frequency limits specified for the channels.

**** Channels A through H may be used by omitting adjacent lettered and numbered channels. Channels 13 and A may be used together with some increase in adjacent channel interference.

center frequency. The channels were chosen to make the best use of present equipment and of the frequency spectrum. There is a ratio of approximately 1.33:1 between center frequencies of adjacent bands, except between 14.5 kHz and 22 kHz, where a larger gap was left for a compensation tone for magnetic tape recording. The deviation is kept at ± 7½% for all bands, with the option of ± 15% deviation on the eight highest bands to provide for transmission of higher data bandwidth information. The nominal frequency response listed for each band is computed on the basis of maximum deviation (7½% or 15%) and a deviation ratio of 5. While deviation ratios of 5 are recommended, ratios as low as 1 or less may be used for a higher data bandwidth, but in that case low signal-to-noise ratios, possibly increased harmonic distortion and cross talk must be expected, Stiltz (1). As a rule, the rms signal-to-noise ratio of a specific channel varies as the 3/2 power of the subcarrier frequency employed.

As flexible and useful as the IRIG proportional bands are, there are many instances in which their progressive channel capacities do not provide a satisfactory distribution of channel bandwidths, particularly when a large number of data channels have the same data bandwidth requirements. A

system of IRIG constant bandwidth channels is listed in Table 2. The column headings state the deviation and frequency response for the three arrangements of subcarrier channels. The two frequency responses indicated in each column are based on deviation ratios of 5 and 1, Gruenberg (3).

Combinations of proportional and constant bandwidth subcarriers may be used, provided proper precautions are taken to avoid crosstalk.

Figure 2 is a simplified block diagram of an airborne FM/FM telemetry package containing several subcarrier oscillators. Physical phenomena within the scientific balloon experiment are converted to analog signals, usually ranging from 0 to 5 volts, to deviate the subcarrier oscillator. The frequency modulated outputs of all subcarrier oscillators are then mixed and amplified, thus providing a source of modulation energy which is used to frequency-modulate the transmitter. The transmitted RF signal is received at one or more ground stations where it is demodulated, Cooper (5).

Figure 2 includes a simplified block diagram of a telemetry receiving station capable of receiving, separating, and displaying signals which are proportional to the analog data or transducer outputs of the balloon-borne equipment. The received RF signal is demodulated by the receiver to produce

Table 2

Constant Bandwidth Subcarrier Channels

A Channels		B Channels		C Channels	
Deviation limits = ±2 kHz Nominal frequency response = 0.4 kHz Maximum frequency response = 2 kHz**		Deviation limits = ±4 kHz Nominal frequency response = 0.8 kHz Maximum frequency response = 4 kHz**		Deviation limits = ±8 kHz Nominal frequency response = 1.6 kHz Maximum frequency response = 8 kHz	
Channel	Center Frequency (kHz)	Channel	Center Frequency (kHz)	Channel	Center Frequency (kHz)
1A	16				
2A	24				
3A	32	3B	32		
4A	40				
5A	48	5B	48		
6A	56				
7A	64	7B	64	7C	64
8A	72				
9A	80	9B	80		
10A	88				
11A	96	11B	96	11C	96
12A	104				
13A	112	13B	112		
14A	120				
15A	128	15B	128	15C	128
16A*	136				
17A*	144	17B*	144		
18A*	152				
19A*	160	19B*	160	19C*	160
20A*	168				
21A*	176	21B*	176		

* Recommended for use in UHF transmission systems only.

** The indicated maximum frequency response is based upon the maximum theoretical response that can be obtained in a bandwidth between deviation limits specified for the channel.

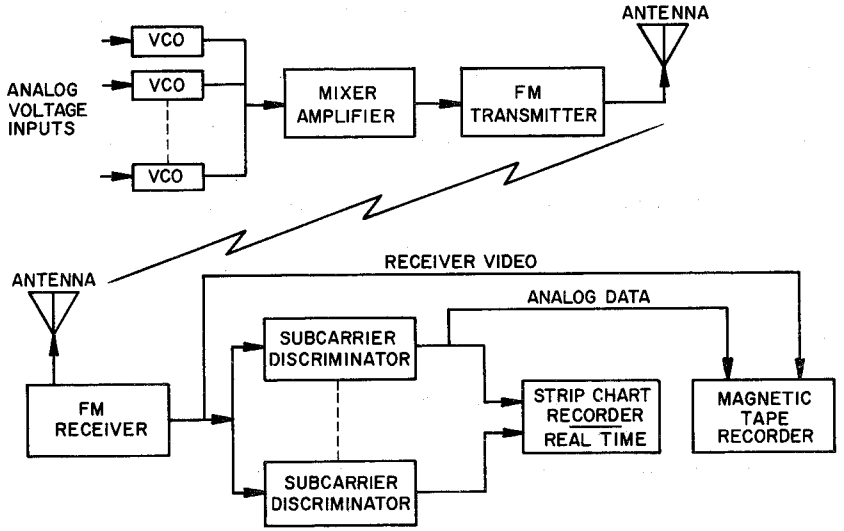

Fig. 2. FM/FM telemetry system block diagram.

the multiplexed signal which is equivalent to that at the output of the mixer-amplifier in the airborne package. The multiplexed signal is then routed to several subcarrier discriminators, corresponding to the subcarrier frequencies used, where the subcarrier signals are separated, and data signals proportional to the analog data are recovered. Separation of the subcarrier signals is accomplished by the use of bandpass input filters in the discriminators. Each filter is capable of passing a band of frequencies centered about the center frequency of the subcarrier channel. The filter bandwidth depends upon the percentage deviation of the channel.

In addition to the bandpass input filter, each discriminator contains a low-pass output filter. Cut-off frequencies of these filters are identical to the subcarrier response frequencies listed in Tables 1 and 2. This filter serves the dual purpose of passing the data frequencies and attenuating any higher undesired frequencies appearing at the discriminator output, Stiltz (1).

The outputs of the discriminators are used to drive graphic chart recorders, to display on meters or oscilloscopes, or to record on magnetic tape. The composite subcarrier signal which comes from the receiver output

may be recorded on magnetic tape for future playback through the discriminators. The response of the tape recorder must be great enough to accommodate the highest subcarrier frequency. If this is not the case, the analog data from the discriminator output may be recorded on a tape track through the use of an FM channel on the tape recorder. When signals are recorded on tape it is very desirable to record timing signals, such as WWV or another digital timing source. Voice annotation is also very desirable. Tape speed compensation or speed control should be used when recording the composite signal to eliminate any wow or flutter. A 17-kHz signal may be recorded with the subcarrier channels or on a separate track for speed control. Some subcarrier discriminators can be corrected for varying tape speed by using the output of a special discriminator tuned to a precision frequency recorded on the tape. The IRIG standards cover tape recording standards and should be referred to for specific detail.

When assembling an FM/FM telemetry system, one must consider the noise in the RF link when weak signals are being received. The receiver output noise spectrum concentrates the noise power in the higher subcarrier bands. The noise power at the subcarrier discriminator is proportional to the width

of the subcarrier bandpass filter. The subcarrier threshold is, therefore, proportional to the square root of the width of the band. It is also a linear function of the subcarrier frequency. For a proportional bandwidth system with a fixed percentage bandwidth, the noise thresholds of the subcarriers vary as the 3/2 power of the subcarrier frequency. The greater the transmitter modulation from a given subcarrier, the lower will be the RF signal strength necessary to provide data with a favorable signal-to-noise ratio. In order to have a system with equal subcarrier thresholds, it is necessary to adjust the subcarriers so that the high channels deviate the transmitter signal more than the low channels. The theoretical pre-emphasis curve calls for the subcarrier amplitude to be adjusted in accordance with the frequency and the square root of the bandwidth. For the straight proportional bandwidth system this is the 3/2 power taper as shown in Fig. 3. Generally, the channels below approximately 10 kHz are allowed to deviate the transmitter about 3 kHz in order to take into account microphonics in the equipment and intermodulation, (Bendix, (4).

The practical technique for assigning RF carrier deviations to the various subcarriers combines the theoretical noise susceptibility relation-

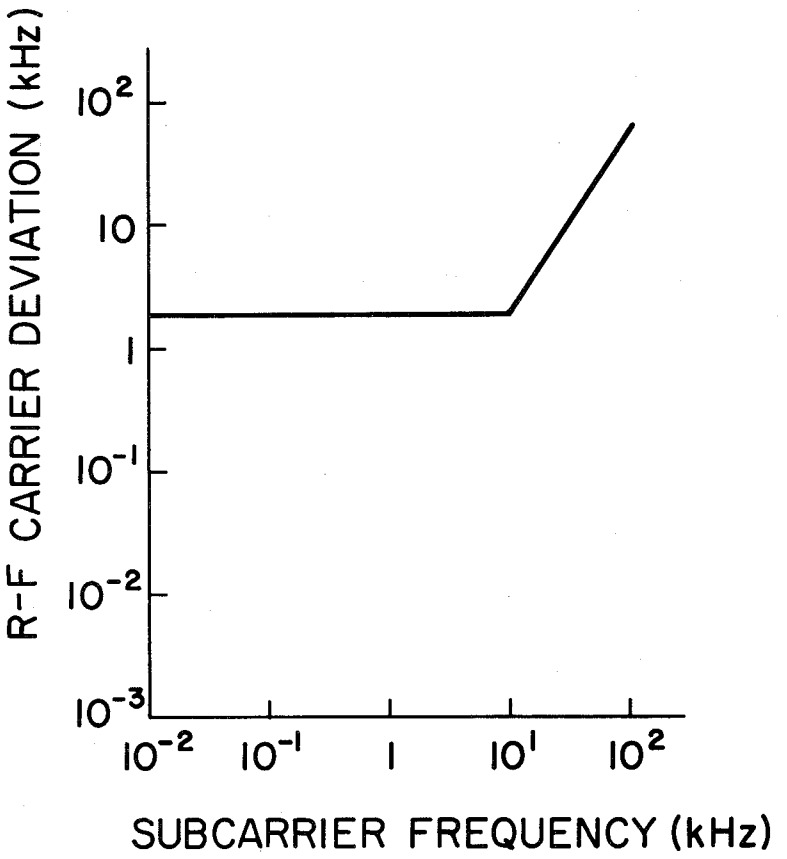

Fig. 3. Pre-emphasis curve for 3/2 power tapers.

ship with considerations involving intermodulation distortion and microphonism, Gruenberg (3). Table 3 is an example of pre-emphasis scheduling involving seven 7½% and one 15% proportional bandwidth channels and two constant bandwidth channels in a VHF system. The channel numbers, center frequencies, and bandwidths are listed in the first three columns and the weighting factor in the next column. This factor is the product of the center frequency and the square root of the bandwidth of the channel normalized by dividing by the product of the center frequency and the square root of the bandwidth of the lowest channel, Gruenberg (3). In this example, 3 kHz is assigned to the lowest five channels, leaving 110 kHz of a total deviation of 125 kHz to be divided among the remaining channels on a pre-emphasis basis. Column 3 shows the deviation for each channel with all channels above channel 9 being deviated by an amount proportional to their weighting factor.

When establishing the deviation of the carrier by the individual subcarrier frequencies, one must take care to avoid having sideband modulation components that exceed the limits established by IRIG, Gruenberg (3). Although normal operation of FM/FM multiplex systems does not create excessive

Table 3

Example of Pre-Emphasis Scheduling

Channel Number	Frequency (kHz)	Bandwidth (kHz)	$\frac{f\sqrt{BW}}{f_1\sqrt{BW_1}}$	RF Deviation (kHz)
1	0.400	0.060	1.00	3.00
3	0.730	0.110	2.47	3.00
5	1.300	0.196	5.88	3.00
7	2.300	0.346	13.80	3.00
9	3.900	0.586	30.47	3.00
12	10.500	1.576	134.38	3.15
14	22.000	3.300	407.85	9.56
B	30.000	9.000	918.36	21.52
5B	48.000	8.000	1385.70	32.47
7B	64.000	8.000	1848.14	43.30

sideband pairs, large deviations assigned to high frequency subcarriers can result in excessive sideband power output.

If the deviation sensitivity of the transmitter is known, the output voltage level of each subcarrier may be adjusted to give its proper transmitter deviation. A deviation meter, such as on a receiver, may also be used for adjusting individual subcarrier oscillators. When all are adjusted and operated simultaneously, the meter will not read the peak deviation, but will read the deviation corresponding to the rms value of the composite deviation voltage.

b. Pulse-code-modulation telemetry. Pulse-code-modulation (PCM) telemetry systems have come into wide usage in the last few years, particularly for space applications. For applications requiring high accuracy or the sampling of large numbers of channels of varying characteristics, PCM systems offer certain net advantages over competing modulating systems.

Basically, a PCM system is a time-multiplexed sampled-data system in which the values of the input channels sampled are expressed in digital, usually binary, form. The modulating signal in a binary PCM system is thus a sequence of ones and zeros which are grouped in binary "words" describing

the value of the particular channel sampled at the instant of sampling. The two-level signal corresponding to the ones and zeros may then be used to modulate a radio-frequency carrier signal in one of several ways: AM, FM, or PM. FM is generally used, and the system is then called PCM/FM modulation.

The primary advantages of PCM systems include the capability for handling both analog and digital signals, flexibility as to the number of channels and channel sampling rates, capability of transmitting data of high accuracy with little or no degradation in the RF link, and generally superior characteristics of information efficiency and noise immunity in the RF link. Offsetting these advantages is the fact that PCM systems are complex and the complexity varies little with the number of channels. PCM may be justifiable for a system with a large number of channels, but for a small number of channels and modest accuracy requirements, an analog system may be more desirable for reasons of simplicity.

(1) PCM data encoding. Figure 4 shows the basic elements of a typical PCM data encoder. Analog signals, after being conditioned, are fed into a multiplexer which is essentially a commutator that samples the analog signals

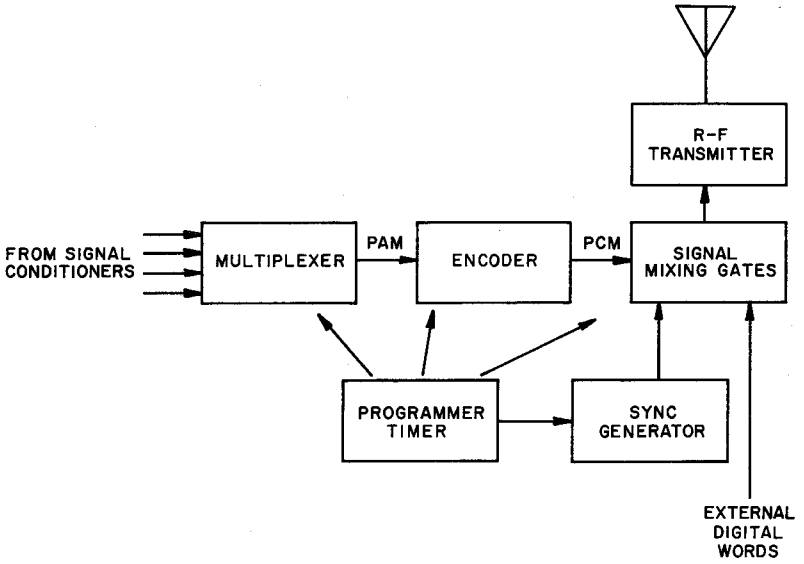

Fig. 4. PCM data transmitting system.

in a sequence and channels them to a common point. The signal at this point is a pulse-amplitude-modulated (PAM) signal, with the amplitudes corresponding to the analog voltages before multiplexing. The multiplexer is controlled by the programmer to sequence the input data in a manner that may be simple, but more often complex, allowing some channels to be sampled more frequently than others.

The PAM signal is fed to an encoder, which consists of an analog amplifier, a sample and hold circuit, and an analog-to-digital (A to D) converter. This converter is controlled by the programmer to make one analog-to-digital conversion per sampling interval. The output of the A to D converter is a sequence of binary digits represented by a two-level signal. The group of binary digits per sample is called a binary word and the number of bits per word determines the resolution. The number of bits per word may vary from 6 to 10. In many cases the resolution of an analog signal from a transducer is less than the resolution capability of the word as determined by the number of bits. The digital output of the encoder is fed to a set of digital gating circuits where they are sequentially mixed with digital data from other sources, such as off-on switches, digital registers and

transducer digital outputs.

The PCM system programmer controls all timing and control functions in the system. It also includes a synchronization generator which develops a pseudorandom binary sequence to synchronize the PCM frame, and in some cases the subframe and words. The largest amount of the programming involves sequencing the multiplexer. In the simple case each data channel is sampled once during the commutation cycle and may be represented by the circular diagram of Fig. 5a. The data format is shown in the adjacent tabulation.

In most applications it will be found that it is not desirable to sample all channels at the same rate. Some data, such as battery voltages and temperature, may be sampled at a much reduced rate. This may be done by attaching one or more subcommutators to the prime commutator in one or more word locations of the main frame. It is also possible to attach sub-subcommutators to the subcommutators. If the basic sampling rate is inadequate, several words in the main frame may duplicate a particular data channel for more frequent sampling called supercommutation. Many data formats may be devised. Modular construction of modern data encoders permits many varia-

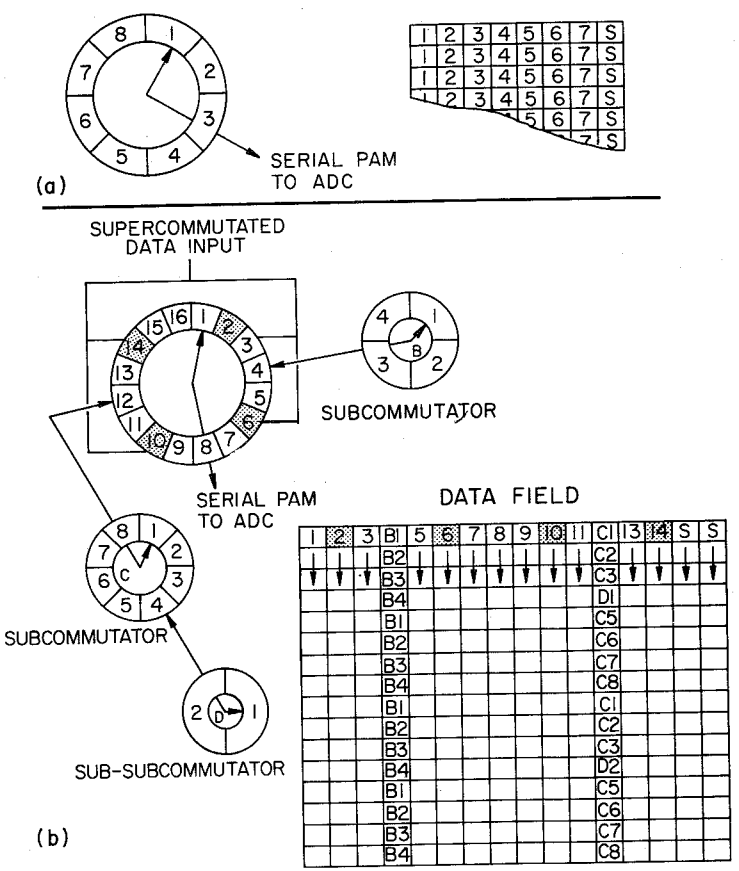

Fig. 5. PCM commutation and data formats using a simple commutator (a) and a commutator with subcommutators (b). Channel 8 in (a) and channels 15 and 16 in (b) are used for frame synchronization.

tions. Figure 5b shows a multiplexer configuration, drawn like commutators, where a 16-word mainframe has two subframes of four and eight words. The eight-word subframe has a two-word sub-subframe. In addition to the subframes, four of the channels on the mainframe are tied together for supercommutation. Channels 15 and 16, in the time sequence, are used for the frame synchronizing pulse. The format diagram of the data field is also shown in Fig. 5b.

The serial bit stream output of the PCM data encoder is used to modulate the telemetry transmitter. There are a number of modulation techniques used to represent the logic levels one and zero. The IRIG standards give a complete description. The most commonly used ones are shown in Fig. 6. NRZL is a non-return-to-zero-level where a "1" bit is one signal level and an "0" bit is a different level. NRZM is a non-return-to-zero-mark. In this waveform the level is meaningless; "1" bits are represented by a change in level in either direction; "0" bits are represented by the absence of a change in level. RZ is return-to-zero. In this waveform, a finite width pulse, usually half-bit width is generated to mark a "1" bit, while "0" bits are not marked. There is an advantage for using NRZ over RZ in that the RF

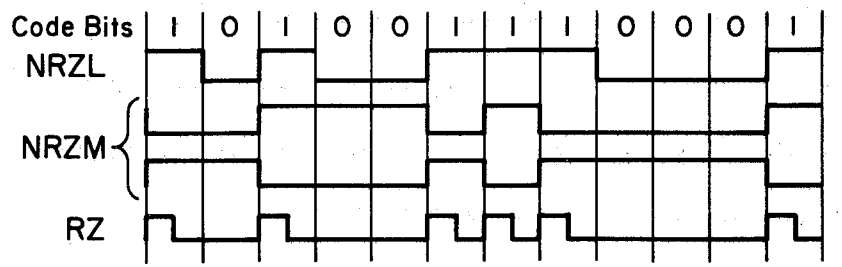

Fig. 6. Waveforms of pulse code information.

link need handle only frequency components of half the bit rate. NRZL is probably the most commonly used code. NRZM is a common form of digital saturation magnetic tape recording, since during tape playback, only the change in magnetic flux is detected, Stiltz (1).

Before the PCM output waveform is used to modulate the AM, FM, or PM transmitter, it is passed through a premodulation filter where the unnecessary high frequency components are removed. It is also possible to have a mixed system such as PCM/FM/FM where a subcarrier channel of an FM/FM system handles the PCM data. The band-width capabilities of the FM channel must be adequate to accommodate the bit rate in this case. In the case of direct frequency modulation of the carrier by the PCM signal, a higher bit rate can be accommodated with a wider deviation. With some balloon telemetry systems, rates as high as 100 kilobits per second are practical.

(2) PCM data recovery. In the PCM encoder, a fixed number of bits constitutes a data word (or sometimes a syllable), and a fixed number of words constitutes a data frame. Ordinarily a word would represent one digitized sample from a data channel and a data channel would occur at least once throughout a frame. The frame is repeated continuously at a fixed

rate. Some channels will provide a data sample once per frame, while others will appear several times in a frame. The subcommutated data samples may appear only once in a total data field.

The purpose of the PCM data recovery system is to detect the incoming data bits, determine the location of the first bit in the frame and then decommutate the data channels. For accurate decommutation, the bit frequency must be established. Also the frame synchronization pulses must be acquired so that the programmed counting pulses may be reset at the proper time. Figure 7 is a block diagram of a PCM data recovery system. The output of the receiver will contain the PCM data in a serial train of bits in NRZL or other data code. In the case of PCM/FM/FM the NRZL data will come from an FM subcarrier discriminator. The bit synchronizer extracts the bit synchronizing rate from the signal and converts the data form to one compatible to the frame and subframe synchronizer input. This unit, which has been preprogrammed to recognize the synchronization word generated by the data encoder, the word lengths, words per frame, and words per subframe, will demultiplex the output data according to the established format. In case some of the digital words are to be converted back to analog data, a digital-to-analog (D to A) converter is programmed to convert those par-

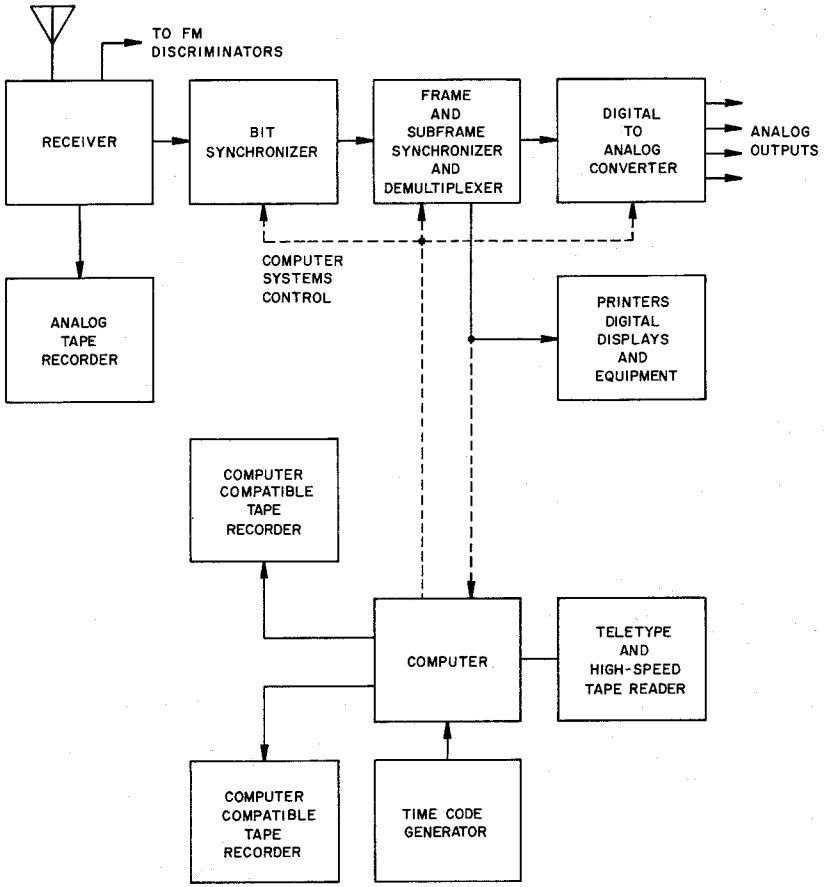

Fig. 7. Block diagram of PCM data recovery system.

ticular channels for graphic chart recorders or other instruments. If the data are to remain in digital form for display on alphanumeric devices, punched tape, magnetic tape, teletype, line printer, or digital voltmeters, then the digital data are taken from the demultiplexer.

It would be feasible to process data in real time if a central processing computer were available and could handle the information as fast as it can be retrieved. A more practical system is to record the data on computer-compatible tape along with a digital time code for future data reduction. This additional system is shown with dashed connections in Fig. 7. The computer here is a minicomputer with a teletype and a high-speed paper tape reader as input-output (I/O) devices. The magnetic tape may also be used for I/O in some cases. The computer is programmed to format the computer-compatible tape with the PCM data.

In some cases the demultiplexing equipment can be computer controlled for data format settings. This saves considerable time and reduces errors in set-up procedure. The system-control program could be stored on magnetic tape or punched tape and transferred to core storage for immediate system set-up.

A photograph of a ground station is shown in Fig. 8.

c. Pulse-amplitude-modulation telemetry. Pulse-amplitude-modulation (PAM) refers to a technique which is essentially the commutation of several sources of quasi-static data into a single telemetry channel, such as an FM/FM carrier or subcarrier. The data bandwidth of the telemetry subcarrier must be large enough to handle the data samples as determined by their duration and commutator speed. The data can be decommutated at the ground station or from a tape recording of the received signal. The IRIG telemetry standards have established standards for the PAM pulse train so that standardized deommmutators can be used.

The duty cycle of the commutation pattern may be 50% (return-to-zero) or 100% (non-return-to-zero). An example of the 50% pattern is shown in Fig. 9. The information channels are allocated equal and constant time intervals within the PAM frame. Each interval T contains a sample pulse beginning at the start of the interval and having an amplitude determined by the amplitude of the data of the corresponding information channel accord-

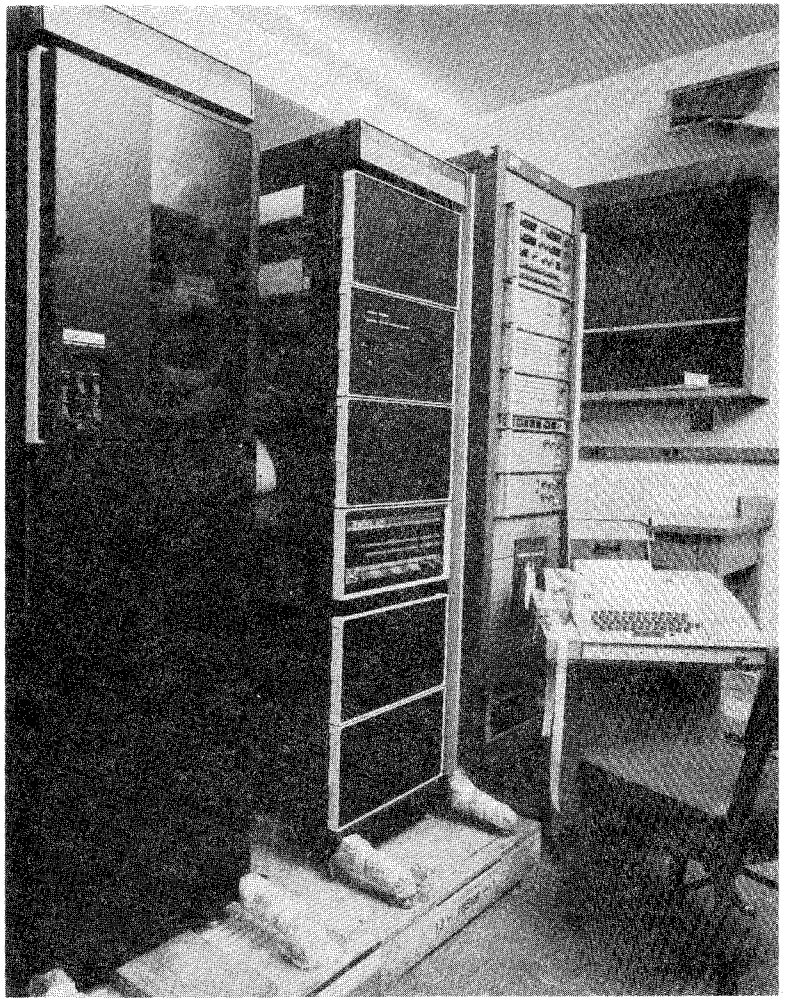

Fig. 8. PCM data recovery equipment.

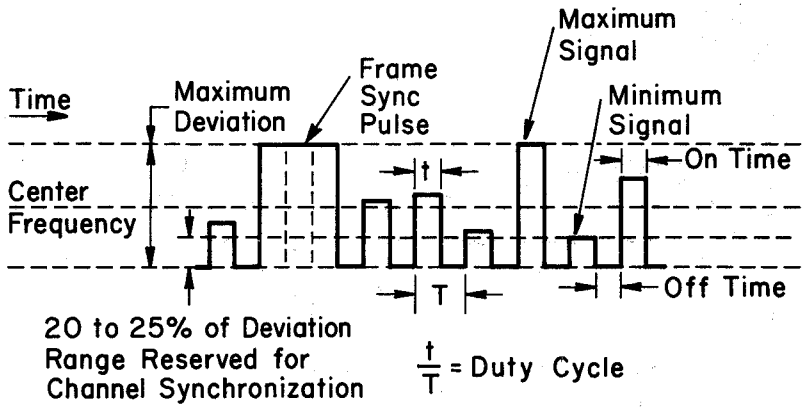

Fig. 9. PAM pulse train waveform.

ing to a fixed relationship, usually linear, between the minimum level (zero amplitude) and the maximum level (full scale amplitude). In this pattern the synchronization interval has a duration of 2T with full scale amplitude for 1.5T followed by the reference level for 0.5T.

Decommutation of a PAM signal is the process whereby the individual channels of the time-division multiplexed sample data are separated. The composite signal, as shown in Fig. 9, is applied to a parallel bank of gates, each of which is closed for a short period, the closures occurring in cyclic order so that only one gate is closed at any instant. The gates are synchronized with the PAM pattern such that each gate will deliver output pulses representing only one channel of sampled data. The voltage levels of each channel are maintained until the next sample appears. With slowly varying data such as temperature or battery voltages there is little need for interpolation. The data can be recorded on individual graphic recorders for each channel, Stiltz (1).

d. Pulse-duration-modulation. Pulse-duration-modulation (PDM) is a time multiplexed system wherein the amplitude of each channel is converted to a pulse, whose duration is directly proportional to the amplitude. It

is sometimes referred to as pulse-width-modulation (PWM). PDM is perhaps a simpler system than PAM but, with modern telemetry components, it is probably less accurate than PAM. PDM was originally adopted because of the noise problems with early mechanical commutators and because the linearity of early FM/FM subcarriers, used with PAM, was not accurate, Stiltz (1).

In the PDM system a commutator is used to sample the analog data signals as with the PAM and PCM systems. To convert the constant width, variable amplitude pulses from the commutator to constant amplitude, variable width pulses, a keyer is inserted between the commutator and the subcarrier oscillator or the FM transmitter for PDM/FM/FM or PDM/FM telemetry. By converting the PAM pulses to PDM pulses a series of data pulses is obtained whose accuracy is not seriously impaired by amplitude fluctuation due to noise. Figure 10 is a diagram of a simple PDM system using a mechanical commutator. In addition to multiplexing the analog data, the commutator provides trigger pulses to the keyer. These trigger pulses are used to initiate the pulse-width data pulses at a fixed rate. The width or duration of these pulses is a direct function of the corresponding data amplitude. One method of accomplishing this is to start a square wave generator and a linear sawtooth

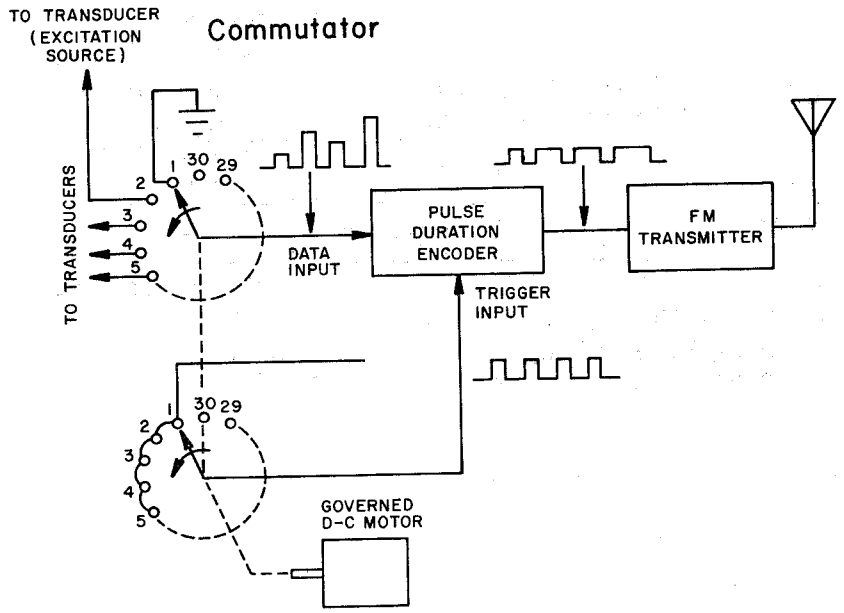

Fig. 10. Block diagram of a typical PDM system.

ramp voltage with the trigger pulse. When the ramp voltage equals the data voltage, a voltage comparator terminates the square wave generator. Since the trigger pulses occur at equal intervals, the data pulses occupy equal time intervals in the commutator sequence. Figure 11 illustrates the PDM pulse train.

As in the PAM technique, one channel is reserved for zero reference, one for full scale reference, such as zero and five volts, respectively, and two channels for decommutator synchronization. There are two types of synchronization formats. One is a full amplitude pulse with a duration of 1.5T where T is the channel interval. The other is the absence of any pulse for an interval of 2T. The maximum frame length should be no greater than 128 intervals, including those used for calibration and synchronization. The IRIG telemetry standards include standards for the PDM pulse train so that standard decommutators can be used, IRIG (2).

The output voltage of the pulse duration encoder is generally applied to a high frequency channel of an FM/FM subcarrier system where the subcarrier frequency is shifted from near one band-edge to near the other band-edge in a manner of frequency-shift-keying. Accuracies of one percent of

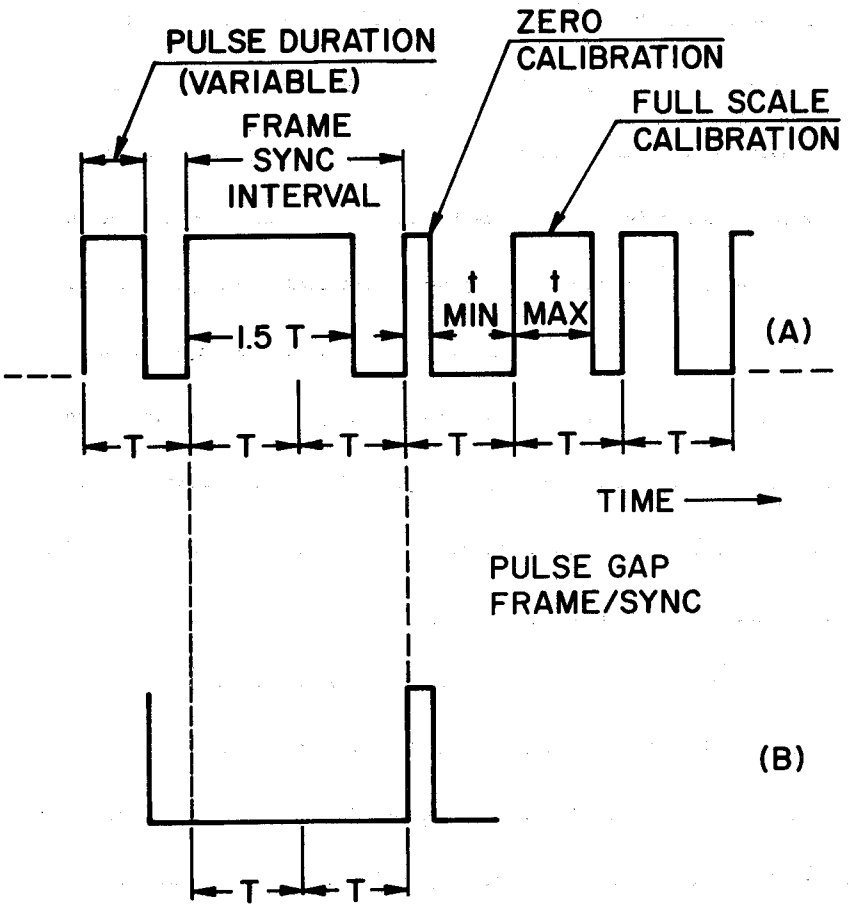

Fig. 11. PDM pulse train waveform.

full scale are readily achieved with PDM systems. The accuracy of the system is primarily determined by the keyer. The output of the encoder may be used to drive the transmitter directly, especially for high commutation rates. When this is done, true FM transmitters should be used because of the large dc or low frequency components contained in the pulse train.

At the ground station the PDM data may be recorded on magnetic tape for future analysis, displayed by means of a bar graph presentation on an oscilloscope, or converted to analog voltages and recorded individually on graphic recorders. It is also possible to convert the information to a form suitable for digital computer processing.

The bar graph display and the waveforms used to generate the display are shown in Fig. 12. The length of the bars is representative of the PDM pulse duration or the amplitude of the analog data. These bars appear on the oscilloscope when it is unblanked by each channel pulse. The pulse durations are used to gate a sawtooth whose duration is the same as the channel data pulse duration. The amplitudes of the sawteeth are proportional to their duration and are used for vertical deflection. The horizontal sweep for the oscilloscope may be linear; however, a stairstep generator, as shown,

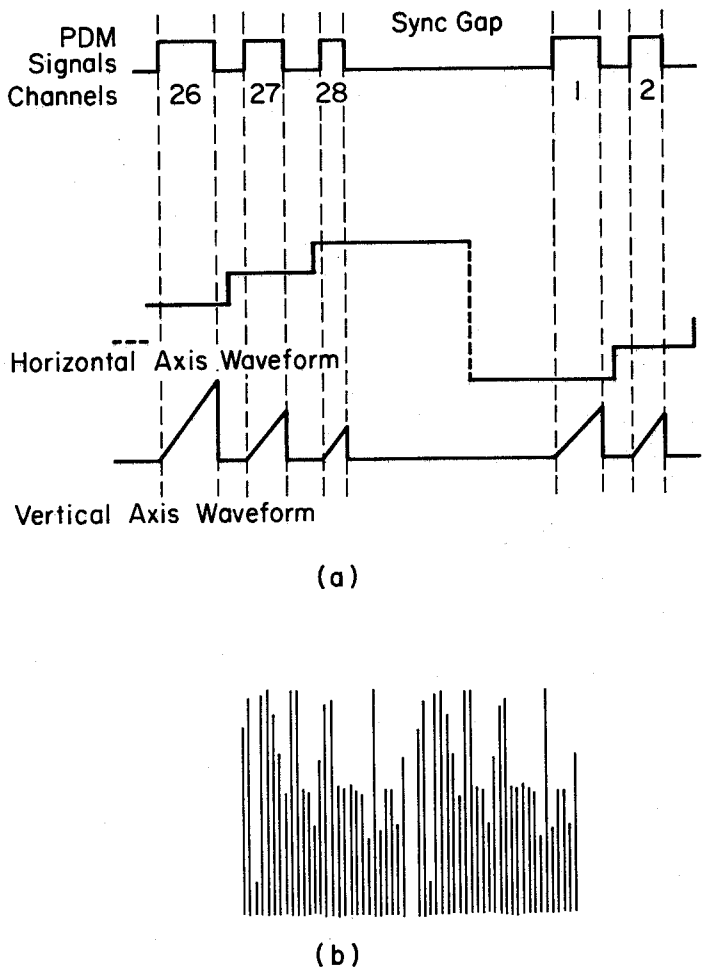

Fig. 12. Waveforms (a) used to create PDM bargraph display (b).

makes a better sweep for this type of presentation, Stiltz (1).

A more satisfactory method of display consists of decommutating the data or separating the information from a serial train of pulses to a parallel configuration where each channel is available on a separate output. For this to be done, the data pulses must be converted from variation in duration to variation in amplitude. This can be accomplished by an integrating circuit, such as used for the bar graph display. The peak amplitude is sampled and held until the next corresponding data channel appears. This process is synchronized by the sampling rate pulses which are derived from the frame synchronization signal and the frame format information.

To convert the PDM data to digital information suitable for computer processing, it is necessary to convert the pulse duration to a digital form compatible to computer application. One method consists of gating a clock oscillator for the duration of the data pulses and counting the clock pulses during these intervals. Another method consists of converting the PDM pulses to PAM pulses, sampling the amplitude of the pulses at the proper time, and converting them to digital form with an analog-to-digital converter.

2. The Radio Frequency Link

It is the purpose of the radio frequency link to connect the inaccessible data to the accessible location. Since we are concerned with balloon telemetry, we are confined to RF links rather than wire links. The RF spectra used for telemetry are the UHF (1435-1535 MHz and 2200-2300 MHz) bands. The VHF (216-260 MHz) band for telemetry was to have been relinquished by January 1, 1970; however, some extensions were made to agencies which were not readily able to make the frequency changes. The UHF band which has been assigned to balloon telemetry is the L-Band (1435-1535 MHz).

The radio frequency link consists, essentially, of the transmitter and its antenna at the data source on the balloon, the receiver and its antenna at the ground station, and the propagation medium between.

The transmitter is generally a frequency modulated or phase modulated radio frequency energy source. The mixed output of the FM subcarrier channels or the direct modulation from the PCM digital data encoder is applied to the modulation input of the transmitter. Precautions are made to avoid the generation of undesired signals. It is the function of the transmitter

to apply this signal to a radio frequency carrier with the addition of as little distortion as possible. For most balloon telemetry the RF energy is nominally about two watts. The RF energy is radiated from the balloon system by means of an antenna with an omnidirectional horizontal pattern. A modified ground plane suspended below the balloon for vertical polarization is generally used.

The receiving system at the ground station consists of the antenna, preamplifier (if used), and the receiver with its detectors and amplifiers. The output of the receiver drives the appropriate demodulation equipment, discussed earlier. In some cases down-converters are used, especially when VHF equipment is available to use with UHF signals.

The receiving antenna may vary in size and configuration from simple ground planes or dipoles to parabolic dish antennas. For VHF telemetry a dipole array, yagi configuration, or an array of helical antennas may be used. Helical antennas are of broad bandwidth; they are simple to construct and accommodate circularly polarized signals. They are more popular for reception of signals from sources such as space vehicles or sounding rockets. For balloon work it is easier to transmit a linear, vertically polarized signal for omnidirectional coverage. Since there will be no Faraday rotation in the course of a balloon flight, it is better to arrange for linear, vertical signal reception. In the case of VHF this dictates the use of dipole or parasitic (yagi) arrays, and for UHF a parabola with a vertical linear feed. Figure 13 is a photograph of a 1485 MHz receiving antenna.

Three important parameters describe a receiving antenna. These are directivity, gain, and effective aperature. Directivity is the ratio of the response of the antenna to signals in the direction of the maximum pattern lobe to its average response to signals in all directions. Gain is the power ratio of the response of the antenna to signals in the direction of its maximum lobe to the response of a reference antenna such as an isotropic antenna, expressed in decibels (dB). The effective aperature, or capture area, determines the amount of signal extracted.

Antennas may be entirely manually positioned, manually controlled but motor driven, or entirely operated by machinery with automatic tracking provisions. The choice of system depends on cost, antenna size and weight, beamwidth, wind loads, and flight path. Manual tracking, which usually relies on a simple indication of relative signal strength to guide the operator, is useful mainly with the simpler antennas.

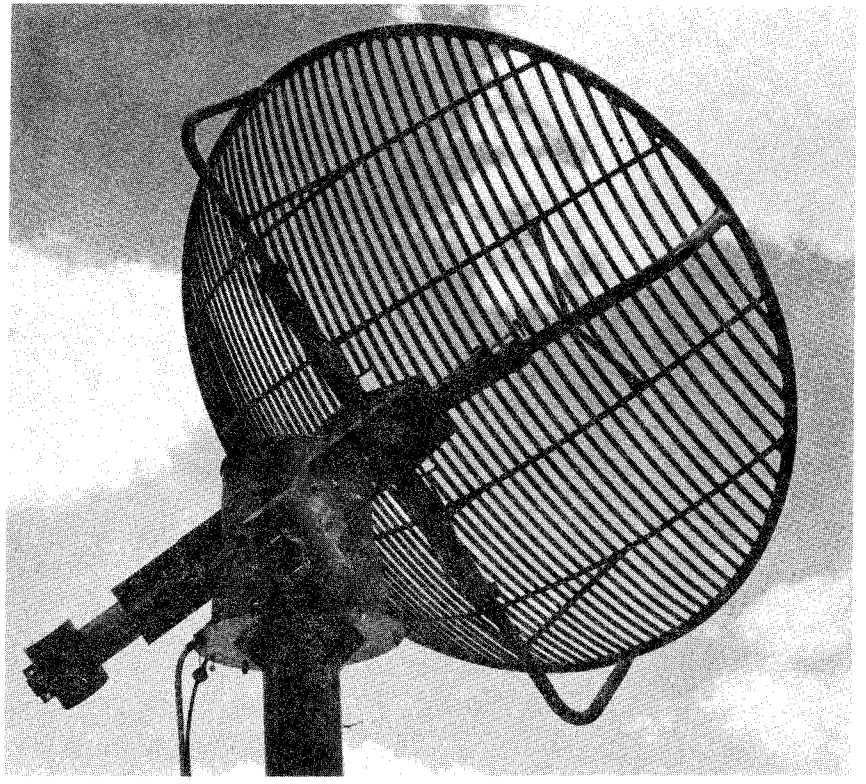

Fig. 13. L-Band telemetry receiving antenna.

The range of operation with UHF and VHF signals is limited to radio-horizon distances as determined by the heights of the balloon and the receiving antenna on the ground. The height of the receiving antenna has little significance for long range reception except that it should clear surrounding objects. The direct radio-horizon distance to a balloon from a ground station may be calculated approximately by the formula, $D = (3h/2)^{\frac{1}{2}}$, where h is in feet and D is in statute miles. The propagation range, which is greater than the tangential distance due to atmospheric refraction, may be approximated by considering the earth's radius to be 4/3 its actual radius. The propagation distance is then approximated by $D = (2h)^{\frac{1}{2}}$. Table 4 gives the radio-horizon range for balloons at several altitudes.

When the balloon is approaching the radio horizon the elevation angle is small and multipath propagation due to reflection from the earth's surface or objects on it may occur. The effect of multipath propagation is the destructive or constructive interference in the RF signal and if the time difference of arrival of the two signals is very small compared to the period of the highest modulating frequency there is no effect on the FM modulation characteristics, Nichols (6). As the range of the balloon from the receiver

Table 4

Radio-horizon Range for Balloons at Various Altitudes

Balloon Altitude	($\times 10^{-3}$)	Maximum Range		
km	ft	km	Statute Miles	Nautical Miles
20	65.62	583	362	314
24.38	80	644	400	347
25	82.02	652	405	352
27.43	90	684	425	369
30	98.43	714	443	385
30.48	100	721	448	389
33.53	110	756	470	408
35	114.83	771	479	416
36.58	120	790	491	426
39.62	130	821	510	442
40	131.23	825	512	445
42.67	140	853	530	460
45	147.64	875	543	472
45.72	150	884	549	476
50	164.04	922	572	497
55	180.45	967	600	522
60	196.85	1010	627	545

increases, a predictable variation in the signal strength will occur. This might be avoided by adjusting the receiving antenna height during flight to insure constructive interference. The antenna height should be

$$h_a = n\frac{\lambda}{4}\quad\frac{d}{h_b}$$

where d is the ground range and h_b is the balloon's height.

Without antenna height adjustments, the predictable signal strength variation with range is suggested as a method of estimating balloon range over a distance of 100-450 km, when other methods are unavailable, Clark (7).

It is very desirable to operate the RF link with a minimum of transmitter power at the signal source on the balloon. This is to reduce the battery ampere-hour requirement and hence the payload weight. VHF transmitters have approximately 40% dc to RF efficiency, while UHF transmitters at present are 10 to 15% efficient. Long duration flights require several ampere-hours of battery reserve, unless the telemetry is programmed, which adds much payload weight.

In order to assemble a system which uses a low power balloon-borne transmitter, emphasis must be placed on low-noise receiving equipment and an

antenna with reasonably high gain. This is necessary to cope with marginal signals which occur when the range approaches the radio-horizon.

The ability of a telemetry receiver to detect the presence of a signal is fundamentally limited by the presence of internally generated noise, such as thermal noise, shot noise, vacuum tube noise, and semiconductor noise. Since noise is always present, amplification in the receiver amplifies noise as well as the desired signal.

Thermal noise is a major contributor to the overall noise in a receiver. It is caused by the random motion of electrons in the circuit components and at absolute temperature T in ^{o}K the maximum available noise power is expressed by the Boltzmann expression kTB_n, where k is Boltzmann's constant (1.38×10^{-23} J/^{o}K) and B_n is the noise bandwidth.

An ideal receiver adds no noise to the signal being amplified; however, a practical receiver will generate noise to some extent. The measure of the noise generated by a practical receiver compared with that of an ideal receiver is called the noise factor F. The noise factor of the receiver may be considered to be the degradation of the signal-to-noise ratio of the receiver. When the noise factor F is expressed in dB, it is called the

noise figure NF, where NF = 10 log F.

Figure 14 shows two amplifiers, such as a preamplifier and a receiver, connected in series. Each has the same noise bandwidth B_n, but different noise factors and gains; it can be shown that the overall noise factor

$$F_o = F_1 + \frac{F_2 - 1}{G_1}$$

where the gains and noise factors are ratios.

If the gain of the first amplifier is large, the contribution of the receiver to the overall noise factor is small; therefore, the system noise factor can be greatly improved with the addition of a preamplifier with a low noise factor, assuming it has a reasonably high gain such as 15 to 20 dB. It is better to place the preamplifier at the antenna where the signal-to-noise ratio is highest. After the signal has been amplified by the low-noise preamplifier, the attenuation and noise generated by long runs of coaxial cable and antenna rotary joints have little effect on the overall signal-to-noise ratio.

The total noise power in dBm (dB below one milliwatt) may be expressed as

$$N = 10 \log \frac{kT_oB_n}{1 \times 10^{-3}} + \log F_o$$

Fig. 14. Block diagram of two amplifiers in series.

where T_o is a reference temperature (290°K) and B_n is the receiver noise bandwidth.

This equation is separated into two parts to show the effect of variations of the overall receiver noise factor. The noise contributed by the first term is due to the kTB_n noise term, Cooper (8).

An example of the power levels at different points in an L-Band UHF radio frequency link, such as illustrated in Fig. 15, are shown in Fig. 16. The power level is plotted in decibels relative to 1 mW (dBm). The transmitter power is 3 W or 35 dBm, which is shown on the upper right side of the diagram. The transmission line loss from the transmitter to the balloon antenna is 1 dB, while the antenna gain is 2 dB. The free space loss for a range of 400 n mi (radio-horizon) is 153 dB, based on the formula

$$L = 20 \log (4 \pi R/\lambda)$$

where λ is the wavelength and R is expressed in meters. The atmospheric loss, caused primarily by oxygen and water vapor is approximately 1 dB per 100 n mi. The signal level is increased by 29 dB with an 8-ft paraboloid antenna and 1 dB is lost in the antenna pedestal and associated cabling. The resultant -93 dBm represents the signal at the preamplifier input terminals.

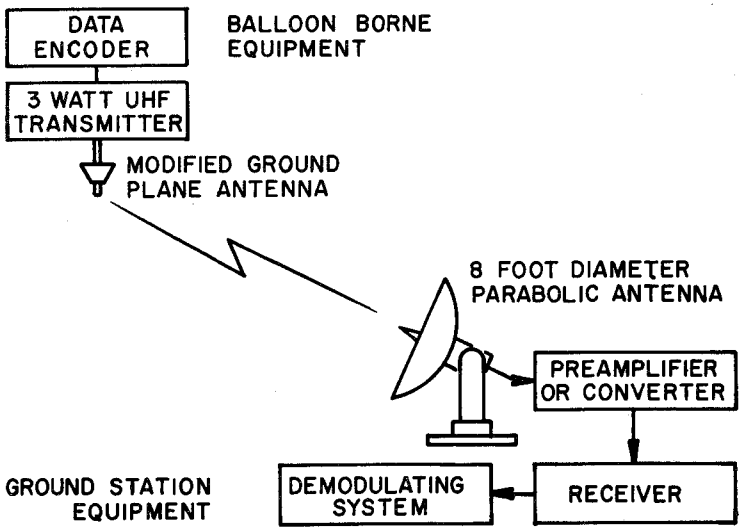

Fig. 15. Block diagram of UHF telemetry system.

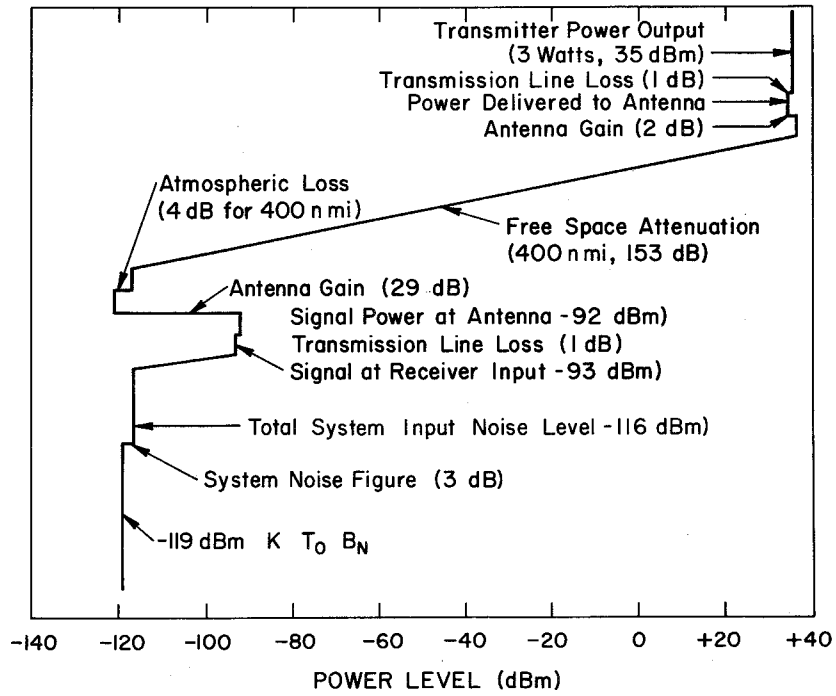

Fig. 16. Signal power-level diagram.

On the lower left side of the diagram, the receiver noise contributed by the kTB_n factors is represented by the -119 dBm level. This level plus the noise figure term represent the noise level of the receiving system. If the noise figure is 3 dB, then there is a -116 dB noise level. A larger noise figure will create a higher noise level and will require a greater signal for a margin of safety. In this case there is a 23 dB signal-to-noise ratio. This provides a margin of safety because 9 to 12 dB is considered adequate for FM/FM telemetry, and 13 dB is adequate for PCM/FM with an error probability of 1 bit in 10^5 bits, Cooper (8).

3. On-Board Data Recording

Scientific data that are not telemetered to ground stations and recorded there are recorded aboard the balloon. On-board recording is not as prevalent now as it was before reliable telemetry was available. It is sometimes used as a back-up for radio telemetry.

The method of recording depends on the type of experiment being performed. For example, if a scientist is counting the accumulation of high energy particles from a source outside the earth's atmosphere, he may use a system of scalar counters which may be displayed with a series of light

sources such as light emitting diodes (LED). These lights may be photographed on continuously moving film with periodic flashes of a clock and a photobarograph. The time and pressure-altitude may also be displayed with the other data in digital form. This technique permits the data, time, and altitude to be presented on the same film record.

Magnetic tape recorders are also used for on-board data recording. These may be analog or digital recorders. Incremental recorders can generate a computer-compatible format, useful for rapid data analysis. Digital time data from a time code generator is desirable for a complete data recording on the tape. Some tape recorders use cassette tapes which are useful for small amounts of data. The recorders may be programmed or commanded on and off as desired with the command-control systems.

Other miscellaneous types of on-board data recording include the measurement of radioactive particles by using photographic emulsion plates; particle collectors for micrometeorite detection; and cameras for photographing on-board phenomena such as the track of a high energy particle in a spark chamber.

C. COMMAND-CONTROL

Scientific balloon flights are practically always equipped with a command-control system for balloon control and scientific package control. Balloon control requires three or four command channels for ballasting, valving, and flight termination or cutdown. The number of channels required by the scientist for control of the experiment depends upon the complexity of the experiment. In some complex experiments the number of command channels may be one hundred or more.

There are several criteria for a reliable command-control system. First, the range over which it will operate successfully should be made as great as possible. With VHF or UHF as the radio link, a practical range is in the order of 400-450 n mi, limited by the radio-horizon. Ranges beyond this are generally unnecessary because the balloon trajectory can be covered by down-range stations or by tracking aircraft capable of command-control. The command system should have an extremely high reliability. The system must be designed to recognize all legitimate commands and to reject extraneous or inadvertent signals that are received. Locally generated noise, such as from dc motors, must not be decoded as commands nor

prevent true commands from being recognized. Finally, the balloon-borne equipment should be small, lightweight, and consume a small amount of power, especially when quiescent. As with all balloon-borne electronics, power consumption is a critical item because excessive power requirements create additional payload weight in the form of batteries.

The command-control technique resembles radio telemetry to a large extent. In the command system, the encoder and transmitter are located at a ground station while the radio receiver and decoder are aboard the balloon payload. The decoder output may be in the form of a voltage level, a closed circuit, a relay closure, or a digital word. The margin of signal-to-noise received at the balloon is much larger than a received telemetry signal primarily because the ground transmitter power is much greater. There are essentially three systems which may be used for balloon command-control. These systems are pure tone modulation of the RF carrier, tone-digital where a system of pulse modulated tones is used to set up a digital command word, and PCM where the digital bits are used to modulate an RF carrier or subcarrier. The modulation formats for any of these systems are limited only by the designer's imagination. The advent of medium scale and large scale integrated

(LSI) circuits have expanded the circuit possibilities tremendously.

1. Tone Modulation

The tone modulation system was the first developed for scientific ballooning and is used where relatively few commands are needed. There are various concepts that can be used with tone commands. Some use the simultansous transmission of combinations of two or more standard Electronic Industries Association (EIA) tones to code a command channel. Others use a sequential series of tones to complete a command.

When the tone command system is used, the function of the tones is to modulate the command transmitter. On the balloon the RF signal is received, and the tones are detected and applied to the decoder where they are separated for their proper function. In the case of simultaneous multitone coding, each tone is decoded and used to establish the state of a circuit, such as a relay. The correct combination of tones will establish the proper combination of decoder circuit states to actuate the command. When tones are used simultaneously, precautions must be taken to prevent the generation of a sum or difference frequency of two tones which may actuate an undesired command channel.

A tone system, shown in the block diagram of Fig. 17, which has been used extensively for scientific ballooning, uses an RF link compatible with an existing VHF narrow band FM communication system. This minimizes the required ground station equipment and allows the transmission of commands from mobile stations, such as land vehicles or aircraft. Two tones are transmitted simultaneously. One tone (number 1), sometimes referred to as a squelch tone, is common to all command channels. It is used to enable the audio circuits at the receiver to allow the command tone to reach the tone decoders.

As many as twelve tone oscillators in the EIA audio frequency range are used to frequency modulate the command transmitter at the ground station. The tone oscillators may be any stable audio generator; however, circuits using resonant reeds are often used. Resonant reed circuits are also generally used as tone demodulators in the balloon-borne equipment, but other filters, such as active filters, could be used. The resonant reed is an electro-mechanical device that acts as an audio frequency filter with a bandwidth of about 1% of the design frequency. It has one or more steel reeds suspended in a magnetic circuit consisting of a permanent magnet and

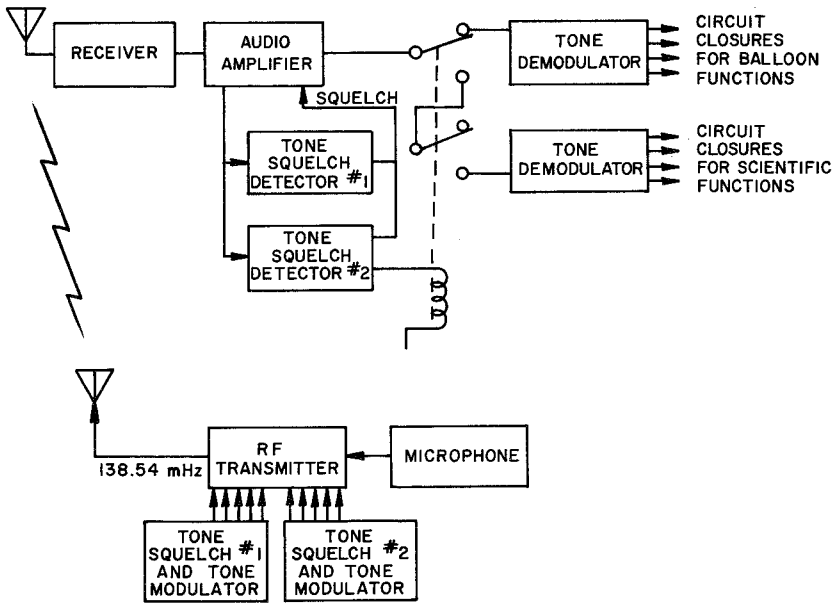

Fig. 17. Block diagram of a tone modulated command system.

a field coil. When operating at its resonant frequency each reed vibrates to make a circuit closure with a large duty cycle. This intermittent closure due to resonant vibration is integrated and used to actuate an amplifier and relay circuit. In all decoder channels, an adjustable delay of one to six seconds is designed into the circuits so that momentary or extraneous signals will not actuate a command function.

Sometimes it is desirable to use a single tone command channel to change the states of a latching relay rather than to use two channels for this purpose. This can be done with an additional miniature relay and an RC charging circuit as shown in the schematic diagram of Fig. 18. When a tone command is received, the decoder relay applies power to actuate the miniature relay and the latching relay to one state and begins to charge capacitor C through resistance R. If the command is transmitted for a time long enough to charge C with enough energy to actuate the latching relay to its other state, this will be done when the command transmission ceases and the decoder and miniature relays return to their de-energized state. For short duration commands the latching relay goes to one state without returning. It takes a short and a long duration command to transfer states se-

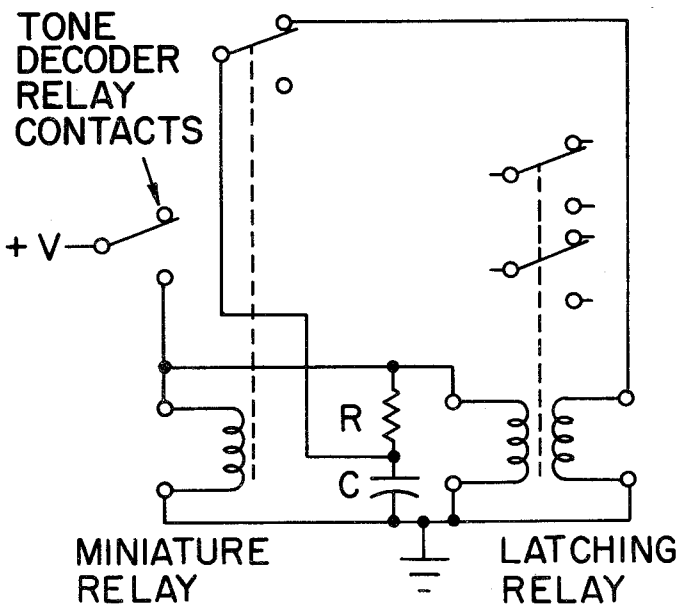

Fig. 18. Latching relay circuit for single command channel operation.

quentially. The RC time constant should be about 10 sec and the capacity of C should be adequate to store the charge necessary to actuate the latching relay.

If the transmitting system is capable of more than one tone squelch modulator, almost duplicate systems may be used on a balloon or two or more balloon systems may be commanded at a time. Figure 17 illustrates an example where two decoders are operating from the same receiver using two tone squelch frequencies. When transmitting a special command such as payload separation, it is necessary to have interlocking circuits on the encoder panel to prevent inadvertent transmission of that command.

A tone command system using sequential tones is the Address-Execute system used by The National Aeronautics and Space Administration on some of the earlier space flights, Coates (9). In this system the RF carrier of the ground command transmitter is modulated with a series of discrete single audio tones, as shown in Fig. 19. Sequential transmission is employed with an address tone sent first to "arm" the decoder. Each command receiving system is assigned to a unique address tone. The execute tones follow to accomplish the particular command function and may consist of up

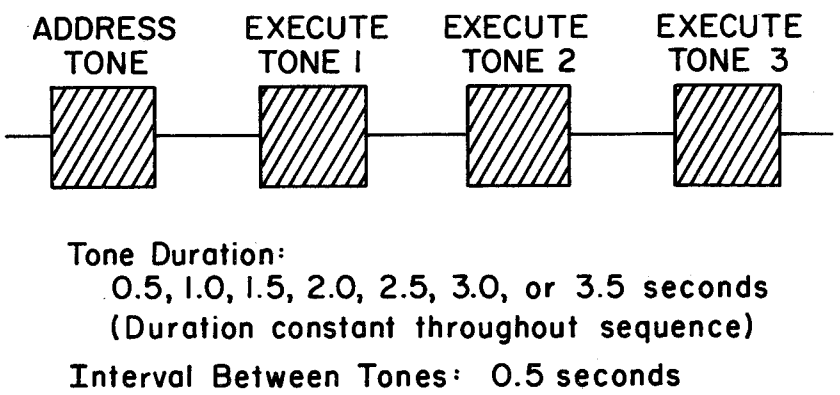

Fig. 19. Address-execute tone command structure.

to three different tones in sequence. The combined detection of these tones by the "armed" decoder causes initiation of the command actions. After a predetermined period of time, equal to the length of the longest execute sequence, the decoder is dearmed and cannot respond to an execute tone until it receives another valid address tone.

2. Tone-Digital Systems

The tone-digital command system was developed by NASA for spacecraft command-control, Coates (9). This particular coding format has not been used for balloon command, but illustrates possibilities for tone-digital systems. It consists of a pulse-duration-modulated (PDM) tone with constant bit ratio word coding and repetitive word formatting as shown in Fig. 20. A series of five words, each consisting of eight bits, one synchronization and one blank period, are sent for each command. The series consists of a unique address transmitted twice, followed by an execute word transmitted three times. The reception of one correct address word and one correct execute word will actuate a command. This redundancy increases the probability that the correct command will be received under weak signal and interference conditions.

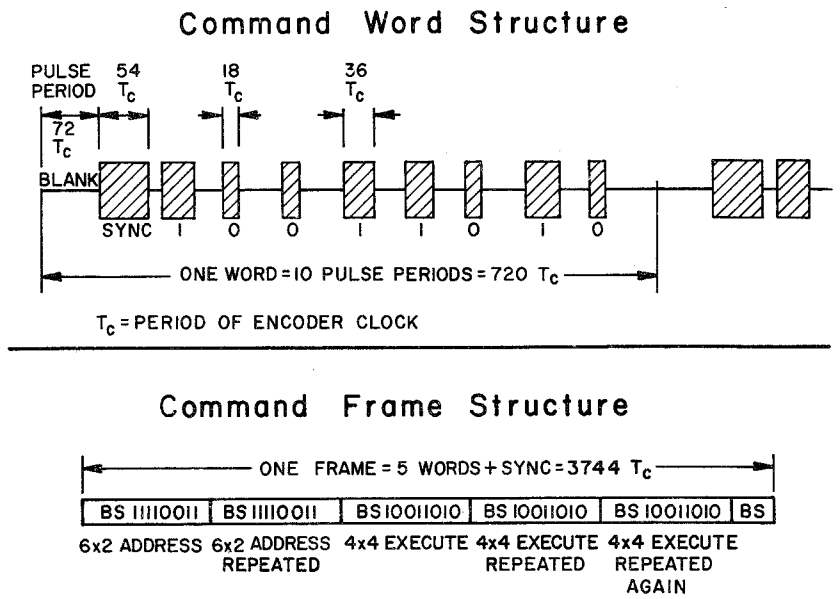

Fig. 20. Tone-digital command word structure and format.

The technique used for error detection and interference rejection consists of forming the code words from a fixed number of zeros and ones. The address code consists of a combination of two "ones" and six "zeros" while the execute code always contains a combination of four "ones" and four "zeros." This 4 X 4 combination provides 70 commands out of a possible 256 combinations of eight data bits. It provides a means of detecting all odd and 43% of all two-bit errors. To further reduce the possibility of spurious commands, the snyc pulse must be detected before the words are detected, and once it is detected, a valid execute word must be read within a fixed period.

Pulse-duration-modulation of an audio oscillator is used, where the bit period is 72 audio cycles, the sync period is 54 cycles, and the "one" bit is 36 cycles and the "zero" bit is 18 cycles. The decoding logic is somewhat more complicated with this digital system than with the simultaneous or sequential tone systems described earlier.

Another form of the tone digital technique has been used for balloon command-control, Cooper (10). In this system the command words are digitally encoded into a train of pulse-duration-modulated 1600 Hz audio signals.

These signals modulate a narrow band FM transmitter. The coded pulses are transmitted in bit pairs (dibits) which represent "ones" and "zeros." An 18 msec pulse followed by an 8 msec pulse forms a one; a reverse sequence forms a zero. A complete command transmission consists of a 3-dibit address, a 28 msec sync pulse, and a 5-dibit command word. Each bit period requires 40 msec, and the complete command 640 msec. It is possible to transmit 8 different addresses and 32 command words; thus up to 256 commands are available to control a single balloon or several balloons simultaneously. A special interlocked command word is reserved for balloon flight termination.

On the balloon, the train of PDM signals is detected at the discriminator of the command receiver, then amplified with audio circuits and passed to the command decoder. An audio, phase-lock-loop, band-pass filter excludes undesired frequencies and noise before the audio signal is converted to dibit and sync pulses. The logic circuits of the decoder detect pulse width, dibit coding, and the presence of the sync pulse. The decoder produces momentary and latching relay closures to actuate the command functions. Six features of the decoder's operation act separately to prevent

inadvertent command activation; the dibit coding, the pulse-width modulation, the audio frequency, the 11-pulse word, the required sync pulse, and the three-dibit address word preceeding the command word. When all of these coding features are performing properly, the command will be accepted by the decoders.

Command encoders for this system can be used both at the ground stations and in mobile vehicles. The radio frequency equipment is the same as is used for VHF-FM communications from the ground stations to the mobile vehicles.

3. PCM Command

A PCM command system may be a high capacity command transmission link. The message configuration is similar to a computer instruction, as partitioning is used to designate various functions, such as addressing, event timing, error checking, and system control. The modulation signal is similar to PCM telemetry such as PCM-NRZ where a voltage-controlled subcarrier oscillator is frequency-shift-keyed (FSK) from one frequency to another.

The word format may vary depending upon the requirements of the command

instruction and, for spacecraft, may be quite long. It may contain word synchronization bits, address bits, and instruction bits or memory load bits and their complements for error checking. In more exotic systems the command word may be transmitted back to the ground station for checking with the command word transmitted and if there is agreement, an execute command is transmitted from the ground.

A PCM command system that has been built for one scientific balloon experiment will transmit up to 32 discrete commands and a 16-bit instruction command to the balloon. The discrete commands can be increased to 64 with a small circuit change. The command word consists of 23 binary bits with the first six bits being the address. This address logic is permanently wired into the encoder; however, thumbwheel switch settings could be used for establishing the address of 00 through 31.

The binary discrete command words are determined by thumbwheel digital switch settings which determine the bit logic beginning with the eighth bit. If the command word is an instruction command, the digital switches are set to position 32 which changes the state of bit 7 and causes a 16-bit instruction command to be generated. The word format is established by the

settings of 16 toggle switches.

The encoder logic voltage levels are used to frequency-shift-key (FSK) a voltage-controlled-oscillator (VCO) such as is used with airborne FM/FM telemetry. For this particular system, a channel 1A VCO is used with 14 kHz being used for logic "zero," 16 kHz for a space, and 18 kHz for logic "one." The VCO output modulates an AM or FM transmitter. The bit rate is 30 bps. The six bit discrete commands are decoded on the balloon into voltage signals for actuating relays or whatever other purpose is desirable. Two channels are necessary for actuating a latching relay into two states.

The instruction commands, consisting of 16 binary bits, are decoded into an NRZ-L format on the balloon. In addition to the decoded binary word there is a clock-pulse, a "data-presence" signal and an end-of-message (EOM) pulse. All of these signals are desirable at the receiving end for handling the binary instruction words.

A recent development of data communication circuits has been made by the Larse Corp. of Palo Alto, California. These circuits are modular in form and are supplied in both transmitting and receiving modules. They can be configured with a large degree of versatility which makes them quite useful for many data transmission systems. These units have been utilized in a PCM command-control system by the National Scientific Balloon Facility.

The code format for this command system consists of 16 bits of data information grouped in eight coded groups. These groups consist of four consecutive bits, starting with a low clock bit followed by two data bits, which represent the status of two data inputs, and followed by one high clock bit. A sync pulse follows the entire group. The coded format is used to frequency-shift-key (FSK) an oscillator operating at 1620 Hz ± 180 Hz at 360 bits per second. The low clock bit and a "zero" data bit are represented by one band edge while a high clock bit and "one" data bit are

represented by the other. This FSK signal is used to frequency modulate the command transmitter.

The 16-bit data word is used to transmit a 6-bit address and a 6-bit command word which can be coded into as many as 64 discrete command functions which appear as open collector transistor sources at the receiver on the balloon. The addresses and commands are established at the transmitter with thumbwheel switches in octal coding. The other switches are used when the system is used for instruction or data commands and for control. A 16-bit data word can be transmitted with the 6-bit address. The data format is established with 16 toggle switches and is transmitted in 2 successive groups of 8 bits.

The system provides several elements of security utilized by the system. No more than two negative transitions occur per code element; all clock bits must be in their proper position of proper polarity and duration; data bits must be in their proper position; and elements cannot have too few or too many transitions.

The 16-bit words are transmitted twice in immediate succession when a command is given. They are compared bit-by-bit by the receiving module to determine the validity of a command.

The binary instruction commands are useful on the balloon in many instances where binary information is desirable, such as setting up memory registers for positioning an instrument on the balloon payload. It is feasible to have an analog-to-digital converter at the ground station ahead of the digital code generator. This would allow one to dial in the desired data in analog form. If a real-time computer were available at the ground station, computer-controlled digital instruction commands with digital telemetry feedback could be used for instrument control. Techniques for using digital command and telemetry are almost unlimited.

4. Verification

There are various schemes for command verification for balloon commands. The obvious way is to use a telemetry channel where a signal is developed on the balloon when the command is decoded and is telemetered to the ground stations for visual observation. In some systems the telemetry signal may be used to turn on visual displays for command verification. In some instances a high-frequency tracking beacon signal frequency is shifted about 1 kHz when the command is actuated on the balloon.

It is more desirable, in some cases, to have verification that the ultimate operation being commanded has performed. This can be done, but because the command system is generally of independent design from the scientific experiment, the verification ends with command reception and decoding.

5. Radio-Frequency Link

For many command-control applications for scientific ballooning in the past, the voice-communications equipment used by launch, recovery and tracking crews has been used as the RF link to the balloon. This is narrow band VHF frequency-modulation equipment (±5 kHz) using a 60-W transmitter with either a vertically polarized, horizontally omnidirectional or a directional antenna with about 8 dB gain at the ground station. The receivers are modules designed for portable VHF-FM gear which has been repackaged for noise suppression. They have a sensitivity of less than 1 μV for 20 dB quieting. The receiving antenna is a vertically polarized coaxial dipole.

By making signal strength calculations, as discussed in sub-Section B.2 for telemetry, it can be seen that there is adequate available signal for reliable operation.

Transmitted power 60 W	+ 48 dBm
Transmitting antenna gain	8 dB
Space loss (400 nmi)	-132 dB
Atmospheric and cable loss	- 2 dB
Available signal	- 78 dBm

This signal is equivalent to 28 μV across 50 ohms. Without the 8 dB antenna there would be -86 dBm or 11 μV, where only a few microvolts are adequate.

Command-control functions are found in many frequency bands including the high frequency bands. The frequency used would depend upon the type of modulation system used, the range of operations, and the desired ground and airborne antenna configurations. The appropriate frequency management organization should be consulted for obtaining a frequency assignment.

When tone commands are used, a set of 20 IRIG tones (different from the EIA tones) are specified by the IRIG standards for radio command-control. These 20 tones range in frequency from 7.5 to 73.95 kHz, IRIG (11). Other tones and modulation formats can be used because the IRIG standards are not restrictive. They establish standards for commercial equipment as well as provide for efficient spectrum usage and reduction of interfering signals.

D. COMMUNICATION REPEATER

It is often desirable to have communication between two ground stations when the VHF-FM communication system will not function because they

are separated by a distance greater than the radio-horizon.

If the command-control system uses the communications RF links, it is a simple matter to create a radio repeater system using the FM/FM telemetry system. The audio output of the command receiver with proper dc offsets and amplitude limiting is applied to the input of a VCO. The VCO channel must have the frequency data capabilities to handle voice frequencies. Channel E with MI = 5 should be adequate. At the ground station the voice can be taken from the telemetry discriminator, amplified, and used to drive a speaker. This system will work between vehicles and aircraft as long as a telemetry receiver-discriminator is available. It is possible to modulate directly the telemetry transmitter by mixing the audio with other VCO signals. This eliminates the need for a discriminator at the receiving station, but may create intermodulation problems with the telemetry.

E. BALLOON CONTROL

Command-control is used for controlling the scientific balloon as well as the experiment. The experiment generally demands the most from the command system; however, the balloon control commands are very important. Command-control is used for dropping ballast, releasing lifting gas, and for

flight termination.

1. Ballasting

A ballast hopper is usually built in the form of a rectangular box with a pyramid shaped bottom opening into a round port. The port is open to ballast flow; however, the presence of a permanent magnet at the port causes the steel pellets to cluster together and prevent the flow. To allow the ballast to flow, an electromagnet is energized to oppose the permanent magnetic field. This action, called ballasting, may be done by command or by a timer.

The usual verification technique for ballast flow is to verify the reception of a command on the balloon. The actual ballast flow can be detected by means of a sensitive flap and switch in the ballast port. Another technique uses an oscillator as a VCO of the FM/FM telemetry system which has, as part of its frequency determining circuit, an inductance wound around a non-metallic part of the ballast port. When the ballast drops through the coil, the oscillator frequency is changed in proportion to the amount of flow.

Before a flight is terminated, it is usually desirable to remove all

ballast from the payload to relieve the load from the recovery parachutes. This can be done by command-control, and a timer may be used as a back-up. As a last resort, the hoppers may be destroyed with pyrotechnic devices at the time of flight termination. Hoppers used this way are made of a fragile material such as cardboard.

2. Valving

For the purpose of releasing gas from a balloon, a valve is usually built into the apex of the balloon at manufacture. It is usually actuated by an electric motor which is controlled by timer or command-control. Limit switches stop the electric motor at the extremes of the valve travel and allow the motor to be reversed when desired.

It is desirable to have the receiver and command decoder located at the apex of the balloon with the valve. This eliminates a long wire run over the balloon. A repeater type command could be conceived with a radio link from the main payload to a simple receiver-decoder at the apex. If a telemetry transmitter can also be installed with the valve, the valve position may be monitored at the ground station. The ultimate vertification of valving is in the response of the balloon.

3. Flight Termination

A flight is usually terminated by releasing the payload on a parachute. This action is initiated by command-control, generally by the pilot of the tracking aircraft who can better determine the recovery problems and impact hazards from his vantage point. The parachute is attached to the balloon with a coupling which is nearly always released with pyrotechnic devices. Reliability is assured by the use of redundant sub-systems in the coupling system. As a precaution against command failure, a timer-activated sus-system which is set at launch for a period longer than the maximum anticipated flight time is also included.

As in the case of the valve, it is desirable to have the command receiver-decoder at the location of the coupling system. This reduces long wire runs and other hook-up problems in the balloon train. If this cannot be done, wires can be run the length of the parachute to fire the pyrotechnic devices. The timer is always located with the coupling system.

When the parachute and its payload are separated from the balloon, a rip cord built into the balloon and attached to the parachute rips a hole in the balloon, allowing it to fall to earth.

4. Timers

Timers for balloons can have various configurations depending upon the complexity of the flight, the expense involved, and accuracy required, Cooper (12). Mechanical, chemical, and electronic timers have all been used for scientific ballooning. Some flights may use simple timers such as motor driven cams, conducting mixtures which are allowed to escape, and electrolytic cells. A precision tuning-fork driven time piece, called an Accutron, is useful for balloon timing. This timer is equipped with several switch contacts and is accurate to within a few seconds a day. A popular mechanical timer consists of a cam actuated switch driven by a chronometric motor and gear train. The motor has an accuracy of 1%. The desired elapsed time can be set by a dial on the cam. Several cams are available for effecting switch closures at different times. The predecessor to this timer was a long motor driven lead screw which drove a screw-follower to actuate a switch. The elapsed time was determined by the position of the follower on the screw.

Recent timer designs use crystal oscillators with binary and decimal dividers using integrated circuit components, such as RCA COS MOS logic

components. The elapsed time can be set with thumbwheel switches. When the states of the time storage registers in the decade divider chain agree with the decade switch settings, a circuit closure is made. If more than one set of switches is used, more than one circuit closure can be made. The circuit closure can be used to actuate a relay or thyrister circuit to handle large amounts of current. A block diagram and photograph of an electronic timer capable of three timed functions is shown in Fig. 21, Cooper (12). This timer can be updated during flight by command-control. It has status monitor circuits so that the elapsed time can be monitored through telemetry. This is useful when updating.

F. TRAJECTORY DETERMINATION

Balloon trajectory determination is necessary for several reasons. Since the scientific and balloon flight support equipment is seldom expended, it is necessary to know the balloon location for recovery purposes. To meet the requirements of the Federal Aviation Agency (FAA), the balloon position must be known to help prevent it from becoming a hazard to air traffic. In many instances it is important to the scientist to know accurately the geographical coordinates of the experiment. It is always important to the

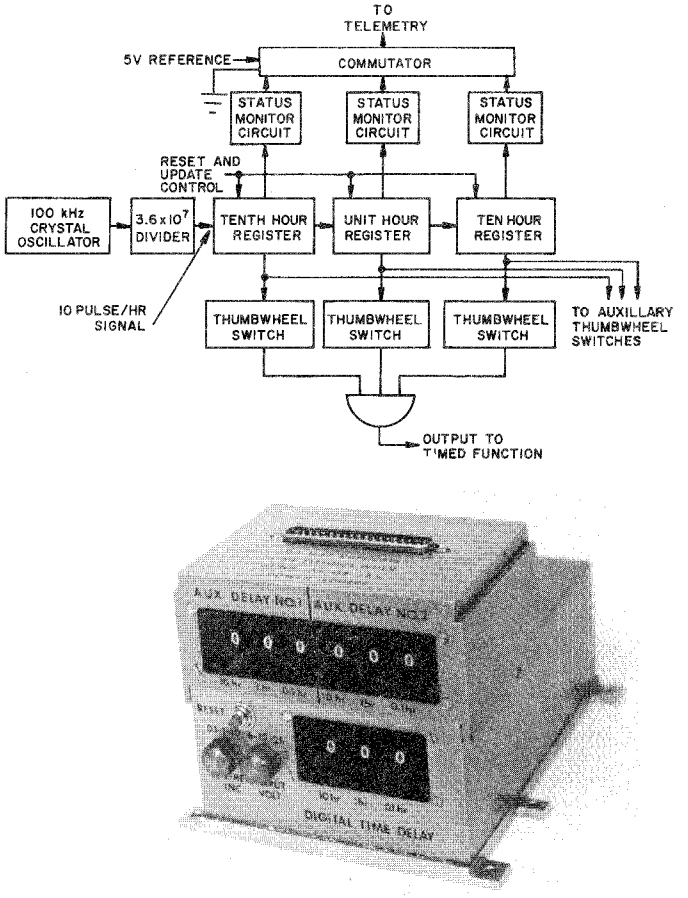

Fig. 21. Digital timer block diagram (a) and a photograph of the timer (b). Pulses from a crystal oscillator are divided to yield a 10 pulse/hr clock. Memory registers store counting bits for tenths of hours, hours, and tens of hours. The timer shown in (b) has two auxilliary sets of switches for additional timed functions, and more can be added if desired.

scientist to have an accurate measurement of the pressure-altitude of the balloon.

1. Radar Tracking

Radar is a contraction of the words, radio detection and ranging. Radar provides a straight-forward method of tracking a balloon. A radar system used for balloon tracking must be capable of providing accurate position information. Its usefulness is limited by its range, which may extend to near the radio-horizon. Range measurements are a function of the elapsed time between the emission of a pulse of a radio-frequency signal and the reception of a reflected signal from the target. The rate at which successive pulses may be transmitted is usually determined by the longest range at which targets are expected. The range beyond which targets start to appear as second-time-around echoes is called the maximum unambiguous range and is $R = c/2f_r$, where f_r is the pulse repetition frequency (PRF) in Hz and c is the velocity of radio propagation, 3×10^8 m/sec.

When no transponder is used the signal is reflected from the balloon and its payload. Some payload configurations with their reflective surfaces provide excellent radar targets, but it is best to provide a corner

reflector target to insure a good reply signal.

If the radar antenna has a vertical fan beam, such as is used for target acquisition, the elevation accuracy will be poor. The more desirable radiation pattern is a narrow pencil beam. This provides more accuracy in azimuth and elevation. The antenna required to provide such a beam, generally a paraboloid, may be made to track the target with a servomechanism actuated by an error signal. The error signal may be generated by sequential lobing, conical scan, and simultaneous lobing or monopulse.

Any good tracking radar may be used for skin tracking a balloon for position determination. The surplus M33 fire control radar has been used for this purpose; however, these units are becoming difficult to maintain because of component aging and obsolescence. The X-band tracking system of this radar operates in the 8500-9600 MHz band with a peak RF power of 250 kW and a PRF of 1000 pps. A tracking antenna with a pencil beam with a half-power width of 2° is used for tracking. An integral computer, originally a part of the M33 fire control system, can provide a range reading on a counter. Typical accuracies for this radar are $\pm 0.1^\circ$ or better in azimuth and elevation and $\pm$ 10 yd at maximum range of 50 n mi (100,000 yd).

2. Rawin Set

Another straight-forward method of tracking a balloon within a limited range with a minimum of airborne equipment is the AN/GMD-1 Rawin set. This is a transportable, radio direction finder, designed for automatically tracking and recovering data from a balloon-borne radiosonde transmitter. A signal from the balloon-borne transmitter, such as radiosonde AN/AMT-12, containing meteorological information in the form of pulse modulation, is received, amplified, and detected by this equipment. The transmitted frequency is 1680 MHz at approximately 0.3 W. This is a continuous wave signal, pulse modulated with a cutoff pulse train ranging in rate between 5 and 200 Hz as determined by a transducer, such as a thermistor for temperature measurements.

The AN/GMD-1 equipment uses a 7-ft paraboloid antenna with a conical scan tracking system. The detected radiosonde signal is passed to separate equipment in the radiosonde system where it is recorded. By reference to calibration data for the airborne unit, the recorded information may be converted to values of temperature, humidity, and pressure. The AN/GMD-1 equipment was originally designed as a tool for sounding the atmosphere to

provide data for weather analysis and forecasting, and to prepare ballistic corrections for the effect of the atmosphere on the trajectory of projectiles.

When the radiosonde system is used with high altitude research balloons for parameters such as temperature and humidity, the measurements are reliable only at the lower altitudes. The temperature sensing system reaches a radiative balance in a rarefied atmosphere and is, therefore, not a reliable air temperature sensor at high altitudes.

Azimuth and elevation angles of the balloon are measured with the AN/GMD-1 antenna to an accuracy of $\pm 0.05^{o}$. These coordinates in conjunction with the altitude are useful in determining the balloon's trajectory. The radiosonde signal is generally accurate to about 150 mi where ground reflections begin to interfere.

3. Phase Shift Ranging

A simple ranging and direction finding system utilizing existing balloon electronic components can be used. This system adds practically no balloon-borne equipment to that normally required for scientific balloon flight support.

This technique utilizes the propagation delay characteristics of a

two-way radio signal from the ground station to the balloon. An audio signal with a convenient wavelength, such as 720 n mi (225 Hz), modulates a transmitter which is used for transmitting command signals to the balloon system. This audio signal is extracted from the command receiver on the balloon and used to modulate the telemetry transmitter, either directly or on an FM/FM subcarrier channel.

At the ground station the audio signal is extracted from the telemetry signal, and a phase comparison is made between the transmitted and received signal. A digital phase meter is used for phase measurements where one degree of phase shift represents one n mi of range, considering two-way propagation delay. More range resolution may be obtained by increasing the modulating frequency by an integral factor such as four, where 360^{o} represents 90 n mi of balloon range. The lower frequency would then be used only for the coarse measurements to eliminate ambiguity.

The azimuth of the balloon from the transmitting station can be determined by using a highly directional telemetry receiving antenna. If the receiving antenna is inherently highly directional, such as a paraboloid used for UHF telemetry, its directional characteristics may be used. If a

signal in the VHF range of 216-260 MHz is used, a system using two receiving antennas may be used. The system consists of two high-gain vertically polarized yagi antennas, horizontally skewed so that the main pattern lobes intersect at the half-power points. The antennas are alternately switched into the telemetry receiver and a visual azimuth error is indicated on an oscilloscope. High resolution pointing accuracy is obtained by rotating the antenna system to null the pointing error. The azimuth readout is provided by a selsyn system and a mechanical counter.

With careful installation and calibration one might expect to get azimuth accuracies of one degree and 0.5 n mi or better in range.

The system could be automated with a servosystem for automatic azimuth tracking. With modern minicomputers, the aximuth and range could be converted to geographical coordinates and also used to drive an X-Y recorder for horizontal mapping.

4. Omega

The Omega navigation system has been used to some extent for following a scientific balloon in its trajectory. Its performance characteristics and the results of tracking experiments indicate that the one-standard-

deviation accuracy of the system is approximately 1 n mi during the daytime and 2 n mi at night, Pierce (13).

Omega navigation is based on the measurement of phase of the signals transmitted from each of several very low frequency (VLF) transmitting stations. Omega is best described as a time-shared CW type of radio navigation system in which the measurements are in terms of the relative phase of the received signals, rather than a comparison of the time of arrival of pulses.

One characteristics of VLF propagation is a low attenuation rate, making it possible to receive the signals at great distances. At the present time, only four Omega stations are in operation. It is anticipated that the system will comprise eight transmitters for global coverage. The existing four transmitters provide a navigation capability for many important geographical regions. The locations of the transmitters are shown below.

Omega Transmitter Locations

Station	Location	Latitide	Longitude
A	Aldra, Norway	66° 25.3'N	13° 09.2'E
B	Trinidad	10° 42.1'N	61° 38.3'W
C	Haiku, Hawaii	21° 24.3'N	157° 49.8'W
D	LaMoure, N. Dakota	46° 22.0'N	98° 20.1'W
E	Reunion Island	20° 58.4'S	55° 17.4'W
F	Argentina	43° 3.2'S	65° 11.5'W
G	Australia	No location established	
H	Japan	34° 36.9'N	129° 27.2'E

The first four stations are permanent stations and radiate from 1 to 3 kW of VLF power. The last four are new stations to begin operation

in the future to make the Omega system a world-wide system which will be useful for global ballooning operations. All except station G are presently under construction. The Trinidad station will eventually be replaced with a station in Liberia. Omega charts and other information may be obtained from the U.S. Naval Oceanographic Distribution Office, Philadelphia, PA or Clearfield, UT.

The frequencies presently being transmitted are 10.2, 13.6, and 11.333 kHz. These transmissions are on a sequential time-multiplexed basis as shown in Fig. 22. The frame repetition interval is 10 sec. Each 10-sec period is divided into eight time segments, A through H. (These letter designations are not to be confused with the station designations.) The time segments are not all equal. Omega navigation receivers, when tuned to one of the VLF frequencies, are synchronized with an internal commutator so that the station transmitting during any particular interval may be identified. The initial receiver commutation cycle may be established by snychronization with WWV or by considering the relative strength of the received

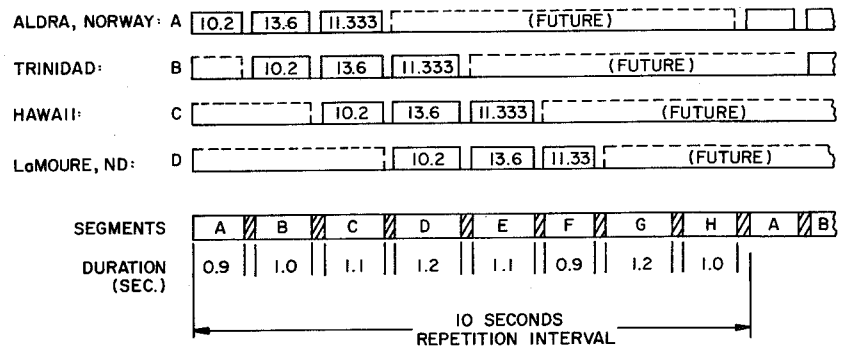

Fig. 22. Omega transmission format.

signals. Automatic segment synchronism may also be established by the unequal segment duration when using more complex receivers. Also, at present, one of the stations transmits a "phase signature" consisting of a 6 μ sec phase advance. This creates a temporary 1 mi error, but identifies the station.

All Omega stations transmit on a phase-locked, synchronized basis. Accurate frequency control is accomplished by employing ultrastable atomic frequency standards at each station. Phase synchronization is maintained by continual phase comparison of signals transmitted by individual transmitters using monitor receivers at the transmitters themselves and at central control locations.

The receiving equipment compares the phase difference of signals of the same frequency transmitted from two stations to determine the hyperbolic line of position (LOP) as shown in Fig. 23. Since the phase difference is repetitive at half wavelength intervals, ambiguous lanes will occur. This lane ambiguity must be accounted for by keeping precise records of the lanes the vehicle has traversed. By using a separate pair of transmitting stations, another set of intersecting lanes can be obtained to establish the position of the vehicle.

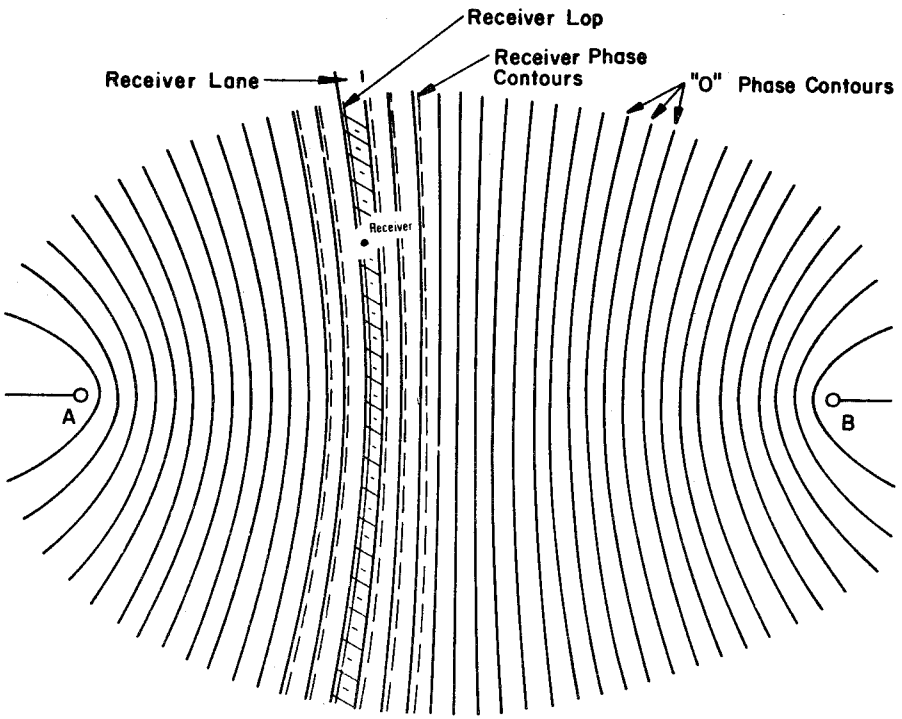

Fig. 23. Omega lane pattern between a pair of stations.

Lane ambiguity can be reduced by using two Omega frequencies. The difference between these two frequencies is used as a third frequency to establish a wider lane. For example, the width of four lanes at 13.6 kHz is equal to the width of three lanes at 10.2 kHz. Similarly, nine lanes at 10.2 kHz equals ten lanes at 11.333 kHz, the total width being the equivalent lane width of the frequency difference of 1.133 kHz, about 72 n mi.

Omega receivers normally present the lane data from pairs of transmitting stations in the form of a voltage on a strip chart recording. The information may be referred to a map or listing where geographical coordinates may be established. A more sophisticated system would use a minicomputer to convert the relative phase information from two pairs of stations (three stations) into geographical coordinates while automatically taking into account the varying skywave factors.

To implement the Omega system for balloon trajectory determination, it is necessary to receive the Omega signals at the balloon and retransmit them to one or more ground stations. A block diagram of a system is shown in Fig. 24. This shows a single frequency Omega signal amplifier on the balloon with its output used to modulate the telemetry transmitter. The

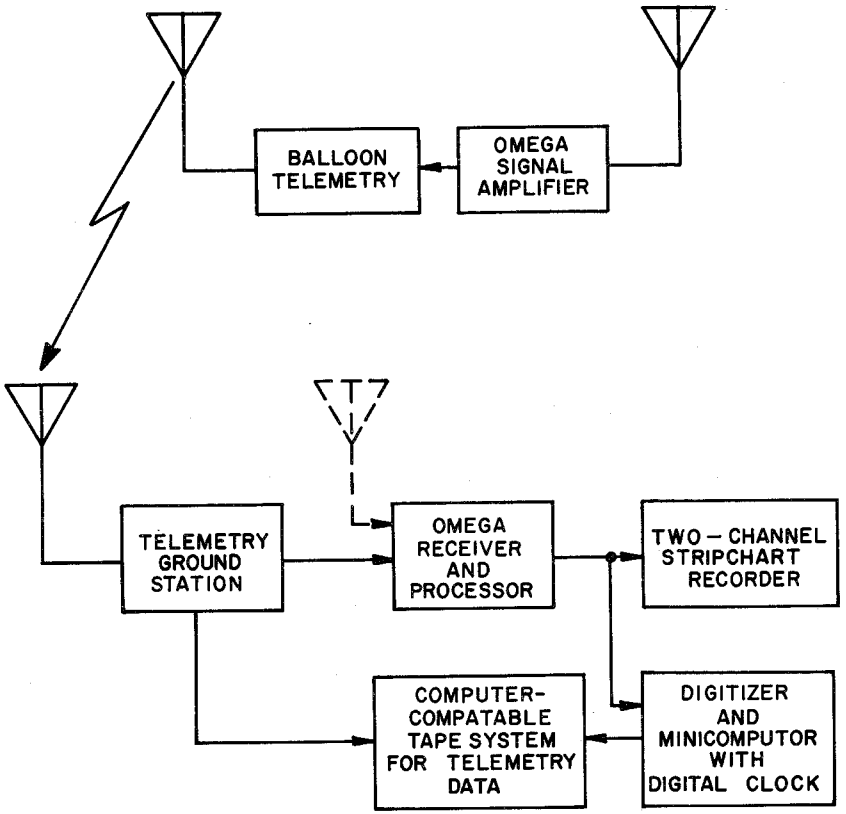

Fig. 24. Block diagram of Omega system for balloon position determination.

transmitter may be directly modulated or the Omega signal may modulate a subcarrier channel if FM/FM telemetry is used. The airborne equipment should be designed for minimum phase variation with Omega signal level variation.

At the ground station the telemetry signal is received and the telemetry information is processed in the usual manner. The Omega signals are extracted from the telemetry signal by demodulation of the carrier and subcarrier, and passed to the Omega receiving and processing equipment. The Omega equipment utilizes the Omega signals as though they were received directly. The fact that they are relayed by the balloon telemetry introduces delays that are determined by the balloon's position. The path from the balloon to the ground station is common to the Omega signals from all transmitters; therefore, the delay for all signals is equal and no relative phase variations occur.

The simplest approach to determining the balloon's ground position is by plotting lane information from the Omega processor onto an Omega map. It may be necessary to initialize the data based on system delays.

A more elaborate system employs digital techniques where appropriate lane tables are stored in a digital computer. These tables, which conform

to Omega maps, can be used to extract geographical coordinates of the balloon.

Another approach uses spherical hyperbolas and the geographical coordinates of the Omega transmitting stations to compute balloon lines of position.

The diurnal variations of propagation of the Omega signals must be considered when making calculations of balloon position using Omega. This variation may create errors of several nautical miles depending upon which transmitting stations are being used. Correction charts are available for these diurnal variations. A local approximation of the error may be determined at the ground station through periodic checks of the Omega position of the station, accomplished by direct reception of the Omega signals. The diurnal correction may be assumed to apply as well at the balloon location, when it is within close range of the ground station.

5. Tracking Aircraft

A method that has been used extensively for balloon trajectory determination is that of aircraft tracking. This method, though not capable of giving extremely accurate position, is necessary for general balloon surveillance as well as for locating the payload impact at the earth's surface.

Most aircraft are equipped with high frequency, automatic direction finding (ADF) equipment for homing on signals such as those radiated from broadcast stations. If the scientific balloon has a signal such as the beacon signal commonly used with the barocoder, the aircraft can determine the location of the balloon by homing on that signal using the ADF equipment. If the geographical position of the balloon is not recognized by the aircraft pilot, he can take bearings to other signals or use the VOR system.

Another aircraft tracking system operates on a principle similar to the high frequency ADF system. It is designed to use the telemetry frequency to determine the bearing of the balloon from the heading of the aircraft. A servo controlled directional antenna locks onto the telemetry signal and a dial displays the bearing of the balloon.

6. FAA Transponder

ATC transponders, similar to those used by many aircraft, may be used on a scientific balloon. The FAA (Federal Aviation Administration) may then determine the balloon position and provide trajectory information. As

the FAA radar scans the horizon, it transmits a pulsed signal which is received by the balloon transponder. The received pulsed signal in turn causes the transponder transmitter to send a pulsed reply which is then received by the radar receiver. This reply signal consists of a digital code identifying the balloon, which has been assigned a special code. The distance is determined by the radar ranging circuits. A complex system of FAA radars provides a wide, though not complete, geographical range of coverage for vehicles carrying transponders, FAA (14).

To conserve power, the transponder may be time-pressure programmed or turned on by command. It is most useful to the FAA when the balloon is operating below 75,000 ft altitude. A programmer can be designed to allow operation constantly to this altitude, and for 5 min at 30-min intervals for the remainder of the flight.

G. PRESSURE-ALTITUDE

The altitude of a free balloon is one of the factors determining the trajectory. Also, scientists using high altitude balloons as vehicles are generally interested in knowing atmospheric pressure at the balloon or the

air mass above the balloon. When pressure and virtual temperature data are available from the balloon altitude to the surface, a pressure-to-altitude conversion can be made by integrating the hydrostatic equation (see Section XI). Atmospheric pressure measurements for scientific ballooning are generally made in millibars, a bar being 10^5 N/m^2 --slightly less than mean sea level atmospheric pressure. Gage pressure is referenced to atmospheric pressure, while absolute pressure is referenced to a vacuum.

Types of gages used to measure pressure include liquid manometers, Bourdon tubes, strain gages, piezo electric devices, capacity diaphragms, variable reluctance diaphragms, rare earth transducers, corona current devices, thermoconductivity measuring devices, radioactive density gages, and solid state pressure sensing devices. Many of these gages are applicable to on-board pressure measurements. The type used for a flight depends upon the accuracy desired, the type of data recovery, and other factors peculiar to the flight, Cooper (15).

1. Barocoder

One of the earliest types of instruments used for pressure measurements is the barocoder. This instrument has usually been used in conjunction with

a low-power transmitter operating at approximately 1680 kHz, and together they are commonly referred to as a beacon-barocoder. The beacon transmitter can be tracked by means of the automatic direction finding (ADF) equipment available on most aircraft; consequently, it provides a means of locating the balloon as well as providing the pilot with balloon altitude information. When the beacon-barocoder was originally designed, it was used on balloon flights where radio telemetry for data recovery was not always available. This made the beacon-barocoder an independent instrumentation item. It is still widely used because of its accepted reliability, redundancy to other pressure systems, and for its compatibility with the tracking aircraft for balloon tracking and payload recovery after termination.

The barocoder consists of a system of aneroid bellows which are mechanically linked to a stylus which is allowed to move longitudinally across the surface of a code drum. The code drum is a motor-driven cylinder which has a systematic configuration of Morse code letter groups etched on its surface in the same fashion that electronic circuits are etched on copper-clad insulation board. As the pressure changes, different code letters are traversed by the stylus as the drum rotates and the circuit closures made by

the stylus on the etched drum key the transmitter on and off. The signal is radiated from a long wire antenna suspended below the balloon payload or attached to a load tape. Receivers are located in the tracking aircraft and at the ground stations.

2. Diaphragm Gages

There are two types of diaphragm gages that are applicable to pressure-altitude measurements. One is a capacitive device using a taut membrane stretched between two stationary capacitor plates. The space between the membrane and one stationary plate is evacuated, while the space between the membrane and the other stationary plate is connected to the gas whose pressure is to be measured. The displacement of the membrane with respect to the stationary plates is a measure of the pressure, and is determined by capacity measurements between the membrane and the stationary plates. An oscillator-detector circuit is used for capacity measurements, the dc output voltage being a direct representation of absolute pressure. The output voltage generally ranges between 0 and 5 V and varies linearily with pressure.

The other type of diaphragm gage is mechanically configured similar to

the capacity type, in that it consists of a taut membrane between two rigid blocks. This unit operates on the principle of variable reluctance rather than variable capacitance. An E-core and coil assembly is embedded in each block. A small gap between the diaphragm and the E-core in a symmetrical arrangement results in a condition of equal inductance with the membrane in an undeflected position. Diaphragm deflection results in an increase in the gap in the magnetic flux path of one core, with an equal decrease in the other. This increases the inductance of one coil while decreasing the inductance of the other. A simple bridge and detector circuit converts the inductance ratio to a dc output voltage of 0 to 5 V, which varies linearly with pressure. The output voltage from the diaphragm gages may be read at the ground station through the telemetry system.

Diaphragm gages have been used to a large degree on scientific balloons in recent years. Various pressure ranges are available, with the most sensitive ranges such as 0 to 0.1 psia (0 to 7 mb) being used for balloon float altitudes. With careful calibration, the accuracy of this most sensitive range should be within 0.1 mb. If the output voltage is digitized rather than being telemetered in analog form, readout accuracy can be improved.

An assembly of diaphragm type gages may be used to cover the complete pressure range traversed by balloons during ascent and descent, Cooper (16). If three gages are used in the assembly, good resolution may be obtained for float altitudes above 18 km. The three transducers cover the full ambient pressure range expected in balloon flights; each is engaged in the pressure interval to which it is most sensitive. Electronic circuits can be used to select the appropriate transducer for each pressure segment and supply calibration voltages for the telemetry system. Typical pressure ranges of transducers of this type are 0-1100 mb for low altitude pressure measurements (below 18 km), 0-70 mb for the range between 18 and 34 km, and 0-7 mb for flights above 34 km.

The dc analog voltage outputs of the transducers are individually applied to the input of a telemetry system. Calibration voltages for the telemetry system may also be supplied at intervals with the pressure analog from the transducer interface electronics. To conserve power, only the transducer required for a particular range need be functioning. They may be selected by command-control or by an electronic circuit which automatically selects the transducer which is most sensitive in the pressure range in

which the balloon is flying. The active transducer may be identified at the telemetry output by some identifying code, such as the manner in which the calibration pulses are applied to the telemetry encoder input.

Since taut diaphragm gages rely upon a reference vacuum for their operation as an absolute pressure gage, care must be taken to insure that the reference vacuum is not allowed to deteriorate. Manufactured gages have a reference as a part of their construction and are subject to leaks through glass seals, welds, or even through the thin metal material of the taut membrane. Careful manufacturing control must be maintained. A small leak may take months to detect. When one occurs, however, the gage suffers with a fixed shift in its output voltage and is more sensitive to ambient temperature changes.

3. Thermoconductivity Gages

A thermoconductivity pressure gage utilizes the change in the thermoconductivity of a gas to detect pressure changes. One transducer of this type uses a thermistor sensing element in a constant temperature environment. The thermistor is an element of a bridge circuit, whose output changes with pressure changes because the equilibrium temperature of the thermistor

changes inversely with the pressure being measured. The output voltage of the bridge is fed to an operational amplifier whose output is fed back to the bridge to bring it into balance. The output voltage of the operational amplifier is a function of the thermoconductivity of the gas surrounding the thermistor sensor, which makes it a pressure sensing device since T is constant. The voltage range can be designed to give an appropriate analog range, such as 0 to 5 V d c over the pressure range to be measured.

The thermoconductive transducer has good performance characteristics with good resolution in the very low pressure range under controlled conditions. The output voltage varies logarithmically with the absolute pressure, giving more resolution at the low pressure end of its range. A typical calibration curve is shown in Fig. 25. Since it measures thermal conductivity, its accuracy depends upon the chemical composition of the gas being measured. When used as a balloon pressure-altitude transducer, it may be exposed to helium or other gases which have a different thermal conductivity from that of air. This will change the calibration of the transducer and cause it to indicate an erroneous pressure.

4. Other Types of Pressure Transducers

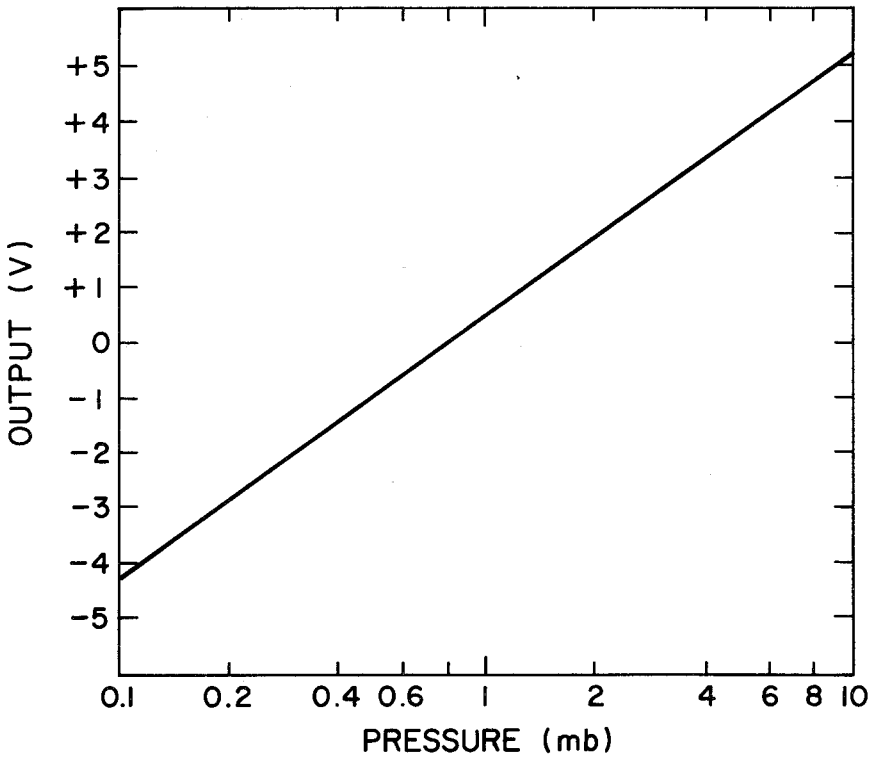

Fig. 25. Typical calibration curve for thermoconductivity pressure gage.

There are several other types of pressure transducers that have been used as balloon altimeters. Some of these transducers have special application and may not lend themselves to routine operational use because of their complexity, calibration problems, or their incompatibility with telemetry.

The hypsometer is an instrument which measures the pressure of a gas through the relationship of the vapor pressure of a liquid to its temperature. If a liquid is maintained at its boiling point, its vapor pressure is equal to the surrounding gas pressure. Thus the vapor temperature is a measure of this gas pressure. Some means, such as a thermistor, must be used to measure the temperature of the liquid. This temperature measurement must then be converted to an analog or digital signal, compatible with the telemetry, before transmission to the ground.

The hypsometer has a slow response and is tedious to prepare for flight. When it is working properly and has been carefully calibrated, it is an accurate pressure measuring device.

A transducer that has been used in scientific balloon flights is a corona transducer which operates on the density dependence of a corona dis-

charge in air. A positive ion flow is generated in a region of high electric field gradient in the immediate vicinity of a fine wire suspended axially within a conducting cylinder. The magnitude of the current flowing between the wire and the cylinder is a function of the gas density in the region between the electrodes. Since the unit is basically a density measuring device, the corona current is sensitive to temperature variations. The transducer has a temperature compensation circuit which makes it function as a pressure measuring system.

Radioactivity pressure transducers have also been used in scientific ballooning. These instruments have sensitive electrometers to measure the ionization currents produced by alpha-particles from a radioactive source. Voltage pulses are generated by a blocking oscillator at a rate determined by the ionization currents. At low pressures, the repetition interval is very long--on the order of 30 to 50 sec at 3 mb. In some cases the pulses are used to change the state of a flip-flop, making it easier to read on telemetry, Howard (17).

The radioactive type of transducer must be temperature controlled or temperature compensated since it is basically a density measuring device.

Some must be calibrated immediately prior to use because of the decay of the radioactive source. Like the thermoconductivity transducer, the radioactive transducer can be affected by the composition of the measured gas.

Early scientific balloon flights were equipped with an instrument called a photobarograph to provide redundancy in pressure measurements. This is a self-contained unit which operates independently from other electronic or telemetry equipment. It consists of an accurate aneroid pressure gage with a dial calibrated in millibars. The pressure dial and an accurate time piece are photographed at appropriate intervals during the balloon flight, and the camera film is processed after payload recovery.

5. Altitude Measuring Devices

A newly developed radio altimeter makes direct geometric altitude measurements of meteorological balloons up to altitudes of 35 km over water and 12 km over land. This radio altimeter is a pulse-radar system in which the elapsed time period between transmitted pulses is a measure of the altitude, Levanon (18), Stremler (19). A single RF superregenerative stage serves as both the transmitter and the receiver. The transmitted pulse is

reflected from the water or earth surface and is received by the altimeter receiving circuits. The repetition frequency of the transmitted pulses is controlled by the round trip propagation time of the pulsed radio signals. At high balloon altitudes, the repetition interval may be less than the propagation time by one or more integral multiples. This creates an ambiguity in altitude but it can be overcome by extrapolating the balloon ascent data or by means of balloon-borne pressure gages.

The maximum altitude of operation is influenced by transmitter power, antenna gain, choice of operating frequency, terrain, etc. The upper limit for altimeters currently being used is 35 to 40 km over water and 12 to 15 km over land using 5-element yagi antennas at 403 MHz. These radio altimeters are obviously more practical to use over water than over land. Because of this, they find more use for meteorological or long duration global flights than for scientific balloon flights.

H. POWER

Solar cells, fuel cells, nuclear sources, and batteries have all been considered as power sources for balloon-borne electronic equipment. Solar cells have been used extensively only on small, long-duration balloon systems,

and batteries are used regularly to power both scientific and support equipment on large scientific flights. Other types of power sources have not been widely used.

Solar cells are p-n junctions, usually silicon, that develop electrical energy by the photovoltaic effect. When a junction is illuminated, photon energy creates electron-hole pairs, and a voltage is developed across the junction. The efficiency of modern solar cells is about 5-10%, and a 1-m^2 panel exposed perpendicularly to the direct rays of the sun at the top of the atmosphere will intercept 1395 W of solar power, see Section III.G. Thus a solar cell panel may be expected to provide a maximum of about 140 Wm^{-2} during the day under ideal circumstances, and it will produce no power at night. In general, a large area of solar cells would be required to provide energy for a scientific flight, and stored energy would be needed to supplement the solar cells if power were required at night.

Mercury, lead-acid, nickel-cadmium, silver-zinc, and silver-cadmium batteries have all been used in scientific ballooning. No one type is clearly superior to all others; therefore, battery selection depends on the application and the type of service desired.

Mercury cells have a high energy density and are rugged and reliable. The terminal voltage during discharge is fairly constant; therefore, some models are useful as voltage references. Unfortunately, they have characteristics which render them incapable of providing power under the conditions generally required for balloon service. They are not rechargeable, they cannot be operated satisfactorily in parallel because circulating currents cause serious discharge of cell capacity, and they are not useful at temperatures below 5°C. They are useful, however, for low-power loads where current drain is well below the design maximum and the temperature can be controlled.

The lead-acid cell is probably the best known of the common storage cells. It has a relatively low energy density, but it has a high terminal voltage and a fairly level discharge plateau. When flown at high altitudes, it should be operated in a sealed container in which a pressure greater than the partial pressure of the electrolyte can be maintained. Also, in the case of liquid electrolyte types, it must be properly oriented to prevent spilling. Because of their low cost and universal availability, lead-acid batteries are sometimes used, but they are not generally recommended for balloon service.

Nickel-cadmium cells employ electrodes of nickel and cadmium in a potassium hydroxide electrolyte. There are two distinct cell forms--the Junger or pocket-plate and the Durac or impregnated, sintered-plate type. The sintered-plate type can sustain a higher current drain and it can be made thinner, and hence smaller, than the pocket-plate type. The principal advantages of the nickel-cadmium cell are that it can be hermetically sealed, it has a high cycle life, and it performs better than other cells at low temperatures. It has a higher energy density than the lead-acid cell.

The silver-zinc cell employs zinc and silver oxide as electrodes in a solution of potassium hydroxide. These cells, designed for high-energy applications cannot be hermetically sealed because of the evolution of oxygen. They may be operated in either series or parallel, provided they are all the same type and size. They have a high energy density and are especially suited for high current drains. The major disadvantages are the limited shelf life when activated and the limited recharge cycles as compared to nickel-cadmium and silver-cadmium. The energy density is good over a range of -30 to +50°C but is reduced at more extreme temperatures. The silver-zinc battery is well suited to balloon applications where the best

energy-to-mass ratio is desired and the recycle life is not important.

Silver-cadmium cells are similar in construction to silver-zinc cells except that the electrodes are silver and cadmium. The electrolyte is potassium hydroxide. The operating characteristics and watt-hour cost are also similar to those of silver-zinc cells. Silver-cadmium cells have better temperature stability and greater cycle life than silver-zinc cells but their energy to mass ratio is not quite as great. As with the silver-zinc cells, they cannot be hermatically sealed for high discharge rate applications. The main advantage over other types of storage cells is their increased cycle life for rechargeable application. This, together with their reasonably high energy density makes them desirable for use as power sources for repeated use where operating cost is a major factor, Garner (20).

I. EQUIPMENT PACKAGING

Equipment which is flown on a balloon must be protected against a rather severe environment during flight. Ambient air temperature may drop as low as -85°C. Air pressure is frequently less than 0.005 atmospheres and may reach values as low as 0.001 atmosphere (~ one mb) on the highest flights. Also moisture may occasionally condense on equipment during ascent or descent even

in the absence of clouds. Finally, equipment which is to be recovered for post-flight evalutation or reuse must be protected against the accelerations associated with the flight. Landing shocks, in particular, can be severe. Experience has shown that equipment which is properly packaged can function satisfactorily in the adverse flight environment while improperly packaged equipment frequently fails.

Pressure and temperature in the atmosphere at balloon flight levels are discussed in Section XI. Heat exchange between a balloon-borne object and its environment is covered in Section III. Potentially damaging accelerations are most likely to occur during the parachute opening or upon landing. These are discussed in Sections X.C. and XII.G., respectively.

Equipment which is flown repetitively for routine flight support is usually packed in a self contained, serviceable configuration. Figure 26 shows one such support package. Its construction and protective covering (not shown in the figure) are the end result of extensive engineering analysis and flight experience. The packaging for scientific equipment, or special support equipment, being flown for the first time is often designed on the basis of engineering analysis alone. A preliminary flight for testing the

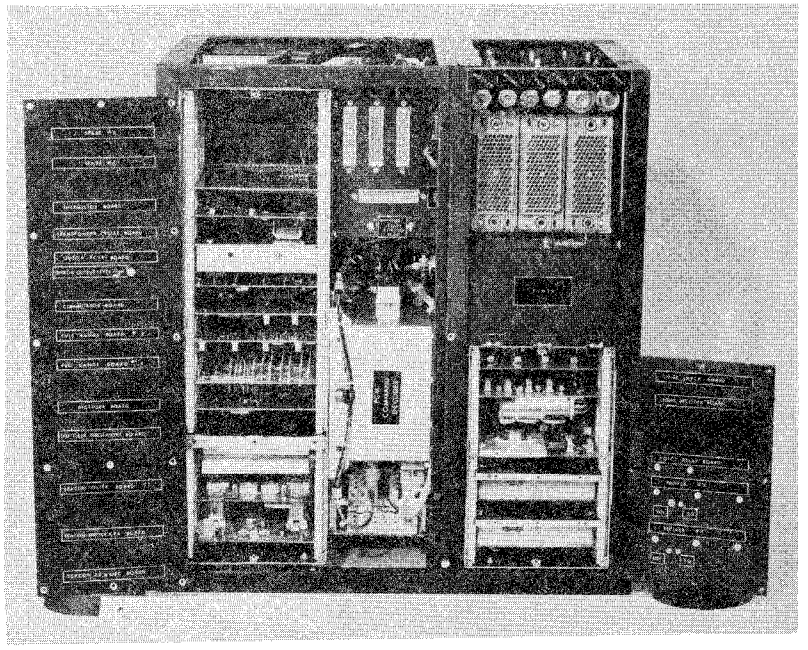

Fig. 26. The NCAR integrated flight support package.

packaging and other engineering features of new flight systems should always be considered. Tests in environmemtal chambers may also be useful.

The location of support instrumentation on a flight payload depends largely on the configuration of the scientific equipment. Large, bulky experiments may have adequate space within their structure to accommodate the support package without causing undue problems, e.g., center-of-gravity shifts. Smaller experiments may be placed above, below, or beside a self contained support package. Each such arrangement creates its own special problems in protective packaging.

The flight support package must be equipped with appropriate circuit connectors to connect the telemetry, command, pyrotechnic, and other circuits used with the scientific experiment and balloon control. Flight antennas should be placed on the payload with much care. Antennas are usually suspended well below the payload at distances and separations that will create a minimum radiation interference with each other. Some payload configurations require a long wire, high frequency antenna to be attached above the payload on a balloon load tape. The Omega tracking antenna whip may sometimes be located above the support package.

A flight package can be protected from low temperature environments with thermal insulation material, such as styrofoam sheets or similar molded material. It is seldom necessary to supply heat from an external source because high dissipation equipment such as telemetry transmitters provide enough heat to warm low dissipation equipment. Because of this, it is necessary to configure flight components within the package for uniform heat distribution and proper heat sinking. It may sometimes be necessary to release heat from highly dissipative components to the outside of the insulated housing by means of metal heat conductors. A part of the payload structure is often used as a heat sink. It is possible to use liquid thermal sinks and electrical or fluid heat exchangers as part of the package design. Liquid thermal sinks are often used with packages containing equipment with low internal heat release such as timers and command-receivers which are isolated from the main support package at the top of the parachute or balloon.

When configuring the flight package it is generally desirable to place the batteries in the lower portion of the package. This concentrates the weight at the bottom, utilizes the heat liberated by the batteries more ef-

fectively, and prevents stray electrolyte from damaging other circuit components.

REFERENCES

(1) Stiltz, Harry L., 1961: Aerospace Telemetry, Vol. I. Prentice-Hall, Inc.

(2) Telemetry Standards, Revised 1973. To be used in conjunction with document 118-73, Test Methods for Telemetry Systems and Sub-systems: Inter-Range Instrumentation Group, Published by Secretariat, Range Commanders Council, White Sands Missile Range, New Mexico, 88002.

(3) Gruenberg, Elliot L., Ed., 1967: Handbook of Telemetry and Remote Control. McGraw-Hill Book Co.

(4) Bendix-Pacific, 1958: The Theory and Application of FM/FM Telemetry, Revised 1958. Bendix Aviation Corp., North Hollywood Calif.

(5) Cooper, Oscar L., 1967: Scientific Balloon Instrumentation, Proceedings of the Thirteenth I.S.A. Aerospace Instrumentation Symposium.

(6) Nichols, Myron H. and Lawrence L. Rauch, 1956: Radio Telemetry, 2nd ed. John Wiley and Sons, Inc., New York.

(7) Clark, T. A., 1969: Telemetry Signal-Strength Variations from Balloon-borne Equipment and a method for balloon range estimation. Journal of Scientific Instruments, Series 2, Vol. 2.

(8) Cooper, Oscar L., 1970: Evaluation of UHF Radio Frequency Equipment for Balloon Telemetry, Proceedings, Sixth AFCRL Scientific Balloon Symposium. (AFCRL-70-0543)

(9) Coates, Robert J., 1969: Tracking and Data Acquisition for Space Exploration. Goddard Space Flight Center, Greenbelt, Maryland. Publication X-520-69-200.

(10) Cooper, Oscar L., 1970: PCM Command Control System, Facilities for Atmospheric Research, No. 12, Mar. 1970. National Center for Atmospheric Research, Boulder, Colo. 80302.

(11) IRIG Standards for Radio Command Control, 406-550 Mcs Band, 1962: Inter-Range Instrumentation Group, published by Secretariat, Range Commanders Council, White Sands Missile Range, N. Mex., 88002.

(12) Cooper, Oscar L., 1971: Timers for Balloons. Facilities for Atmospheric Research, No. 16, Mar. 1971. National Center for Atmospheric Research, Boulder, Colo. 80302.

(13) Pierce, J. A., W. Palmer, A. D. Watt, R. H. Woodward, 1966: Omega, A World Wide Navigational System, 2nd Rev. U.S. Navy Dept. Bureau of Ships, submitted through Office of Naval Research P and B, publ. No. 886B, Project No. 347.

(14) Federal Aviation Regulations, Vol. II, Part 37.180, July 1969: Supt. of Documents, Wash., D.C. 20402.

(15) Cooper, Oscar L., 1968: Pressure Altitude Transducers, Facilities for Atmospheric Research, No. 7, Dec. 1968. National Center for Atmospheric Research, Boulder, Colo. 80302.

(16) Cooper, Oscar L., 1970: Pressure Altitude Assembly for High-Altitude Balloons, Facilities for Atmospheric Research, No. 15, Dec. 1970. National Center for Atmospheric Research, Boulder, Colo. 80302.

(17) Howard, R. L., S. W. Nelson, J. R. Winckler, 1968: An Alphatron Pressure Gauge for High Altitude Constant Level Balloon Flights. School of Physics and Astronomy, Univ. of Minnesota, Minneapolis, Minn.

(18) Levanon, N. and F. G. Stremler, 1969: Accurate Pulse-Radar Altimeter for Meteorological Balloons, Proceedings of IEEE, Vol. 57, No. 9, Sept. 1969.

(19) Stremler, F. G., N. Levanon, V. E. Suomi, 1970: Applications of Radio Altimetry to Balloons, Proceedings, Sixth AFCRL Scientific Balloon Symposium. (AFCRL-70-054B)

(20) Garner, Ruford V,, 1964: Investigation of Electrical Power Sources for Missile-Borne Applications, Report No. RE-TR-64-29, DA Proj. No. IX27919D687, U.S. Army Missile Command, Redstone Arsenal, Ala.

Part0001 NCAR-TN/IA-99 Scientific Ballooning Handbook - Link Page

Next PART0002